

博士論文

Undrained behavior of sand with non-plastic silt and its application to ground deformation analysis

(非塑性シルトを含む砂の非排水せん断実験と地盤変形予測への応用)

アルベルト エルナンデス ヨランダ

東京大学
東京, 日本
夏 2014

**UNDRAINED BEHAVIOR OF SAND WITH NON-PLASTIC
SILT AND ITS APPLICATION TO GROUND
DEFORMATION ANALYSIS**

**非塑性シルトを含む砂の非排水せん断実験と地盤変形予測への
応用**

by

Yolanda Alberto Hernández

B.E. (Universidad Nacional Autónoma de México) 2007

M.Sc. (University of California, Berkeley) 2009

A dissertation submitted to the
Department of Civil Engineering
of the
University of Tokyo
in partial fulfillment of the
requirements for the degree of
Doctor of Philosophy
In
Civil Engineering

University of Tokyo

Tokyo, Japan

Summer 2014

THESIS APPROVAL

University of Tokyo

Department of Civil Engineering

Laboratory of Geotechnical Engineering

Title: Undrained behavior of sand with non-plastic silt and its application to ground deformation analysis

This is to certify that we have read this thesis and that in our opinion it is fully adequate, in scope and quality, as a thesis for the degree of Doctor of Philosophy

Research Supervisor

Prof. Ikuo Towhata

Advisory Committee Members

Prof. Susumu Yasuda

Prof. Junichi Koseki

Assoc. Prof. Keiko Kuwano

Assoc. Prof. Taro Uchimura

ABSTRACT

Undrained behavior of sand with non-plastic silt and its application to ground deformation analysis

By

Yolanda Alberto Hernández

Doctor of Philosophy in Civil Engineering

University of Tokyo

Prof. Ikuo Towhata, Chair

ABSTRACT: The presence of non-plastic fines during liquefaction has caused divergent conclusions regarding its effects. While field test data with fines has been added in charts for design and some criteria has been adopted regarding the liquefaction potential according to water content, liquid limit and plasticity index, there are not clear provisions for non-plastic fines. The use of density measures for comparison in laboratory testing, such as void ratio, relative density or sand skeleton void ratio, has led to contradictory results given the restrictions of each parameter and the impossibility to keep them all constant at the same time. Results appear to be conflicting, yet they can be integrated under the same frame if the differences between density measures are understood. Mineralogy, size distribution, sphericity, roundness and surface roundness all affect packing and compressibility of sands. Minimum and maximum void ratio are the most meaningful measures of packing behavior, nonetheless these measures are not easy to define for sands containing more fines than 30%. To understand this, it is important to point out that there are three different states in sand containing silt: 1) when fines are within the voids in the sand matrix, 2) when fines exceed the volume of voids 3) when fines start controlling the overall response. These values depend on the ratio of sand and fine grains sizes, particle shape and mineralogy. Seeking to avoid the selection of a particular parameter for comparison of different fines contents, a different approach was used in this work.

Sand retrieved from Tokyo Bay after the liquefaction events in 2011 was used for the series of tests presented herein. Sand was sieved to separate fines from coarser sand grains. After washing and drying, fines were thoroughly mixed with sand from 0 to 80% of content. Constant energy for sample preparation was used in this study to compare different fines contents and to simulate a natural process. This methodology looks to overcome the issue of selecting a density index for evaluation. The samples were prepared by air pluviation, keeping a constant height of fall of 5 cm and 50 cm. A hollow cylindrical torsional shear device was used. Saturation was achieved using the double vacuum method.

During the first series of tests, samples prepared with 5 cm of height of fall (AP-5 cm) were consolidated to an effective confining stress of 100 kPa and then cyclic loading was applied at different cyclic stress ratios. After studying the stress-strain curves, stress paths, excess pore pressure distributions and liquefaction curves it was found that when a small amount of fines is added to clean sand, liquefaction resistance decreases. More addition of fines causes a reverse behavior until once more a reduction in resistance is observed. After this, liquefaction resistance increases again with fines. Monotonic tests were also run for samples made by 5 cm of height of fall from 0 to 60% of fines content. The behavior was similar to the one found by cyclic tests.

In the second stage samples were prepared with a height of fall of 50 cm (AP-50 cm). A comparable response was found although the fines content, where the reverse behavior was found in the previous group, varied slightly. In both sets the variation of the volumetric strain after consolidation was measured to obtain the relation of the volumetric compressibility with fines content. The shear modulus for the first cycle (shear strain of 0.1%) was also measured to observe the effect of fines content.

The presence of two important fines contents was confirmed in these experiments: the threshold fines content F_{thr} and the limiting fines content, F_{lim} . These values defined three different groups of behavior: the first controlled by sand, the second where there was a transition, and the third controlled by fines. In both cases, AP-5 cm and AP-50 cm, clean sand exhibited the largest resistance. However it was still necessary to know how this

response related to field values used for design, as the SPT-N value. It was assumed that two laboratory parameters could be used to establish this connection: relative density, D_r , and the coefficient of volume compressibility, m_v . At this stage, there was a clear image of the relation between fines and volumetric deformation, hence, this parameter was used to run a third set of tests that compared fines contents at similar values of m_v .

The last series of test was conducted for a value of $m_v=1.20 \times 10^{-4}$ (1/kPa) which is expected to be inversely proportional to a single value of SPT-N. Different heights of fall were used to obtain this value after consolidation. The smallest height of fall, 2 cm, was used for clean sand and the highest for 80%, 50 cm. Liquefaction curves showed that from 0 to 20% there is a decrease in resistance, having a small difference between 10 and 20%. Then there was a slight increase from 30 to 40%. From 60 to 80%, liquefaction curves shifted to the left side, but samples with 80% were more resistant than those of 60%. This confirmed the results obtained for the previous groups of experiments.

Later, using the same approach of similar m_v , samples of 0, 20, 30 and 80% were prepared to study the post-liquefaction behavior. A series of random loads were applied to these samples until a certain shear strain was reached and then drainage was opened to measure the volumetric deformation. The samples with 20 and 80% reported the major volumetric strain, while the 0% had the smallest.

TABLE OF CONTENTS

Chapter 1. INTRODUCTION	2
1.1. Introduction.....	2
1.2. Research motivation.....	5
1.3. Scope and objectives.....	7
1.4. Thesis outline.....	8
Chapter 2. LIQUEFACTION IN TOKYO BAY	11
2.1. Liquefaction in silty soil	11
2.1.1. Liquefaction in the 1989 Loma Prieta Earthquake.....	11
2.1.2. 1999 Chi-chi Earthquake, Taiwan.....	13
2.1.3. 2010 and 2011, Christchurch New Zealand	15
2.2. Liquefaction in Tokyo Bay	16
2.2.1. Liquefaction in Urayasu City	18
2.3. Characteristics of Tokyo Bay sand	29
2.3.1. Index tests.....	30
2.3.2. Microscope pictures.....	34
Chapter 3. LIQUEFACTION OF SILTY SAND	40
3.1. Previous research on liquefaction potential of silty soils.....	40
3.2. Previous laboratory research on liquefaction of non-plastic silty sand	41
3.2.1. Other parameters of comparison.....	42
3.2.2. Results of different researchers in laboratory testing	44
3.3. Particle packing.....	48
3.4. Liquefaction of mine tailings.....	51

Chapter 4. EXPERIMENTAL PROGRAM.....	54
4.1. Specimen preparation.....	54
4.1.1. Moist tamping.....	55
4.1.2. Water pluviation	55
4.1.3. Slurry deposition	55
4.1.4. Dry deposition	56
4.1.5. Effect of sample preparation	56
4.2. Sample saturation.....	57
4.2.1. Carbon dioxide	59
4.2.2. Double-vacuum saturation.....	59
4.3. Consolidation tests	60
4.4. Undrained monotonic shear tests	61
4.5. Stresses and strains in a hollow cylindrical torsional shear device	62
4.6. Torsional shear tests.....	67
4.6.1. Selection of sample preparation method	67
4.6.2. Specimen preparation	68
4.6.3. Preparation of de-aired distilled water	71
4.6.4. Saturation.....	72
4.6.5. Preparation of the sample for consolidation.....	76
4.6.6. B-value	77
4.7. Consolidation tests.....	82
4.8. Monotonic tests.....	83
4.9. Cyclic shear tests	84
Chapter 5. ANALYSIS OF EXPERIMENTAL RESULTS	88

5.1.	Tests formed by air pluviation	89
5.2.	AP – 5 cm	93
5.2.1.	Consolidation.....	93
5.2.2.	Monotonic shear tests	97
5.2.3.	Stress-strain curves and stress paths.....	100
5.2.4.	Excess pore-water pressure development.....	106
5.2.5.	Liquefaction curves	107
5.3.	AP – 30 cm	110
5.3.1.	Consolidation.....	110
5.3.2.	Stress-strain curves and effective stress paths.....	112
5.3.3.	Liquefaction curves	117
5.4.	AP – 50 cm	120
5.4.1.	Consolidation.....	120
5.4.2.	Stress-strain curves and effective stress paths.....	122
5.4.3.	Liquefaction curves	127
5.5.	Tests at the same penetration resistance, SPT N-value (S _{mv}).....	130
5.5.1.	Relative density	131
5.5.2.	Coefficient of volumen compressibility	135
5.6.	Slurry deposition procedure.....	144
Chapter 6.	APPLICATION TO DEFORMABILITY ANALYSIS	148
6.1.	Shear modulus degradation.....	148
6.2.	Calculation of lateral displacement.....	155
6.1.	Stress-strain modified curves.....	160
6.2.	Post-liquefaction deformation.....	166

6.2.1.	Random loading.....	169
Chapter 7.	RECONCILIATION OF PREVIOUS RESEARCH.....	180
7.1.	Laboratory tests on the effect of fines content.....	180
7.1.1.	Binary packing.....	180
7.2.	Reconciliation of previous results.....	183
7.3.	Monotonic tests for effective confining pressure, $\sigma'_c=50$ kPa	187
7.4.	Low-plasticity fines	190
7.5.	Simplified procedures for evaluation of liquefaction potential	196
7.5.1.	Youd and Idriss (2001).....	196
7.5.2.	Japanese Highway Bridge Design Code.....	198
7.5.3.	Tokimatsu and Yoshimi (1983).....	202
7.5.4.	Assessment through cone penetration test (CPT).....	204
7.5.5.	Results obtained in this research program.....	206
Chapter 8.	CONCLUSIONS AND RECOMMENDATIONS.....	210
8.1.	Recommendations.....	213
Chapter 9.	REFERENCES	214

FIGURES

Figure 1.1. Charts for Chinese criteria. From Wang (1979).....	4
Figure 2.1. San Francisco Bay’s areas of liquefaction	11
Figure 2.2. Liquefaction in the Valencia Street Hotel.....	12
Figure 2.3. Localization of affected areas by the Chi-chi Earthquake	14
Figure 2.4. Liquefaction-induced tilting in a residential building (from Hung 2012).....	14
Figure 2.5. Location of Darfield and Christchurch	15
Figure 2.6. Comparison of CSR for Darfield and Christchurch Earthquakes with CRR for FC=9%. From Cubrinovski et al. (2011).....	16
Figure 2.7. Intensity map.....	18
Figure 2.8. Map of Urayasu City (From Yasuda et al. 2012).....	19
Figure 2.9. Boiled sand in Urayasu City	19
Figure 2.10. Differential settlement observed around the City	20
Figure 2.11. Damage observed around the metro station	21
Figure 2.12. Liquefaction on the streets	21
Figure 2.13. Tilting of houses.....	22
Figure 2.14. Liquefaction in the harbor area	23
Figure 2.15. Floating of manholes.....	24
Figure 2.16. Bs – FC vs N1 (Urayasu City Council, 2012).....	26
Figure 2.17. As – FC vs N1 (Urayasu City Council, 2012)	26
Figure 2.18. Fs – FC vs N1 (Urayasu City Council, 2012)	27
Figure 2.19. Variation of fines content and SPT-N1 for different kind of soils (Urayasu City Council, 2012)	28

Figure 2.20. Variation of FC and SPT- N_1 value in Urayasu City (Urayasu City Council, 2012)	28
Figure 2.21. Tokyo Bay sand	29
Figure 2.22. Gradation of Tokyo Bay sand as retrieved from the site	30
Figure 2.23. Grain size distribution for different fines content	31
Figure 2.24. Liquid limit by the Casagrande device.....	32
Figure 2.25. Liquid limit by the fall-cone test.....	33
Figure 2.26. Minimum and maximum void ratios.....	34
Figure 2.27. (a) 0% fines content; (b) 30% fines content and (c) 100% fines content.....	35
Figure 2.28. Microscope pictures	36
Figure 2.29. Colored microscope picture. FC=0%	37
Figure 2.30. Colored microscope picture. FC=30%	37
Figure 2.31. Colored microscope picture. FC=50%	38
Figure 2.32. Colored microscope picture. FC=100%	38
Figure 3.1. Relation between fines content and N_1 . From Tokimatsu and Yoshimi (1983)	40
Figure 3.2. Soil classification chart for electric cone. From Robertson and Campanella (1985)	41
Figure 3.3. Definition of sand skeleton void ratio, intergranular contact index void ratio and equivalent void ratio	43
Figure 3.4. Definition of state parameter and equivalent granular state parameter (After Baki et al., 2012)	44
Figure 3.5. Binary mechanical packing of coarse spheres and smaller sizes. From McGeary (1961)	50
Figure 3.6. Theoretical variation of void ratio in binary packings with fines. After Lade et al. (1998)	51

Figure 4.1. Sample formation.....	54
Figure 4.2. Influence of sample preparation on the liquefaction resistance. From Mulilis et al. (1977)	57
Figure 4.3. Pore pressure parameter B and degree of saturation, S (%) (After Black and Lee, 1973).	58
Figure 4.4. Scheme of pressures for isotropically consolidated samples at 100 kPa	61
Figure 4.5. Undrained effective stress paths for loose sands (from Yamamuro and Covert 2001)	62
Figure 4.6. Hollow cylinder torsional shear device.....	63
Figure 4.7. Stresses in a hollow cylinder specimen.....	65
Figure 4.8. Pedestal and top cap.....	69
Figure 4.9. Sample preparation.....	70
Figure 4.10. Air pluviation	71
Figure 4.11. Deairing water.....	72
Figure 4.12. Saturation process	73
Figure 4.13. Flushing water.....	74
Figure 4.14. Saturation of the OP-PP differential pressure transducer	75
Figure 4.15. Chamber filling	77
Figure 4.16. Schematic view of the machine.....	78
Figure 4.17. Considerations during pre-consolidation	79
Figure 4.18. Procedure to check B-value	80
Figure 4.19. Consolidation in a hollow cylinder torsional device.....	82
Figure 4.20. Volumetric strain during consolidation.....	83
Figure 4.21. Monotonic test sample results.....	84

Figure 4.22. Stress conditions during cyclic shear tests	85
Figure 4.23. Typical stress-strain curves and effective stress paths during cyclic loading ..	86
Figure 5.1. Load scheme for cyclic loading	88
Figure 5.2. Load scheme for monotonic loading.....	89
Figure 5.3. Uniformity of FC=30% sample for AP-5 cm.....	90
Figure 5.4. Uniformity of FC=30% sample for AP-50 cm.....	90
Figure 5.5. Void ratio for AP-5 and 50 cm samples.....	92
Figure 5.6. Relative density for AP-5 cm samples	93
Figure 5.7. Volumetric strain during consolidation.....	94
Figure 5.8. Volumetric strain and mean effective stress during consolidation AP-5 cm	95
Figure 5.9. Obtaining m_v from consolidation curves.....	96
Figure 5.10. Coefficient of volume compressibility for AP-5 cm.....	97
Figure 5.11. Stress-strain curves during monotonic loading for $\sigma'_c=100$ kPa.....	99
Figure 5.12. Effective stress paths during monotonic loading for $\sigma'_c=100$ kPa.....	99
Figure 5.13. Stress-strain curves and effective stress paths for FC=0%, AP-5 cm, CSR=0.15	
101	
Figure 5.14. Stress-strain curves and effective stress paths for FC=30%, AP-5 cm,	
CSR=0.15 102	
Figure 5.15. Stress-strain curves and effective stress paths for FC=80%, AP-5 cm,	
CSR=0.15 103	
Figure 5.16. Comparison of stress paths for FC=0, 30 and 80%	104
Figure 5.17. Tangent shear modulus during cyclic undrained shear for AP-5 cm	105
Figure 5.18. Definition of tangent shear modulus	105
Figure 5.19. Excess pore pressure ratio for AP-5 cm	106

Figure 5.20. Liquefaction curves for AP-5 cm.....	108
Figure 5.21. Cyclic resistance ratio and fines content for AP-5 cm.....	109
Figure 5.22. Variation of CRR_{20} with m_v for AP-5 cm	110
Figure 5.23. Volumetric strain during consolidation.....	111
Figure 5.24. Volumetric strain and mean effective stress during consolidation AP-30 cm 111	
Figure 5.25. Coefficient of volume compressibility for AP-30 cm.....	112
Figure 5.26. Shear-strain curves and effective stress paths for FC=0% and AP-30 cm.....	113
Figure 5.27. Stress-strain curves and effective stress paths for FC=10 and AP=30 cm.....	114
Figure 5.28. Stress-strain and effective stress path for FC=20% and AP-30 cm	115
Figure 5.29. Stress-strain curves and effective stress paths for FC=30 and AP-30 cm	116
Figure 5.30. Liquefaction curves for AP-30 cm.....	117
Figure 5.31. Sample A. FC=30% $e=1.10$ $D_r=42\%$ AP-5 cm	118
Figure 5.32. Sample B. FC=30% $e=1.08$ $D_r=44\%$ AP-30 cm	118
Figure 5.33. Comparison between samples A and B.....	119
Figure 5.34. Volumetric strain during consolidation. AP-50 cm	120
Figure 5.35. Mean effective stress and volumetric strain during consolidation.....	121
Figure 5.36. Coefficient of volume compressibility for AP-50 cm.....	122
Figure 5.37. Stress-strain curves and effective stress paths for FC=0%, AP-50 cm, CSR=0.15	123
Figure 5.38. Stress-strain curves and effective stress paths for FC=30%, AP-50 cm, CSR=0.15	124
Figure 5.39. Stress-strain curves and effective stress paths for FC=80%, AP-50 cm, CSR=0.15	125

Figure 5.40. Comparison of effective stress paths AP-50 cm	126
Figure 5.41. Tangent shear modulus during cyclic undrained shear for AP-50 cm	127
Figure 5.42. Liquefaction curves. AP-50 cm.....	128
Figure 5.43 Cyclic resistance ratio and fines content for AP-50 cm.....	129
Figure 5.44. Variation of CRR_{20} and m_v for AP-50 cm	129
Figure 5.45. Cyclic resistance ratio and coefficient of volume compressibility for AP-5 and 50 cm	130
Figure 5.46. Correlation between void ratio range and mean grain size (From Cubrinovski and Ishihara, 1999)	132
Figure 5.47. Correlation between C_D and void ratio range (From Cubrinovski and Ishihara, 1999)	132
Figure 5.48. Void ratio range with fines content.....	133
Figure 5.49. Relative density for $N_1=3$ and $N_1=5$	134
Figure 5.50. Variation of f_2 with PI. After Stroud and Butler (1975)	135
Figure 5.51. Coefficient of volume compressibility variation with fines content	136
Figure 5.52. Selected range of m_v	136
Figure 5.53. Volumetric strain during consolidation. S_{mv}	137
Figure 5.54. Mean effective stress and volumetric strain during consolidation. S_{mv}	138
Figure 5.55. Concept of dissipation energy	139
Figure 5.56. Dissipated energy for the same m_v	139
Figure 5.57. Double amplitude shear strain for $m_v=1.20 \times 10^{-4}$ (1/kPa), $CSR=0.15$	140
Figure 5.58. Excess pore pressure ratio for $m_v \approx 1.20 \times 10^{-4}$ (1/kPa), $CSR=0.15$	141
Figure 5.59. Liquefaction curves. S_{mv}	142
Figure 5.60. Comparison of CRR_{20} for the three different experiments	143

Figure 5.61. Stress-strain curve for slurry deposition sample FC=10%, e=1.10, CSR=0.15	
	144
Figure 5.62. Effective stress path for slurry deposition sample FC=10%, e=1.10, CSR=0.15	
	145
Figure 5.63. Layering observed in samples made by SD	146
Figure 6.1. Shear modulus for the first cycle of loading $\gamma=0.1\%$	148
Figure 6.2. Cyclic resistance ratio and shear modulus for 0.1% of shear strain for AP-5 cm	
	149
Figure 6.3. Cyclic resistance ratio and shear modulus for 0.1% of shear strain for AP-50 cm	
	150
Figure 6.4. Cyclic resistance ratio and coefficient of volume compressibility for AP-5 and 50 cm	151
Figure 6.5. Definition of the secant shear modulus	152
Figure 6.6. Normalized shear modulus degradation for AP-5 cm.....	153
Figure 6.7. Degradation of shear modulus for AP-50 cm.....	154
Figure 6.8. Degradation of shear modulus for similar m_v value.....	155
Figure 6.9. Model of lateral displacement.....	157
Figure 6.10. Calculation of lateral displacement.....	159
Figure 6.11. Stress-strain modified curve for FC=0% CSR=0.15 by S_{mv}	161
Figure 6.12. Larger scale FC=0% CSR=0.15 by S_{mv}	161
Figure 6.13. Curves of stress ratio τ/p -strain for FC=0, 10 and 20%	162
Figure 6.14. Curves of stress ratio τ/p -strain for FC=30 and 40%	163
Figure 6.15. Curves of stress ratio τ/p -strain for FC=60 and 80%	164
Figure 6.16. Ratio of shear stress over mean effective stress versus strain for FC=0, 30 and 80%	
	165

Figure 6.17. Modified stress-strain curves for FC=0, 30 and 80%	166
Figure 6.18. Volumetric strain after uniform loading CSR=0.15 AP-5 cm	168
Figure 6.19. Volumetric strain after uniform loading CSR=0.15 AP-5 cm	168
Figure 6.20. Random loading	169
Figure 6.21. Variation of volumetric strain with shear for different shear strains (From Toriihara et al., 2000)	170
Figure 6.22. Stress-strain curves of random undrained loading on FC=0% sample	171
Figure 6.23. Effective stress path for random undrained loading on FC=0% sample.....	171
Figure 6.24. Stress-strain curves of random undrained loading on FC=20% sample	172
Figure 6.25. Effective stress path for random undrained loading on FC=20% sample.....	172
Figure 6.26. Stress-strain curves of random undrained loading on FC=30% sample	173
Figure 6.27. Effective stress path for random undrained loading on FC=30% sample.....	173
Figure 6.28. Stress-strain curves of random undrained loading on FC=80% sample	174
Figure 6.29. Effective stress path for random undrained loading on FC=80% sample.....	174
Figure 6.30. Ratio of shear stress over current mean effective stress versus shear strain for random loading. AP=5 cm, CSR=0.25	175
Figure 6.31. Ratio of shear stress over corrected current mean effective stress versus shear strain for random loading. AP=5 cm, CSR=0.25	176
Figure 6.32. Shear strain DA with number of cycles for random loading	177
Figure 6.33. Volumetric strain after random undrained loading for different void ratios. AP-5 cm	178
Figure 6.34. Volumetric strain after random loading for different fines contents.....	178
Figure 7.1. Stages of binary packing	181
Figure 7.2. Influence of D50/d50. From Lade et al. (1998)	182

Figure 7.3. Variation of e_{\min} with D_{50}/d_{50}	183
Figure 7.4. Void ratio kept constant	184
Figure 7.5. Relative density kept constant.....	185
Figure 7.6. Relative density for Monterey sand at the same sand skeleton void ratio	186
Figure 7.7. Relative density for Yatesville sand at the same sand skeleton void ratio.....	187
Figure 7.8. Stress-strain curves for monotonic loading at $\sigma'_c=50$ kPa. AP-5 cm.....	188
Figure 7.9. Effective stress paths for monotonic loading at $\sigma'_c=50$ kPa. AP-5 cm.....	189
Figure 7.10. Effect of fines on the critical state line. (In Bouckovalas et al. 2003)	189
Figure 7.11. Decrease in resistance with fines content for the same compaction energy. From Lade and Yamamuro (1997)	190
Figure 7.12. Plasticity index and cyclic resistance ratio for soil with fines (From Ishihara 1993)	191
Figure 7.13. Cyclic loading on TBS, FC=10% prepared by AP-50 cm	192
Figure 7.14. Cyclic loading on TBS, FC=10% prepared by AP-5 cm	192
Figure 7.15. Cyclic loading on LPTBS, FC=10% prepared by AP-5 cm	193
Figure 7.16. Excess pore pressure ratio for LPTBS	194
Figure 7.17. LPTBS – Liquefaction curves.....	195
Figure 7.18. Liquefaction curves of LPTBS compared to non-plastic fines liquefaction curves	196
Figure 7.19. SPT clean-sand base curve (From Seed et al., 1985).....	198
Figure 7.20. Variation of the coefficient c_1 with fines content.....	200
Figure 7.21. Variation of the coefficient c_2 with fines content.....	200
Figure 7.22. Variation of the corrected blowcount N_a with fines content.....	201

Figure 7.23. Variation of resistance with the adjusted value N_a modified for fines content	201
Figure 7.24. Field correlation and laboratory results for silty sands. From Tokimatsu and Yoshimi (1983).....	203
Figure 7.25. Correlation between modified cone penetration resistance and cyclic stress ratio (From Robertson and Campanella 1985).	204
Figure 7.26. Correlation between cone penetration resistance and cyclic stress ratio for sands and silty sands. From Robertson and Campanella (1985).....	205
Figure 7.27. Effect of non-plastic fines content on the correlation between normalized cone resistance and cyclic resistance ratio. (From Carraro et al., 2003).....	206
Figure 7.28. Comparison of results with current curves for SPT N-value and cyclic resistance ratio	208

TABLES

Table 1.1. Literature review on laboratory testing	6
Table 2.1. Relationship between the amount of subsidence. Subsidence measured and estimated amount.....	25
Table 3.1. Previous laboratory research on the undrained behavior of sands with fines	46
Table 5.1. Relative densities and peak shear strength	98
Table 6.1. Parameters for calculation of lateral displacement of an anonymous site.....	158
Table 7.1. Relationship among earthquake magnitude, number of cycles and r_n	202
Table 7.2. Correlation between fines content and ΔN_f	203

ACKNOWLEDGEMENTS

First of all I thank God for all the blessings received, for bringing strength and hope to my life through my family and my dear ones.

I would like to thank the guidance and encouragement of my Advisor, Prof. Ikuo Towhata. He supported me in every single way and always kept me focused on the goal. I have learnt so much these years but I still get surprised by how much I can keep learning from him. Mi más sincero agradecimiento Sensei.

I want to thank my husband, Jesus. His love and support during these years led me through this journey of discovery, wonder, sacrifice and sometimes even heartbreak. He stayed with me and shared it all, always thoughtful and affectionate. He's the cornerstone of my life and words cannot describe my gratitude. This accomplishment is a much his as mine.

I am grateful for my referees: Prof. Susumu Yasuda, Prof. Junichi Koseki, Prof. Reiko Kuwano and Prof. Taro Uchimura. Being able to learn from them was very rewarding. Their advices and corrections helped me gain more insight into my topic. Thank you very much.

I am indebted to all my lab partners and friends. I shared very special moments that I'll always treasure. Especially, I would like to thank Otsubo san and Aoyama san who not only became my dear friends but also helped me through the laboratory and into Japanese life.

I want to thank my family for their loving support and constant prayers. To my mom, Lucia, for her immeasurable love during my whole life, she's the strongest woman I'll ever meet. To my sister, Fernanda, who is an example of dedication and always keeps me motivated. To my brother, David, who has always been there for me, feeding my spirit with joy and happiness, my debt to him is boundless that's why I'm so lucky to be his sister.

I am very grateful for my uncle Ino and my aunt Peaya, they are like my second parents and their unconditional love and support is overwhelming. I also would like to thank my

grannie Coti, my aunt Mary, my uncle Jesus, my adorable family in-law and all my friends, they are the most wonderful persons who always trusted us and cared about our wellbeing.

I would like to thank to all the staff from FSO, Hirano san and Aoyama san from the Civil Office, who were always eager to help and made my life so much easier. I really appreciate their hard work for all the international students.

I have to thank my sponsor CONACYT for their continuous support during my graduate education.

Chapter 1

INTRODUCTION

Chapter 1. INTRODUCTION

1.1. Introduction

Liquefaction is a hazard that has caused a large number of casualties and economic losses. A $M_w=7.9$ earthquake stroke San Francisco in 1906 generating severe damage on areas that were reclaimed areas that previously were bay or marshland. Jefferies & Been (2006) pointed out that Dutch engineers recognized the phenomenon of strength loss and pore pressure increment after the severe flow slides caused by vibration near a railway bridge at Weesp in 1918. However, the problem was addressed and defined later as spontaneous liquefaction by Terzaghi & Peck (1967), who indicated that it occurred in fine silty sands more frequently. Mogami & Kubo (1953) reported small heavings of sand at some places as Amagasaki during an earthquake in 1951, therefore performed experiments using a metal box able to move vertically and sinusoidally on Kumiho sand and other materials. They found that as acceleration increased, shearing strength decreased to almost zero which made the soil behave as a liquid and they decided to call this phenomenon liquefaction.

Nevertheless, it was until the earthquakes of 1964, in Anchorage, Alaska and Niigata, Japan, that liquefaction was acknowledged as an important engineering problem. Ever since, a vast research has been conducted on this matter.

In the late 70's researchers as Seed and Tokimatsu developed different procedures for evaluating the liquefaction potential. Observations of liquefied sites, where it was observed that liquefaction also occurred in deposits formed by different materials as gravel and silt, were added to various databases and used for guidelines. Currently, some of the simplified procedures used worldwide are the ones proposed by Seed et al. (1985), the Japan Road Association (1990 and 1996), Tokimatsu and Yoshimi (1983), Chinese Building Code (1989) or the Arias intensity method (Kayen and Mitchell 1997).

Once it was seen that liquefaction could be triggered in soils other than clean sands, several criteria for evaluating the liquefaction susceptibility of fine-grained soils were developed. The first approach to liquefaction of sands containing fines was taken on by Wang (1979)

who compiled a series of liquefaction events in different soils to estimate the liquefaction potential of silty soils according to its fines content, FC, plasticity index, PI, water content, w_c , and liquid limit, LL . Later Seed et al. (1983) summarized Wang's findings into the three following conditions for soils vulnerable to liquefaction:

- $FC < 15\%$ (percent finer than 0.005 mm)
- $LL < 35\%$
- $w_c > 0.9 LL$

After the liquefaction events in Adapazarı during the Kocaeli Earthquake of 1999, Bray and Sancio (2006) studied the limits proposed by the so-called Chinese criteria. They concluded that the use of FC for separating liquefiable from non-liquefiable soils should be avoided, redefined the relation between water content and liquid limit as $w_c > 0.85 LL$ and stated that plasticity index, PI, was a good index of liquefaction susceptibility since soils with $PI < 12$ can liquefy.

Donahue et al. (2007, 2008) also performed tests on fine grained soils from Adapazarı, Turkey. They used the slurry deposition and in-place wet pluviation methods for reconstituting the samples. When tested at the same void ratio, they found that a soil with $PI=2$ had greater static shear strength and cyclic shear strength than a soil with $PI=10$. In liquefaction resistance evaluation, researchers have recommended liquefaction screening criteria based on liquid limit, fines content (the percentage of particles finer than 5 μm or 2 μm), plasticity index, and w_c/LL and also suggested that there is a significant difference in the cyclic response of fine-grained soils due to minor changes in PI for low plasticity soils. However, Donahue et al. (2007, 2008) concluded, based on their results, that the ratio w_c/LL and the overconsolidation ratio, OCR, are the most significant elements regarding liquefaction potential assessment. For values of $PI < 12$, they found that there is actually small influence of PI on the soil response.

Nevertheless, the two last groups of researchers coincided on avoiding the use of fines content as a determining parameter for establishing whether soils are liquefiable or not.

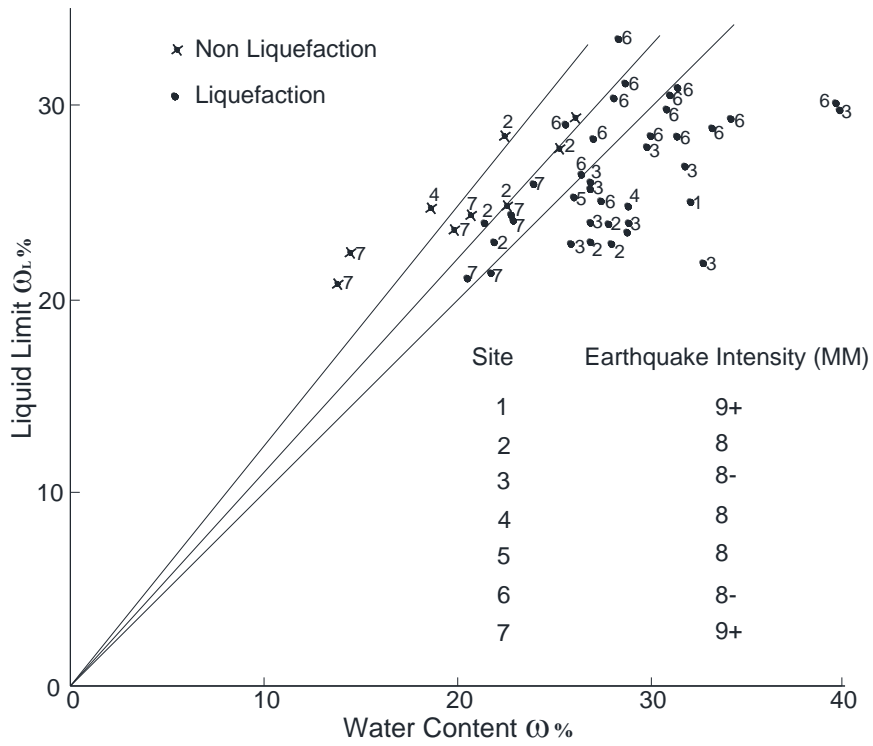
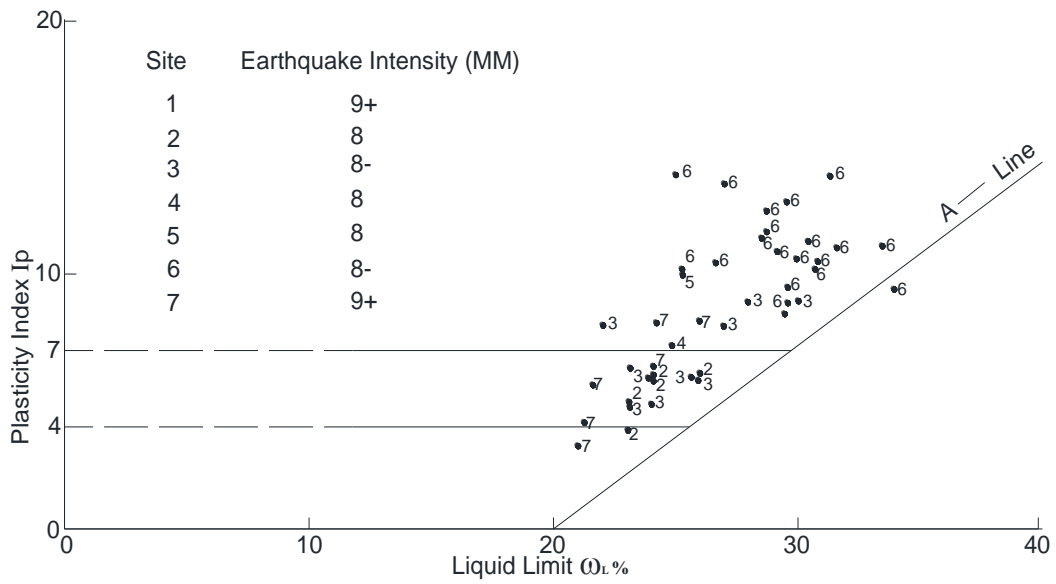


Figure 1.1. Charts for Chinese criteria. From Wang (1979)

Boulanger and Idriss (2006) studied a series of monotonic and cyclic tests on sand, clay, tailing slimes and artificial mixes of silt in order to find out the threshold for soils that would be better evaluated using appropriate procedures for sand or those with behavior similar to clay. They concluded that the clay-like response will be exhibited in soils with $PI \geq 7$ and otherwise soils should be considered as having sand-like behavior.

These criteria for susceptibility have tried to make a clear distinction of the soils that are expected to liquefy, but once those soils have been identified, it is also important to know how the content of non-plastic fines might increase or decrease the liquefaction susceptibility. This work has been undertaken in several studies and is the main focus of the present dissertation.

1.2. Research motivation

Reclamation of soils, mining activities and offshore construction among others have encouraged the study of soils containing large amount of fines content with no plasticity. The study of the undrained behavior of these soils has been of major interest because liquefaction is one of the most expensive hazards.

Given the complexities of evaluating the mechanical characteristics of these soils in the field under controlled and systematic conditions, laboratory studies have been carried out. These requirements imply laboratory studies being carried out having a reference basis; and having different references have led to unalike results. Table 1.1 shows a summary of the research that has been conducted on this topic over the years, where it is noted that divergent effects of fines content have been observed regarding liquefaction resistance of soils. However, there is no distinction in the range of plasticity index of the soils listed.

In Chapter 3, a more detailed explanation of the conditions that led to these conclusions in laboratory testing is provided, including materials, range of fines content, plasticity and parameters used for comparison.

Table 1.1. Literature review on laboratory testing

Researcher	Year	Conclusions
Lee and Fitton	1969	Resistance decreases with fines content
Seed and Idriss	1976	Resistance decreases with fines content
Iwasaki and Tatsuoka	1977	Resistance decreases with fines content
Shen et al.	1977	Resistance decreases with fines content
Ishihara et al.	1980	Resistance decreases with fines content
Ishihara	1985	Resistance decreases with fines content
Troncoso and Verdugo	1985	Resistance decreases with fines content
Thevanayagam	1988	Resistance decreases with fines content
Ishihara	1993	Resistance decreases with fines content
Verdugo and Ishihara	1996	Resistance decreases with fines content
Zlatovic and Ishihara	1997	Resistance decreases with fines content
Lade and Yamamuro	1997	Resistance decreases with fines content
Amini and Qi	2000	Resistance increases with fines content
Polito	2000	Resistance decreases with fines content
Polito and Martin	2001	Resistance decreases and increases
Carraro et al.	2003	Resistance decreases with fines content
Bouckovalas et al.	2003	Resistance decreases and increases
Huang	2003	Resistance decreases and then increases
Nabeshima and Matsui	2003	Resistance decreases with fines content
Xenaki and Athanosopolous	2003	Resistance decreases with fines content
Huang et al.	2004	Resistance decreases with fines content
Papadoulou	2008	Resistance decreases with fines content
Carraro et al.	2009	Resistance decreases with fines content
Cubrinovsky	2010	Resistance decreases with fines content
Ishihara and Lee	2012	Resistance decreases with fines content
Noda and Hyodo	2013	Resistance increases and decreases

As it will be described in Chapter 7, most of the simplified procedures currently used, compute the resistance of soils based on the SPT N-value. These methods apply a correction factor for fines content that, as described in Chapter 2, has sometimes inadequately consider the effect of non-plastic fines on the liquefaction resistance.

In order to understand the real effect of the fines on the liquefaction of sands, it is necessary to relate the laboratory experiments to the methods used for assessing liquefaction resistance for design. This thesis focuses on the need to relate laboratory results to field tests and omit the use of density measures that have led to contradictory results.

1.3. Scope and objectives

The problem of liquefaction potential in silty sand is a controversial issue that has been observed in different earthquake events. Several studies in laboratory testing programs have led to divergent conclusions, particularly when using a density measurement as a parameter of comparison. This thesis tries to find a different approach to understand this issue and to integrate the results that have been found so far. This thesis is also focused on the damage that can be provoked by silty sand deposits under liquefaction.

The main objective of this work is to define the influence of non-plastic fines on the liquefaction resistance of sands. It covers the monotonic and cyclic undrained behavior of loose to medium samples of natural sand with fines varying from 0 to 80%, retrieved from Tokyo Bay after the liquefaction events of 2011.

After conducting monotonic and cyclic shear tests, post-liquefaction behavior was studied. All results gathered were used to investigate the effect of fines on ground deformation.

The aims of this research are, in general terms:

1. Identify the influence of cohesionless fines content on liquefaction potential by finding which parameters should be kept constant for comparison during laboratory testing.
2. Integrate the results obtained with previous research in order to make conclusions compatible with simplified procedures for estimation of liquefaction potential.
3. Find the relation between fines content and shear modulus, through the use of cyclic shear tests. Relate the shear modulus with the strain amplitude and factor of safety for liquefaction resistance to evaluate seismic performance of geotechnical structures
4. Identify the effect of fines on the post-liquefaction behavior.
5. Provide a framework that integrates the studies on fines content and can be also incorporated into the simplified procedures for assessing liquefaction potential.

1.4. Thesis outline

This experimental study is presented in the following structure:

Chapter 2 discusses the liquefaction in silty sand and Tokyo Bay Area sand. It explains the liquefaction events in silty sand around the world and provides a description of the liquefaction events on March 11th, 2011. Moreover, it discusses briefly the physical properties of Tokyo Bay Sand and microscope pictures of different fines contents.

Chapter 3 is about the background on fines content effect on the liquefaction resistance of sands. Field and laboratory research on fines content in previous years is described in detail. The particle packing theory is explained, as well as different measures of density for silty sand. Some discussion on mine tailings is also provided, given the large amount of non-plastic fines contained in these soils.

Chapter 4 describes the experimental program. Methods of sample reconstitution, procedures for sample saturation, consolidation tests and, monotonic and cyclic tests, are described. The hollow cylindrical device used to conduct these experiments is also explained, along with the calculation of stresses and strains. Finally the detailed is the experimental method, including specimen preparation and sample saturation is given, including sample results. Relevant findings of testing silty sand are also provided.

Chapter 5 presents the analysis of experimental results. Both torsional monotonic and cyclic shear tests results are given and explained according to the effects of fines for same energy compaction. Three different heights of fall were used for air pluviation: 5, 30 and 50 cm. The influence of fines content on the coefficient of volume compressibility, m_v , is also showed. Finally, a link between field and laboratory tests is intended, through two different approaches. Results of tests conducted at the same m_v value are given and compared to previous results.

Chapter 6 discusses the deformability analysis and post liquefaction deformation. In this chapter the shear modulus degradation curves measured are given and their utility for deformability analysis is explained. Also the results of post-liquefaction deformation for

silty sand are explained. Modified stress-strain curves are given in order to compare the skeleton curves.

Chapter 7 conciliates the results of the effect of fines influence on the liquefaction and post-liquefaction behavior of sands in previous research and the present dissertation. First the theory of binary packing that can be used to explain the results obtained in this research is explained. Later, the effect of comparing the undrained response of silty sand at different density parameters and the results by other researchers are clarified.

Some other relevant aspects while testing sand with fines content, such as different confining pressures and low plasticity are considered.

Finally, this chapter discusses the integration of the obtained results into the simplified procedures for evaluating liquefaction potential.

Chapter 8 finalizes with the conclusions and recommendations. It provides relevant outcomes and their applications for design as well as suggestions for future studies.

Chapter 2

LIQUEFACTION IN
TOKYO BAY

Chapter 2. LIQUEFACTION IN TOKYO BAY

2.1. Liquefaction in silty soil

Different seismic events around the world caused severe liquefaction-induced damage in silty sands, which have raised the importance of studying the influence of non-plastic fines on the liquefaction resistance.

2.1.1. Liquefaction in the 1989 Loma Prieta Earthquake

On October 17, 1989 a $M_w=6.9$ the San Andreas fault northeast of Santa Cruz, California, ruptured over a length of approximately 45 km. In the San Francisco Bay Area there were hydraulic fills that had 3 to 9 meters of loose, silty sand. Liquefaction-induced damage in building, infrastructure and pipelines was found mostly in the South Market area, Mission Creek and Mission District (Figure 2.1).

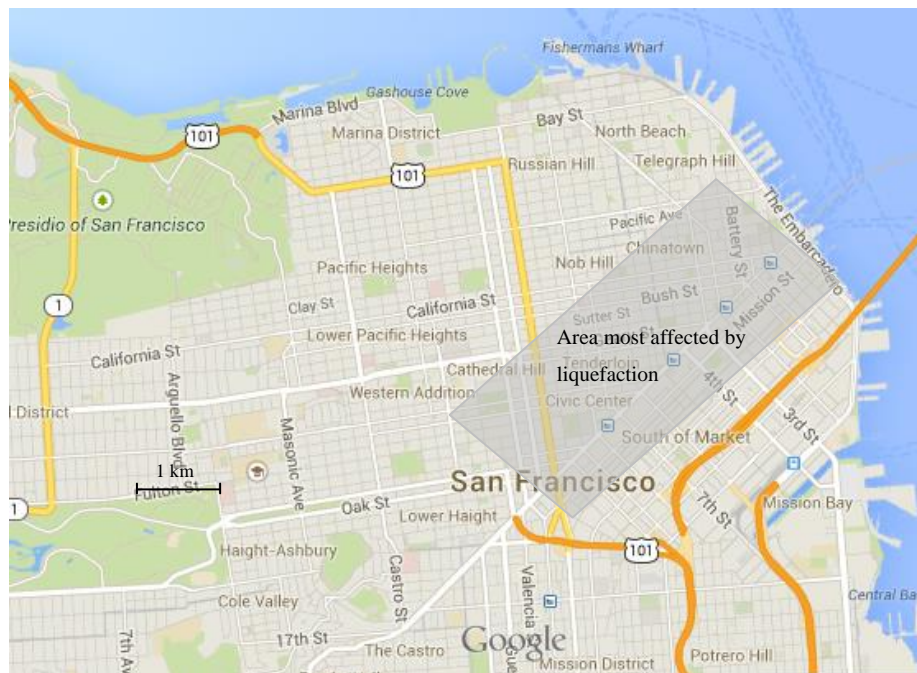


Figure 2.1. San Francisco Bay's areas of liquefaction¹

¹ Google Maps (2014). San Francisco Bay.

One of the most representative proves of liquefaction during the 1989 Loma Prieta Earthquake, was the extreme damage of the Valencia Street Hotel (Figure 2.2). Most of these fills were placed during the 1900s and were composed of sand that was deposited in hydraulic suspension and allowed to settle freely (Holzer 1998). Sand dredged from San Francisco Bay contained fines compared to clean Dune sand that was also present as fill material. It was reported that sand with fines had lower values of density and had more tendency to liquefy than clean sand (Clough et al. 1994).

Rollings and McHood (1998) computed the liquefaction-induced settlement in Marina District and compared it to the measured values. They used a correction for fines adjusting the volumetric-strain curves as pointed out by Seed et al. (1984) instead of modifying the SPT N-value. Their results had a difference to the measured value of about a factor of 2, which led them to conclude that more studies should be done on defining the effect of fines on the correlations.



Figure 2.2. Liquefaction in the Valencia Street Hotel²

² Image taken from http://mceer.buffalo.edu/1906_Earthquake/city_destroyed/city-trembles.asp

2.1.2. 1999 Chi-chi Earthquake, Taiwan

On September 21, 1999 the mountainous village of Chi-Chi was the epicenter of a $M_w=7.6$ earthquake causing extensive liquefaction damage in foundations, embankments, riversides, retaining walls, etc. The counties affected, Yunlin, Zhonghua, Nantou and Taichung, are in Central Taiwan (Figure 2.3) where soils were mostly compressible sands with large amounts of low to medium plastic fines. These soils originated from the process of weathering and abrading of shales, slates and sandstones from the central mountains; at some spots there are layers of very loose sand susceptible to liquefaction, their fines content ranges from 10 to 50% and some of these layers are capped by thick layers of clay material (Juang et al. 2005).

Back analyses performed on the liquefaction potential of the soil showed discrepancies between the results using simplified methods and the actual observed response. For instance, Ni and Fan (2002) evaluated the methods by Seed et al. (1985) and Tokimatsu and Yoshimi (1983) to observe the adequacy of these procedures to be applied on the soil conditions in Central Taiwan. They found that one of the major differences is the correction factor used for fines content, while the factor of safety computed for the liquefied area was similar in both methods for fines content less than 35%. Tokimatsu and Yoshimi's correction for fines caused an overestimation and Seed's, an underestimation for the real correction in their study. Ni and Fan suggested correction of fines for the simplified methods they discussed.

Similarly, Juang et al. (2005) proposed a model based on artificial neural network of limit-state data that resulted in more accuracy for considering more fines than 35%, than the method by Youd and Idriss (2001).



Figure 2.3. Localization of affected areas by the Chi-chi Earthquake³

Figure 2.4 shows a bearing capacity failure caused by liquefaction. The extensive economic loss during this earthquake also enforced the development of new methods for sampling, testing and evaluating the liquefaction potential of sands containing large amounts of fines.



Figure 2.4. Liquefaction-induced tilting in a residential building (from Hung 2012)

³ Google Maps (2014). Central Taiwan.

2.1.3. 2010 and 2011, Christchurch New Zealand

In September 2010, an earthquake of $M_w=7.1$ hit the island of New Zealand, in the southeast side near the city of Christchurch with epicenter in Darfield. Later on February, 2011 a $M_w=6.3$ earthquake close to the Christchurch Central Business District (CBD) caused 181 casualties and extensive damage in buildings, infrastructure and pipelines.



Figure 2.5. Location of Darfield and Christchurch⁴

As seen in Figure 2.5, the City of Christchurch is located on the east coast of New Zealand and it was mainly built on reclaimed swamp. Soils in the area are clean sands around the Avon River, along with loose silts and peat in the southeast part of CBD. Boiled sand along the Avon River contains 5~20 % of silty fines and the fines are low to non-plastic.

Damage in the residential area was extensive in the east and northeast of the Central Business District, where soils are mostly clean fine sands with non-plastic silts. More than 15,000 residential properties/buildings were affected particularly due to lateral spreading and differential settlement. Cubrinovski et al. (2011) performed spectral analysis of surface waves (SASW) and dynamic cone penetrometer (DCP) tests to calculate the cyclic resistance ratio for a $M_w=7.5$ event. Figure 2.6 shows the comparison they made for cyclic

⁴ Google Maps (2014). Christchurch

resistance ratio in Darfield and Christchurch for a site with FC=12%. It was observed that estimated values for clean sand showed a satisfactory comparison with measured values. Some other remarkable characteristics in these events are the cumulative effects of these strong earthquakes and repeated liquefaction.

The evaluation of the liquefaction potential of these soils is of major interest in the prevention of future damage in the City. Some studies have been conducted on the effect of fines content in the sandy soils of the surroundings in this area, finding a more contractive behavior with the addition of fines when density measures as void ratio or relative density are used (e.g., Arefi 2013; Rees 2010).

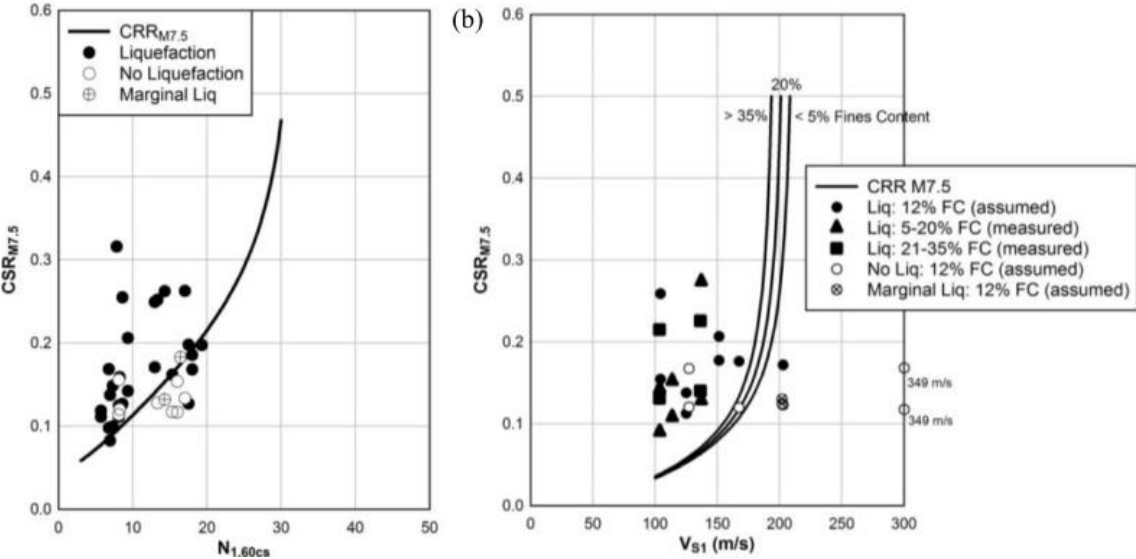


Figure 2.6. Comparison of CSR for Darfield and Christchurch Earthquakes with CRR for FC=9%. From Cubrinovski et al. (2011)

2.2. Liquefaction in Tokyo Bay

On March 11, 2011 a $M_w=9.0$ stroke the east coast of Japan, triggering a tsunami and several impacts. This event, one of the five most powerful earthquakes in the world since 1900, was followed by two aftershocks inducing additional damage of $M_w=7.4$ and $M_w=7.7$,

15 and 30 minutes after the first event. Figure 2.7 shows the epicenter of the earthquake and the affected zones, according to the intensity.

Severe liquefaction-induced damage was observed in Tokyo Bay, where reclamation of the coastline started around 1600, from Sumida to Yokohama and expanded to Kanagawa and Chiba Prefectures around the 50's. These areas were affected before by other seismic events. On December 17, 1987 a $M_w=6.7$ Earthquake hit eastern Chiba Prefecture (Chibaken Toho-oki Earthquake) causing liquefaction in many areas of the city, including Kairaku 1-chome, Mihama 3-chome and Irifune 4-chome. Therefore, some zones that experienced liquefaction in 1987 liquefied again.

On March 2011, boiled sand was observed in the reclaimed cities of Urayasu, Ichikawa, Narashino, Odaiba, Shinonome, Tatsumi, Toyosu, Seishin, Yokohama, Kawasaki, Kizarasu and Chiba (Yasuda et al. 2012). However, the most devastating effects were found on lands reclaimed after the 70's where differential settlement and lateral displacement affected private houses, roads, sea walls, pipelines and other structures. Amid those areas, Urayasu City was the most affected, where more than 9,000 private properties had detriment.

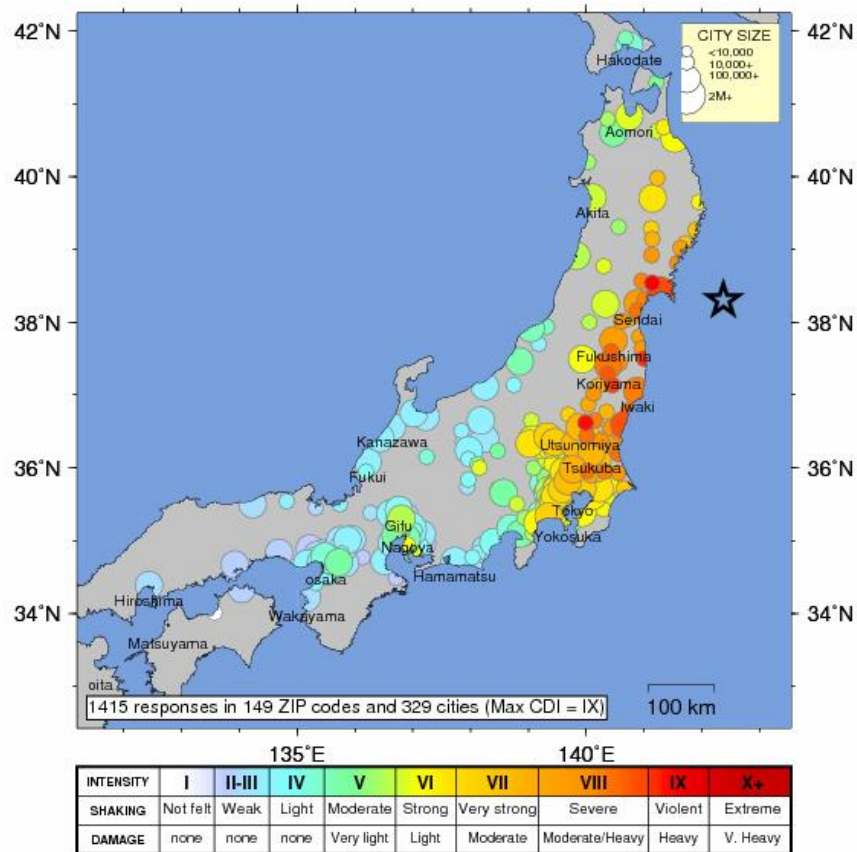


Figure 2.7. Intensity map⁵

2.2.1. Liquefaction in Urayasu City

Urayasu City is a man-made peninsula that has been grown through the years until having an extension of 17.29 km². It is divided into three parts, according to the period when they were reclaimed. The first is Motomachi mostly natural alluvium, later from 1968 to 1975 more land was added and was designated as Nakamachi. Finally Shinmachi was constructed from 1978 to 1980. Figure 2.8 shows the location of Urayasu City and the division into sectors (A, B, C, D, E, F) that suffered different extents of damage.

The sand used for reclamation is the same as the seabed of the original city. Regarding the grain size distribution, boiled sand contained 15 to 70% of fines content; these fines are non-plastic and correspond to the composition of the sand layer in reclaimed land up to

⁵ USGS Community Internet Intensity Map, 2011

10 m below the sea level (Figure 2.9). After analyzing the several cases of liquefaction it could be concluded that the dissimilitude in reclamation materials and method of reclamation has an effect on the liquefaction potential and extent of damage (Ishihara 2011).

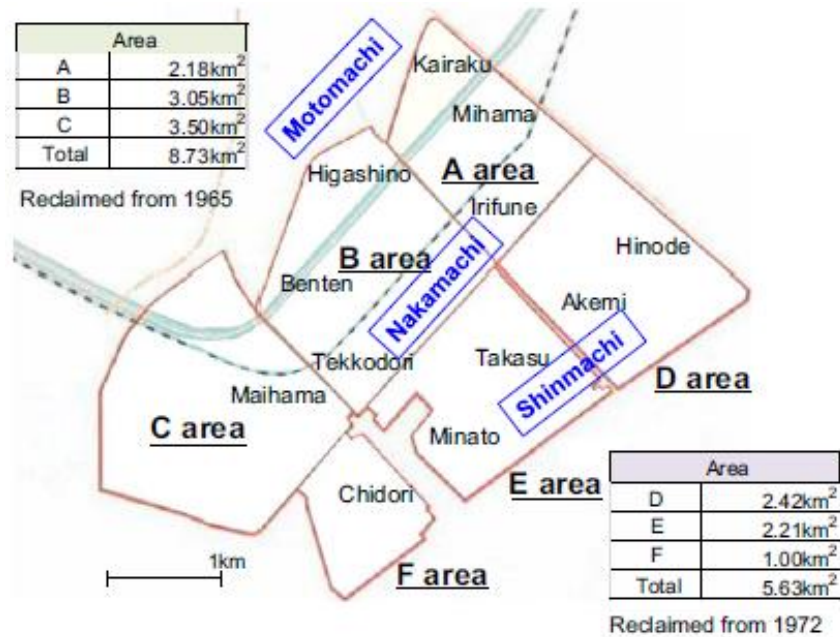


Figure 2.8. Map of Urayasu City (From Yasuda et al. 2012)



Figure 2.9. Boiled sand in Urayasu City

One year after the liquefaction events of 2011, a field trip was conducted to report on the damage that could still be observed in the City.

Figure 2.10 illustrates some of the countermeasures taken for differential settlements in the structures in the City.



Figure 2.10. Differential settlement observed around the City

Figure 2.11 shows deformation in Urayasu Station. In Figure 2.12 liquefaction in the streets of Urayasu City can be observed. Figure 2.13 shows houses affected by tilting, which was the most significant problem in the private properties of the City. Figure 2.14 presents the conditions at the port areas, where bearers were placed at the border. In Figure 2.15 some of the manholes that floated can be seen, even one year after the earthquake. The damage in pipelines and manholes due to liquefaction, as well as countermeasures, has also been addressed by different researchers (e.g., Ishihara 2011; Towhata et al. 2012)



Figure 2.11. Damage observed around the metro station



Figure 2.12. Liquefaction on the streets



Figure 2.13. Tilting of houses



Figure 2.14. Liquefaction in the harbor area



Figure 2.15. Floating of manholes

Table 2.1 is a compilation of the estimated and measured subsidence at different sites of the city reported by the Government of the City. It can be seen that at some places the actual subsidence exceeded the estimated values of settlement, especially for larger fines content.

Table 2.1. Relationship between the amount of subsidence. Subsidence measured and estimated amount

Location	Calculated settlement [m]									Measured settlement [m]		
	FC=15			FC=25			FC=35			Max.	Av.	Min.
	Max.	Av.	Min.	Max.	Av.	Min.	Max.	Av.	Min.			
Urayasu Station	19	9	3	14	6	2	11	5	2	0	0	0
Maihama	30	25	18	22	18	13	17	14	10	-	-	-
Tomiooka	22	18	17	16	13	12	13	10	9	30	26	15
Imagawa	30	23	16	22	16	11	18	12	9	50	22	5
Mifune, Infune	36	32	4	26	23	3	21	18	2	45	19	7
Minato	41	26	17	31	19	13	25	15	10	60	22	5
Takasu	49	38	9	37	28	7	30	23	5	50	23	2
Akemi, Hinode (Northwest)	56	44	45	43	33	32	35	27	27	65	32	3
Akemi, Hinode (Southwest)	23	17	15	19	11	11	15	9	9	15	8	2

It is important to remark, that Japanese standards for calculation of settlement assume that shear strain is equal to volumetric strain which is an inaccurate hypothesis, therefore estimations made by this procedure should be carefully considered.

The following figures show the relations between fines content and SPT N-value. Bs stands for the fill material, As is the alluvial layer and Fs refers to reclaimed soil. Data for FC>80%, FC<5% were excluded. FC was considered to be 5 when N₁=20. Figure 2.16 shows the relation between fines content and the corrected SPT N-value for the fill layer.

Figure 2.18 shows the relation for SPT N-value and fines content for the layer As of alluvial soils. Figure 2.18 exhibits the relation between fines content and N₁ for the dragged soils, Fs.

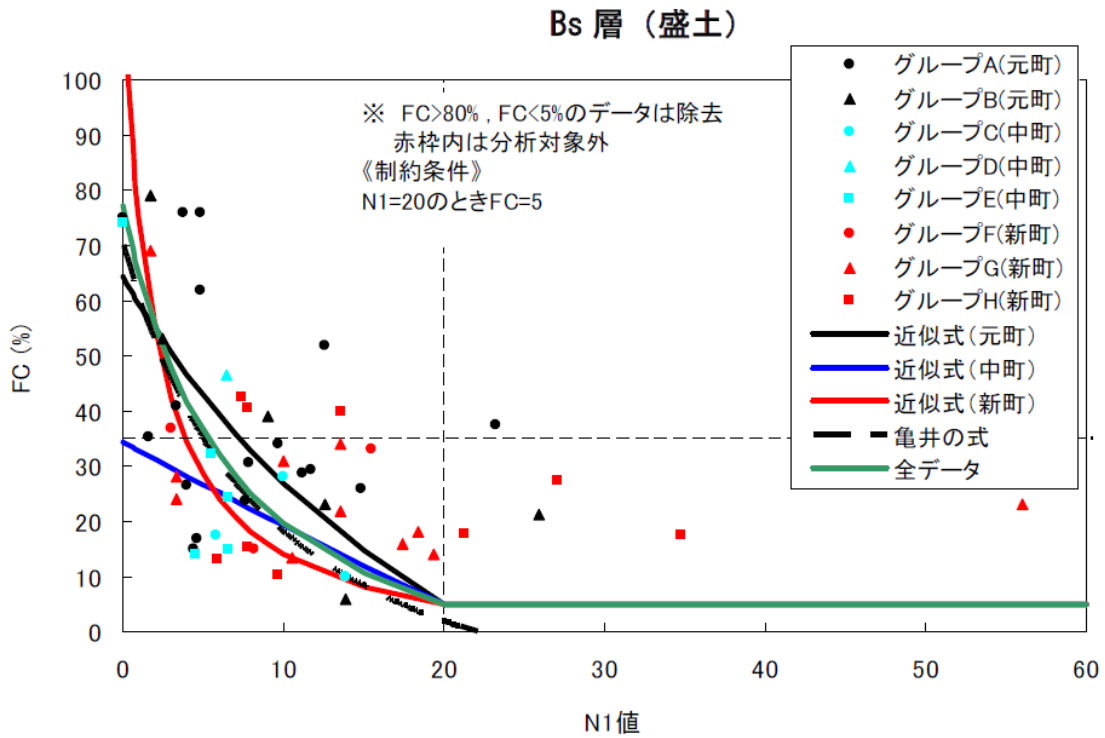


Figure 2.16. Bs – FC vs N1 (Urayasu City Council, 2012)

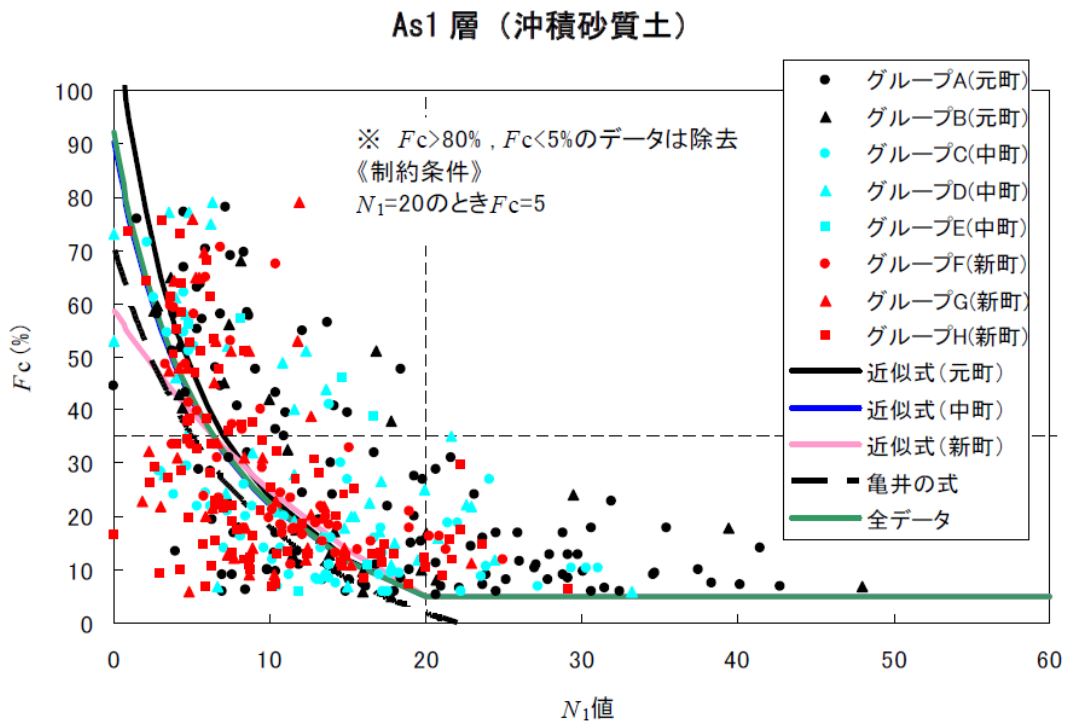


Figure 2.17. As – FC vs N1 (Urayasu City Council, 2012)

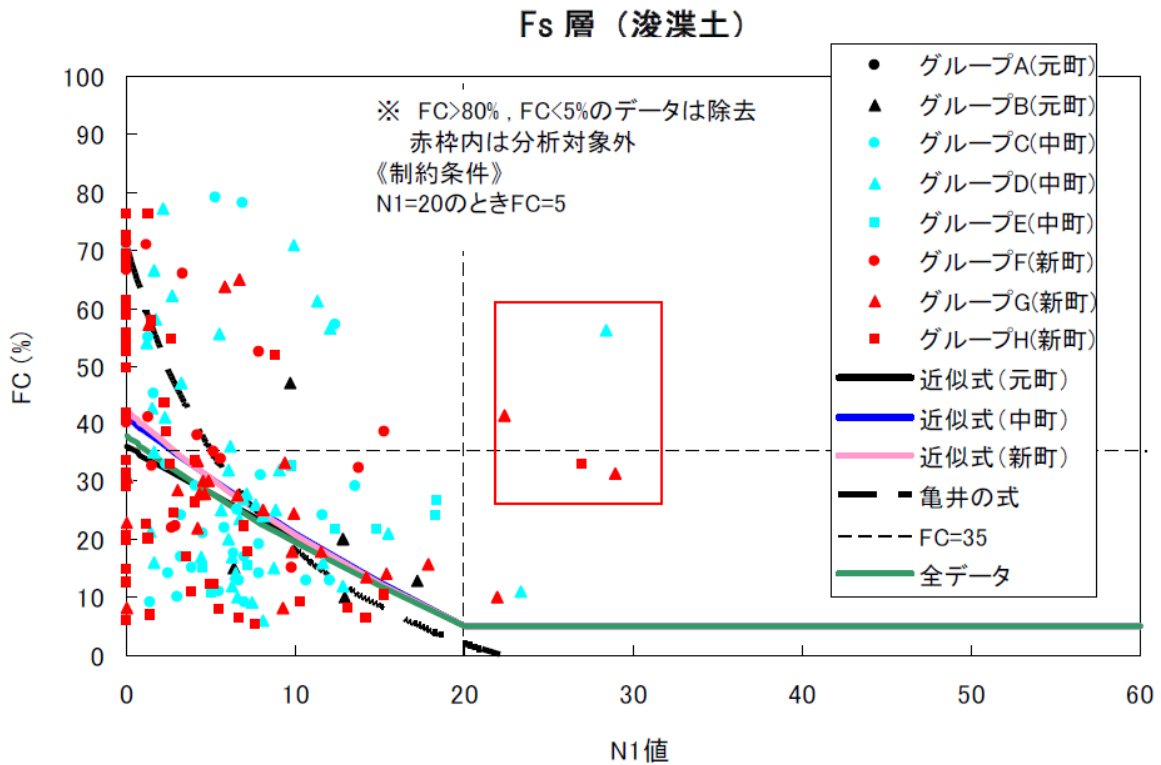


Figure 2.18. Fs – FC vs N1 (Urayasu City Council, 2012)

Figure 2.19 shows the trendiness of fines content and SPT N1-value for the different strata presented in the previous figures. Figure 2.20 shows the data points of FC and N1-value for different zones of Urayasu City in the Fs soil. It can be observed that Nakamachi and Shinmachi exhibit low values of SPT N for all fines contents, given that most of these soils were deposited relatively recently, compared to the soils of the original part of the City, Motomachi.

This difference is mostly attributed to ageing effects. For instance Towhata et al. (2012) did a study on the effect of ageing on the factor of safety of reclaimed land since 1867. Kokusho et al. (2012) performed miniature cone tests with different cement contents to simulate longer geological age and found that these specimens had greater resistance.

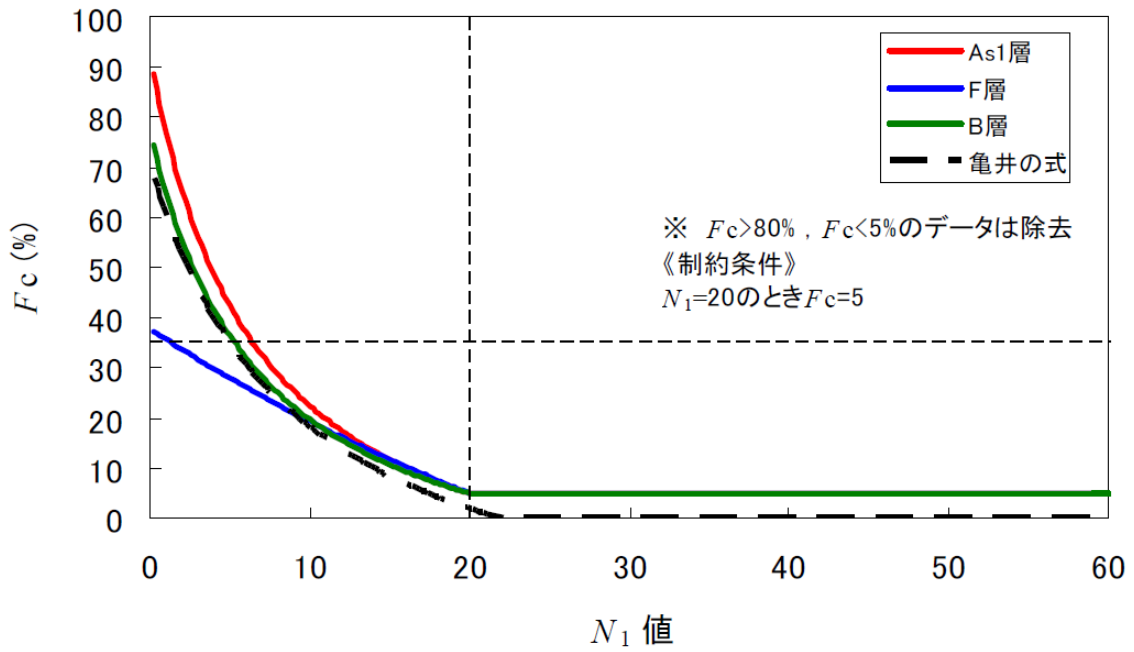


Figure 2.19. Variation of fines content and SPT- N_1 for different kind of soils (Urayasu City Council, 2012)

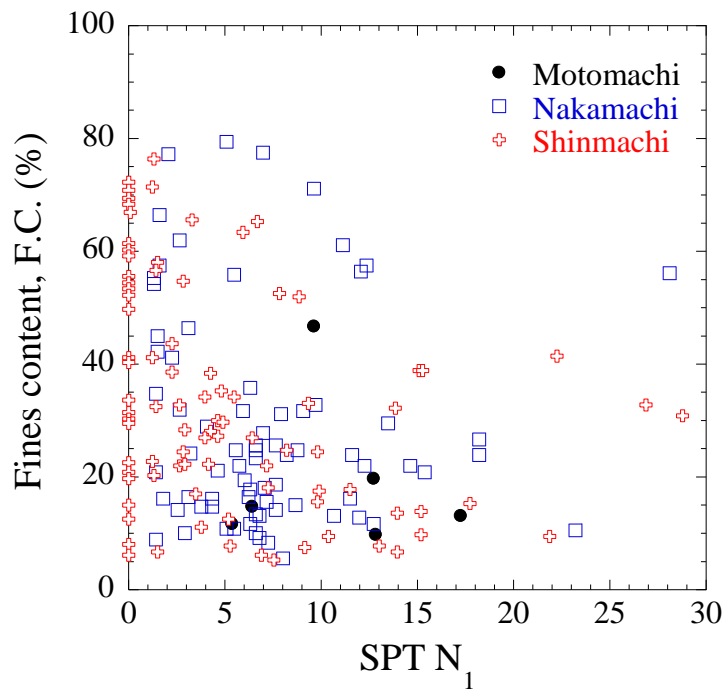


Figure 2.20. Variation of FC and SPT- N_1 value in Urayasu City (Urayasu City Council, 2012)

The large amount of fines of Tokyo Bay sand will have a significant influence on the evaluation of settlement and lateral displacement caused by liquefaction. Considering these data, the importance of knowing the effect of fines content on the liquefaction potential of soils is remarked.

2.3. Characteristics of Tokyo Bay sand

Boiled sand from Urayasu City was collected in 2011 and used for these experiments. Tokyo Bay sand is a non-plastic silty sand, with high fines content. Figure 2.21 shows the appearance of sand in its natural angle of repose.



Figure 2.21. Tokyo Bay sand

2.3.1. Index tests

Tokyo Bay sand is a gray sand with a density of solids $G_s=2.69 \text{ Mg/m}^3$. A grain sieve analysis was conducted to identify the percentage of size distribution in sand. It was found that this sand has a fines content of 32% and its grain diameter corresponding to 60% passing is $D_{60}=0.12 \text{ mm}$ (Figure 2.22).

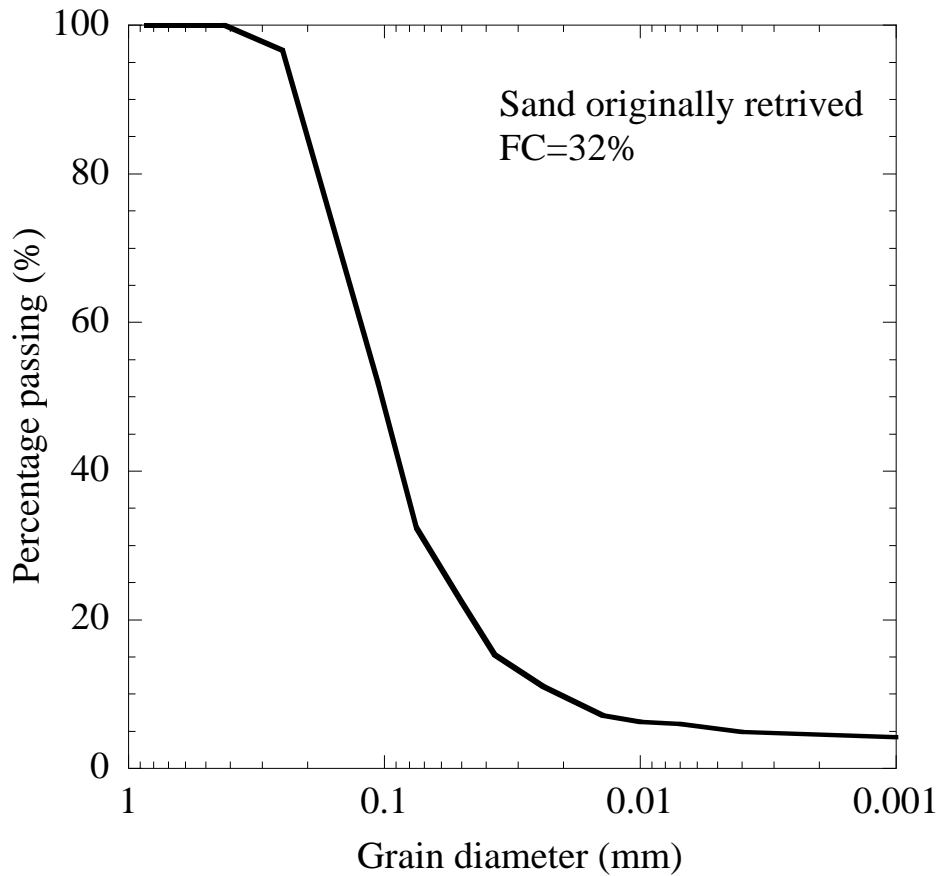


Figure 2.22. Gradation of Tokyo Bay sand as retrieved from the site

Grain size diameter of the sand and fines used for the experimental program in this thesis is shown in Figure 2.23.

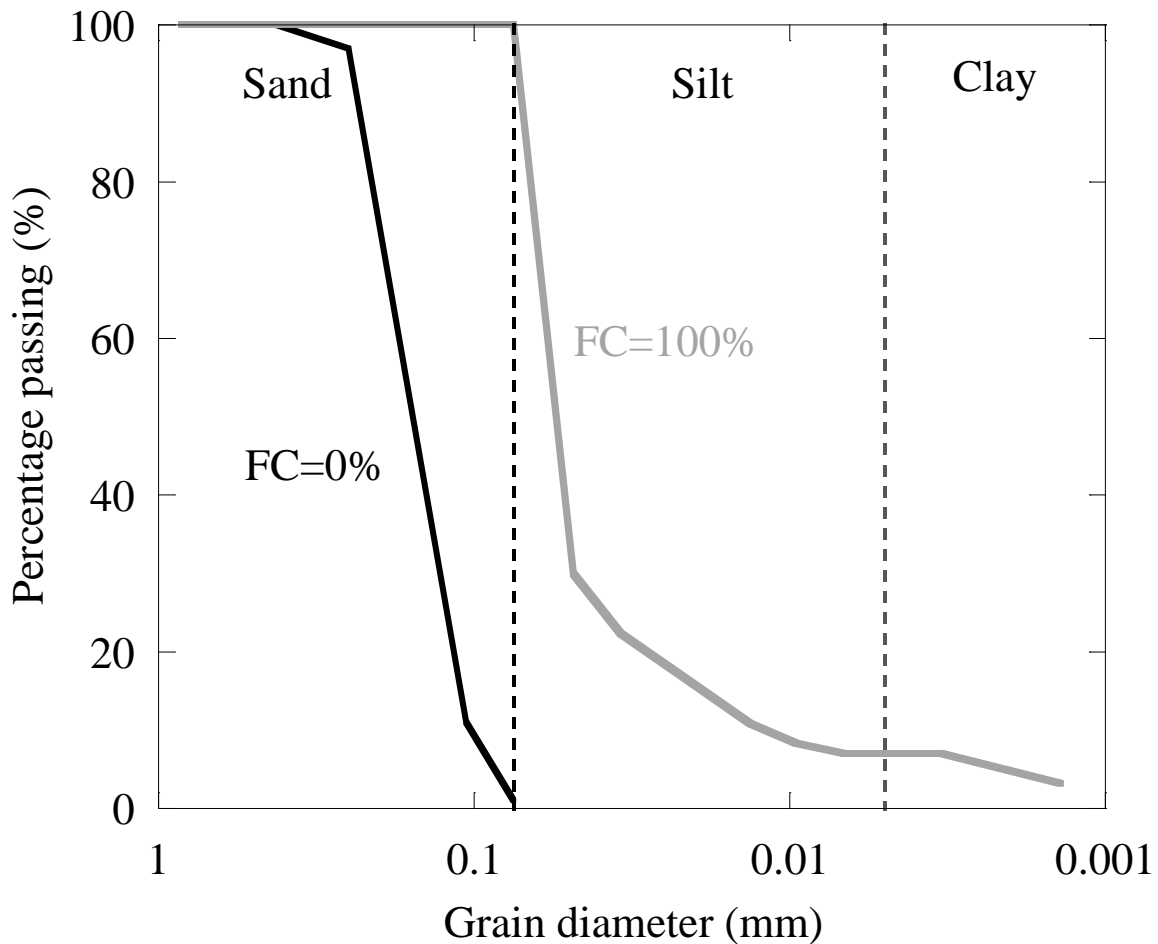


Figure 2.23. Grain size distribution for different fines content

In order to calculate plasticity index, liquid limit was determined by the Casagrande device and by the fall-cone test, conducted by the Japanese Geotechnical Society (JGS) standards.

The liquid limit shown in Figure 2.24 is $LL=41.33\%$; it was determined by using the standard brass cup and finding the water content for 25 blows.

This procedure is very commonly used; however it has different downsides, being the first one the effect of the operator of the cup on the number of blows. In this regard, it was important to verify the value of liquid limit with an alternative procedure in order to ensure the validity of the results.

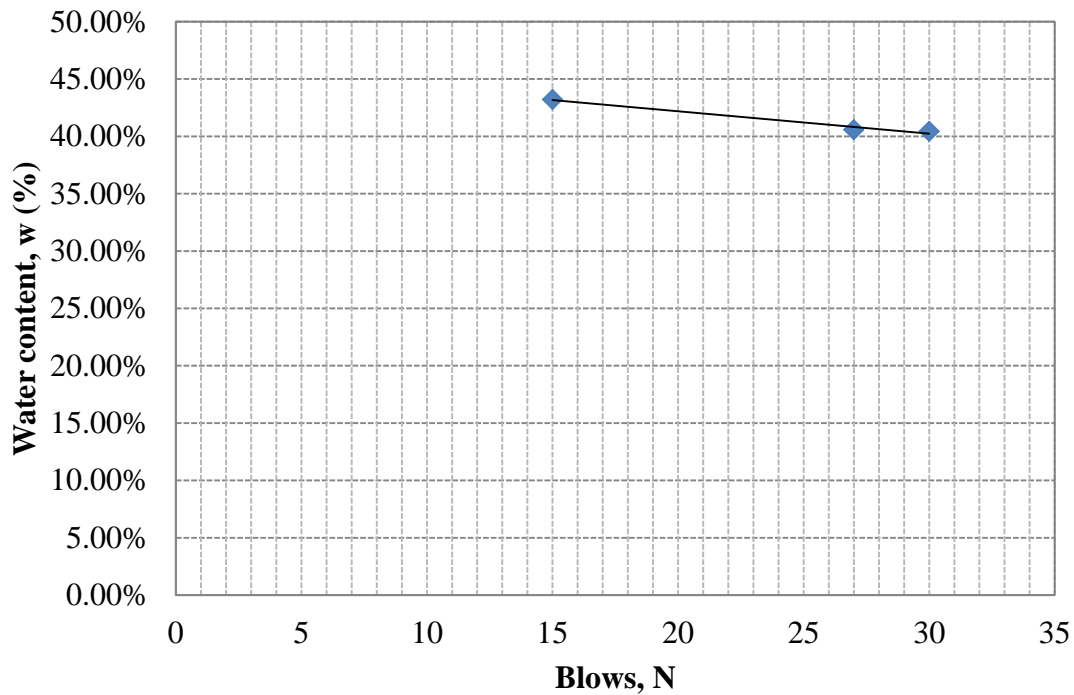


Figure 2.24. Liquid limit by the Casagrande device

Consequently, the liquid limit was also evaluated using the method of the fall-cone device, where the liquid limit is determined as the water content when the cone is released for 5 seconds and penetrates the soil 11.5 mm. This method has the advantage of not being so influenced by the operator, since a button releases the cone that penetrates the cup filled with soil. The button is released only for 5 seconds and the device allows for measuring the penetration distance every time. There are other versions of this test, such as the Swedish cone or the English cone, where the penetration for the liquid limit is 10 and 20 mm, respectively.

As in the Casagrande device, several water contents are aimed in order to define a curve that can be used to interpolate the value. In Figure 2.25, the liquid limit was found to be $LL=40.78\%$.

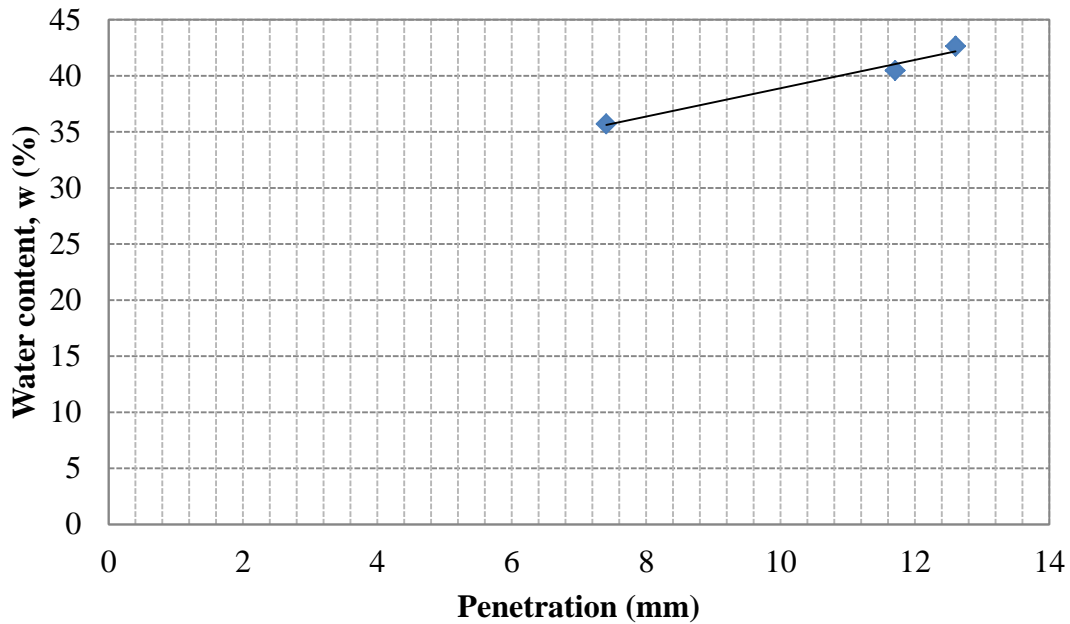


Figure 2.25. Liquid limit by the fall-cone test

Plastic limit was determined rolling out a thread until it breaks at a diameter of 3.2 mm. Six different rolls were made and the plastic limit was considered to be the average of the water contents obtained. Plastic limit is $PL=40.51\%$.

Plasticity index, PI, was calculated as:

$$PI = LL - PL$$

Two values were obtained, $PI=0.82$ and $PI=0.28$. With this result, it is evident that fines from Tokyo Bay sand can be regarded as non-plastic.

For determining the relative density of each sample, minimum and maximum void ratio tests were carried out following Japanese Standards. Considering the large amount of fines and its variability throughout the city, several samples with different fines content from 0 to 80% were prepared. Results are shown in Figure 2.26. It is observed that the curves have a V-shaped form, having the minimum value between $FC=20$ and 30% for e_{max} and between $FC=30$ and 40% for e_{min} .

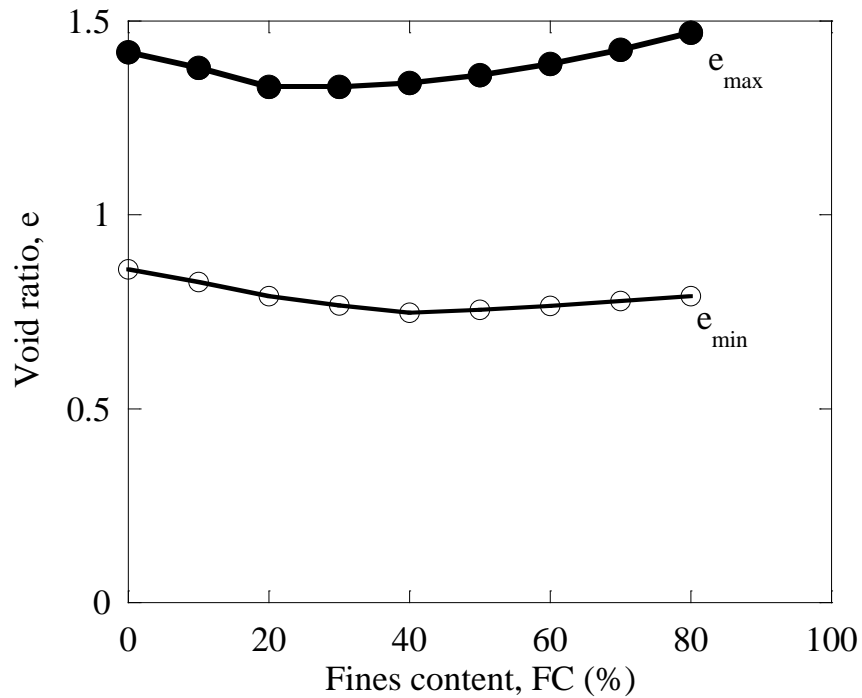


Figure 2.26. Minimum and maximum void ratios

2.3.2. Microscope pictures

Initially three samples of pure sand were mixed with fines of 0, 30 and 80% to observe the microscopic distribution of sand and silt particles. Figure 2.27 shows the variation in shape and size as the fines content increases. Sand particles appear to be sub rounded while silt particles seem to be mostly sub angular.

Images include different colors given that both laser and regular pictures are combined in the same figure. However, in the following pictures, the laser image is removed to observe the colors of the sand and the fines.

These pictures are relevant because the arrangement of the particles and voids is observed, and the complexity of the contacts that can be generated such as: sand-to-sand, sand-to-fine, sand-to-fine-to sand, fine-to-sand, etc. As it will be explained later, the method of reconstitution and the density have also a large impact on the fabric created in the specimen and thus, on the liquefaction resistance/

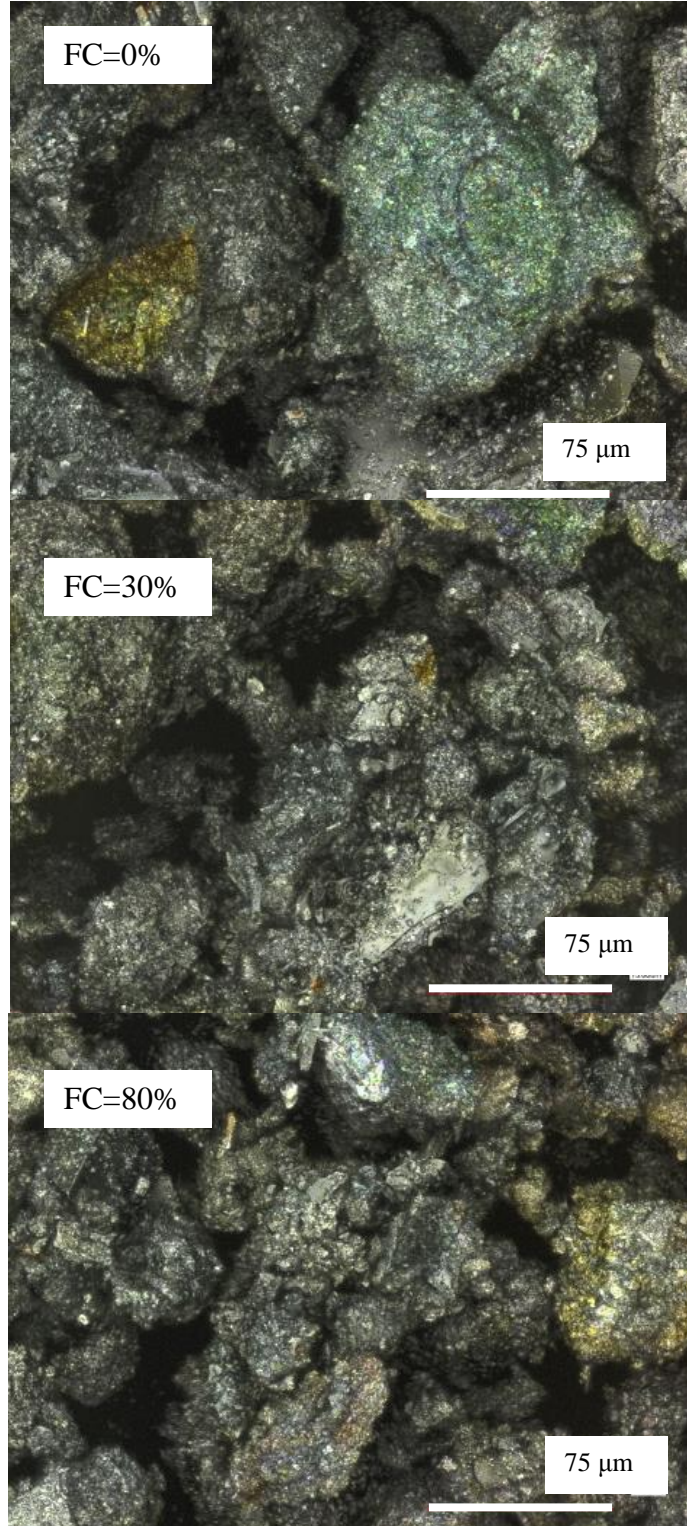


Figure 2.27. (a) 0% fines content; (b) 30% fines content and (c) 100% fines content

Later different microscope pictures were taken for 4 fines content that were thought to be more representative of the microstructure: 0, 30, 50 and 100%. Figure 2.28 shows the pictures of the samples formed. It is observed that the particles in clean sand (0%) are angular and the voids in the sand matrix are easily seen.

For the sample with 30% fines content, there is a mix between the large particles and the fines, it can be seen that this structure seems to be rather unstable regarding the contacts fine-void-grain.

Samples with 50 and 100% show similarities. In the 50% sample large particles can still be observed but the contacts among coarse particles reduced as those compared to the 30% sample.

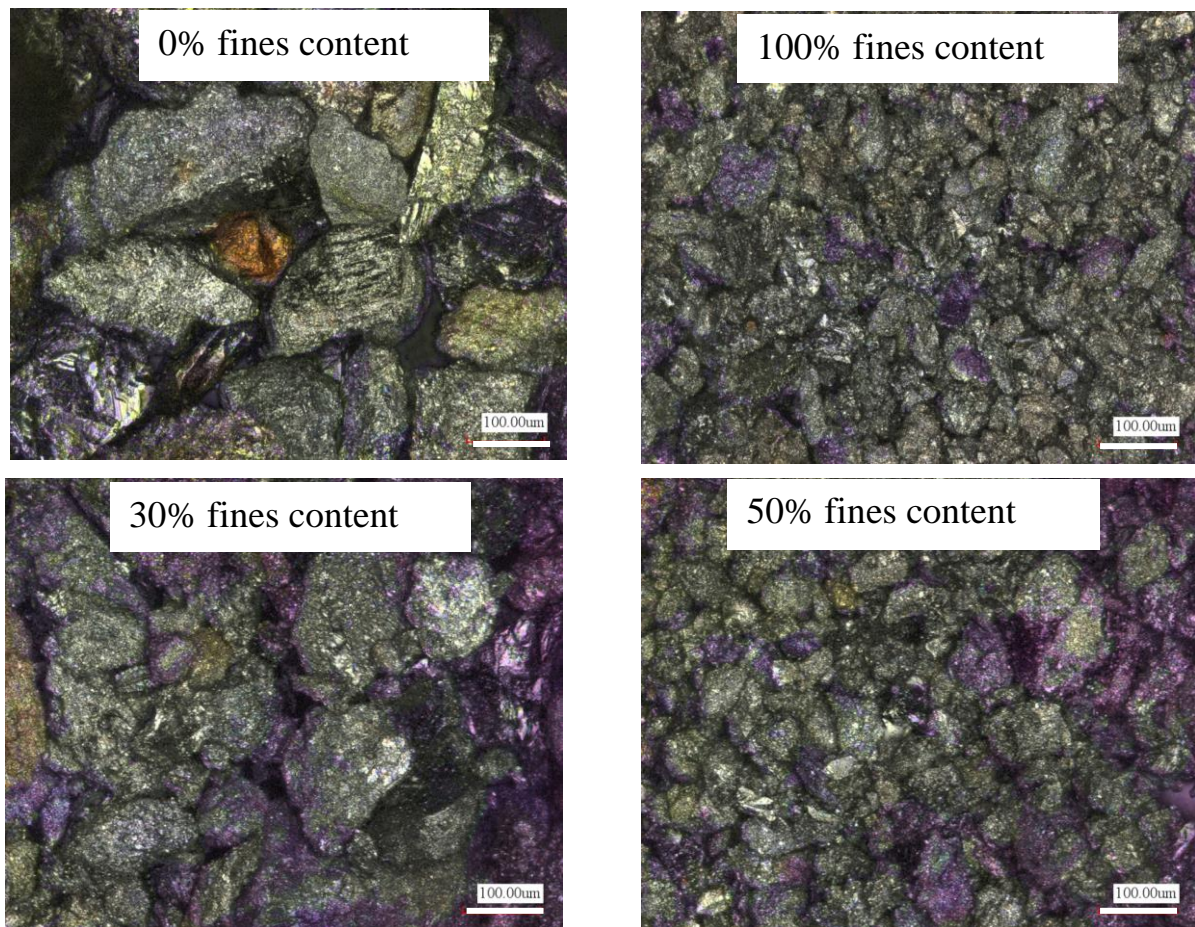


Figure 2.28. Microscope pictures

Colored microscope pictures are shown from Figure 2.29 to Figure 2.32, from 0 to 100% fines content. In these pictures the nature of the grains can be observed in more detail. It is observed that the color of the



Figure 2.29. Colored microscope picture. FC=0%

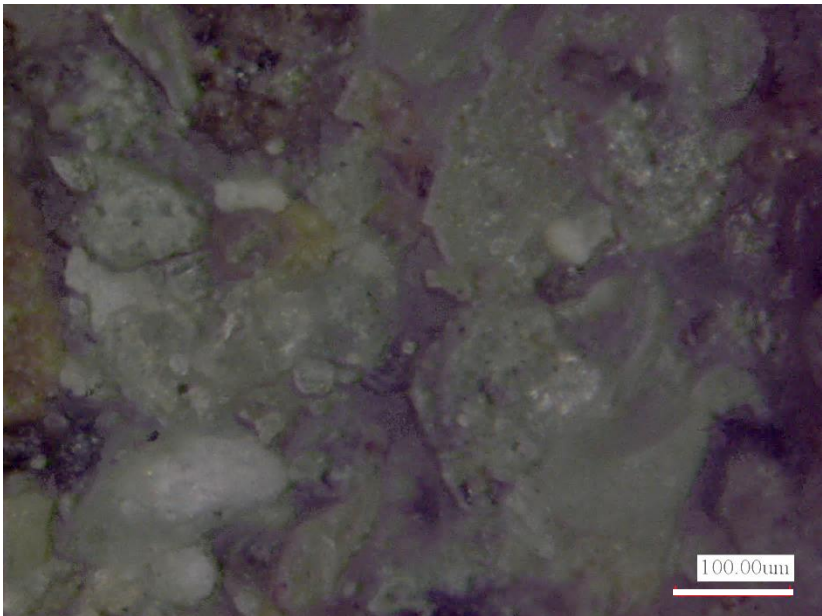


Figure 2.30. Colored microscope picture. FC=30%

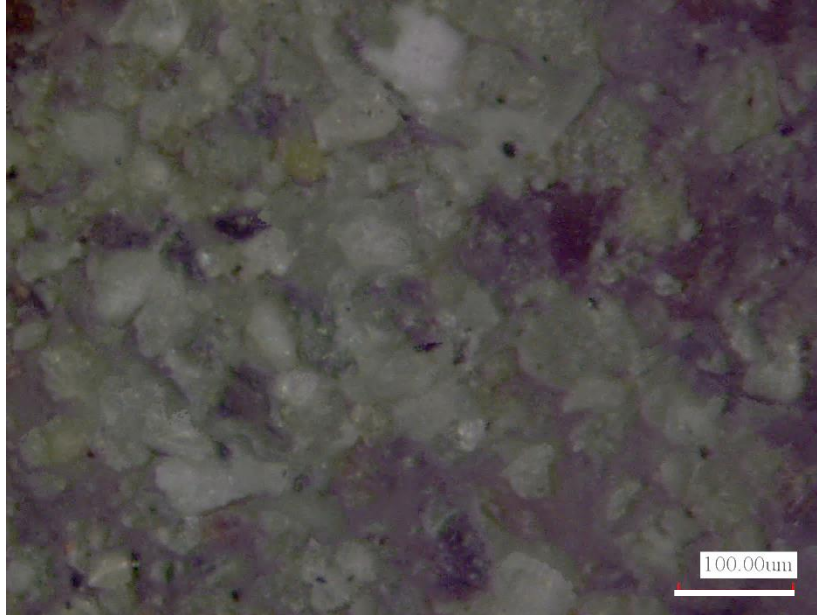


Figure 2.31. Colored microscope picture. FC=50%

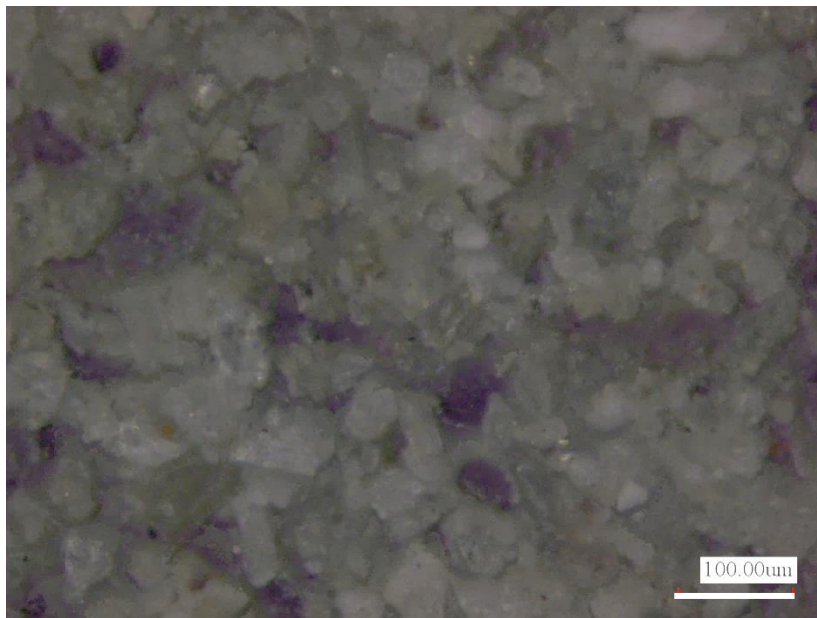


Figure 2.32. Colored microscope picture. FC=100%

Chapter 3

LIQUEFACTION OF SILTY
SAND

Chapter 3. LIQUEFACTION OF SILTY SAND

3.1. Previous research on liquefaction potential of silty soils

The presence of fines during liquefaction has caused divergent conclusions regarding its effects. While field test data of sites with fines has been added in charts for design (e.g., Seed et al. 1984; Robertson & Campanella 1985) there is no clear differentiation between plastic and non-plastic fines.

Wang (1979) defined a criterion for evaluation of silty soil. From gathered data, he stated that any soil, with less than 15 to 20% of clay particles (less than 0.005 mm of diameter), $PI > 3$, and $w > 0.9w_L$, is susceptible to liquefaction. Tokimatsu and Yoshimi (1983) gathered the data in Figure 3.1 from liquefied soils. It can be observed that the normalized value of SPT N , N_1 , decreases with fines content.

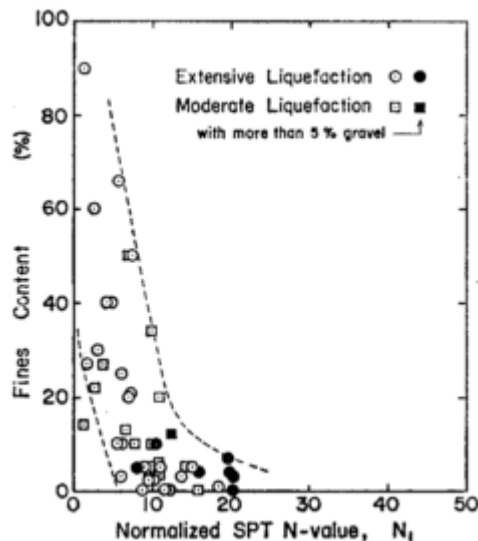


Figure 3.1. Relation between fines content and N_1 . From Tokimatsu and Yoshimi (1983)

Later Seed et al. (1983) compiled data of silty sand from liquefied sites and added them to a chart of cyclic stress ratio and modified penetration resistance. They concluded that the boundary between liquefiable and non-liquefiable soils is significantly higher for silty sands than that for clean sands.

Robertson and Campanella (1985) in their studies on cone penetration tests, proposed the chart in Figure 3.2, where it can be observed that silty sands and silts cause a decrease in penetration resistance. According to this, soils with fines at the same penetration resistance have greater liquefaction resistance than clean sand.

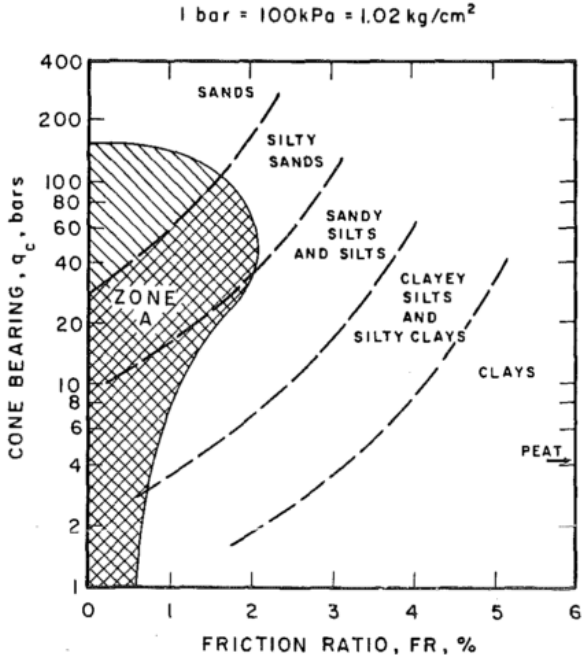


Figure 3.2. Soil classification chart for electric cone. From Robertson and Campanella (1985)

3.2. Previous laboratory research on liquefaction of non-plastic silty sand

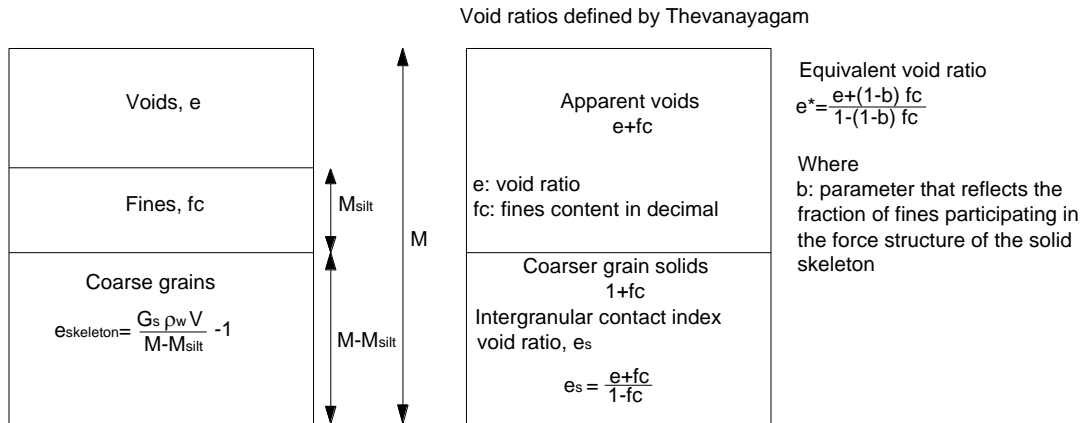
Given the advantages of testing soil in controlled environments, laboratory testing has been a very recurrent choice when dealing with the influence of fines on the undrained behavior of sands. While testing it becomes necessary to keep one parameter constant to observe the effect of the variation of others. Some of the most common parameters to keep constant during comparison are overall void ratio or simply void ratio, e , and relative density, D_r , which are good measures of particle contact. When testing clean sand it is easy to compare results while keeping constant both of them, which has made these parameters quite useful and widespread. For that reason, in experiments with silty sand, most researchers have employed them. However, there are different issues when testing sand containing fines

which have encourage researchers to not only understand the limitations of void ratio and relative density, but also to develop different parameters for comparison, as explained in the following section.

3.2.1. Other parameters of comparison

Although gradation and mineralogy of sand as well as the amount of fines tested are key factors, the difference in the results obtained by several researchers might be explained by considering the concept of void ratio. While sand has no fines, voids are only occupied by water (in a saturated soil) and void ratio is an index of particle contact and force transmission. As a small amount of fines is added to the sand matrix, voids are occupied by water and fines, reducing global void ratio although there is no contribution of the fines to the intergranular force transmission. If fines content increases, it reaches a threshold point B (Figure 3.6) when fines fill all the voids. From such point, fines start influencing gradually the mechanical behavior, until sand grains are fully surrounded by them and do not make contact with each other anymore; then the force is totally supported by fines. It can be deduced that the concept of void ratio as an index of particle contact is not valid after the threshold point. In this regard, variations of void ratio have been used to be representative of the behavior of silty sand, such as the intergranular contact index void ratio (Thevanayagam 1998) and the equivalent void ratio (Thevanayagam et al. 2002) both shown in Figure 3.3. These parameters seem to solve the disjunctives concerning real particle contact. However, there are still uncertainties regarding the values that must be used when fines content is very high or regarding the parameter that reflects the fraction of fines participating in the force structure of the solid skeleton (b). Some researchers as Rahman and Lo (2008) have shown formulas for estimating b but they require different assumptions and an iterative process.

Nevertheless, since it is important to be able to compare soils with different fines content at their natural state in ground, in this paper another standpoint is taken.



M: mass
 M_{silt} : mass of silt
 G_s : specific density
 V: volume
 ρ_w : density of water

Figure 3.3. Definition of sand skeleton void ratio, intergranular contact index void ratio and equivalent void ratio

Another parameter used to represent an index of active contacts for large fines contents is the inter-fine void ratio, e_f , which disregard the influence of sand grains (Thevanayagam 2000):

$$e_f = \frac{e}{FC}$$

Baki et al. (2012) conducted tests on Sydney sand and a mixture of fines from Majura River and kaolin. They focused on the concept of equivalent void ratio and used it to redefine the state parameter, ψ , proposed by Been and Jefferies (1985) as the equivalent granular state parameter:

$$\psi^* = e^* - e_{ss}^*$$

This parameter is the distance from the initial equivalent void ratio to the void ratio on the equivalent granular steady state line (Figure 3.4a), which is also a redefinition of the steady state line (Figure 3.4b).

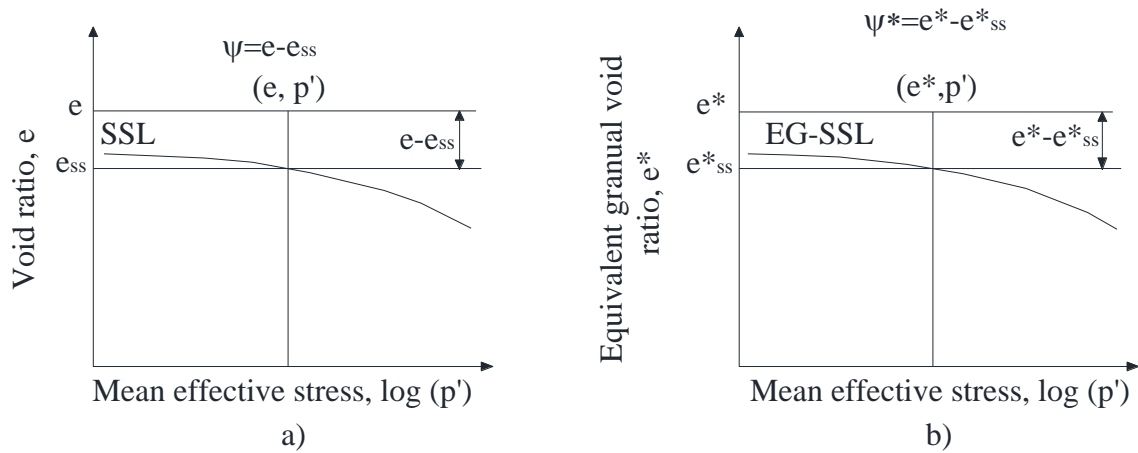


Figure 3.4. Definition of state parameter and equivalent granular state parameter (After Baki et al., 2012)

When studying the monotonic and cyclic behavior of sand with fines, they found that if the tests are run at the same equivalent granular state parameter, there are no effects of fines content or initial void ratio.

3.2.2. Results of different researchers in laboratory testing

The use of density measures for comparison has made the laboratory research on liquefaction of silty sand ambiguous, given the restrictions of each parameter and the impossibility to keep them all constant at the same time.

Lee and Fitton (1969) performed tests on alluvial sand and gravel deposits at El Monte, Los Angeles, California. Grain particles were composed of quartz, feldspar and dark minerals; fines varied from 0 to 90%, the fines being a mixture of silt and clay. Samples were isotropically consolidated to 15 psi (100 kPa) and pulsating loading triaxial tests were conducted at relative densities of 50 and 75%. They found that very fine sands and silty sands showed the weakest response.

Iwasaki and Tatsuoka (1977) performed tests with a resonant column apparatus with a hollow cylindrical specimen of sands with different gradations and fines content from 0 to

33%. While keeping constant void ratio, it was seen that sands other than clean sands had smaller shear moduli.

Shen et al. (1977) conducted one of the first researches carried out on the effect of fines in the liquefaction potential. In their tests, they used a triaxial machine that allows for cone penetration tests on specimens with the same stress conditions as those of the static and cyclic triaxial tests. They used Ottawa sand and clayey silt with $PI=11$ and observed that, at the same sand skeleton void ratio, fines increase the liquefaction resistance.

These primal experiments on sand with fines provided some insight on the expected influence of fines, according to the parameter used for comparison for further research. For instance, when keeping constant void ratio it has been found that liquefaction resistance decreases as fines rise (e.g., Amini & Qi, 2000; Polito & Martin, 2001; Huang et al., 2004; Belkhatir et al., 2010). If relative density is held constant used for comparison, liquefaction resistance grows with the addition of fines (e.g., Polito & Martin, 2001; Carraro et al. 2003; Carraro et al., 2009; Belkhatir et al., 2010). Some researchers as Kuerbis (1989) found the sand skeleton void ratio, which assumes that the volume occupied by fines is part of the volume of voids, to be a more appropriate parameter because it seemed to be independent of fines content; yet, Polito & Martin (2001) identified a growth in liquefaction resistance with fines content for Monterey sand when maintaining constant sand skeleton void ratio.

Liquefaction resistance in silty sand has demanded the attention of many researchers throughout the years. Table 3.1 is a review of the literature focused on this topic. As it is observed, when researchers compared the same parameter they found similar conclusions. It is important to note that most researchers have focused only on fines content below 30%, which is usually the limit for using parameters as void ratio, relative density, sand skeleton void ratio or even equivalent void ratio.

However, as it will be shown later, the difference in the limiting densities of the materials used is also an important factor, that depends on D_{50}/d_{50} , range of fines contents and type of soil.

Table 3.1. Previous laboratory research on the undrained behavior of sands with fines

Researcher Example	Material	Fines content, FC (%)	Parameter kept constant	Conclusion
Lee and Fitton (1969)	El Monte sand	0 to 90% NP&P	Relative density, D_r	As FC increases, CRR increases
Shen et al. (1977)	Ottawa sand and clayey silt	0 to 25 PI=11	Sand skeleton void ratio	As FC increases, CRR increases
Kuerbis (1989)	Brenda sand and silt	0 to 20 NP	Sand skeleton void ratio	As FC increases, CRR increases
Law and Ling (1992)	Chalk River sand and Little Jackfish silt	0, 15, 30, 100 NP	Void ratio, e	As FC increases, CRR decreases
Zlatovic and Ishihara (1995)	Toyoura sand with non-plastic silt	0 to 40 NP	Maximum void ratio (defined by JGS standards)	As FC increases, peak strength decreases
Lade and Yamamuro (1997)	Nevada sand and Nevada fines	0 to 50 NP	Compaction energy	As FC increases, peak strength decreases
Amini and Qi (2000)	Ottawa sand 20-30 and non-plastic fines	10 to 50 NP	Void ratio, e	As FC increases, CRR decreases
Salgado et al. (2000)	Ottawa sand and non-plastic fines	0, 5, 10, 15 NP	Relative density, D_r	As FC increases, peak strength increases
Polito and Martin (2001)	Yatesville sand and fines	0 to 20 NP	Sand skeleton void ratio, e_s	As FC increases, CRR increases
Thevanayagam et al. (2002)	Ottawa sand III with crushed silica fines	7, 15, 25, 40 and 60, 100 NP	Equivalent intergranular void ratio, e^*	Peak strength is independent of FC
Bouckovalas et al. (2003)	Different sands and silt	0 to 30 NP	Void ratio	As FC increases, CRR decreases but for low confining stress, as FC increases, CRR increases
Carraro et al. (2003)	Ottawa sand and ground silica fines	0 to 15 NP	Relative density, D_r	As FC increases, CRR increases

Researcher Example	Material	Fines content, FC (%)	Parameter kept constant	Conclusion
Nabeshima and Matsui (2003)	Toyoura sand with non-plastic fines	30.6, 32.2, 33.5 NP	Relative density, D_r	As FC increases, CRR decreases
Xenaki and Athanasopoulos (2003)	Shinias-Marathon sand and silt	0, 10, 30, 42, 55, 100	Void ratio, e	As FC increases, CRR decreases
Huang et al. (2004)	Mai Liao sand and fines	0, 15, 30, 50 NP	Void ratio after consolidation, e_c	As FC increases, CRR decreases
Naeini and Baziar (2004)	Ardebil sand and fines	0 to 100	Void ratio	As FC increases, peak strength decreases for $FC < 35\%$, then the trend is reversed
Chang and Hong (2008)	Silica sand and kaolinite	0 to 35 NP	Void ratio, e	As FC increases, CRR decreases
Hara et al. (2008)	Tone River sand	0 to 30 Silty and clayey fines	Relative density, D_r	As FC increases, CRR decreases
Rahman and Lo (2008)	Sidney sand and Majura fines	0 to 20 NP	Equivalent granular void ratio, e^*	CRR is independent of FC
Carraro et al. (2009)	Ottawa sand with silt and kaolin	0, 5, 10, 15-NP, 0, 2, 5, 10-P	Relative density, D_r	Non-plastic fines increase dilatancy of sand while plastic fines impart a more contractive behavior
Belkhatir et al. (2010) and Belkhatir et al. (2011)	Chlef sand and silt	0 to 100 NP	Relative density, D_r and intergranular void ratio, e_s	As D_r increases CRR increases As e_s increases, CRR decreases
Dash and Sitharam (2011)	Ahmedabad sand and quarry dust	0 to 100 NP	Void ratio, e	As FC increases, CRR decreases for $FC > FC_{thr}$ the opposite is observed
Huang and Chuang (2011)	Mai Liao sand	0, 15, 30 NP	Void ratio, e , and equivalent void ratio, e^*	For the same e , as FC increases CRR decreases. CRR is independent of

Researcher Example	Material	Fines content, FC (%)	Parameter kept constant	Conclusion
				finer when tested at the same e^*
Bayat et al. (2012)	Sand with kaolinite and bentonite	0 to 30 NP	Void ratio, e	As FC increases CRR decreases for $FC > FC_{thr}$ the opposite is observed
Kokusho et al. (2012)	Futtsu beach sand	0 to 30 PI=6	Relative density, D_r	As FC increases CRR decreases
Missoum et al. (2012)	Silty sand from Chlef, Algeria	0 to 40 NP	Equivalent void ratio, e^* Thevanayagam (2002)	As FC increases, CRR decreases
Lee et al. (2013)	Hsin Hwa sand	0 to 34 NP	Void ratio	As F_c increases, CRR decreases
Noda and Hyodo (2013)	Silica sand and marine clay	0 to 98 NP	Compaction energy	For dense soils, as FC increases, CRR decreases. For loose soils, as FC increases CRR decreases.

NP: non-plastic

P: plastic

Although these results appear to be conflicting, they can be integrated under the same frame if the differences between density measures are understood.

3.3. Particle packing

Fabric is the arrangement of particles and pore spaces in a soil (Mitchell and Soga 2005).

Three kinds of fabric elements can be uttered:

- 1) Pore spaces. Gas or fluids in the voids of soil
- 2) Particle packing. Arrangement of particles with physical frontiers
- 3) Elementary particle arrangements. Particle interaction of single elements of clay, silt or sand.

In order to understand the influence of choosing a density parameter for comparing the undrained behavior of silty sand, it is necessary to understand the basic concepts of particle packing.

As stated by Panayiotopoulos (1989) there are two important factors to consider:

- (1) The minimum and maximum void ratios are the most meaningful measures of packing behavior.
- (2) For particles greater than 50 mm, particle size has no influence on packing of sands.

When considering a single particle size there are different arrangements:

- a) For a cubic deposit, particles are on top of each other in an unstable structure, achieving the loosest possible packing, with void ratio defined by:

$$e = \frac{6 - \pi}{\pi} = 0.90986$$

- b) In a orthorhombic or tetrahedral packing, particles lay on top of the contact of two particles in the previous layer, achieving a void ratio of:

$$e = \frac{3\sqrt{3} - \pi}{\pi} = 0.65399$$

- c) Another packing is the double stagger or nested, where particles in a layer fall down and touch particles in the second layer. Void ratio for this array is:

$$e = \frac{9 - 2\pi}{2\pi} = 0.43239$$

- d) Other arrays are the pyramidal and the close-packed hexagonal or tetrahedral, whose void ratio is the same:

$$e = \frac{3\sqrt{2} - \pi}{\pi} = 0.35047$$

When considering silty sand, it is practical to assume a binary packing where soil particles are spherical and void ratio is supposed to be independent of grain diameter or specific density. McGeary (1961) combined several fine spheres with coarse spheres and drew a

packing-density diagram for binary mixes with theoretical density and percentage of coarse spheres in mixture (Figure 3.5).

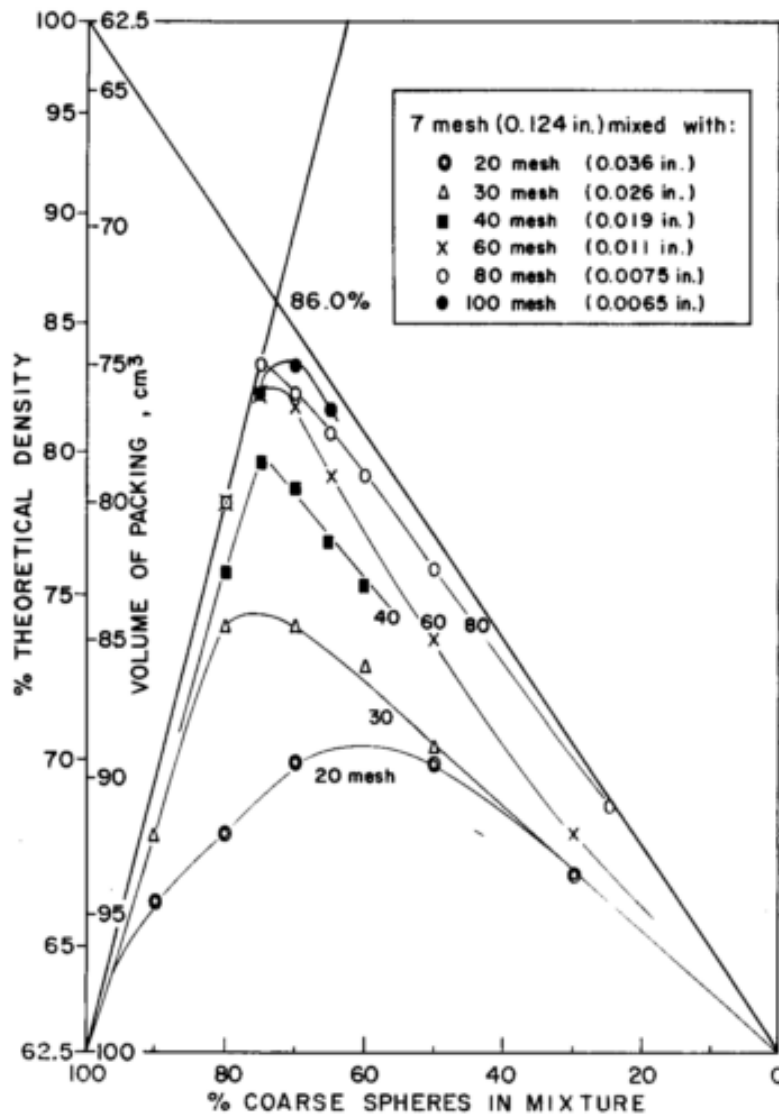


Figure 3.5. Binary mechanical packing of coarse spheres and smaller sizes. From McGearry (1961)

This can be a first approach to binary packing, however if a similar specific gravity is assumed, packing can be expressed in terms of volume. Lade et al. (1998) presented a scheme of the theoretical variation of void ratio with fines where the smaller particles have

a much smaller size than the coarser grains, avoiding the issue of the effect of the ratio between the two grain sizes. In Figure 3.6 the ABC line forms a V-shape having a minimum value at B. These lines were derived assuming that fines have a much smaller diameter than the large grains.

In fact, the V-shape will be defined by the ration between mean diameter of sand, D_{50} , and the mean diameter of fines, d_{50} . As this ratio increases, the shape of the curve is more pronounced and the use of the binary packing is more appropriate.

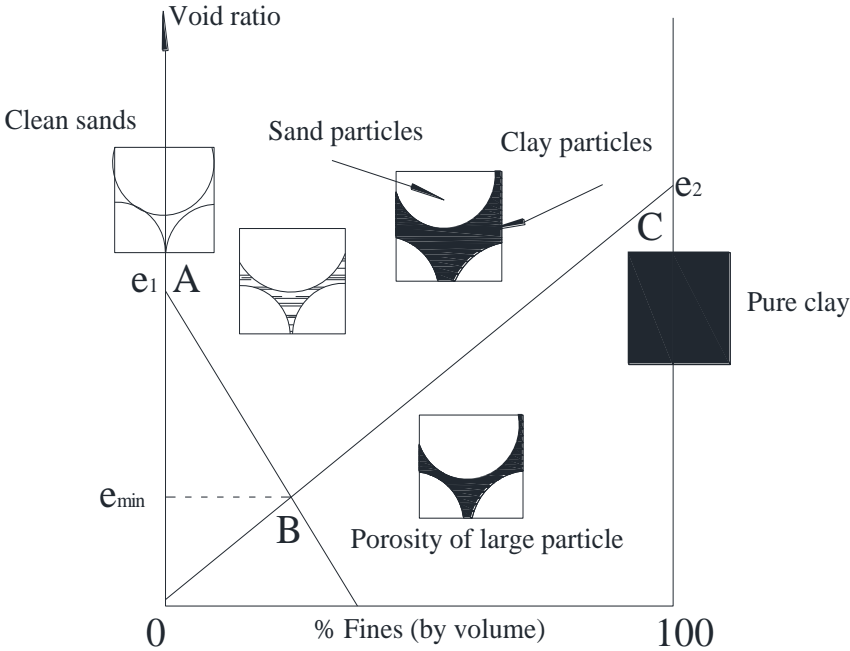


Figure 3.6. Theoretical variation of void ratio in binary packings with fines. After Lade et al. (1998)

3.4. Liquefaction of mine tailings

Materials resulting as residual of ore are usually discharged hydraulically in slurry form without densification. Being a liquefaction-prone material, it can lead to dam or impoundment failures that result in casualties and economic losses.

Tailings are mostly comprised of fine-grained non-plastic materials, therefore understanding the mechanical response of fines is very significant for the treatment of these materials.

Kuerbis (1989) performed tests on Brenda tailings sand and found that at a very loose density, as fines increased, cyclic resistance increased as well for the same void ratio. When using the sand skeleton void ratio as the parameter of comparison, he found that resistance is almost independent of fines content. Wijewickreme et al. (2005) performed constant volume cyclic direct simple shear tests (DSS) and cyclic shear tests on laterite, copper-gold and copper-gold-zinc. Laterite had a clay content of 35%, while for copper-gold clay content varied from 7 to 14% and copper-gold-zinc had no clay content. They found that the cyclic resistance ratio of the latter appears to be independent of the initial density and confining stress, exhibiting a response similar to normally consolidated clay.

Study of the undrained behavior of fine-grained material will contribute to prevent and mitigate liquefaction of mine tailings.

Chapter 4

EXPERIMENTAL

PROGRAM

Chapter 4. EXPERIMENTAL PROGRAM

4.1. Specimen preparation

Given the difficulties of retrieving undisturbed samples in cohesionless soils, reconstitution of samples is used to replicate field conditions to obtain insight into the mechanical properties of soil through laboratory testing.

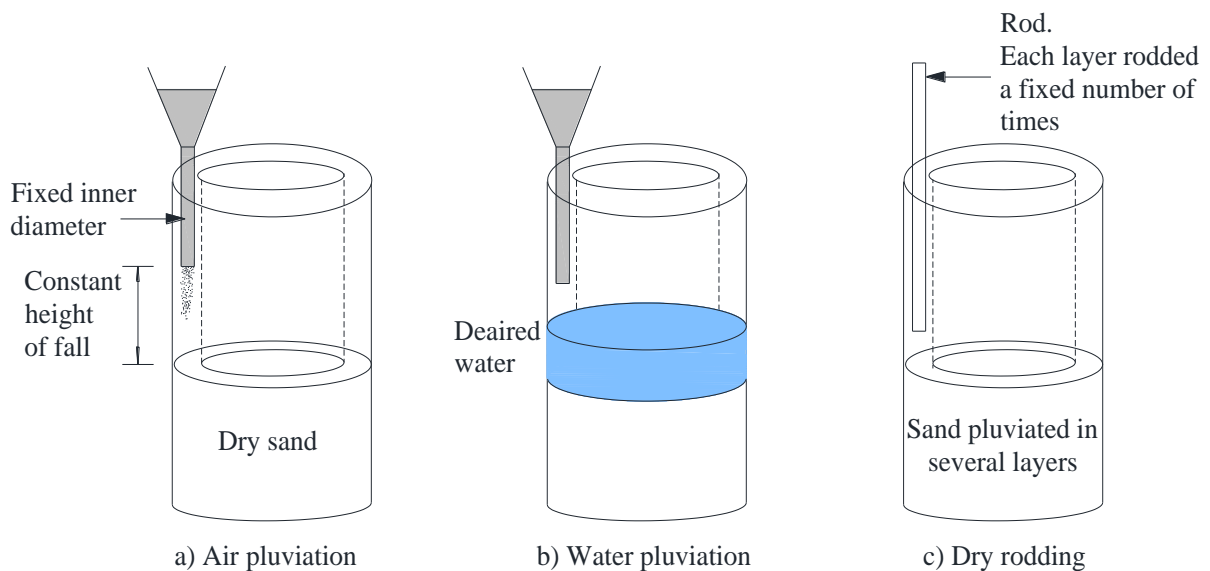


Figure 4.1. Sample formation

There are different kinds of sample formation depending on the form of deposition either wet or dry. Some of these methods intend to reproduce particular conditions of natural depositions, the following are the most common:

- Moist tamping
- Water pluviation
- Slurry deposition
- Dry deposition

4.1.1. Moist tamping

For this procedure, soil is mixed with a certain amount of water to handle and saturate the sample more easily. This method consists of placing a number of layers of a definite thickness into a mold, tamping each layer with a specified force and frequency of tamping until achieving a target density. Then place the next layer and tamp it in the same way until the desired height is obtained.

By using this method, very loose densities can be achieved given the water tension forces between the grains. Large densities can also be obtained by increasing the compaction energy while tamping. However, this method is not appropriate for silty sands since it produces non-uniform samples (Miura et al. 1984).

4.1.2. Water pluviation

Wet pluviation is used to simulate soils deposited in nature through water as alluvial soils or hydraulic fills. In this method, dry sand flows through a funnel into a membrane containing boiled de-aired water. Since soil is already deposited in water, saturation of the sample is warranted and is ideal for testing poorly-graded soil. Nevertheless, the different terminal velocities of silty sand falling through water produces particle segregation. Samples produced by this method are also more compressible than dry-deposited samples during consolidation and exhibit a more dilatant behavior during undrained loading (Kuerbis 1989), however triaxial and simple shear resistance of a water pluviated sample is very close to that of an undisturbed frozen sample of a clean sand (Vaid et al. 1999)

4.1.3. Slurry deposition

Kuerbis and Vaid (1988) developed a variation of the wet pluviation method to avoid particle segregation. In this method a batch of soil is initially mixed with water and boiled to de-air the sample. Once the mix is cool, more water is added and then poured into a mixing tube, where soil is blended thoroughly to finally be deposited into the membrane.

4.1.4. Dry deposition

Dry deposition has different variants as tapped funnel deposition, fast funnel deposition, air pluviation and dry rodding.

Tapped funnel deposition consists of using a funnel to pour the soil into the container without a height of fall and then tap the mold in a symmetrical pattern to achieve the desired density.

Fast funnel deposition is a variant of tapped funnel deposition, where the funnel is raised rapidly without any height of fall to increase density.

Air pluviation consists of pouring soil through air using a funnel. Soil is deposited varying the height of fall to increase density.

Dry rodding consists of pouring sand in a dry state into several layers; each layer is rodded by a fixed number of times until the required density.

4.1.5. Effect of sample preparation

As stated by Mulilis et al. (1977), sample reconstitution has a large influence on the liquefaction resistance of sands. Figure 4.2 shows the influence of sample preparation on the liquefaction resistance of sand. It is observed that vibrated samples have a higher liquefaction resistance. The sample formed by moist tamping shows the higher resistance while air pluviation exhibits the lower cyclic resistance ratio. Samples formed by water pluviation and dry rodding have a medium response for the same relative density.

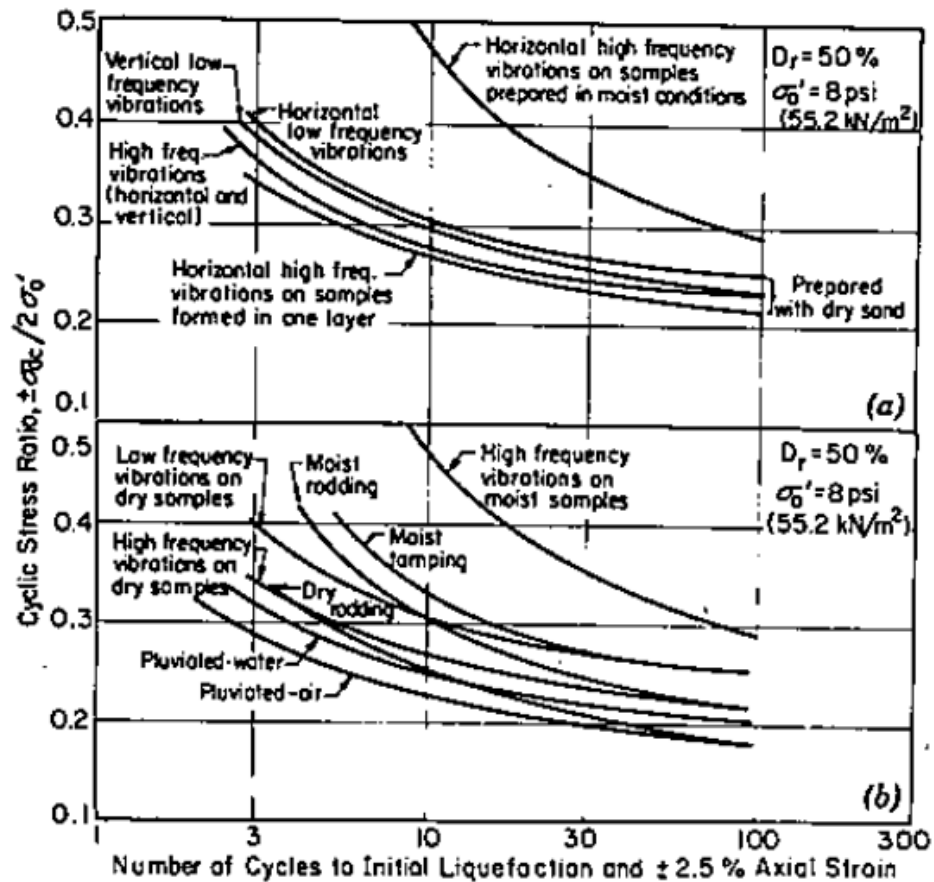


Figure 4.2. Influence of sample preparation on the liquefaction resistance. From Mulilis et al. (1977)

Tatsuoka et al. (1986) also conducted a series of triaxial and cyclic torsional shear tests on Toyoura and Sengeniyama sands. They used air pluviation, wet tamping method, wet vibration method and water vibration method. They found similar results as those seen in Figure 4.2, having the largest resistance for wet-vibration and the smallest for air-pluviation. However resistance was not only a function of sample preparation, but also of sand type, relative density and the strain value for which failure was defined.

4.2. Sample saturation

When samples are reconstituted for testing it is necessary to ensure full saturation to conduct undrained loading. The extent of water saturation can be measured through

Skempton's B value; this parameter is described as the ratio between the increments of pore pressure, Δu , and undrained stresses, $\Delta\sigma_1$ and $\Delta\sigma_3$:

$$B = \frac{\Delta u}{\Delta\sigma_3 + A(\Delta\sigma_1 - \Delta\sigma_3)}$$

The relation between B value and saturation ratio is shown in Figure 4.3 where different soils are presented. It is observed that for clean sands full saturation is achieved for $B \approx 0.8$ while higher values of B are required to fully saturate a clayey material.

After saturating a sample in a triaxial or shear device, saturation can be evaluated measuring the increments in pore pressure while carrying out isotropically undrained compression of the sample. B can be considered to be the ratio of those increments as:

$$B = \Delta u / \Delta\sigma_3$$

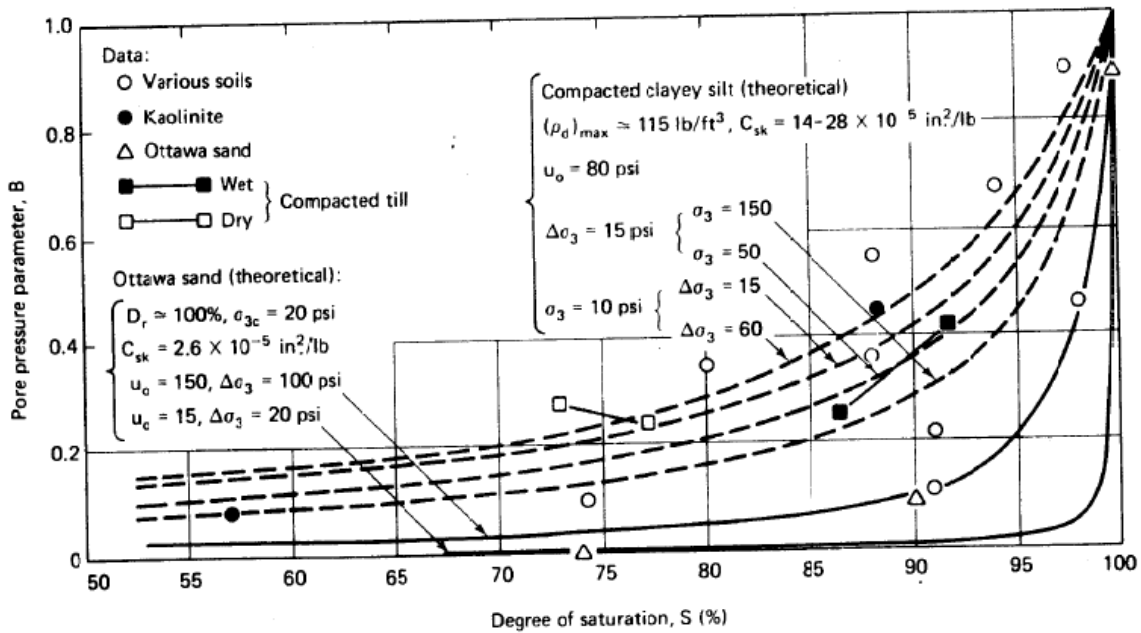


Figure 4.3. Pore pressure parameter B and degree of saturation, S (%) (After Black and Lee, 1973).

For wet-deposition samples saturation is fully achieved using backpressure to dissolve the remaining air in the sample. Sometimes the use of carbon dioxide is necessary to avoid undesirably large backpressures.

For dry samples, de-aired water has to be percolated through the sample until reaching full saturation. Backpressure can also be applied for increasing B value.

Some of the most common procedures for saturation of dry samples are described in the following paragraphs.

4.2.1. Carbon dioxide

This procedure consists of flowing carbon dioxide gas, CO₂, through the sample to eliminate the air. Sample is formed and sustained with an initial isotropic effective stress; then a source of CO₂ is used to circulate gas through the specimen from bottom to top. After some time de-aired water is introduced into the sample to saturate it. One drawback of using CO₂ for saturation is the possible reaction with soil components. Yet, this method is very effective to eliminate the air from the pores and ensure full saturation.

4.2.2. Double-vacuum saturation

This procedure was first introduced by Rad and Clough (1985) for uncemented and cemented sands and later Ampadu and Tatsuoka (1993) showed the application for clays and silty sands.

The method is based on the application of initial vacuum to dissipate the air inside the sample. Two water tanks are needed, one as a source of water and the other as reservoir. First, vacuum is applied to the specimen, and then less vacuum is applied to the cell, creating a negative backpressure that will result in an effective stress on the specimen.

Once this system is maintained for a while, de-aired water under a low head is allowed into the sample to be nominally saturated. More vacuum is applied and then total confining pressure is increased to measure the induced change in pore pressure and calculate the coefficient B. Once again the desired effective stress is adjusted and more water is

percolated through the sample for a brief time. When the needed B value is reached, pressures in the cell and in the specimen are increased until the confining stress becomes positive and the desired effective stress is achieved. More details on this procedure will be provided on section 4.6.4.

4.3. Consolidation tests

Consolidation tests are necessary to gain insight into compressibility of soils. During laboratory testing, consolidation is a process of deferred volumetric deformation caused by the application of stresses on the soil sample. There are two main interests:

- 1) Magnitude of the compression instantaneously generated by different loading conditions
- 2) Evolution of deformation over time

The parameters that can be obtained from this test are the coefficient of consolidation, c_v , and the coefficient of volume compressibility, m_v . Figure 4.4 shows the change in pressures for samples being consolidated at 100 kPa. It is observed that after saturation samples have an effective stress (e.g., 30 kPa) and then an increment in confining stress is applied to achieve the desired effective stress for shearing.

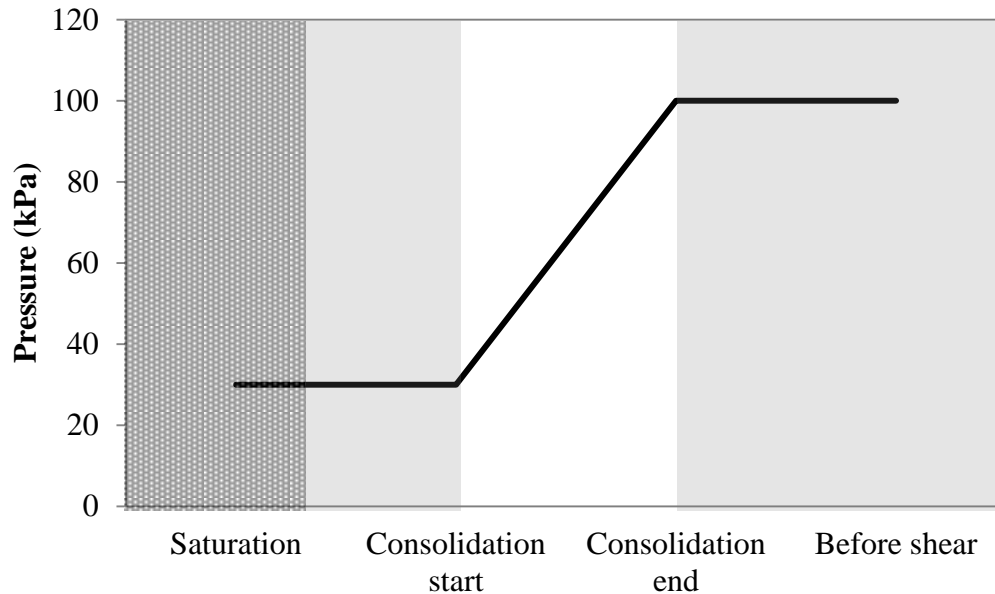


Figure 4.4. Scheme of pressures for isotropically consolidated samples at 100 kPa

4.4. Undrained monotonic shear tests

Figure 4.5 shows the effective stress paths during undrained loading for loose sands at different confining stresses. The regions in this figure are liquefaction, temporary liquefaction and stable region. Yamamuro and Covert (2001) pointed out that the behavior of loose silty sands made through air pluviation exhibited what they called a reverse behavior because maximum shear strength was found for clean sands although silty sands exhibited larger relative density.

The reason to call this phenomenon reverse behavior was explained by Lade and Yamamuro (1997) who found that when conducting experiments with different fines content, found an opposite behavior to that of clean sand for which peak strength increased with relative density.

They concluded that the addition of fines to the structure caused contractive volumetric tendency and the use of air pluviation produced a fabric more unstable that explained the reduction of liquefaction resistance of silty sand.

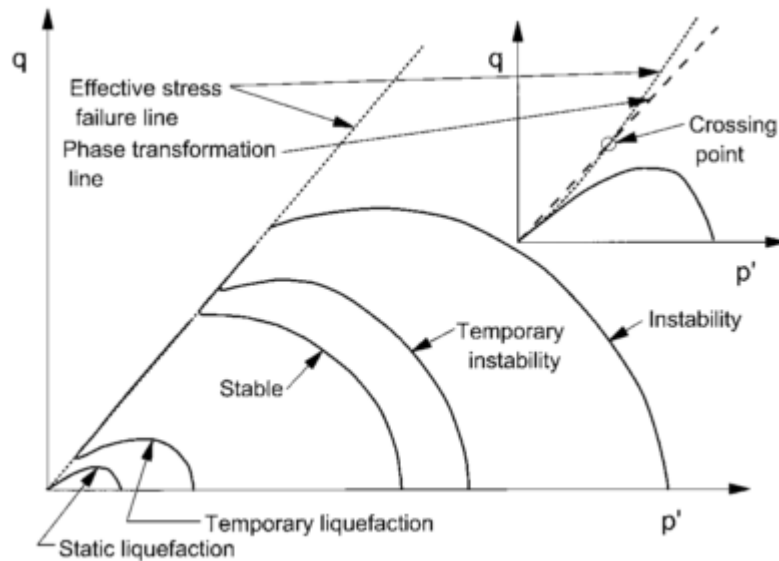


Figure 4.5. Undrained effective stress paths for loose sands (from Yamamuro and Covert 2001)

It is observed that static liquefaction is reached for low confining stresses. For larger confining stresses, in the stable region the stress path does not have a decrease in shear stress. As confining stresses increases, soil behavior approaches to an instability region where soil exhibits larger contraction.

4.5. Stresses and strains in a hollow cylindrical torsional shear device

The apparatus used for this dissertation is the hollow cylindrical torsional shear device. This machine subjects a 190 mm height of a specimen (internal diameter of 60 mm and external diameter of 100 mm) to a combination of axial and torsional stresses, in addition to the fluid stresses inside and outside the cylindrical surfaces. The loading system enables the independent control of torque, axial load, inner cell and outer cell pressures. A computer program controls all the loading devices through a digital-to-analogue (D/A) converter board. Servo-motors apply vertical load and torque. The loading system of this motor is suitable for strain controlled loading and is limited to 10% shear strain. The device can be observed in Figure 4.6. The independence control of load application allows for developing

stress paths more similar to real conditions. Besides it also permits the rotation of the principal stresses axes.



Figure 4.6. Hollow cylinder torsional shear device

Figure 4.7 shows schematically the stresses applied in a hollow torsional shear device. The principal parameters to be considered are:

F: vertical force

T: torque

σ_v : vertical stress

σ_h : horizontal stress

τ_{vh} : shear stress

O: outer cell pressure

I: inner cell pressure

H: height of the specimen

θ : angle of rotation

r_i : inner radius

r_o : outer radius

A_s : cross section of the specimen

A_r : cross section of the axial rod

W_s : weight of the specimen

W_c : weight of the cap

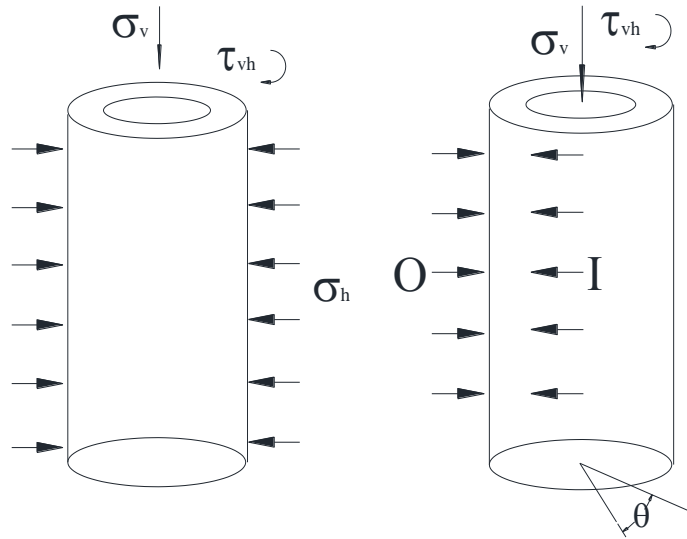


Figure 4.7. Stresses in a hollow cylinder specimen

The static equilibrium in the vertical, radial and circumferential directions (z, r, θ) is given by:

$$\frac{\partial \sigma_r}{\partial r} + \frac{\partial \tau_{r\theta}}{r \partial \theta} + \frac{\partial \tau_{rz}}{\partial z} + \frac{\sigma_r - \sigma_\theta}{r} = 0$$

$$\frac{\partial \sigma_\theta}{r \partial \theta} + \frac{\partial \tau_{r\theta}}{\partial r} + \frac{\partial \tau_{\theta z}}{\partial z} + \frac{2\tau_{r\theta}}{r} = 0$$

$$\frac{\partial \sigma_z}{\partial z} + \frac{\partial \tau_{rz}}{\partial r} + \frac{\partial \tau_{\theta z}}{r \partial \theta} + \frac{\tau_{rz}}{r} = 0$$

The axy-symmetric distribution in a hollow cylinder specimen leads to:

$$\tau_{r\theta} = \tau_{rz} = 0$$

Equations are reduced to:

$$\frac{\partial \sigma_r}{\partial r} + \frac{\sigma_r - \sigma_\theta}{r} = 0$$

Considering the boundary conditions of outer cell pressure, O , and inner cell pressure, I , the solutions for σ_r and σ_θ

$$\sigma_r = \frac{Or_0^2 - Ir_i^2}{r_0^2 - r_i^2} - \frac{r_i^2 r_0^2 (O - I)}{r_0^2 - r_i^2} \frac{1}{r^2}$$

$$\sigma_\theta = \frac{Or_0^2 - Ir_i^2}{r_0^2 - r_i^2} + \frac{r_i^2 r_0^2 (O - I)}{r_0^2 - r_i^2} \frac{1}{r^2}$$

Assuming that the work done by the applied forces and torques is equal to the sum of the work done by the stresses and strains, the average values of stresses and strains can be obtained (Saada 1988):

$$\sigma_z = \frac{F}{\pi(r_0^2 - r_i^2)} + \frac{Or_0^2 - Ir_i^2}{r_0^2 - r_i^2}$$

$$\sigma_r = \frac{Or_0 + Ir_i}{r_0 + r_i}$$

$$\sigma_\theta = \frac{Or_0 - Ir_i}{r_0 - r_i}$$

With corrections for the rod and cap:

$$\sigma_z = \frac{F + W_c + 0.5W_s + \pi(Or_0^2 - Ir_i^2) - A_r O}{A_s}$$

Then horizontal stress is the average of inner and outer cell pressures:

$$\sigma_h = \frac{O + I}{2}$$

Shear stress can be integrated from:

$$dT = \tau_{z\theta} r^2 d\theta dr$$

The limits for r are r_0 and r_i , and for θ , 0 and 2π , then the double integration results in:

$$T = \frac{2}{3} \pi \tau_{z\theta} (r_0^3 - r_i^3)$$

$$\tau_{\theta z} = \frac{3T}{2\pi(r_0^3 - r_i^3)}$$

The principal stresses are given by:

$$\sigma_1 = \frac{\sigma_z - \sigma_\theta}{2} + \sqrt{\left(\frac{\sigma_z - \sigma_\theta}{2}\right)^2 + \tau_{z\theta}^2}$$

$$\sigma_2 = \sigma_r$$

$$\sigma_3 = \frac{\sigma_z + \sigma_\theta}{2} - \sqrt{\left(\frac{\sigma_z - \sigma_\theta}{2}\right)^2 + \tau_{z\theta}^2}$$

Considering u_o and u_i the deformations in the outer and inner diameters, respectively, the average strains ε_z , ε_r , ε_θ and $\gamma_{\theta z}$ are:

$$\varepsilon_z = \frac{\Delta H}{H}$$

$$\varepsilon_r = -\frac{u_o - u_i}{r_o - r_i}$$

$$\varepsilon_\theta = \frac{u_o + u_i}{r_o - r_i}$$

$$\gamma_{\theta z} = \frac{2\theta(r_o^3 - r_i^3)}{3H(r_o^2 - r_i^2)}$$

4.6. Torsional shear tests

4.6.1. Selection of sample preparation method

Seeking to eliminate the use of a density measure for testing, constant compaction energy was selected as the parameter of comparison. Taken into account the characteristics described in previous sections as well as the fact of working with large fines contents, air pluviation and slurry deposition were the methods considered for reconstitution of samples. Given the convenience for controlling compaction energy and repeatability, the first was preferred. However, some samples were made with slurry deposition, the procedure and results are explained in Chapter 5.

Air pluviation was selected as the method for sample reconstitution, given that, as observed in Figure 4.2, air pluviation does not overestimate the liquefaction resistance of the soils, it

represented a convenient method for keeping the compaction energy constant in hollow cylinder samples and it can generate uniform samples. Miura et al. (1984) performed cone penetration tests on minitriaxial samples formed with air pluviation and moist tamping and found that the latter did not produce uniform samples while air pluviation did. Huang et al. (2004) compared the methods of water pluviation, moist tamping and dry deposition for samples with 30% of fines content and found that the samples made through air pluviation exhibited little deviation from the expected grain size distribution.

Following, a brief procedure of the complete undrained test is provided with generalities of the actions taken during each phase.

4.6.2. Specimen preparation

Sand used for these experiments was retrieved from the field containing different amount of fines. In order to make samples with different fines contents, Tokyo Bay sand was sieved to separate the fines passing the #200 mesh (0.074 mm) from the coarser grains. Fines were set apart while sand was washed thoroughly to remove fine particles. Then it was air-dried for 5 to 6 days to finally blend it with fines to achieve the desired mixture.

As mentioned earlier, the specimen is a hollow cylinder, therefore two membranes and two molds are used to form the sample. The inner diameter is 60 mm and the outer diameter is 100 mm. The height is of 190 mm. The pedestal and top cap are shown in Figure 4.8. It can be observed that both pedestal and top cap have 6 blades and porous stones.

The outer membrane has 25 cm of height, 10 cm of diameter and 0.3 mm of thickness. The inner membrane has 39 cm of height, 6 cm of diameter and 0.3 mm of thickness. Both membranes have a Young's modulus of $E=1400$ kPa.

Appropriate corrections for membrane forces are already implemented in the software used to collect the data.



Figure 4.8. Pedestal and top cap

To attach the membranes to the pedestal and top cap, a thin layer of vacuum grease is applied to avoid leakage. Once both inner and outer membranes have been properly attached to the pedestal with 3 rings, inner and outer molds are placed to form the sample (Figure 4.9). It is important that at this stage, the hoses that connect the valves to the specimen are firmly attached in order to avoid leakage. Both membranes to be well attached and no wrinkles should form between the membrane and the mold. When placing the molds, given their sharp edges, especial care shall be put to avoid tearing the membranes or creating gaps that could prevent the sample from getting the initial pressure to stand. Once the membranes are set, a line must be connected to the outer mold to transmit the vacuum. At this stage, 20 or 30 kPa can be used to support the sample.

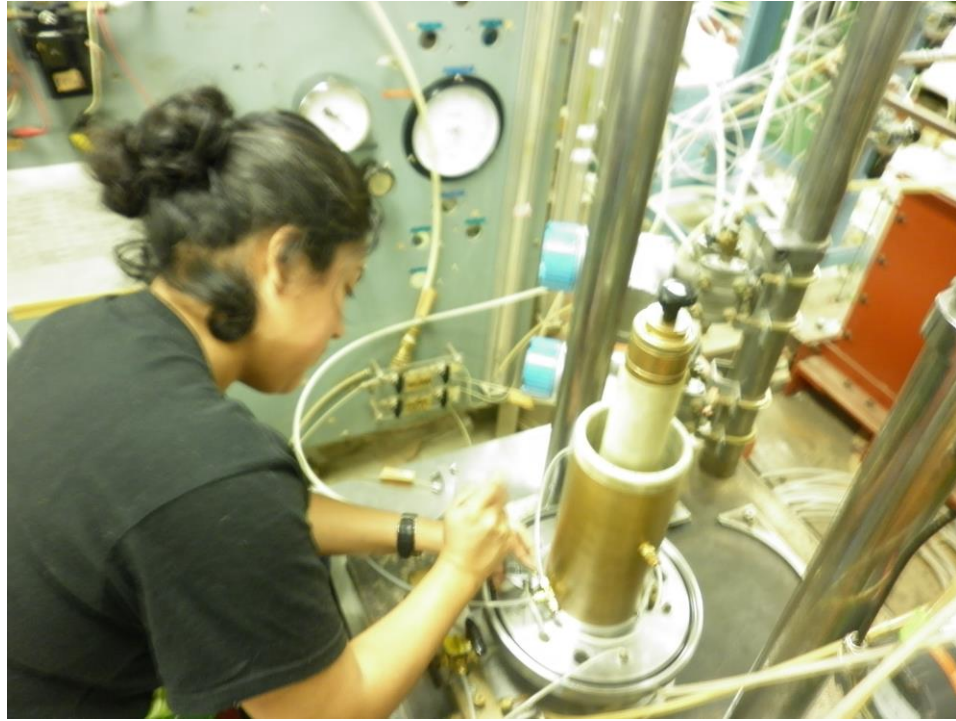


Figure 4.9. Sample preparation

Air pluviation method is shown on Figure 4.10. It consists of pouring dry sand using a funnel with a fixed inner diameter and a constant height of fall. The funnel should be turned slowly around the sample, first clockwise and then counterclockwise to allow for even distribution of the grains.

This method was selected given that, if the height of fall is kept constant, it creates a very natural deposition. It does not overestimate the cyclic resistance of soil and it also is useful to make uniform samples when using sand with fines (Huang et al. 2004)

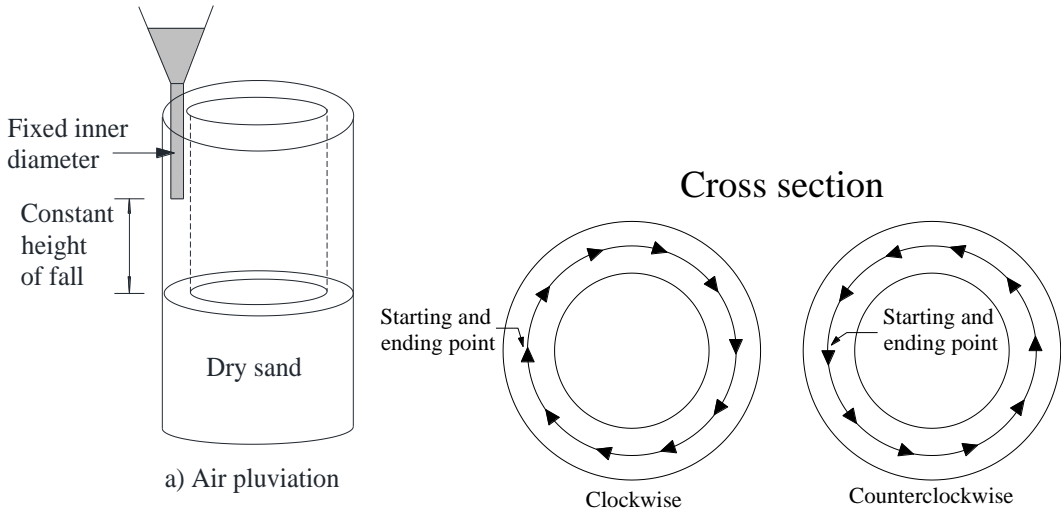


Figure 4.10. Air pluviation

After filling the whole mold, the surface must be smoothed and remaining sand must be removed from the edges to place the cap and cover it with the membrane. Again 3 rings have to be attached to each membrane to avoid leakage.

4.6.3. Preparation of de-aired distilled water

Deaired water must be used to saturate the specimen to avoid dissolved air into the sample. A tank of distilled water needs to be connected to a pump for at least 24 hours to assure that no dissolved air is remaining inside. Figure 4.11 shows the schematic array of the water

container connected to the pump. To check the process, hit softly the tank with a stick to observe the presence of bubbles. Water is completely deaired when no more bubbles appear.

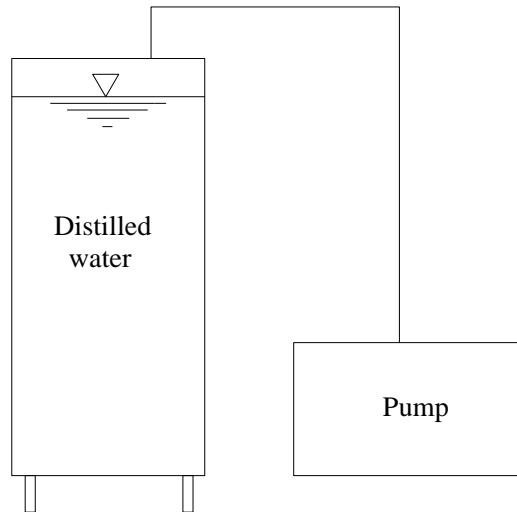


Figure 4.11. Deairing water

4.6.4. Saturation

After the sample and the chamber have been properly attached to the load piston, it is possible to start the double vacuum saturation process.

At this point the sample is kept stable with a pressure of -20 kPa or -30 kPa and the pressure in the inner and outer cell is 0 kPa, obtaining a 20 kPa or 30 kPa effective stress. In order to maintain this condition during the procedure for saturation it is important to apply vacuum to the sample but also to the inner and outer cells. The inner and outer cells should be connected to vacuum and the top part of the sample should also be connected to another source of vacuum as shown on Figure 4.12, all valves are closed at this point. Using the regulators, pressure in the chamber (inner and outer cell) and in the sample should be decreased carefully to reach -70 kPa and -90 kPa, respectively. To do this, the pump regulator has to be set initially to -20 kPa, the sample's top valve is opened and then the inner and outer cell valves in the top part are opened as well. Using both regulators, pressure should be decreased at a rate of about 3 kPa/min keeping always the 20 kPa

difference between the sample and the chamber until achieving -90 kPa and -70 kPa, respectively.

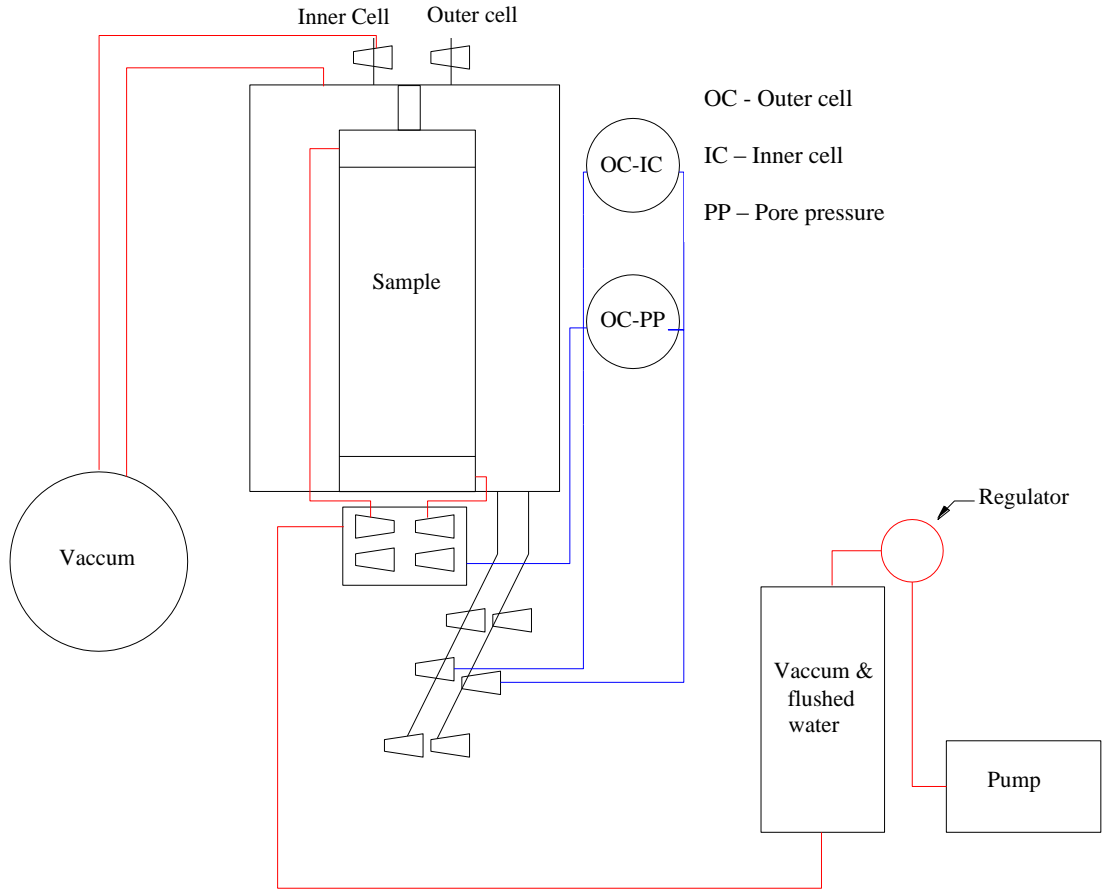


Figure 4.12. Saturation process

After one hour, a line must be connected to the bottom part of the deaired water tank and has to be saturated before attaching it to the valve of the sample’s bottom part as shown in Figure 4.12. As shown in Figure 4.13, the sample’s top valve should be connected to the bottom of the container and this has to have deaired water inside. The flushing should continue until the tank is almost empty.

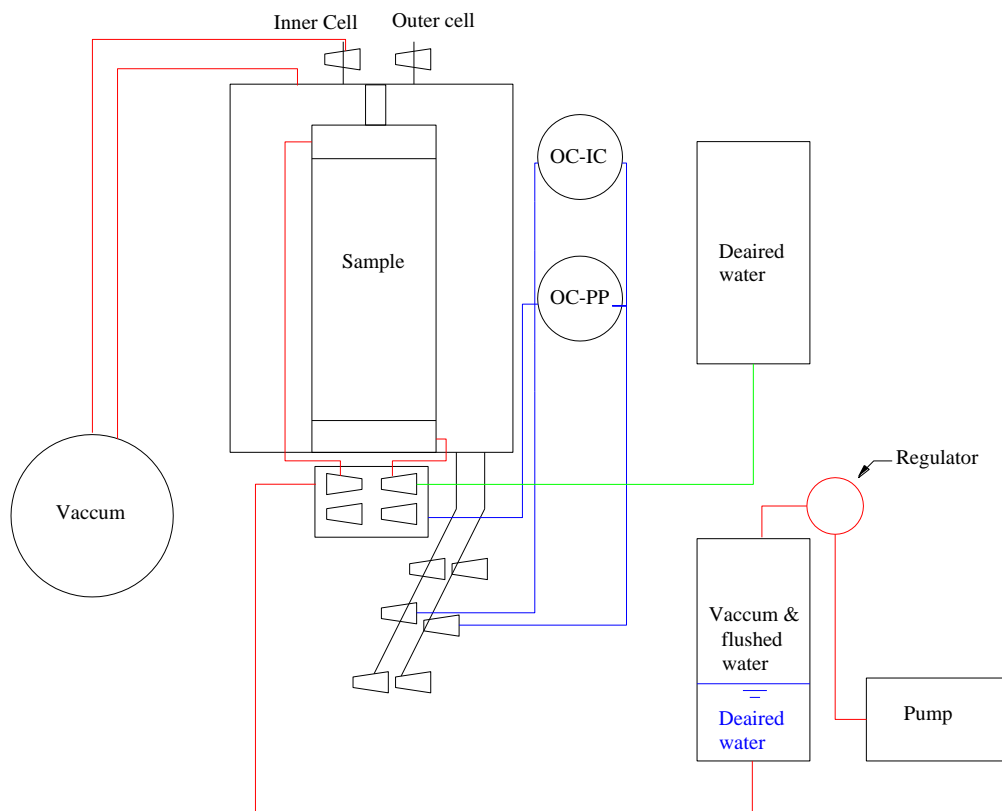


Figure 4.13. Flushing water

During this process it is important that the line which connects the sample to the OC-PP differential pressure transducer (red line in Figure 4.14) is well saturated, by opening all the valves and passing water through the transducer.

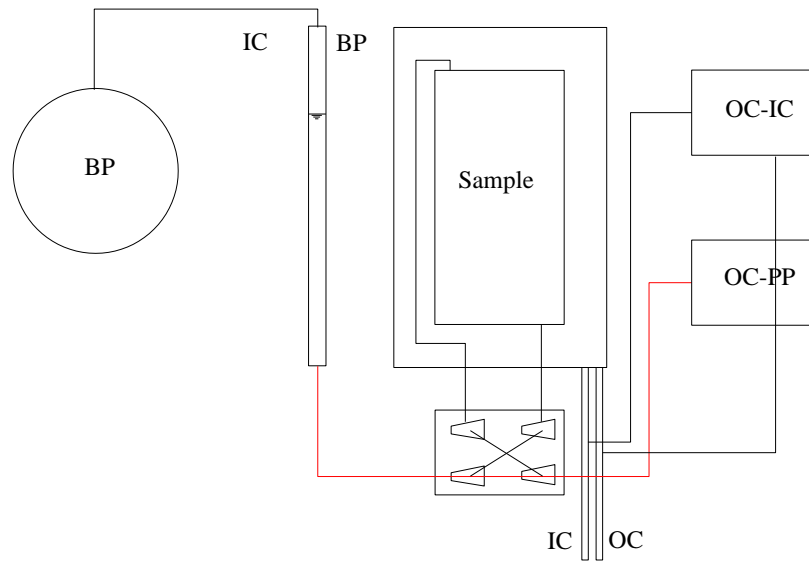


Figure 4.14. Saturation of the OP-PP differential pressure transducer

4.6.4.1. Findings for saturation of silty sand

Saturation is one of the most challenging tasks to undertake when testing sands with fines. In cases where dry deposition is conducted, as the one presented in this thesis, the process is long and can turn to be unsuccessful if the appropriate measures are not considered.

First, the amount of water for flushing during saturation should be 1.5 to 2 times the volume of the sample. The flow should be controlled to avoid undesirable particle movement, especially when dealing with fines content greater than 40%.

The tank used for flushed water should contain water since the beginning of the process and all tanks should be cleaned and checked for leakage periodically.

The most important process during saturation is the stage where vacuum is initially applied to the sample, the decrease of pressure has to be in small decrements. It was found that 1 hour of vacuuming was typically enough for samples containing 0, 10 and 20% of fines content. For samples containing 30 and 40% fines content, the time was usually 2 hours. For larger fines contents, such as 60 and 80%, the suggested time is 3 hours in order to remove the air and make easier the actual saturation.

The use of perfectly deaired water is very important and should not be overlooked. A tank connected to a pump usually will take four to five hours to be totally deaired, yet, if more tanks are connected to the same source, all of them have to be perfectly sealed and the time will increase up to 24 or 36 hours. If a tank is disconnected after deairing, it will only be useful after 10 hours, later the deairing process will have to be conducted again.

4.6.5. Preparation of the sample for consolidation

After the flushing process is finished, the chamber and sample pressures can be set to their original values. In order to do so, the sample's bottom valve is closed and using the regulators for the chamber and the sample's pressure the vacuum should be decreased very slowly until reaching 0 kPa and -20 kPa, respectively. It is important that the cell pressure is measured by the regulator of the vacuum source, as well as by the pressure transducer to verify the values that go in and out. Once the pressure in the inner and outer cells is fully released and the sample is set to -20 kPa again, the sample's top valve can be closed.

Then, the large water tank can be connected to the outer cell entry and a small water of deaired distilled water can be also connected to the inner cell entry, as shown in Figure 4.15. An air source must be connected to the top of both water containers at a very low pressure and the filling of the inner and outer cells can start.

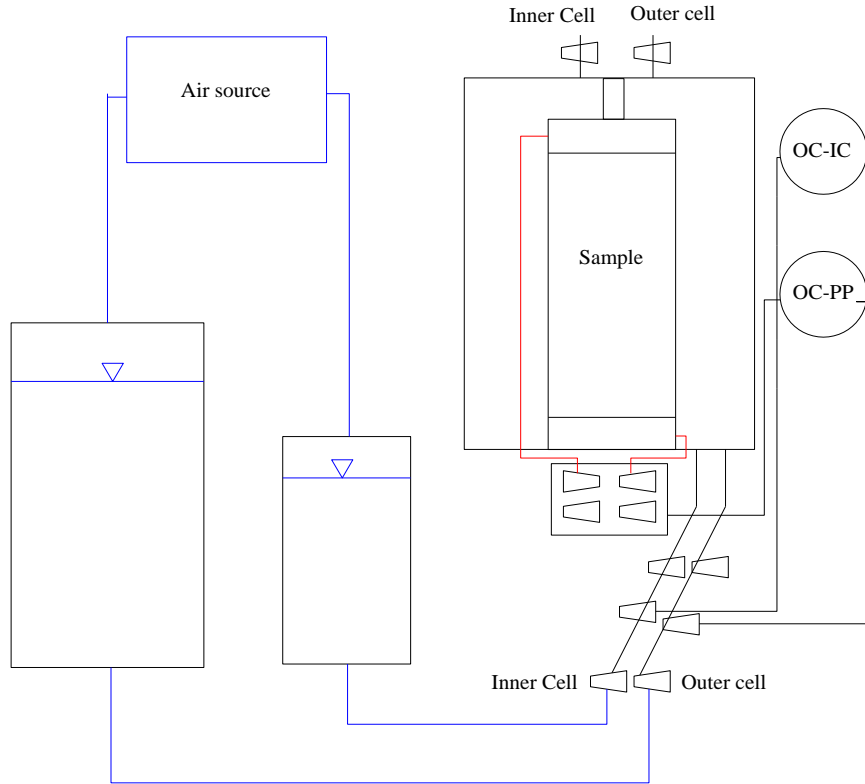


Figure 4.15. Chamber filling

4.6.6. B-value

After carrying out the double vacuum saturation method, a preconsolidation stage is conducted to check the B-value. The volume transducers have to be saturated and, the LVDT and potentiometer have to be properly placed on the chamber.

To this stage, the outer and inner cell pressures are equal to 0 kPa and pore pressure is - 20 kPa. The line that comes from the inner and outer cell gauges has to be connected to the top part of the chamber. Both, inner and outer valves in the top have to be closed. To change the pressure in the sample, this has to be connected to the back pressure gauge as shown on Figure 4.16 and the valve has to be opened while increasing the pressure.

When everything is connected, the pressure will be increased carefully using the inner and outer cell gauges as well as the back pressure gauge. It is important that the difference

between sample and chamber remains 20 kPa, therefore pressures should increase very slowly until the chamber is set to 70 kPa and the back pressure to 50 kPa.

The lines are schematically shown on Figure 4.16.

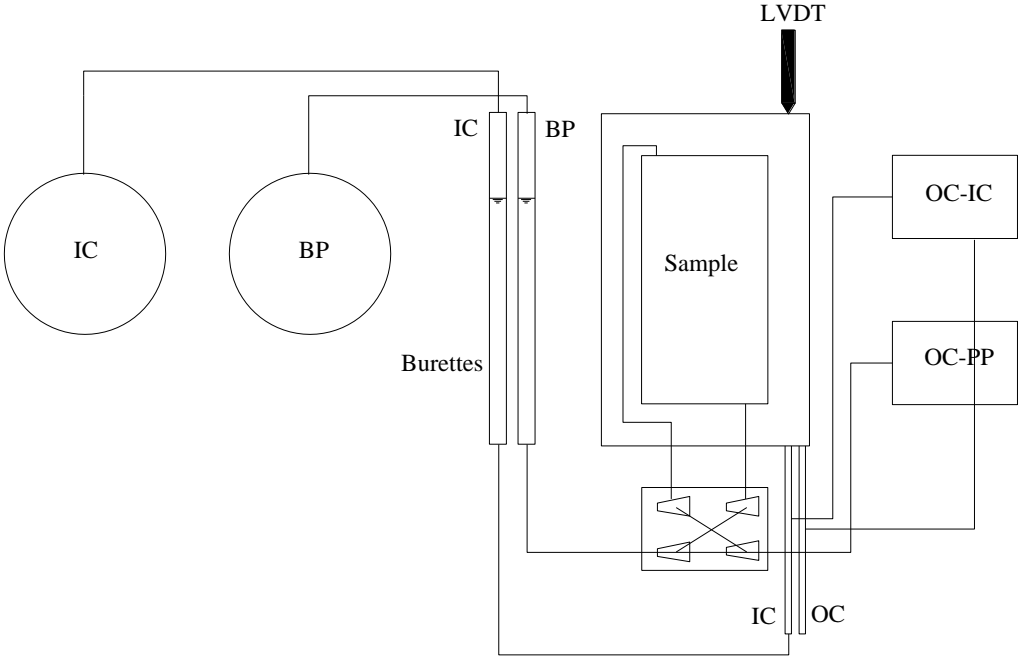


Figure 4.16. Schematic view of the machine

When the back pressure is set to the desired value, three or four minutes are allowed for it to stabilize. Once stable, the drainage valve is closed as shown in Figure 4.17.

The load piston has to be released very cautiously to avoid any displacements. It is important that the LVDT is tightly screwed to avoid tilting or any sudden movement not related to the sample deformation (Figure 4.17).

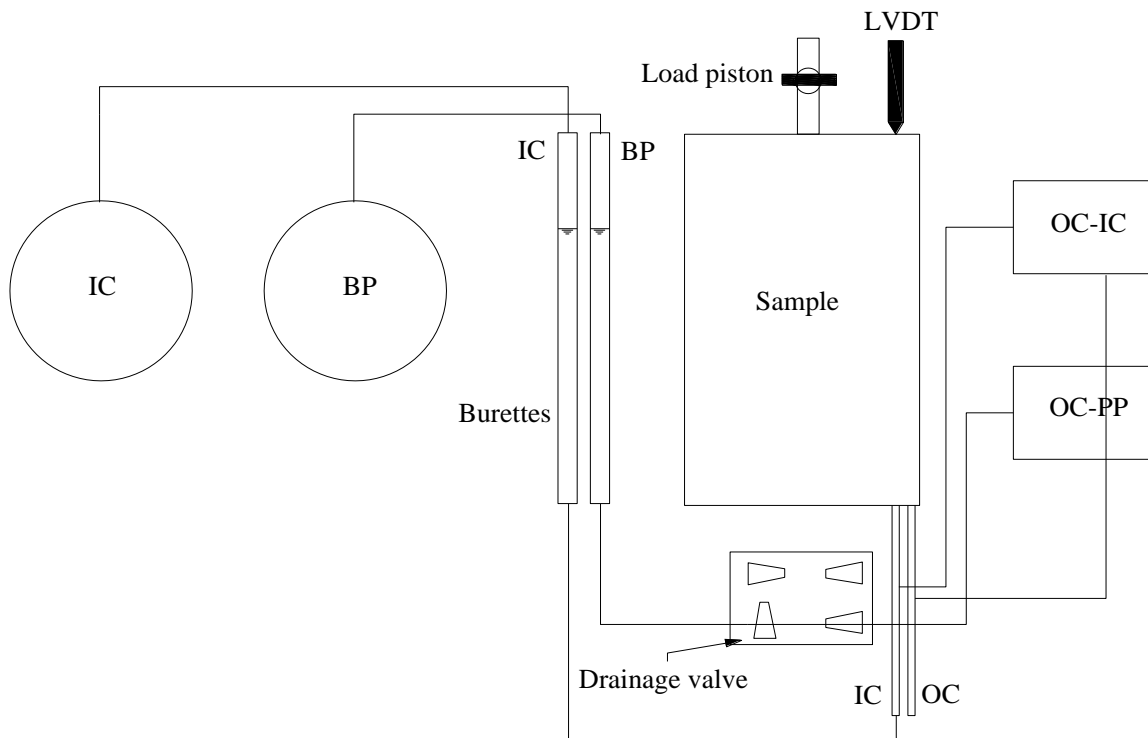
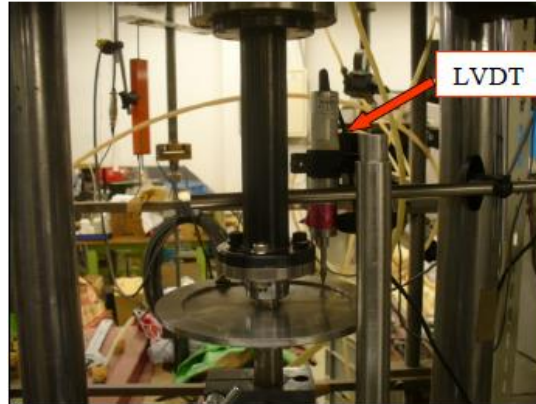


Figure 4.17. Considerations during pre-consolidation

Then isotropic compression is made by applying equal total stress increments to the specimen with the drainage valve closed. The increment of pore water pressure is measured and then the extent of saturation is computed as $B = \Delta u / \Delta \sigma_3$.

After the desired state is reached, the back pressure is raised to the same level as the measured pore water pressure, and the drainage valve is opened. When B-value is not satisfactory the back pressure is raised to higher values so that pore gas solves into water, then the drainage valve is closed and the procedure is repeated until obtaining $B \geq 0.95$.

When this procedure is successful the pressures time history is similar to the one shown in Figure 4.18 where it can be seen that after checking B-value, an increment of 50 kPa is made and the checking is carried out again until B is greater than or equal to 0.95.

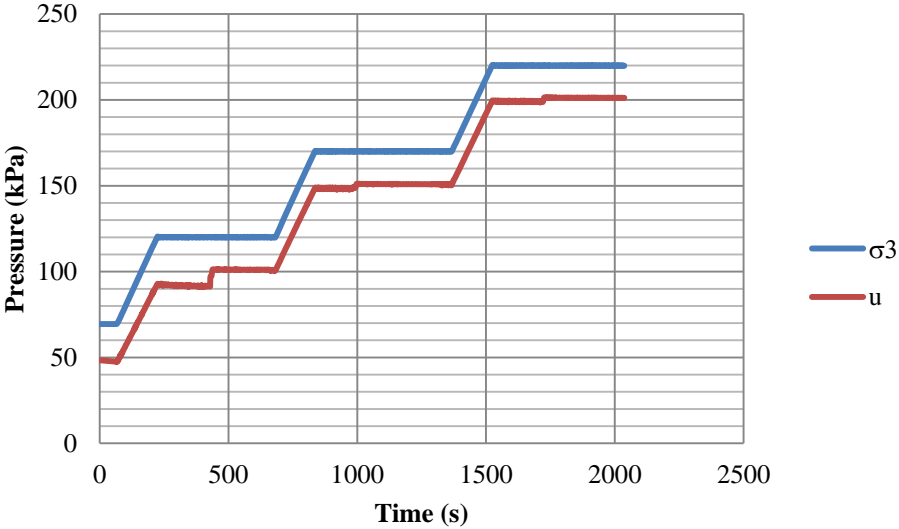


Figure 4.18. Procedure to check B-value

4.6.6.1. *What to do if $B < 0.95$.*

Following the compression, the back pressure should be set to the pore water pressure measured and the drainage valve is opened again. Sometimes 3 or even 5 increments (of 50 kPa each) are necessary to guarantee a $B\text{-value} > 0.95$, so the chamber pressure can reach up to 320 kPa and pore pressure, 270 kPa.

However, if B-value is not satisfactory after increasing the back pressure for several times, it is possible to go back to the flushing process and more water should be passed through the sample. This will ensure a higher B-value when the checking is repeated.

Nevertheless, to avoid this problem it is important to take care of all the lines that are connected to the sample by fully saturating them. Once the back pressure is used for increasing pore pressure it is important to manage the gauge very carefully to avoid undesirable volumetric strains. LVDT has to be very straight and the load piston has to be released very slowly to keep small displacements.

4.6.6.2. *Some issues during testing*

1. Leakage of the sample or the chamber can be a troubling situation. After sample is completed, leakage can be checked by closing the valve that conducts the vacuum, the value can be observed in the computer. If there is no leakage, the pressure will remain stable after closing the valve, however if the pressure starts dropping there is leakage. There are several causes: poor attachment of the membranes to the pedestal and the cap, deterioration of the lines that connect the sample, deterioration of the T-valves in the pedestal or the cap, and even poor connections of the sample to the base. However, the most common cause is the existence of pinholes or scratches in the membrane, this can be checked by applying water pressure inside the membrane and once the pinhole is located it can be sealed with silicon.
2. Saturation. Fully deaired water is essential to obtain good saturation; hence, if after 24 hours the water still has bubbles it should remain vacuuming until they disappear. The volume of water that has to go inside the sample during saturation should be around twice the sample's volume; nevertheless, when the fines content is greater than 40% it is important to use more water even 3 or 4 times the sample's volume to achieve full saturation. All the lines must be properly saturated before starting this procedure to avoid air getting inside the sample.
3. To always achieve acceptable B-values it is important to pass enough water through the sample, to saturate the lines that are connected to it and to control volumetric and axial strains by carefully managing the devices that measure those values. The chamber has to be well fixed to the base and all pressures should be increased very slowly.

4. Before starting saturation, vacuum in the chamber and in the specimen have to increase slowly to avoid large effective stress or deformation in the sample and effective stress has to be constant during the whole process. At the end of saturation, pressures should be increased slowly, at a rate of about 3 kPa/min.

4.7. Consolidation tests

After sample preparation, all samples were isotropically consolidated to an effective confining pressure of 100 kPa for 1 hour. Other samples were confined to confining stresses lower than 100 kPa, as 50 and 36 kPa.

The stress conditions during consolidation in a cyclic shear device are shown in Figure 4.19.

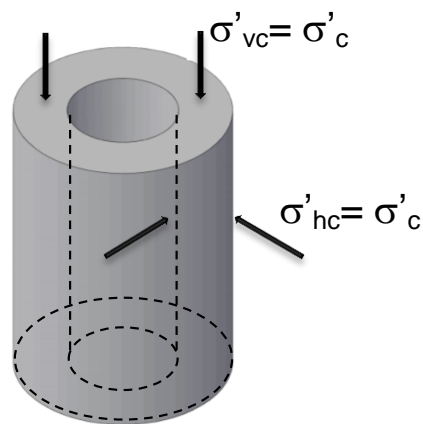


Figure 4.19. Consolidation in a hollow cylinder torsional device

One important factor to understand the effect of different fines contents is the amount of volumetric strain during consolidation. Volumetric strain was measured during this process to compute the coefficient of volume compressibility, m_v , as:

$$m_v = \frac{\Delta P}{\varepsilon_{vol}}$$

Figure 4.20 shows a typical result of the volumetric strain measured during consolidation.

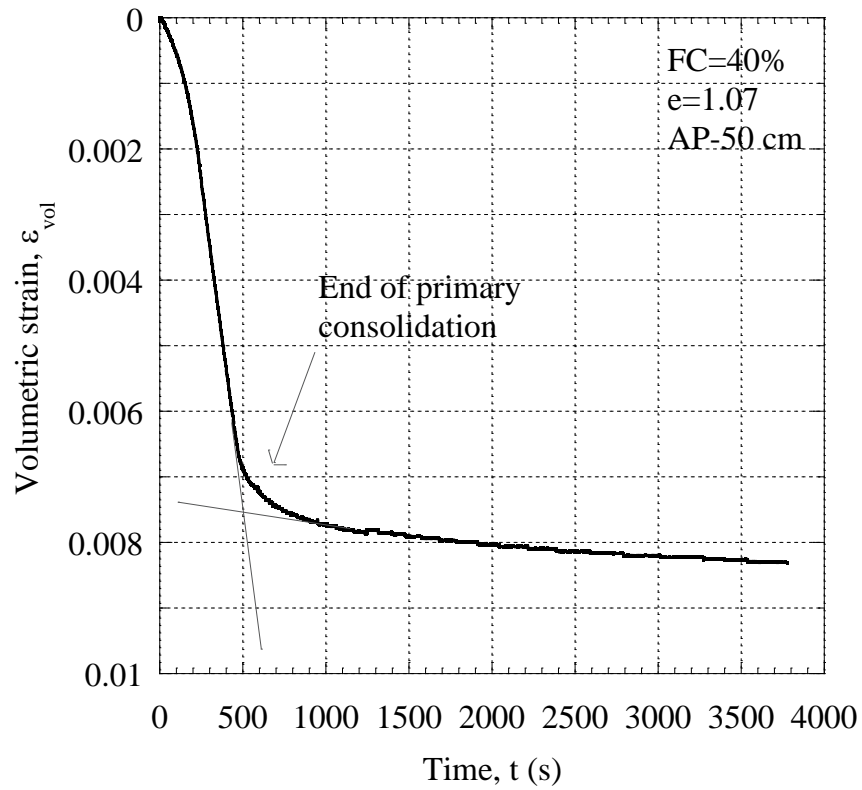


Figure 4.20. Volumetric strain during consolidation

4.8. Monotonic tests

After isotropically consolidated the samples to either 100 or 50 kPa, a torsional shear was applied in a monotonic way to measure the static response of Tokyo Bay sand.

Figure 4.21 shows some typical results of the monotonic tests, for strain-hardening behavior (FC=0%) and plastic stress response (FC=50%).

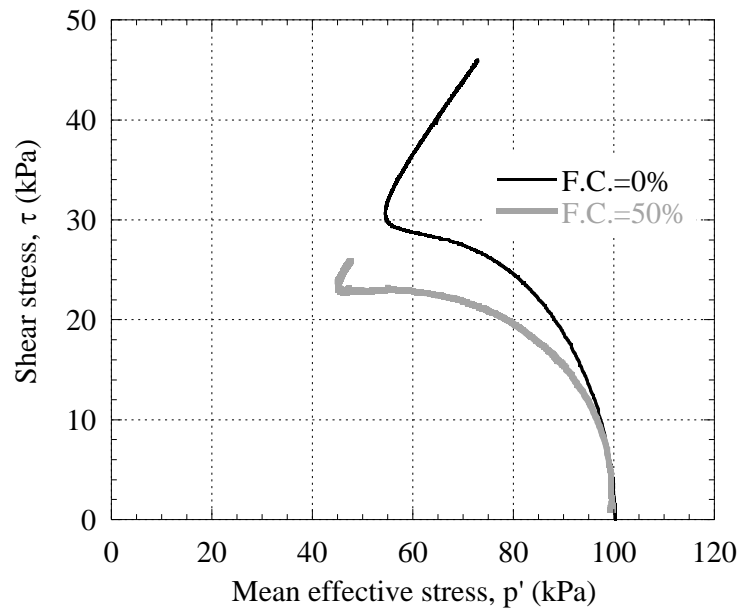
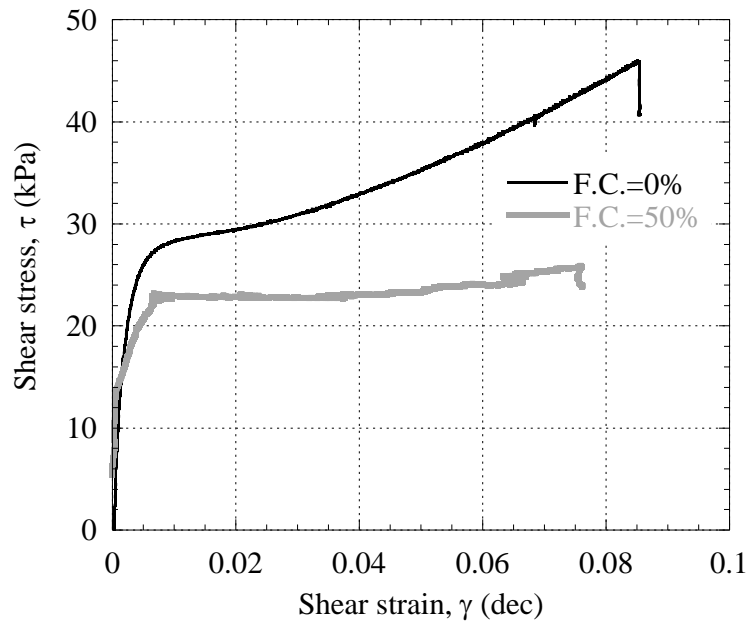


Figure 4.21. Monotonic test sample results

4.9. Cyclic shear tests

After consolidation, cyclic shear test were performed at 100 kPa. This test was run under undrained conditions and consisted of applying a selected shear stress.

Figure 4.22 shows the conditions during the application of cyclic shear stress in a hollow cylinder torsional device.

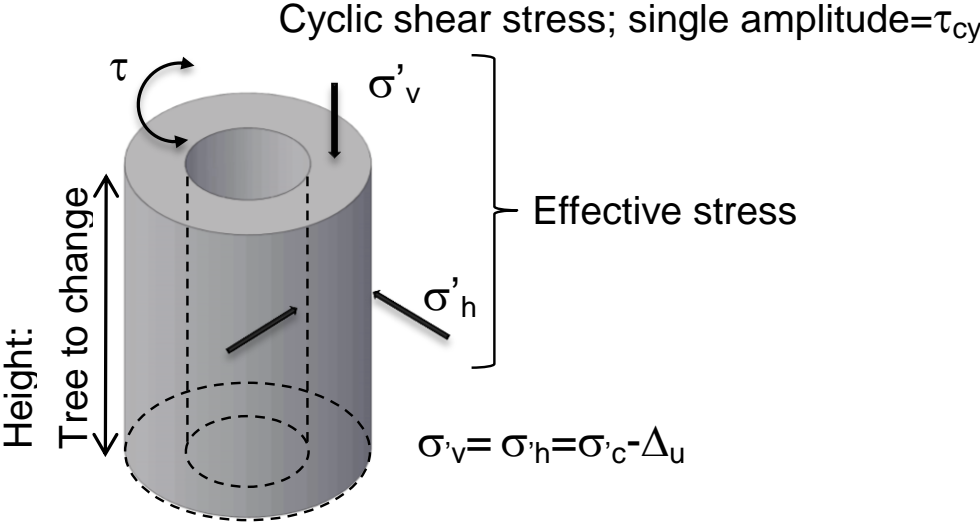


Figure 4.22. Stress conditions during cyclic shear tests

In Figure 4.23 a typical example of cyclic loading is shown. The stresses and strain measured from applying a cyclic shear stress of 15 kPa to a FC=0% sample with void ratio, $e=1.29$, are depicted. In the first figure it is observed the stress-strain curve until shear strain reaches 10% in the negative direction. The second curve is the effective stress paths, where the loss in effective stress is observed until initial liquefaction is observed, when the excess pore pressure ratio, r_u , reaches 1. Where r_u is defined as:

$$r_u = \frac{u_i - u_0}{p'_0}$$

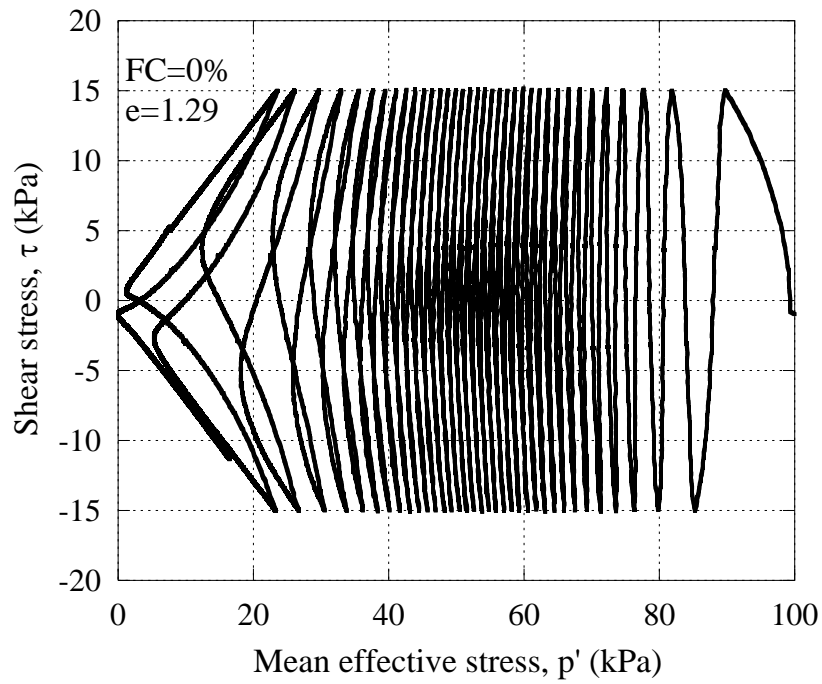
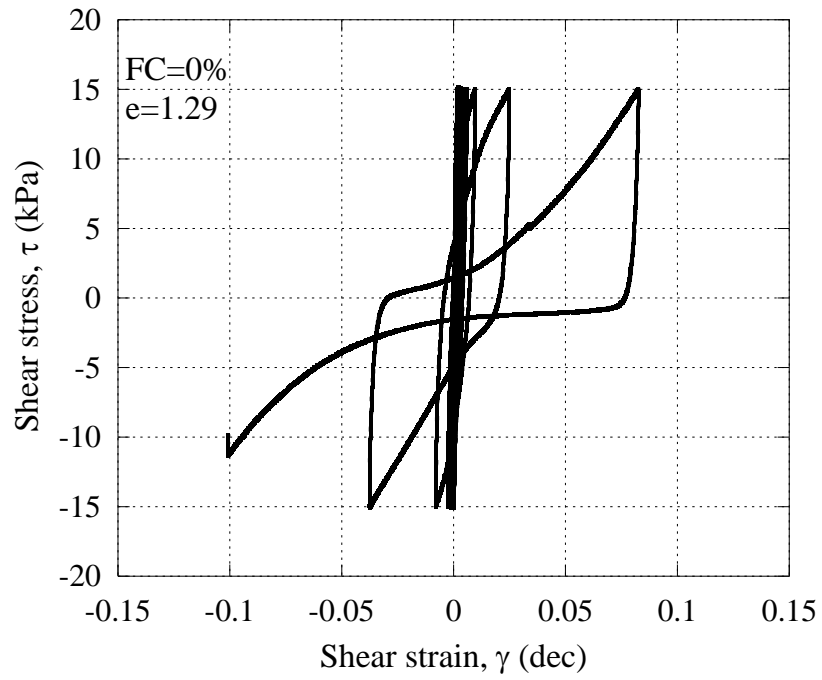


Figure 4.23. Typical stress-strain curves and effective stress paths during cyclic loading

Chapter 5

ANALYSIS OF

EXPERIMENTAL RESULTS

Chapter 5. ANALYSIS OF EXPERIMENTAL RESULTS

Results of the tests explained in Chapter 4 are described and analyzed in the present chapter. Three different groups of tests were conducted, the first two according to the height of fall and the third at the same coefficient of volume compressibility:

1. Air pluviation with height of fall 5 cm (AP-5 cm) and 30 cm (AP-30 cm)
2. Air pluviation with height of fall 50 cm (AP-50 cm)
3. Same coefficient of volume compressibility (Smv)

The experimental program includes consolidation tests, undrained cyclic shear, undrained monotonic shear and post-liquefaction loading. Figure 5.1 depicts the load program for cyclic shearing while Figure 5.2 presents the monotonic shearing.

It should be remarked that all samples were consolidated to 100 kPa and then, for cyclic loading, sheared under uniform shear stress amplitude with different values: 25, 20, 18, 16, 15 and 13 kPa. This ensured that different cyclic stress ratios were obtained for drawing liquefaction curves.

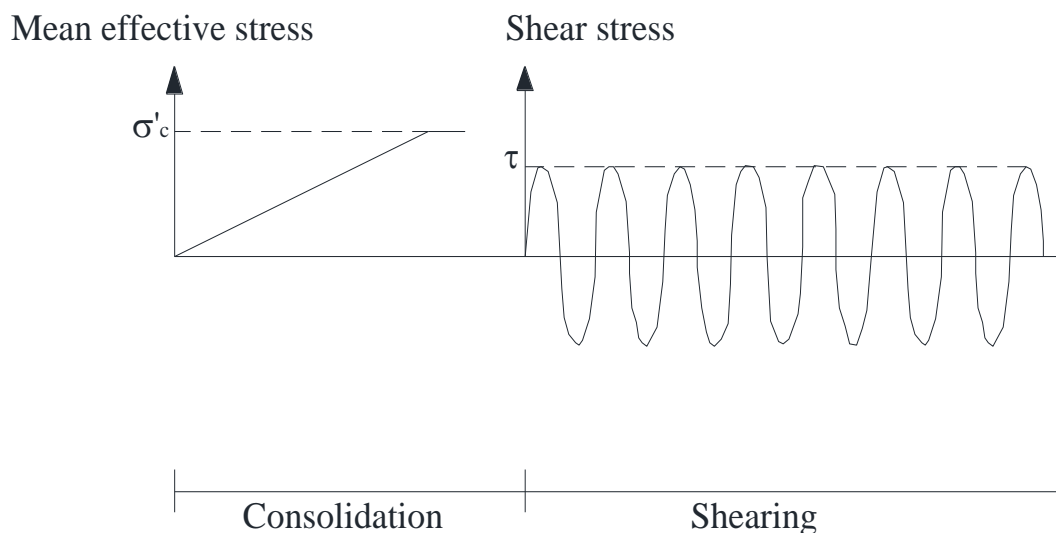


Figure 5.1. Load scheme for cyclic loading

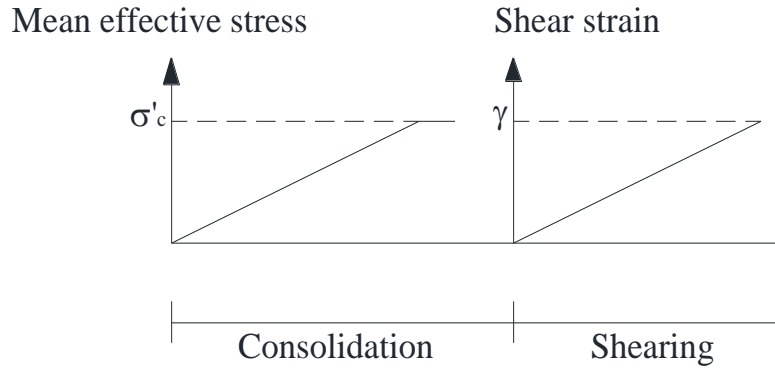


Figure 5.2. Load scheme for monotonic loading

5.1. Tests formed by air pluviation

As stated in Chapter 4, air pluviation was selected as the reconstitution method in this dissertation. When testing sand with fines, it is important to ensure uniformity and this method allows for an acceptable level of uniformity as compared to water deposition methods. Although it could be argued that the velocity during free fall for fine particles is smaller than for coarser grains, this might be overlooked given the repeatability and the advantage of comparing samples at the same compaction energy.

Moreover, this methods allows for recreating what would be a natural deposition of sand with different fines contents.

One of the main concerns was the uniformity in samples with fines. To verify this, samples were formed by AP-5 cm and AP-50 cm, saturated using the double vacuum procedure and consolidated to an effective confining pressure of 100 kPa. Then, samples were removed from the hollow cylinder torsional device, they were cut into three pieces and air dried. The pieces were then sieved to compare their grain size distribution to the original soil used for the sample. In Figure 5.3, the comparison for AP-5 cm can be seen while Figure 5.4 shows the distribution for AP-50 cm.

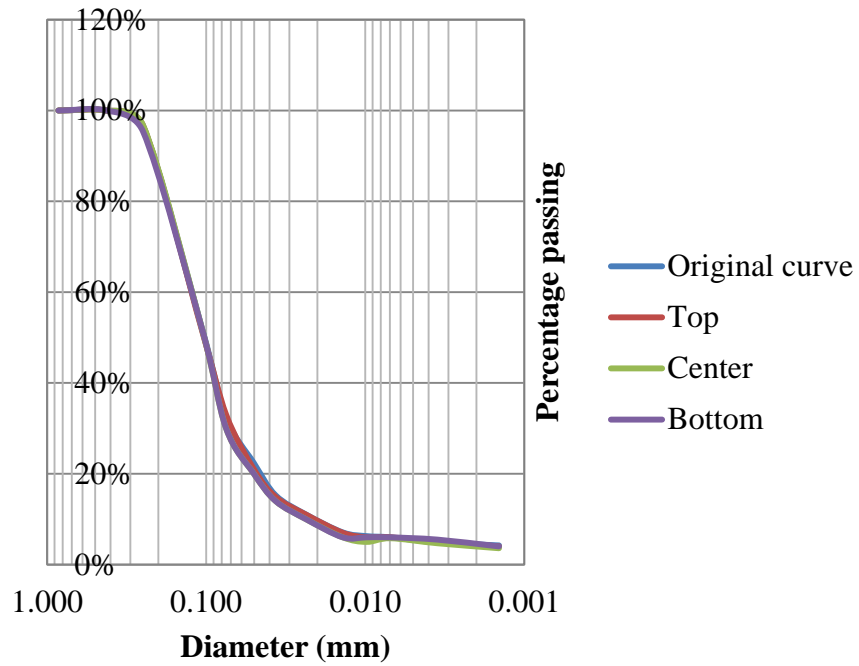


Figure 5.3. Uniformity of FC=30% sample for AP-5 cm

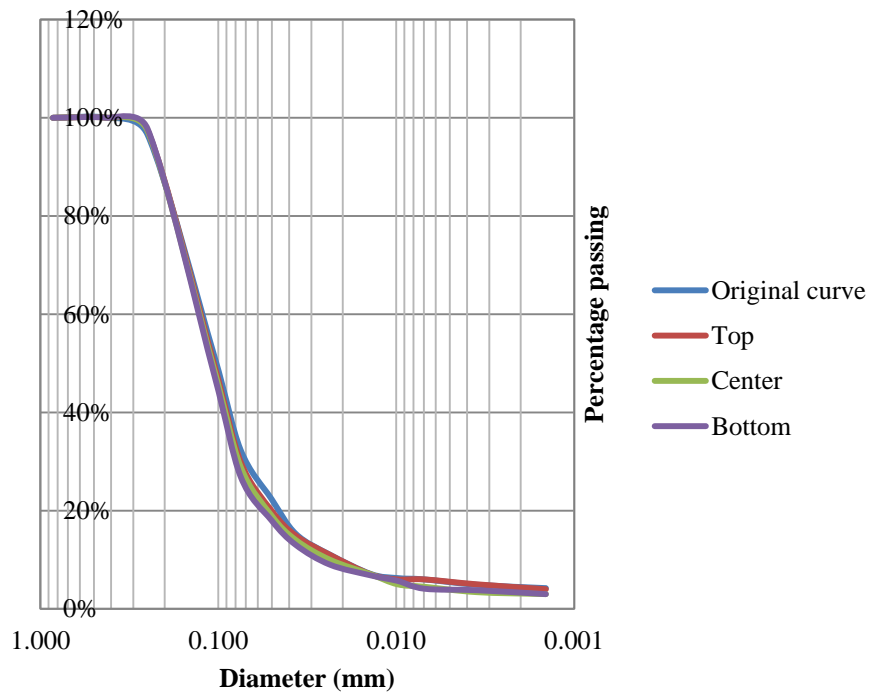


Figure 5.4. Uniformity of FC=30% sample for AP-50 cm

The grain size distribution curves are very similar for AP-5 cm, which proves that using air pluviation can provide uniform samples, even for 30% of fines content, where the combination between fines and sand can be very unstable.

Although some variations are observed in the grain size distribution for AP-50 cm, fines content only changes from 30% to 28 or 27% which is still acceptable considering that the three parts exhibit a similar distribution. This discrepancy can be due to the difference in velocity of fall of the particles; it is observed that in the top part, there are slightly more fines than in the center and bottom parts. Nevertheless, the distribution is still satisfactory for aims of comparison with different fines contents.

The void ratios for samples made by air pluviation, AP-5 cm and AP-50 cm, are shown in Figure 5.5. It is observed that the trend followed by different fines contents is similar to the curves for maximum and minimum void ratios. While the samples prepared by AP-5 cm show very large void ratios, samples prepared by AP-50 cm show lower values, especially for FC= 30, 40 and 50%. Void ratios for 80% are very similar for both heights of fall, this showed that change in height of fall has a large influence in clean sands and sands with small amount of fines, but barely affects the density of larger fines content. The fact of using dry samples is also an important factor to be considered while pursuing a large range of void ratios, which can be more easily obtained by moist tamping (Ishihara 1993). However, the scope of this work is more focused on the trend of the behavior of loose sands and the void ratio ranges obtained are adequate for this purpose.

Later, the use of slurry deposition, the use of slurry deposition which is a method that allows for wet deposition and uniformity of silty sands, is described.

However, as shown by Zlatovic and Ishihara (1995), who used different sample preparation methods, the trend of behavior expected will be similar when using air pluviation or water deposition, although the liquefaction resistance values will be higher for wet deposited samples given the forces developed by water.

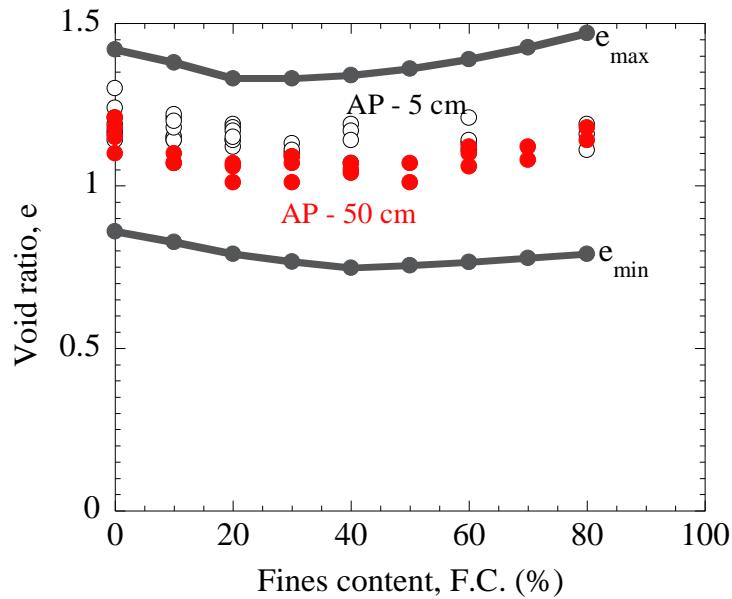


Figure 5.5. Void ratio for AP-5 and 50 cm samples

Although the use of relative density is not appropriate for fines content beyond the threshold fines content, given that most methods for calculation of minimum and maximum void ratio are restricted to less than 30% of fines, relative density was computed to have a reference of the values. In Figure 5.6 the range of relative density for AP-5 cm is shown. As noted, the variation in relative density can occur even from similar values of void ratio, because of the difference in void ratio range ($e_{max}-e_{min}$).

It is also observed that the range of void ratios and relative densities is actually small and for practical terms it would be safe to consider that values are similar, however, some decrements and increments are observed as fines content changes.

From this point, there will be no references as relative density or void ratio to avoid confusion regarding the parameter of comparison. However, when considered necessary, values will be provided just to compare with other researchers or to give an idea of the values of density used for some samples.

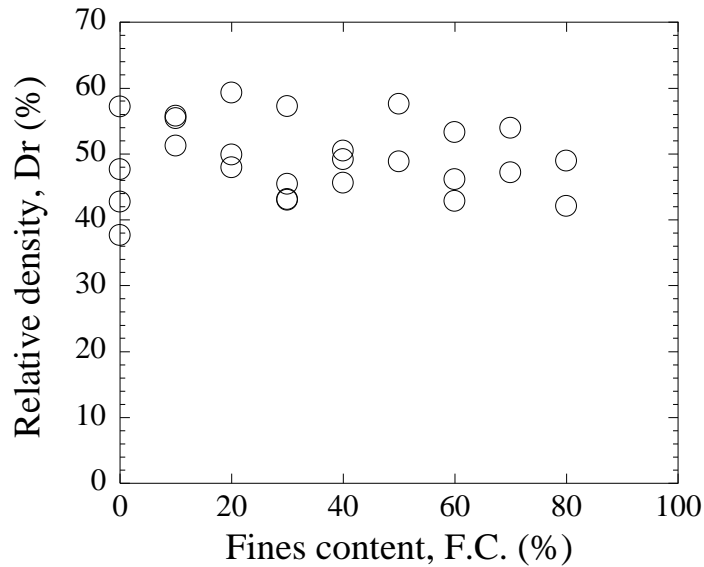


Figure 5.6. Relative density for AP-5 cm samples

5.2. AP – 5 cm

5.2.1. Consolidation

Once the sample was saturated, consolidation tests were carried out. During this process effective stress, pore pressure, axial strain and volumetric strain are measured (Figure 5.7).

Figure 5.8 shows one example of the measured volumetric strain for different fines contents. It is observed that the more pronounced slopes are those for 20 and 60% fines content. The curves for 40 and 30% show less volumetric strain. The 0, 80 and 10% curves show a medium response. It is important to remark that the initial confining stress for the samples is 30 kPa, except for 80% which sample was confined to 20 kPa. This curve is presented in this graph only for the sake of showing the two initial confining pressures used at the beginning of this experimental procedure. Later, the initial confining stress was set to 20 kPa for samples consolidated at 50 kPa, and 30 kPa for the samples consolidated at an effective confining stress of 100 kPa.

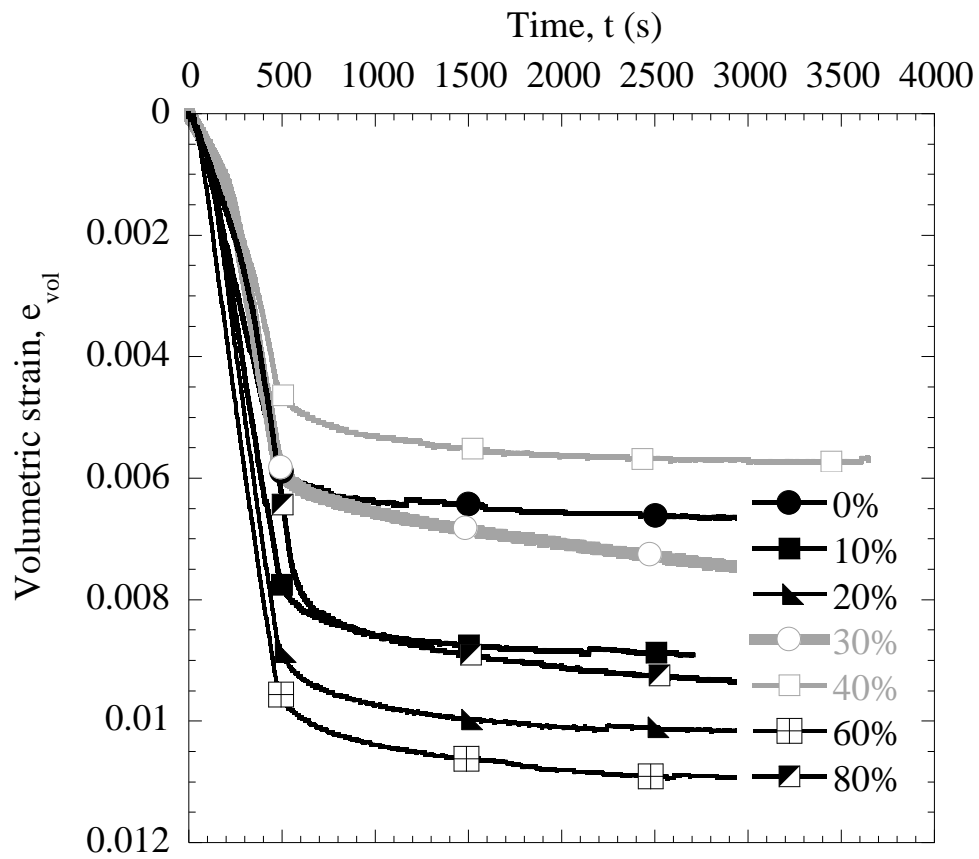


Figure 5.7. Volumetric strain during consolidation

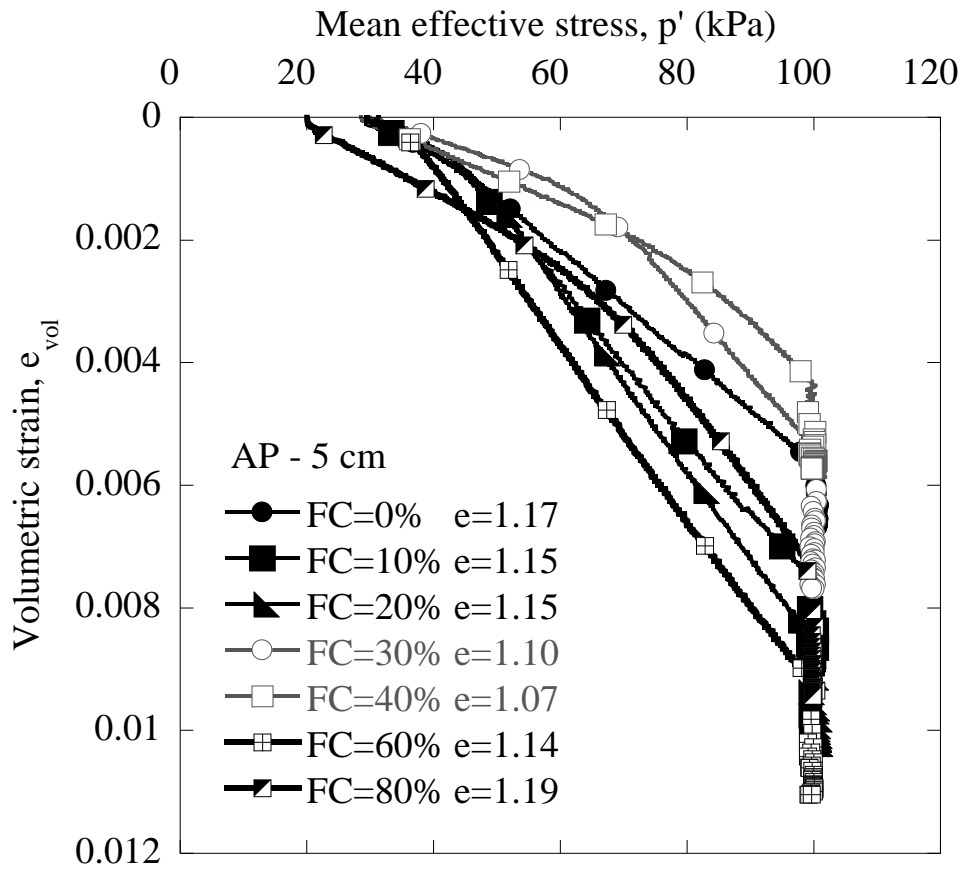


Figure 5.8. Volumetric strain and mean effective stress during consolidation AP-5 cm

One of the most important parameters for this thesis is the coefficient of volume compressibility, m_v , which was calculated as the increment in confining pressure over the volumetric strain measured during consolidation, as:

$$m_v = \frac{\Delta P}{\epsilon_{vol}}$$

Where ΔP is the increment in effective confining pressure. Samples were initially sustained under 20 or 30 kPa during preparation and saturation, and then consolidated to an effective confining pressure of 50 or 100 kPa. Therefore, ΔP was calculated as the difference between the initial and the final pressures. Samples with a large amount of fines exhibit creep which is not considered for volumetric strain. To obtain the volumetric deformation,

curves as shown in Figure 5.9 are drawn to identify primary consolidation and secondary compression. Extrapolations are drawn to each phase and the intersection between both curves is considered to be the volume compressibility during primary consolidation. This is the value used for computing m_v .

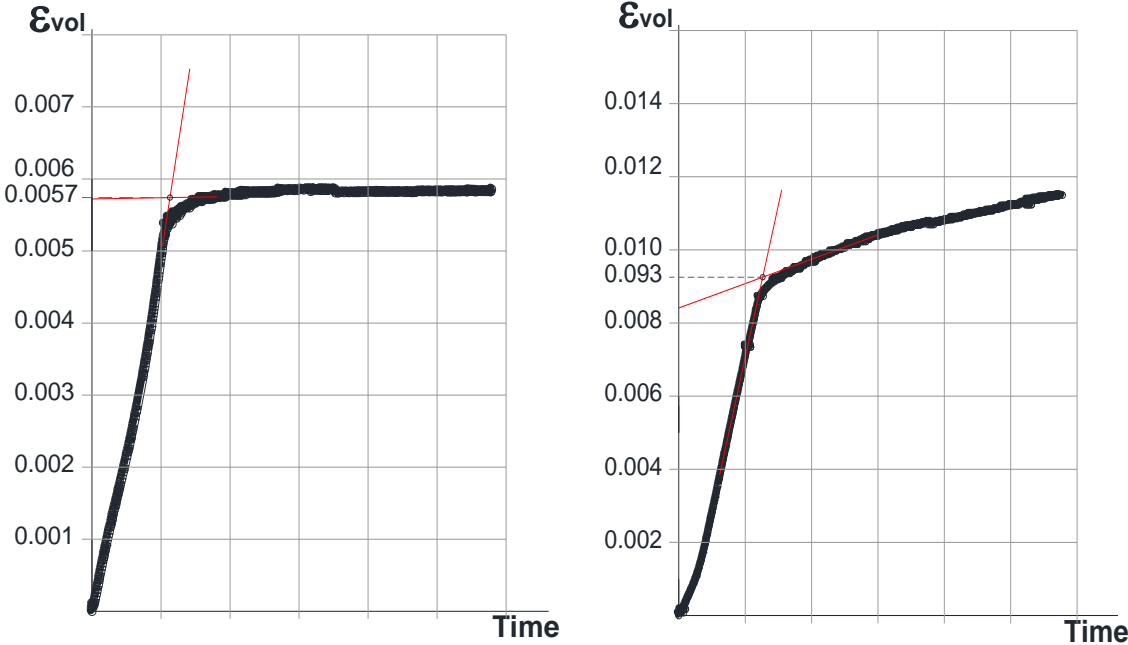


Figure 5.9. Obtaining m_v from consolidation curves

In Figure 5.10 the coefficient of volume compressibility for samples prepared through air pluviation and a height of fall of 5 cm. From 0 to 20% there is an increase in m_v , while there is a decrease from 20 to 40%. The higher values of m_v are those for the 60% fines content and then they reduce for 80%.

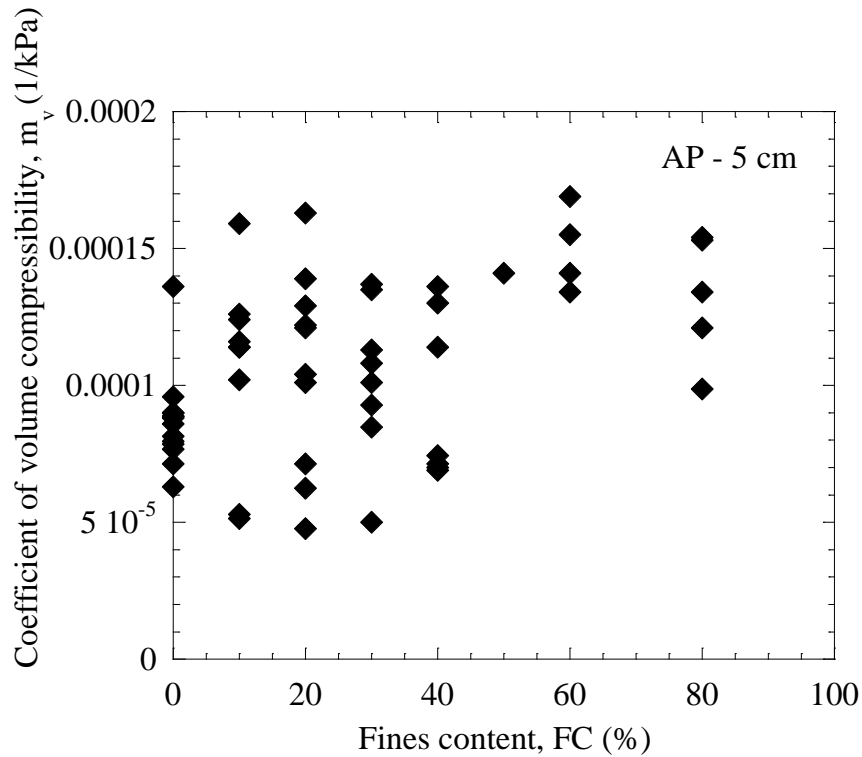


Figure 5.10. Coefficient of volume compressibility for AP-5 cm

5.2.2. Monotonic shear tests

Figure 5.11 shows the stress-strain curves and the stress path of the monotonic shear tests conducted on fines content from 0 to 60% by AP-5 cm. It can be observed that clean sand exhibits the larger resistance while silty sand depicts smaller values of shear strength. Three different groups of fines can be identified, from 0 to 20% where a decrement in shear stress can be observed as more fines are added; from 30 to 40%, both curves show similar stress paths, though the 40% sample has larger shear strength. From 50 to 60%, resistance diminishes as more fines are added. In this group the strain-hardening behavior exhibited from 0 to 40%, is switched to a constant shear stress (perfectly plastic) response. As for the stress paths, the curves from 0 to 40% initially move left toward the failure envelope, followed by phase transformation and a dilative path at a relatively constant slope. The stress paths for 50 and 60% fines content show a decrease of effective stress until the failure line. These results agree with the ones presented by Lade & Yamamuro (1997) who

performed tests on Ottawa and Nevada sands with Nevada fines at the same depositional method to obtain a quasi-natural void ratio. In all cases they found clean sand to be more resistant and liquefaction potential increased with fines content.

Table 5.1 shows the values of fines content, void ratio, relative density and peak shear strength, for monotonic tests. It is observed how peak shear strength decreases as relative density increases due to the differences in maximum and minimum void ratio for the diverse fines contents. This behavior was called “reverse” by Lade and Yamamuro (1997) given the typical results obtained when testing sand while increasing values of relative density.

Table 5.1. Relative densities and peak shear strength

FC	e	Dr (%)	Peak shear strength (kPa)
0	1.23	35	29.5
10	1.19	40	26.0
20	1.13	38	25.5
30	1.08	44	24.0
40	1.07	45	24.5
50	1.09	44	23.0
60	1.15	39	20.0

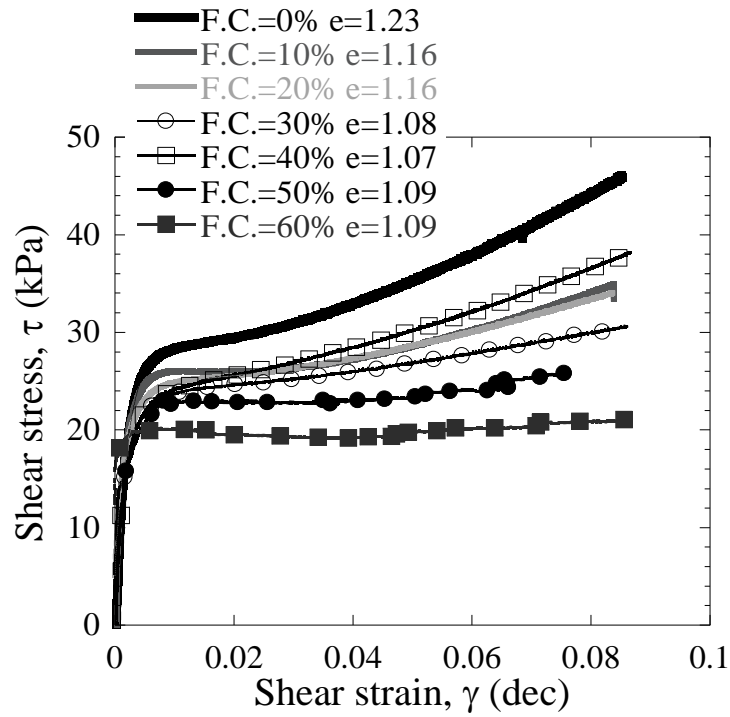


Figure 5.11. Stress-strain curves during monotonic loading for $\sigma'_c=100$ kPa

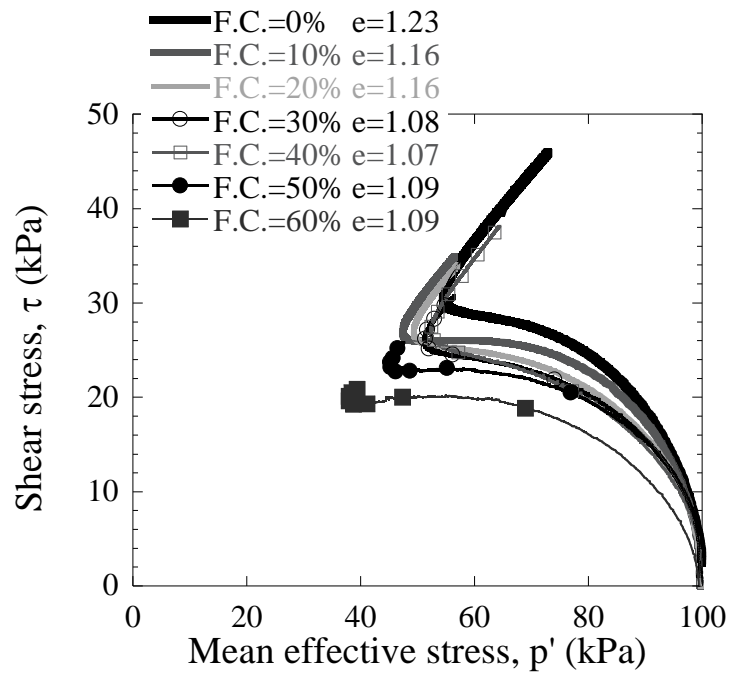


Figure 5.12. Effective stress paths during monotonic loading for $\sigma'_c=100$ kPa

5.2.3. *Stress-strain curves and stress paths*

For cyclic loading, the stress-strain curves and stress paths were also measured to observe the effects of the different fines content. Results showed that there are three different behaviors, according to their relation to the threshold fines content. Typical curves of stress-strain and effective stress paths, for a cyclic resistance ratio $CSR=0.15$ and effective confining stress $\sigma'_c=100$ kPa, are presented in Figure 5.13 for $FC=0\%$, Figure 5.14 for 30% and Figure 5.15 for 80% . These three fines contents were considered to be representative of different behaviors according to the theory discussed in Chapter 3: below the limiting fines content, from 0 to 20% there is response dominated by the sand grains, from 30 to 50% there is a transition stage between sand and fines behavior, then, above the threshold value, from 60 to 80%, the behavior seems to be dominated by the contacts along the fines. Outcomes are described considering this perspective. In the stress-strain curves it is noted that strain amplitude is in the range of -9% to 10% . It can be seen that degradation of the tangent shear modulus seems to be smaller as the fines content increases. In the effective stress paths is also observed that for the same cyclic stress ratio, it takes more cycles for the sample with 0% to develop large deformations and reach the zero effective stress state.

Samples with 30% and 80% take a smaller number of cycles to reach zero effective stress although the 80% sample does not actually reach this state. Figure 5.16 shows a clear comparison of the effective stress paths.

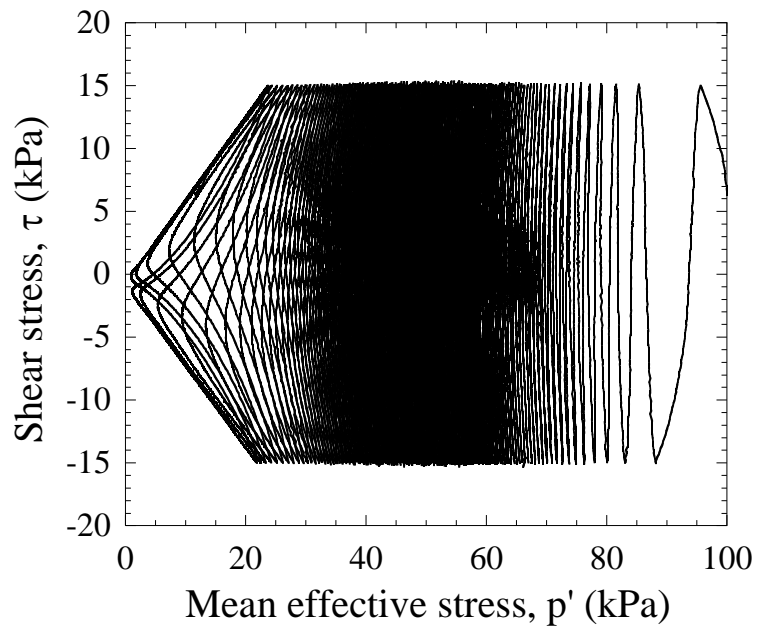
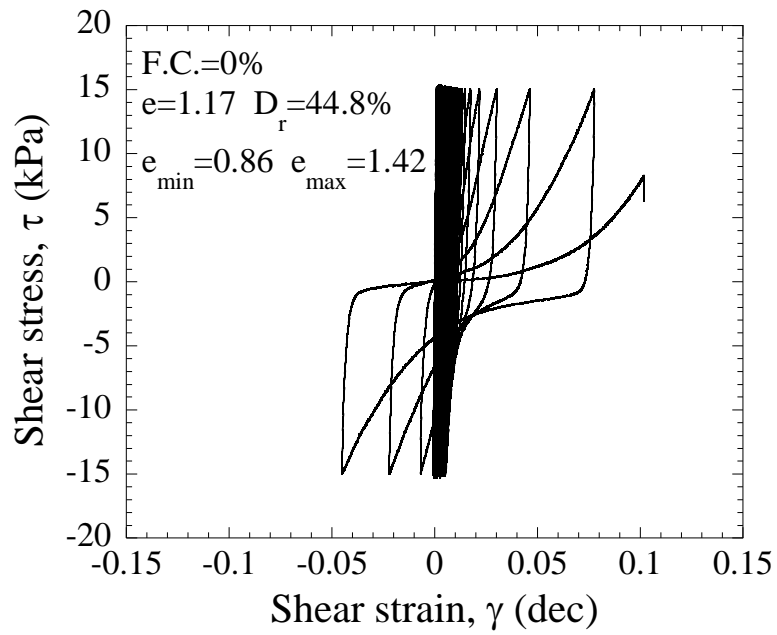


Figure 5.13. Stress-strain curves and effective stress paths for FC=0%, AP-5 cm, CSR=0.15

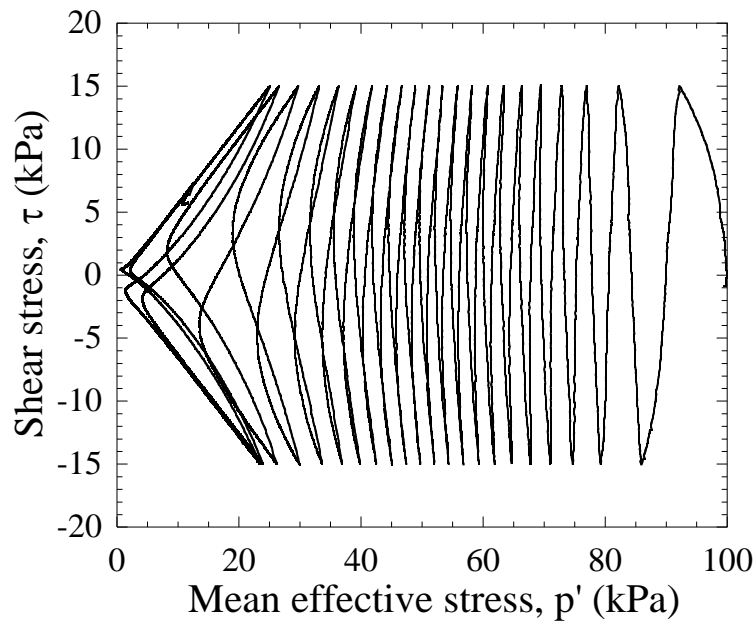
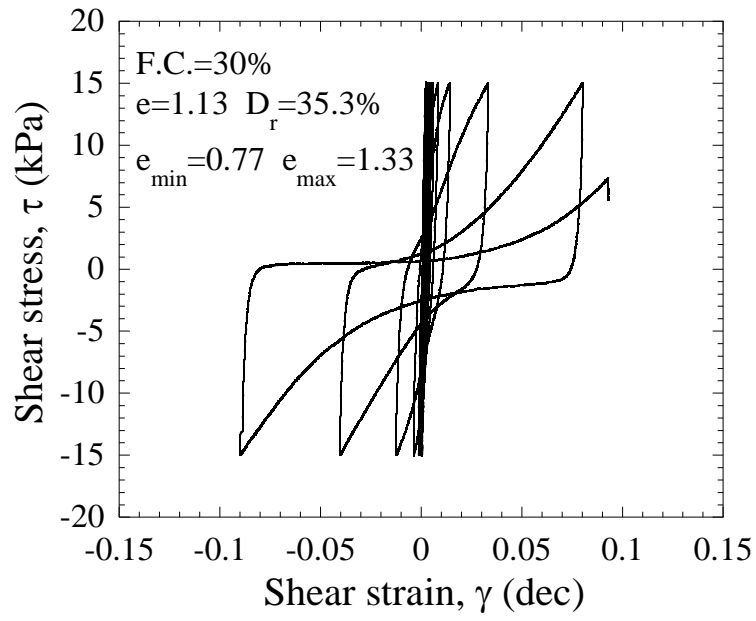


Figure 5.14. Stress-strain curves and effective stress paths for FC=30%, AP-5 cm, CSR=0.15

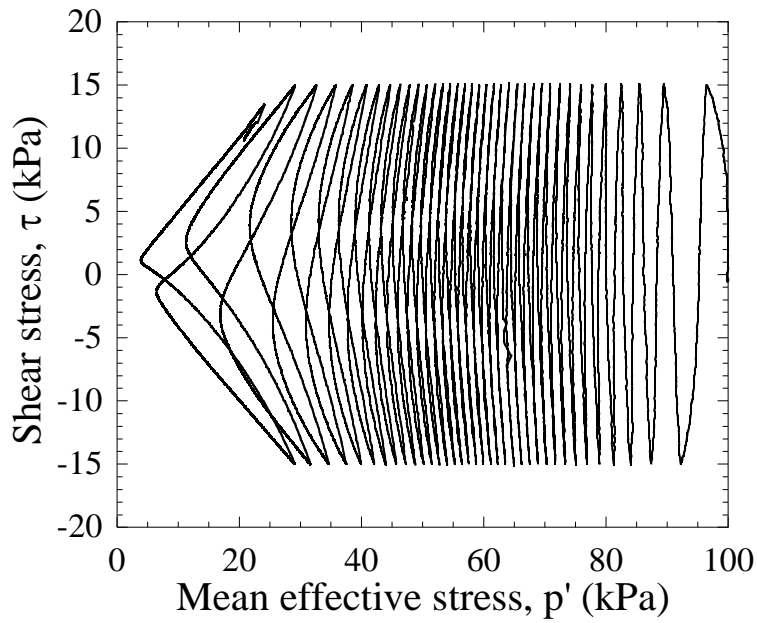
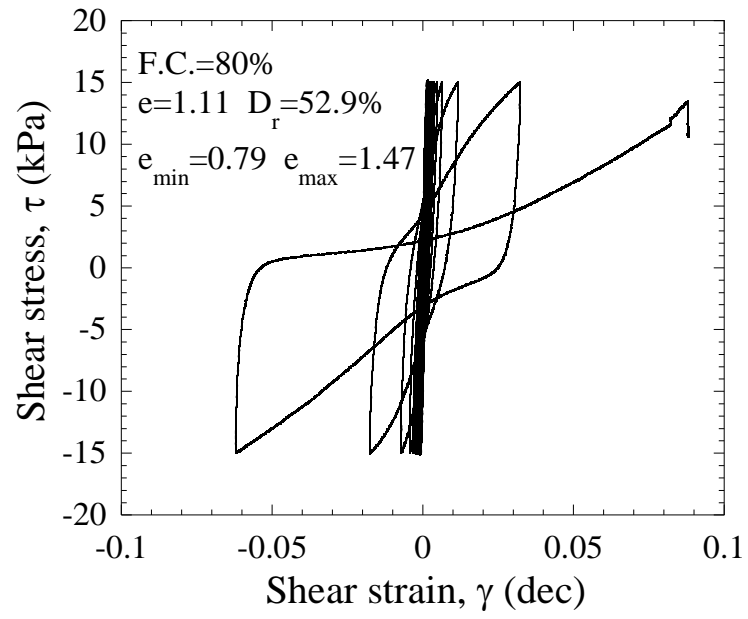


Figure 5.15. Stress-strain curves and effective stress paths for FC=80%, AP-5 cm, CSR=0.15

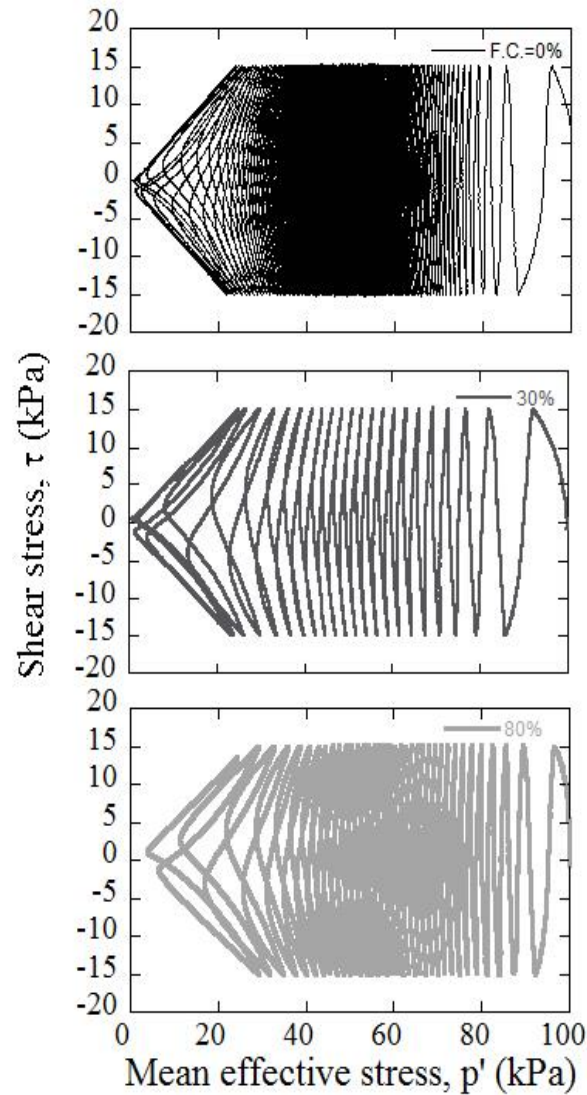


Figure 5.16. Comparison of stress paths for FC=0, 30 and 80%

The tangent shear modulus of samples formed by AP-5 cm was measured and is shown in Figure 5.17. This tangent modulus is the minimum value in the concerned cycle of stress-strain behavior and stands for the extent of decay or softening caused by pore pressure rise. Three samples were used for comparison with 0, 30 and 80% fines content for AP-5 and 50 cm. In the AP-5 cm tests, the curve of FC=0% exhibits more substantial shear modulus degradation, while FC= 80% shows less extent of degradation.

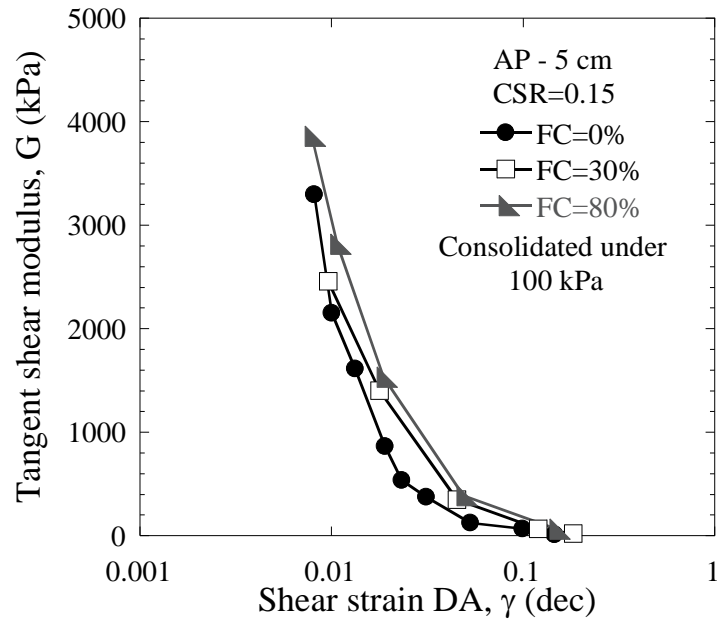


Figure 5.17. Tangent shear modulus during cyclic undrained shear for AP-5 cm

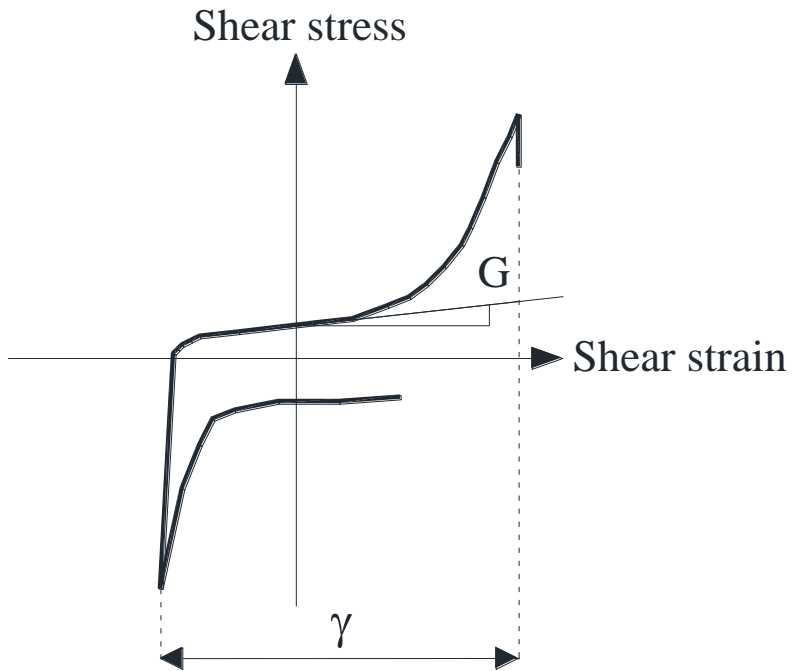


Figure 5.18. Definition of tangent shear modulus

5.2.4. Excess pore-water pressure development

Excess pore pressure build-up was also studied to understand the effect of fines. The values of 0, 30 and 80% for AP-5 cm were taken as representatives of the three groups of behavior observed. Figure 9 depicts the excess pore water pressure ratio against the number of cycles to 5% double amplitude of shear strain. The applied cyclic stress ratio for the three samples is equal to 0.15. The 80% curve rises slower than the other curves until $r_u=0.3$, then it increases rapidly in a similar rate as the 30% curve. The first curve to reach $r_u=1$ is the 30% at 22 cycles, then the 80% curve reaches $r_u=0.95$ as maximum value at 36 cycles and then the 0% curve reaches initial liquefaction at 177 cycles. Results indicate that the 0% specimen is more resistant than others. The arrangement of particles for 30% is the least stable and the excess pore pressure buildup is faster at the beginning of cyclic loading. It can be seen that there is a clear difference between the excess pore pressure ratio increase of silty specimens and clean sand.

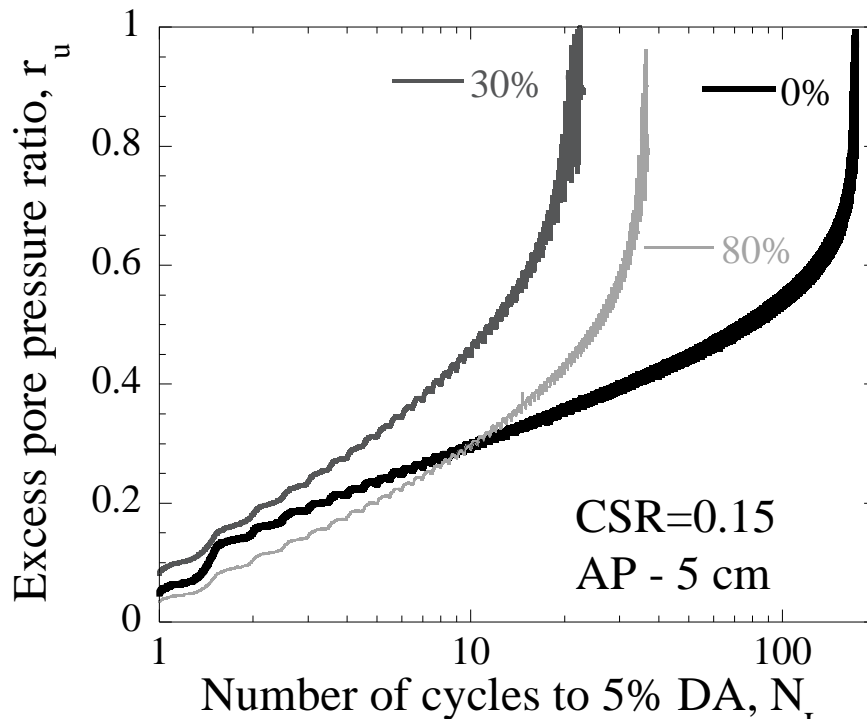


Figure 5.19. Excess pore pressure ratio for AP—5 cm

5.2.5. *Liquefaction curves*

Two criteria were used for defining liquefaction, the generation of total excess pore pressure ratio, $r_u=1$ and the 5% double amplitude of shear strain. Given the nature of loose samples, both criteria yielded similar results for AP-5 cm. Curves shown in Figure 5.20 were constructed using the criterion of 5% double amplitude of shear strain for liquefaction.

From the series of tests it can be seen that there are three noteworthy groups within the fines content, from 0 to 20% where the resistance drops as the fines content increases; from 30 to 40%, where there is the threshold of the maximum amount of fines that can be fit in the sand matrix voids, there is a rise in resistance as fines content augment. Finally the samples with large amount of fines, from 60 to 80%, where the sand loses contact between grains and each grain is surrounded by silt which controls the response of soil, exhibit a slight increase in resistance when more fines are added.

In these curves, three different behaviors can be identified: sand-like, intermediate and clay-like. Being sand-like and clay-like, terms that refer to a response similar to that which sand or clay will exhibit. It can be observed that the clean sand specimen has larger resistance than the samples that have fines.

This agrees to the results obtained previously with monotonic tests and to the results obtained by researchers who have used the same approach for sample formation (e.g., Lade and Yamamuro 1997; Zlatovic and Ishihara 1995)

However the response of samples formed by sand and high fines content as 60 and 80% are quite different from what it would be expected after finding the first two groups of behavior. As explained in Chapter 3, not many researchers have conducted tests on such high values of fines content and following the previous results, it would be expected that FC=60 and 80% will have greater resistance than samples of FC=30 or 40%.

In the next set of tests, intermediate fines contents as 50 and 70% will be tested to prove the results found by AP-5 cm.

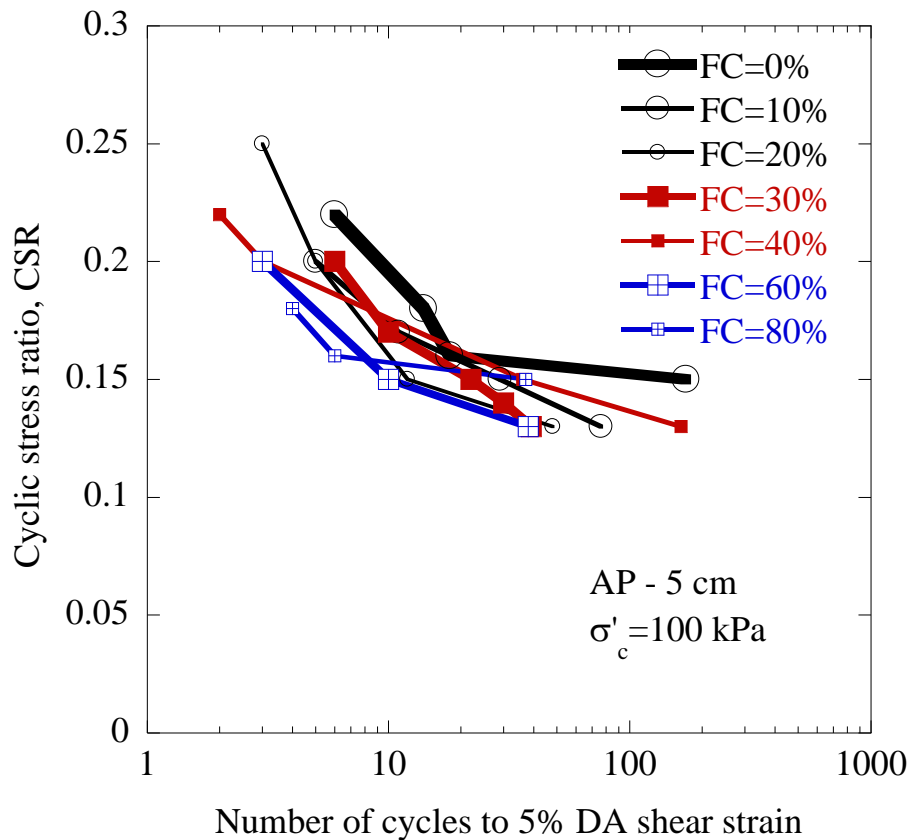


Figure 5.20. Liquefaction curves for AP-5 cm

Cyclic resistance ratio was defined as the cyclic stress ratio for 20 cycles of 5% of double amplitude shear strain. Although some other researchers have found 7.5% of double amplitude as the most accepted criteria for hollow torsional shear tests, since samples are loose, the results obtained by the criteria of 5%, 7.5% and even $r_u=1$ are similar and the same cyclic resistance ratios are obtained.

The variation of CRR_{20} with fines content is shown in Figure 5.21. It is observed that cyclic resistance ratio decreases from 0 to 20% fines content. There is a slight increase of resistance from 30 to 40%. Later there is a major reduction in the group of larger fines content from 60 to 80%.

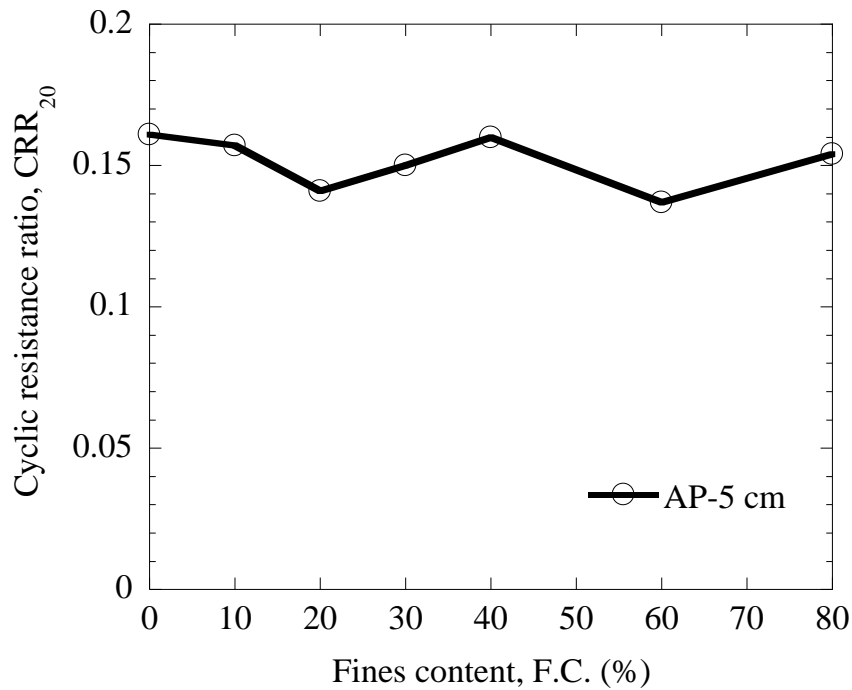


Figure 5.21. Cyclic resistance ratio and fines content for AP-5 cm

Using the values of cyclic resistance ratio, the variation of CRR_{20} and m_v was observed considering the fines content (Figure 5.22). It is observed that the coefficient of volume compressibility has an inversely proportional relation with the cyclic resistance ratio, as expected. When observing the effect of fines content on the relation between the liquefaction resistance and the volumetric strain is still difficult to discern what is the actual influence, given that the greater values of m_v were obtained for the FC=60% samples, while the smaller values were found for FC=0%. In this regard, there is not a conclusive effect of the fines content, but it can be observed that values obtained after liquefaction but before shearing are actually related to those obtained after shearing. This will be useful for further discussions in the following sections.

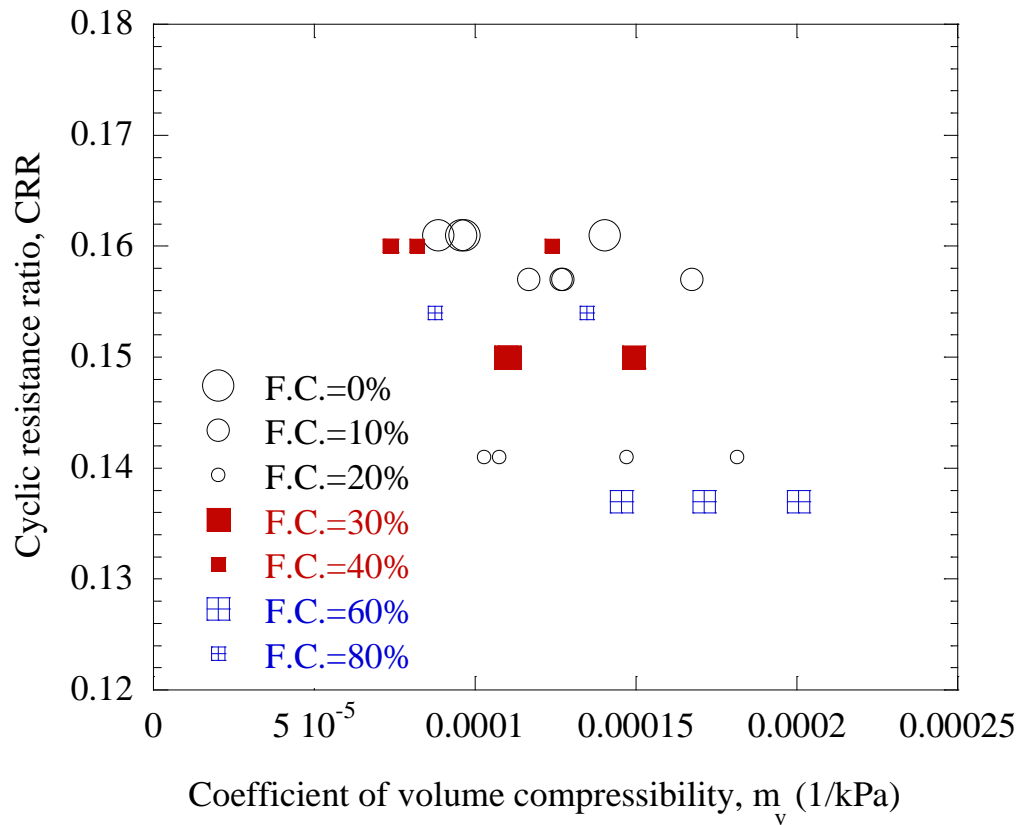


Figure 5.22. Variation of CRR_{20} with m_v for AP-5 cm

5.3. AP – 30 cm

In order to increase the density of samples, height of fall was first increased to 30 cm. Nevertheless, when it was observed that density did not increase significantly, height of fall was increased to 50 cm. For this reason, only tests with fines content FC=0, 10, 20 and 30% were conducted for AP-30 cm.

5.3.1. Consolidation

Figure 5.23 depicts the volumetric strain developed during consolidation for four samples: 0, 10, 20 and 30%. It is observed that volumetric strain is greater as fines content grows.

The stress-strain curves during consolidation are shown in Figure 5.24. For samples formed by AP-30 cm, they were confined initially to 30 kPa and then consolidated at 100 kPa.

After consolidation, coefficient of volume compressibility was computed considering the volumetric strain measured during primary consolidation, values are shown in Figure 5.25.

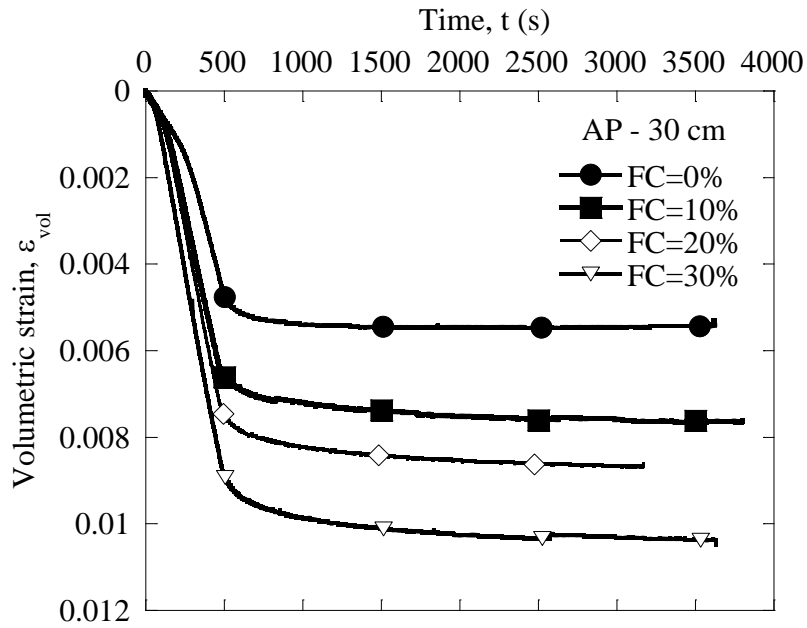


Figure 5.23. Volumetric strain during consolidation

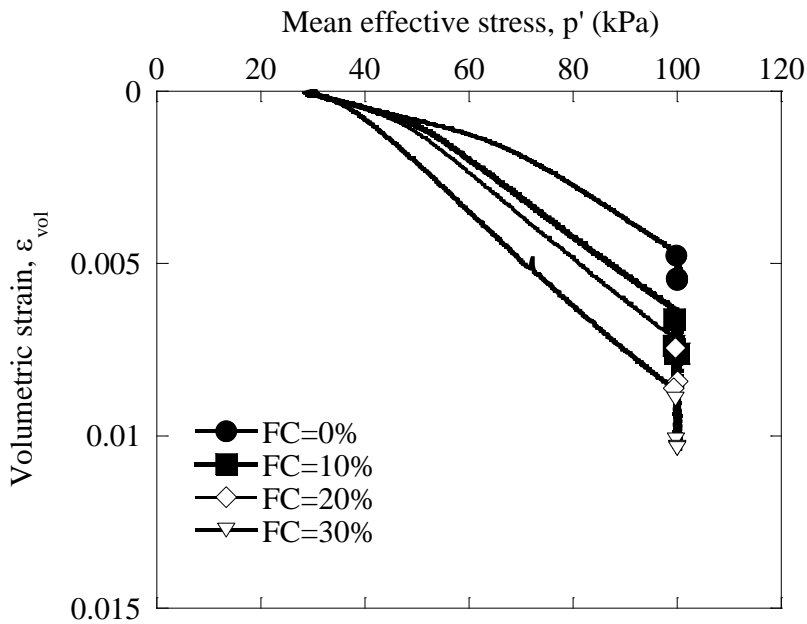


Figure 5.24. Volumetric strain and mean effective stress during consolidation AP-30 cm

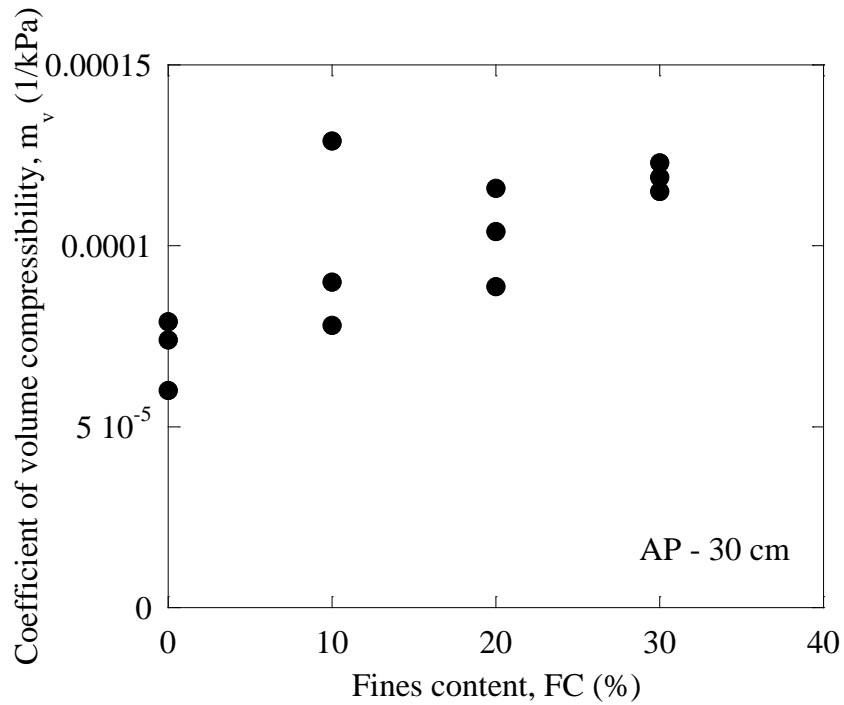


Figure 5.25. Coefficient of volume compressibility for AP-30 cm

5.3.2. *Stress-strain curves and effective stress paths*

Sample stress-strain curves and effective stress paths measured for FC=0, 10, 20 and 30% are shown from Figure 5.26 to Figure 5.29.

It can be observed that the stress-strain curves for FC=0% are different compared to those obtained by AP-5 cm. This was expected since the height of fall was increased in 6 times the previous value. However as fines content goes from 10 to 30% the effect of the increase in height of fall is reducing.

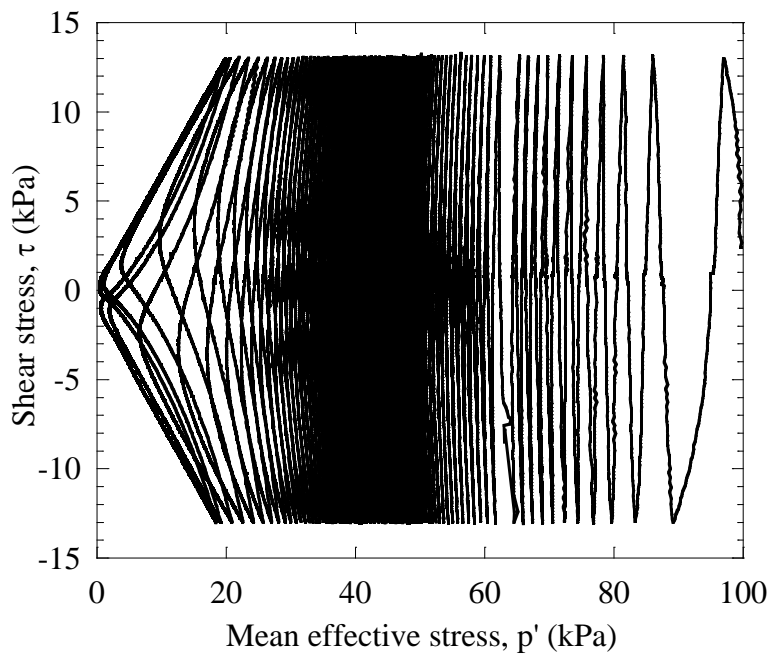
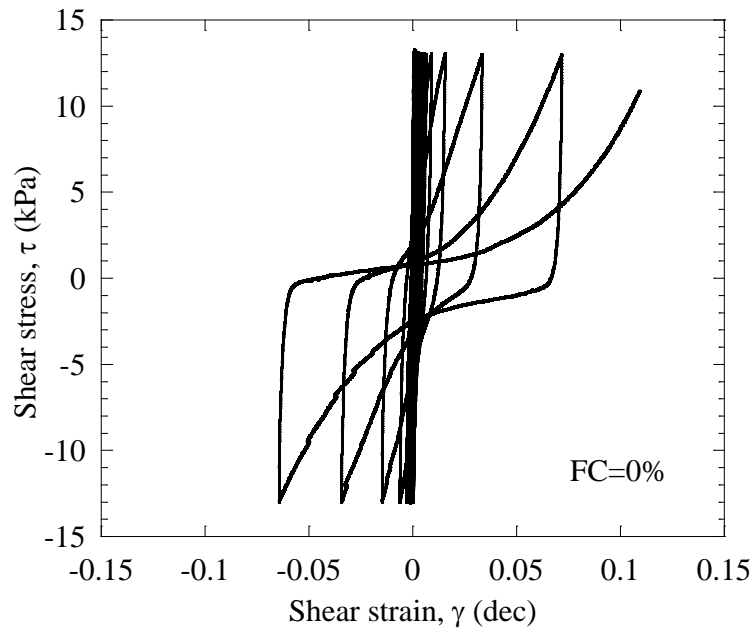


Figure 5.26. Shear-strain curves and effective stress paths for FC=0% and AP-30 cm

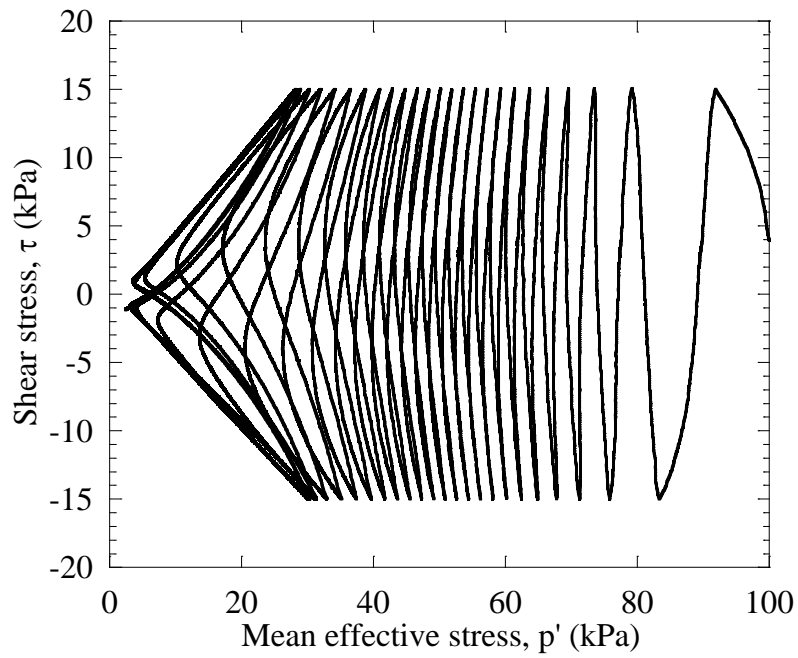
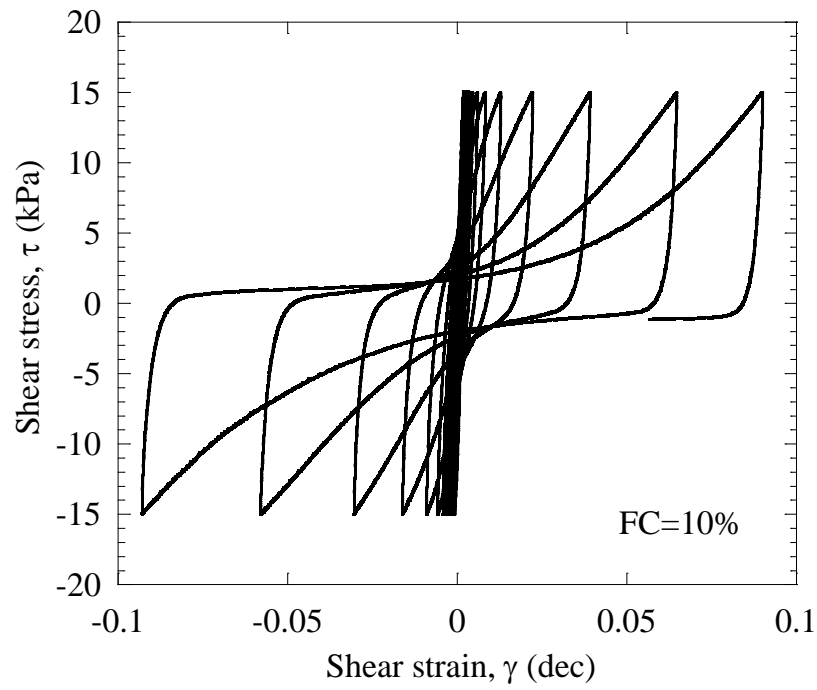


Figure 5.27. Stress-strain curves and effective stress paths for FC=10 and AP=30 cm

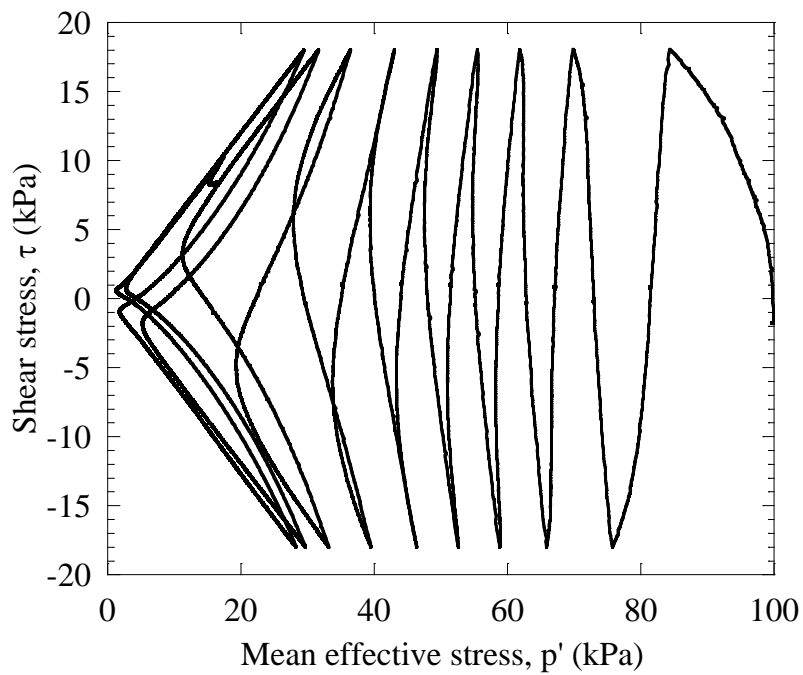
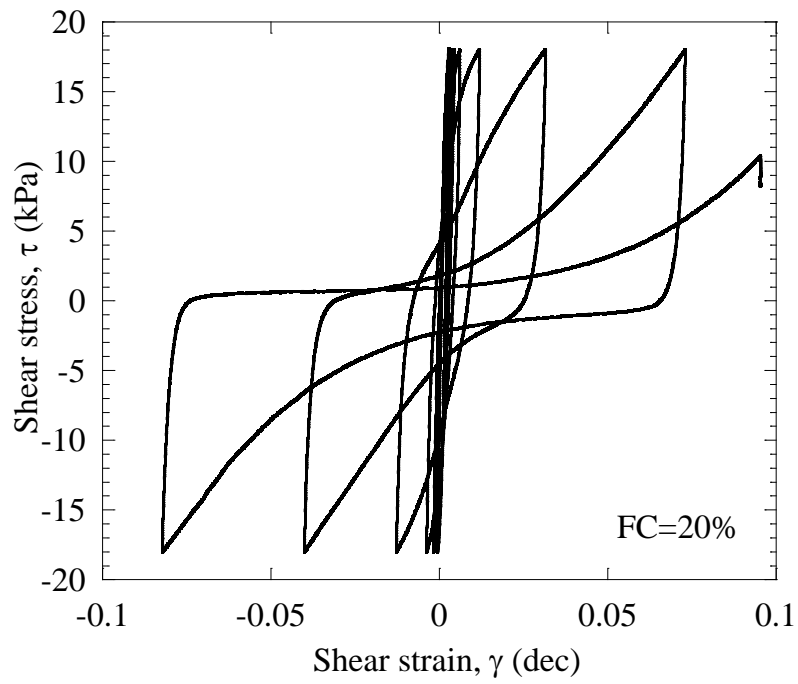


Figure 5.28. Stress-strain and effective stress path for FC=20% and AP-30 cm

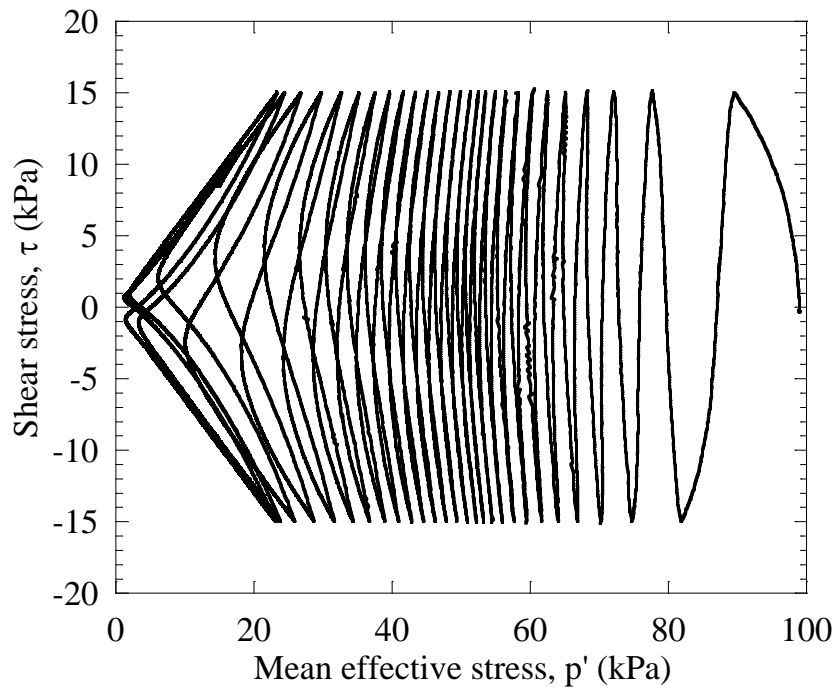
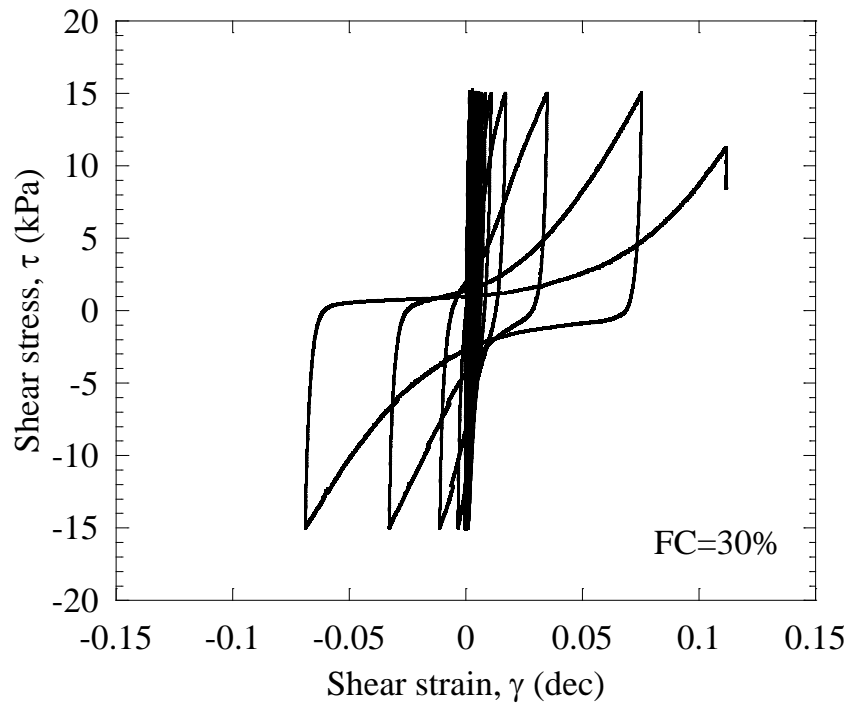


Figure 5.29. Stress-strain curves and effective stress paths for FC=30 and AP-30 cm

5.3.3. Liquefaction curves

Liquefaction curves of samples formed by AP-30 cm can be seen in Figure 5.30. It is observed that clean sand exhibits greater resistance while samples with FC= 10 and 30% have the same cyclic resistance ratio and the sample with FC=20% exhibits the lower value of cyclic resistance ratio. These liquefaction curves are consistent with the results obtained for samples formed by AP-5 cm.

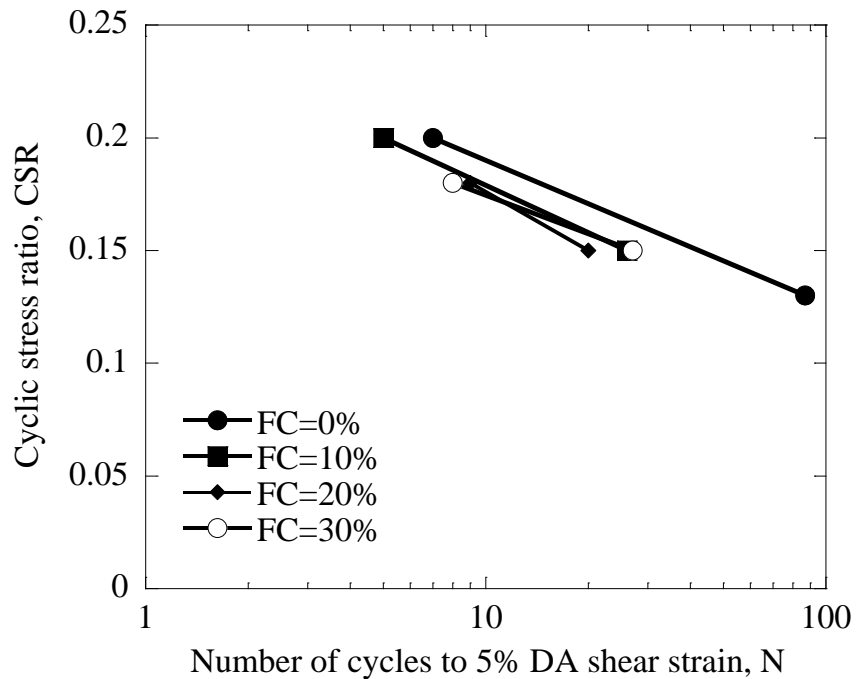


Figure 5.30. Liquefaction curves for AP-30 cm

A comparison was made between two samples with FC=30%, formed by AP-5 cm (Sample A) and 30 cm (Sample B). Figure 5.31 shows the stress-strain curves and effective stress paths for sample A while curves for sample B are observed in Figure 5.32. A similar number of cycles to 5% double amplitude is observed, although more degradation of shear modulus is exhibited in the sample formed by AP-30 cm.

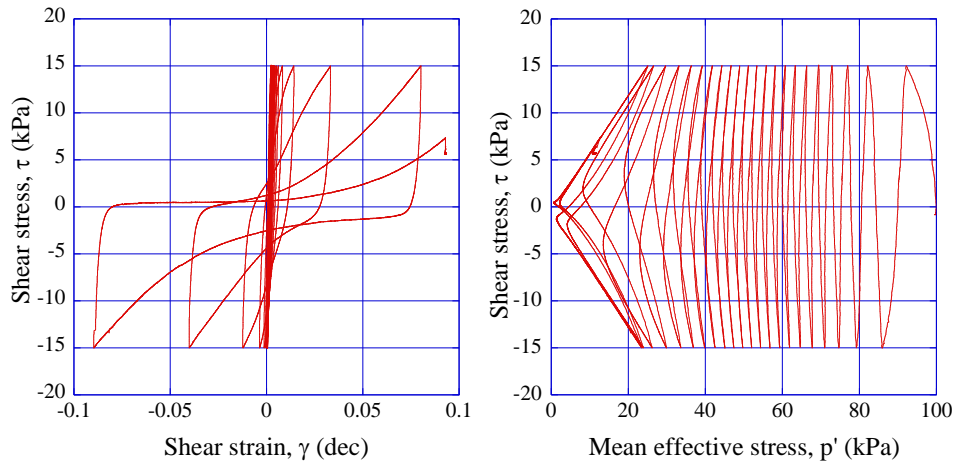


Figure 5.31. Sample A. FC=30% e=1.10 Dr=42% AP-5 cm

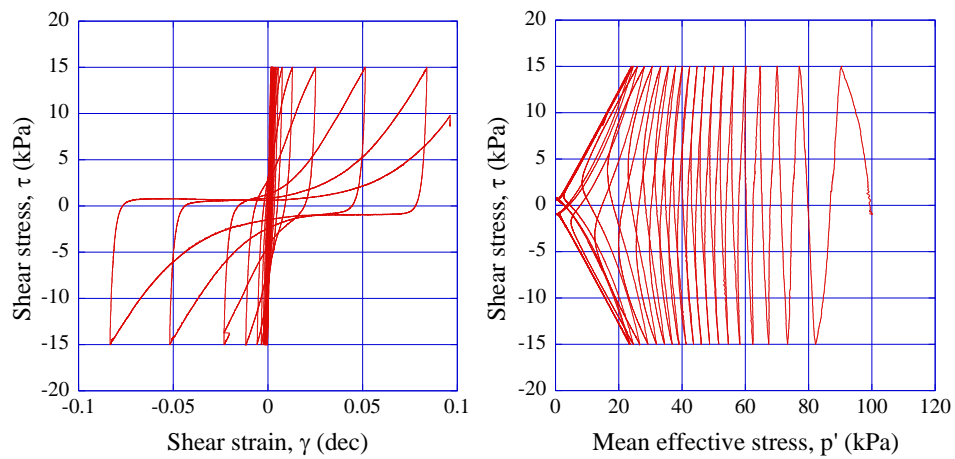


Figure 5.32. Sample B. FC=30% e=1.08 Dr=44% AP-30 cm

Figure 5.33 shows the comparison between samples A and B regarding development of excess pore pressure and shear strain. It can be observed that both samples behave in a similar manner and do not exhibit significant variability in shear strain, therefore it was decided to increase the height in order to make denser samples.

Yet, these results are useful to support the findings in the previous set of tests by AP-5 cm, which led to similar conclusions for samples with $FC \leq 30\%$.

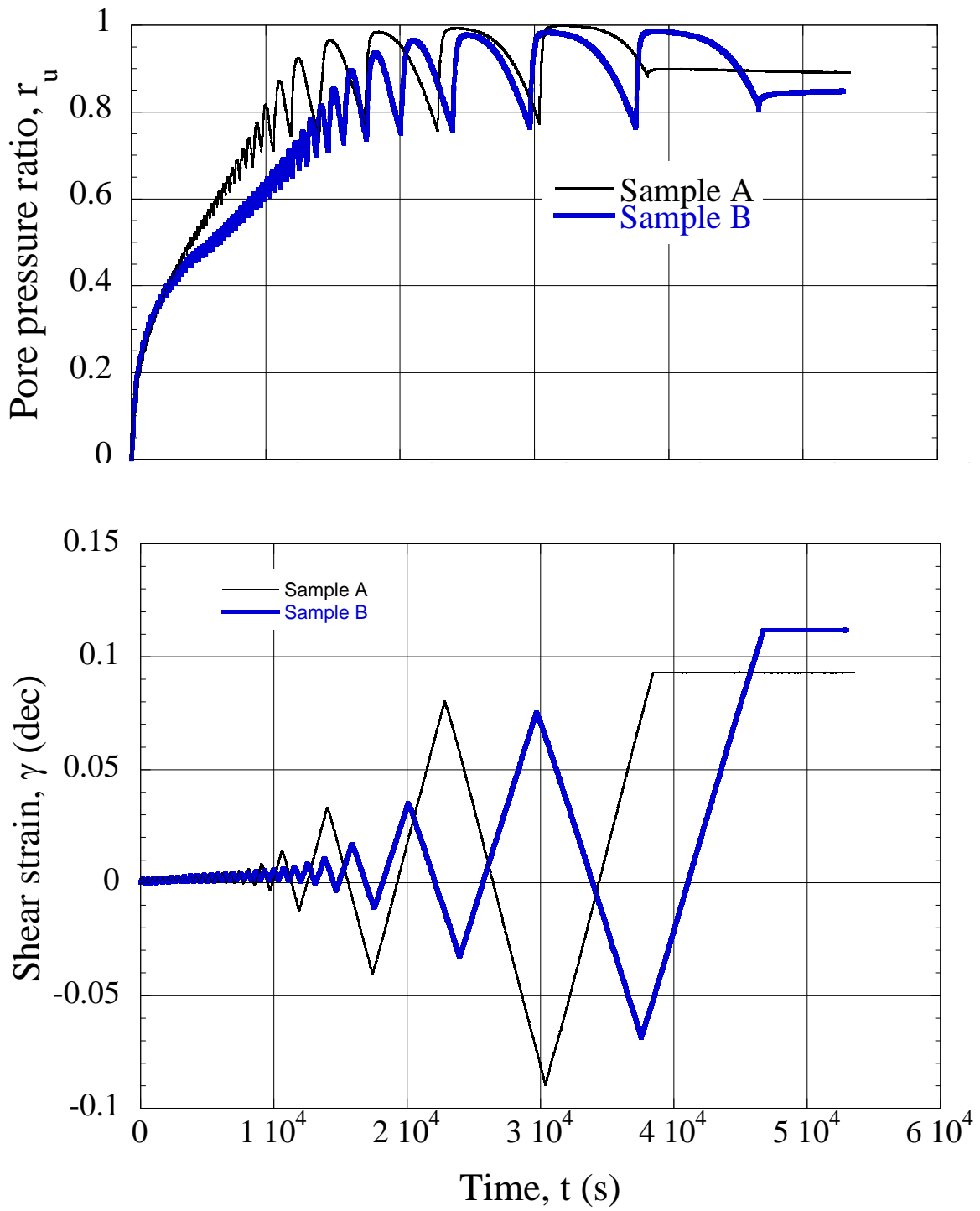


Figure 5.33. Comparison between samples A and B

5.4. AP – 50 cm

5.4.1. Consolidation

Once samples were prepared at 50 cm, they were saturated and consolidated to 100 kPa. Volumetric strain was measured during the process to compute m_v (Figure 5.34).

Figure 5.35 depicts the increase in volumetric strain with mean effective stress during consolidation. It is observed that the slope in this graph is steeper for lower values of FC.

Figure 5.36 shows the variation of m_v with fines content for AP-50 cm samples. In this case, it is observed that m_v increases almost linearly with FC.

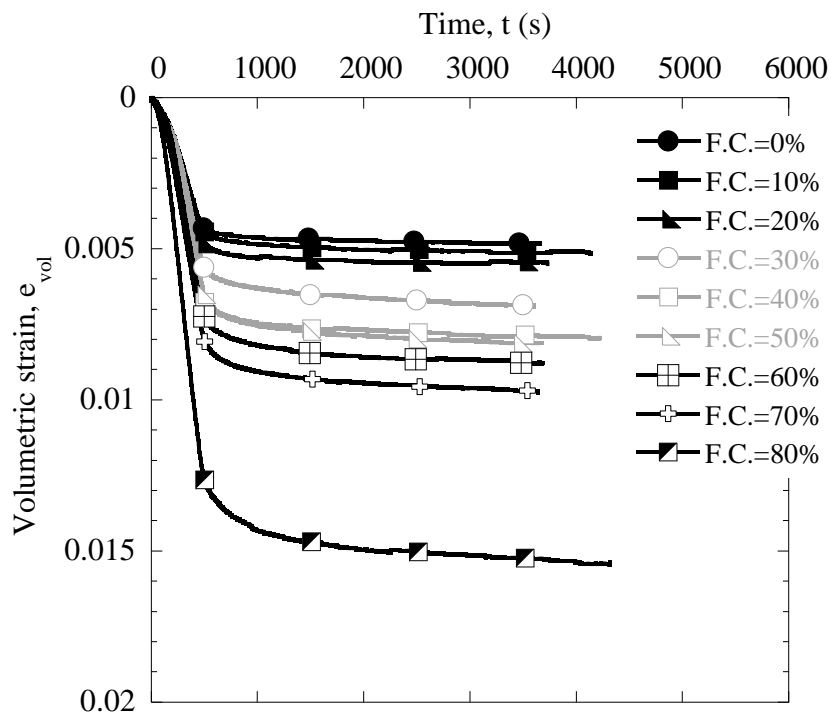


Figure 5.34. Volumetric strain during consolidation. AP-50 cm

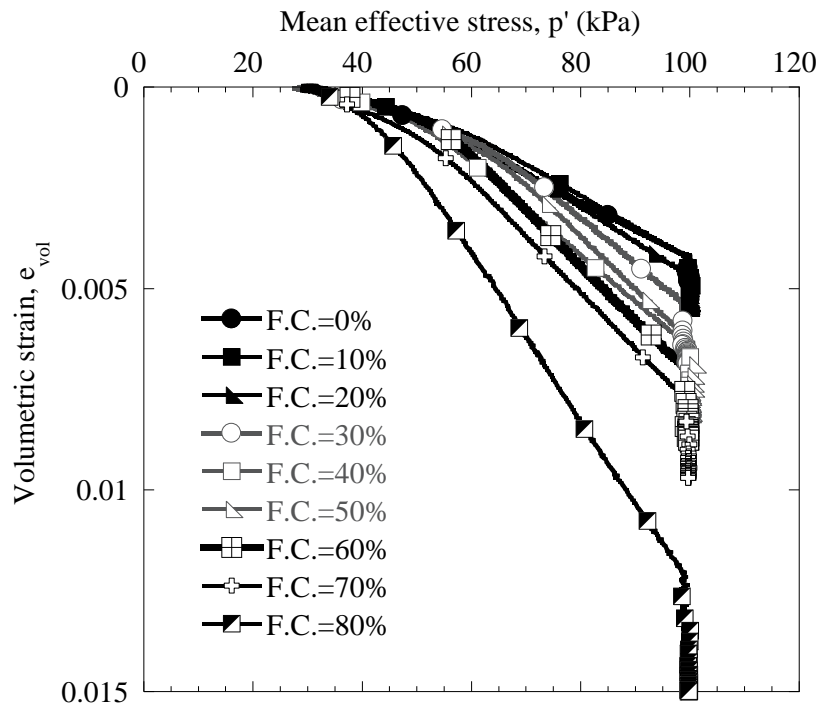


Figure 5.35. Mean effective stress and volumetric strain during consolidation

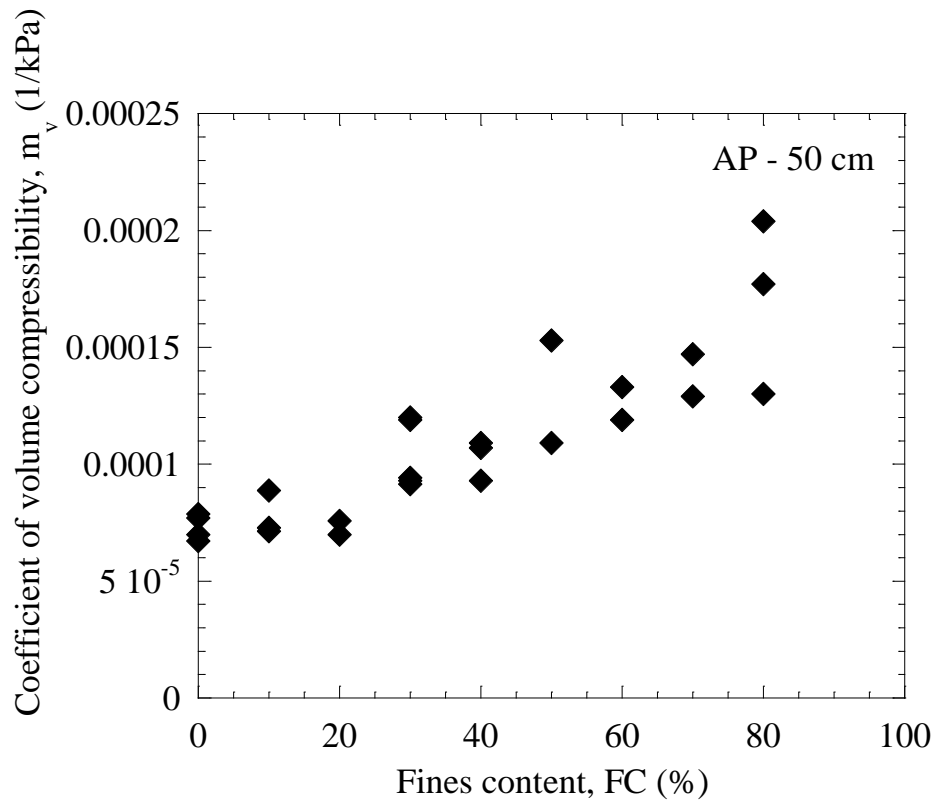


Figure 5.36. Coefficient of volume compressibility for AP-50 cm

5.4.2. Stress-strain curves and effective stress paths

Some examples of the stress-strain curves and effective stress paths of samples formed by AP-50 cm with fines content: 0, 30 and 80% and cyclic stress ratio CSR=0.15, can be observed from Figure 5.37 to Figure 5.39. Figure 5.37 in particular, exhibits a large difference with Figure 5.13 (AP-5 cm) because more cycles were applied to achieve 5% double amplitude shear strain and at that point the condition of zero effective stress was already achieved. Samples with 30 and 80% of fines, however, display a similar behavior compared to AP-5 cm samples.

Figure 5.40 presents the comparison of the effective stress paths for different fines contents: 0, 30, 40 and 80%. It can be seen that for the same CSR=0.15, clean sand exhibits the greatest resistance of all samples with the largest number of cycles to reach the zero

effective stress state. Samples with 30, 40 and 80% have approximately the same number of cycles.

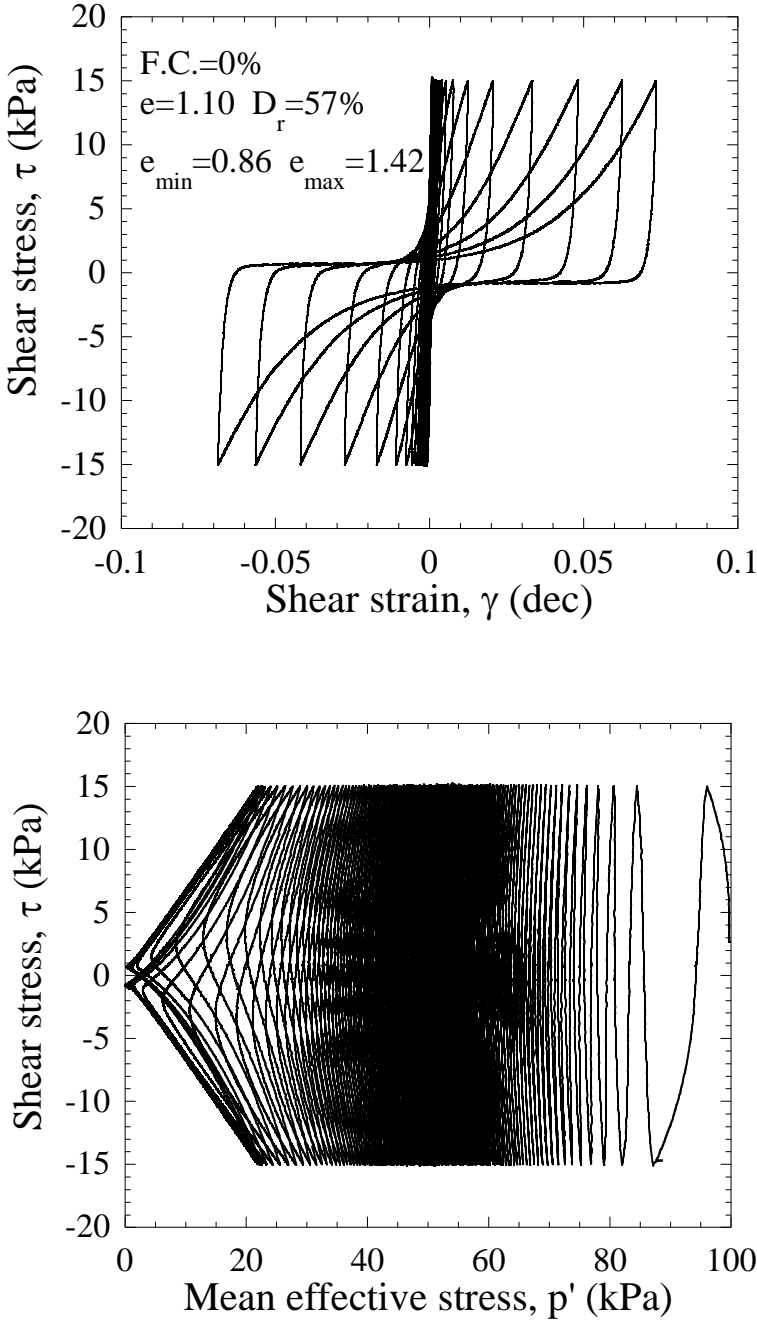


Figure 5.37. Stress-strain curves and effective stress paths for FC=0%, AP-50 cm, CSR=0.15

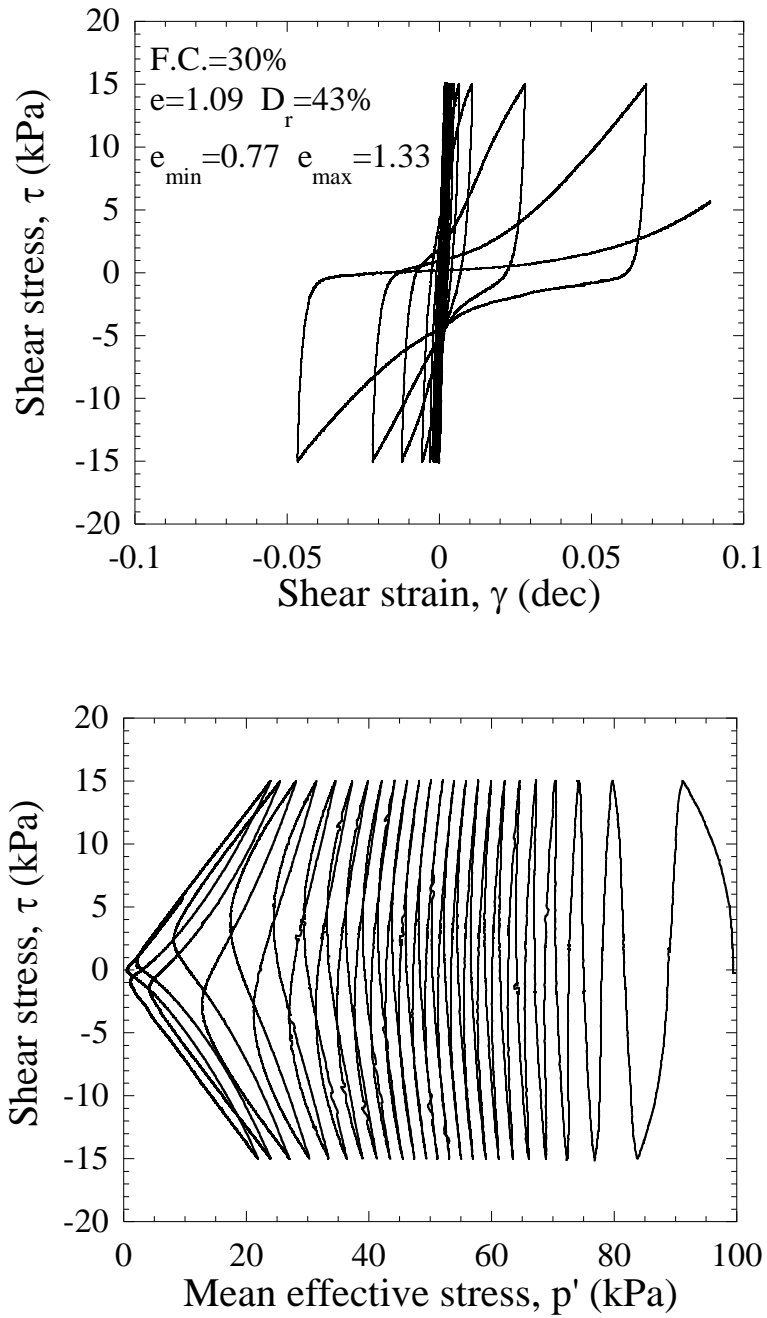


Figure 5.38. Stress-strain curves and effective stress paths for FC=30%, AP-50 cm, CSR=0.15

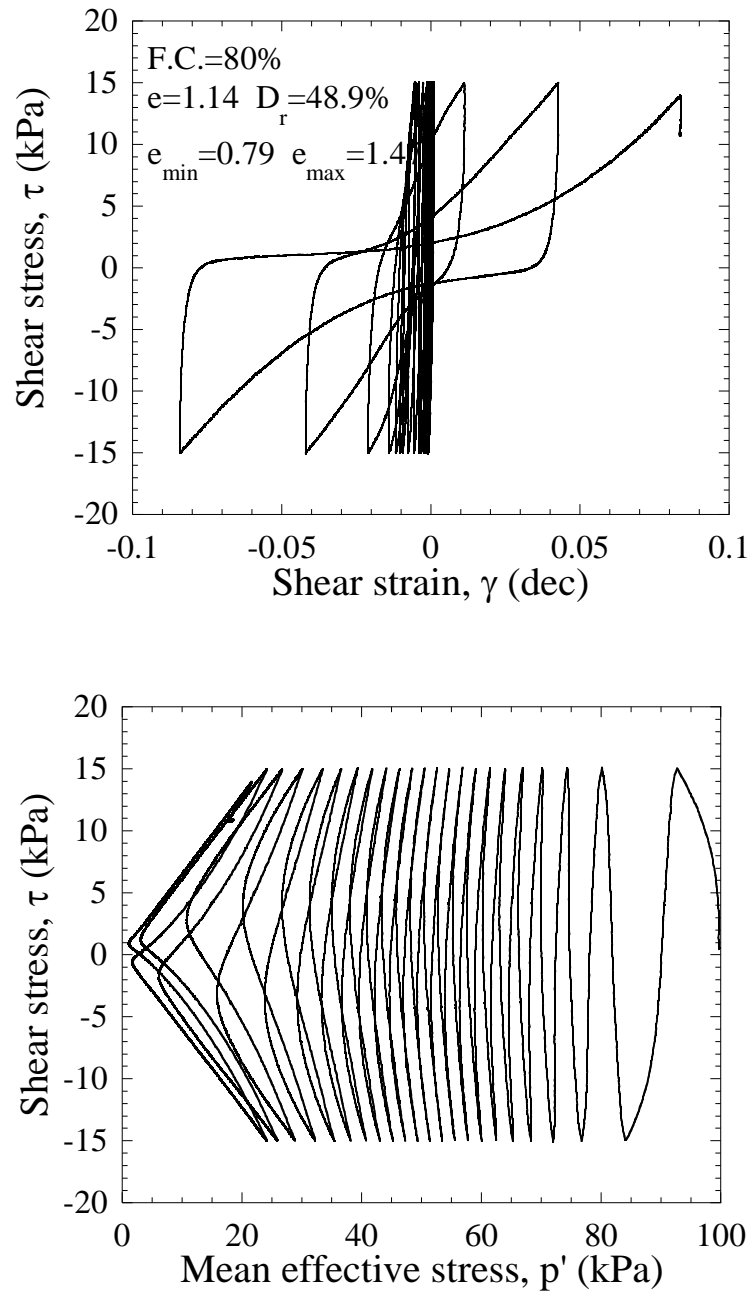


Figure 5.39. Stress-strain curves and effective stress paths for FC=80%, AP=50 cm, CSR=0.15

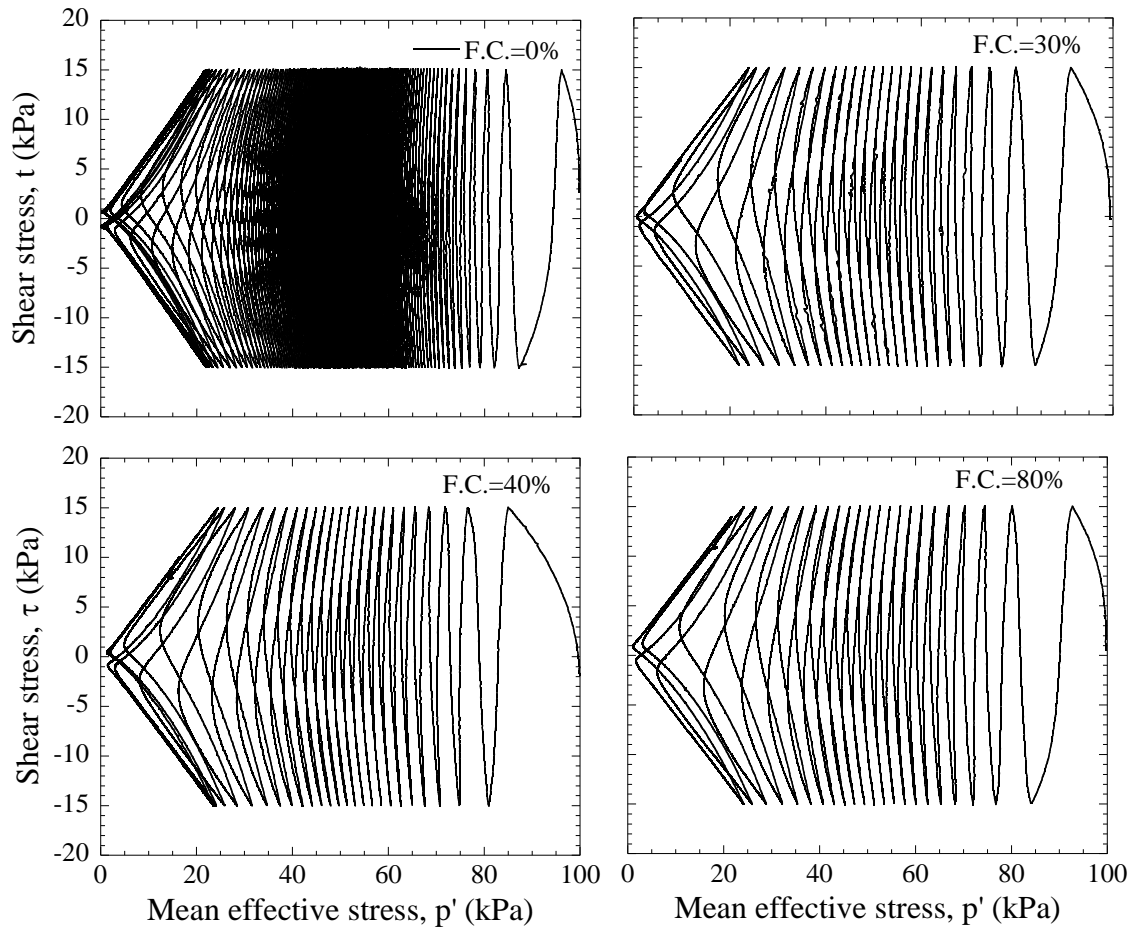


Figure 5.40. Comparison of effective stress paths AP-50 cm

A similar trend as that for AP-5 cm, is observed for AP-50 cm in Figure 5.41, where clean sand (FC=0%) displays more significant shear modulus degradation along with 30% curves. The 80% fines content sample exhibits less degradation, which is subject to further discussion. These data indicate the influence of fines content on the deformability characteristics.

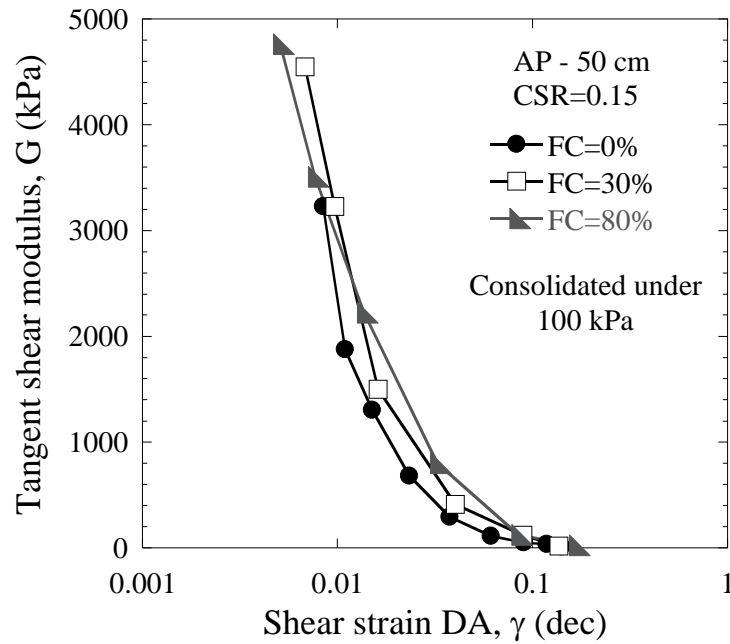


Figure 5.41. Tangent shear modulus during cyclic undrained shear for AP-50 cm

5.4.3. Liquefaction curves

A similar response to that for AP-5 cm is found in Figure 5.42, where three different behaviors are also found. In this case, there is a reduction of resistance from 0 to 30%, then a small increase is observed from 40 to 50%, and the group from 60 to 80% has a response comparable to the one in Figure 5.20 for the same group. The difference in the point of reversal behavior can be found in Figure 2.26, where the threshold fines content for e_{\max} is between 30 and 40%, while in the curve for e_{\min} , the bottom point of the V-shape curve is shifted to right, between 40 and 50%. This provides a clear indication on the locus of fines content where a reversal of behavior can be expected.

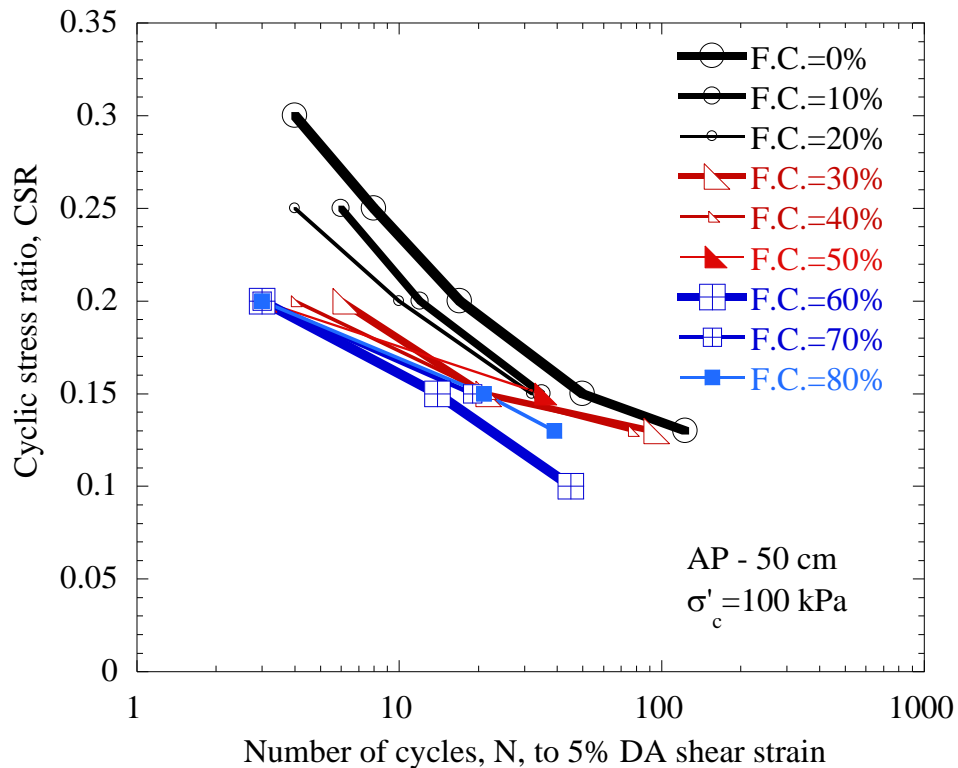


Figure 5.42. Liquefaction curves. AP-50 cm

The variation of cyclic resistance ratio for 20 cycles with fines content can be observed in Figure 5.43. A clearer decrement of CRR_{20} is observed from 0 to 30% fines content and then a small increment was observed from 30 to 50%. Once fines control the behavior of the matrix, resistance decreases for FC=60% fines content and increases for FC=70 and 80%. This proves the observations made in the set conducted of samples formed by AP-5 cm. Therefore, it is safe to admit that samples with fines contents beyond 60% will gain resistance as more fines are added.

Figure 5.44 and Figure 5.45 show the variation of CRR with m_v for different fines contents. As it was seen in the AP-5 cm tests, there is still not a clear correlation when comparing samples at the same m_v value. This parameter, however, showed the same trend for AP-5 cm and AP-50 cm, which gives consistency to the obtained results.

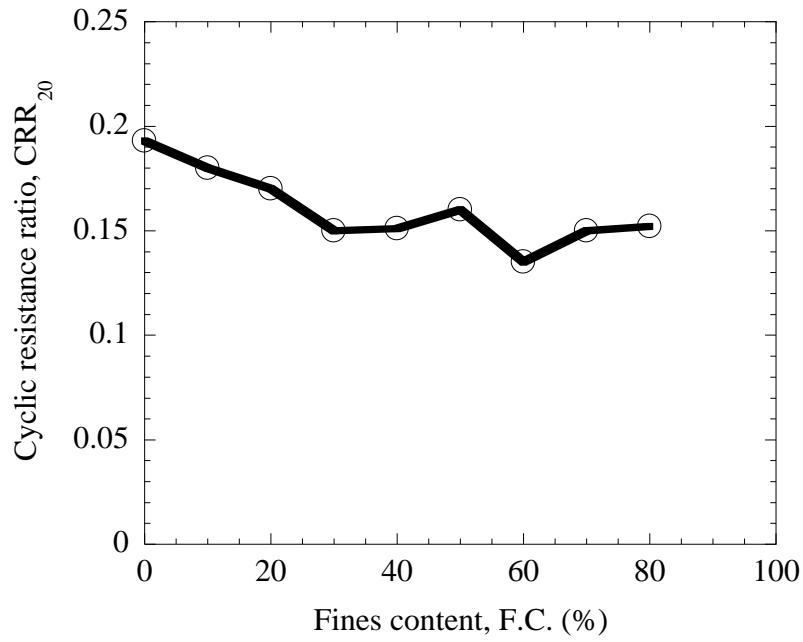


Figure 5.43 Cyclic resistance ratio and fines content for AP-50 cm

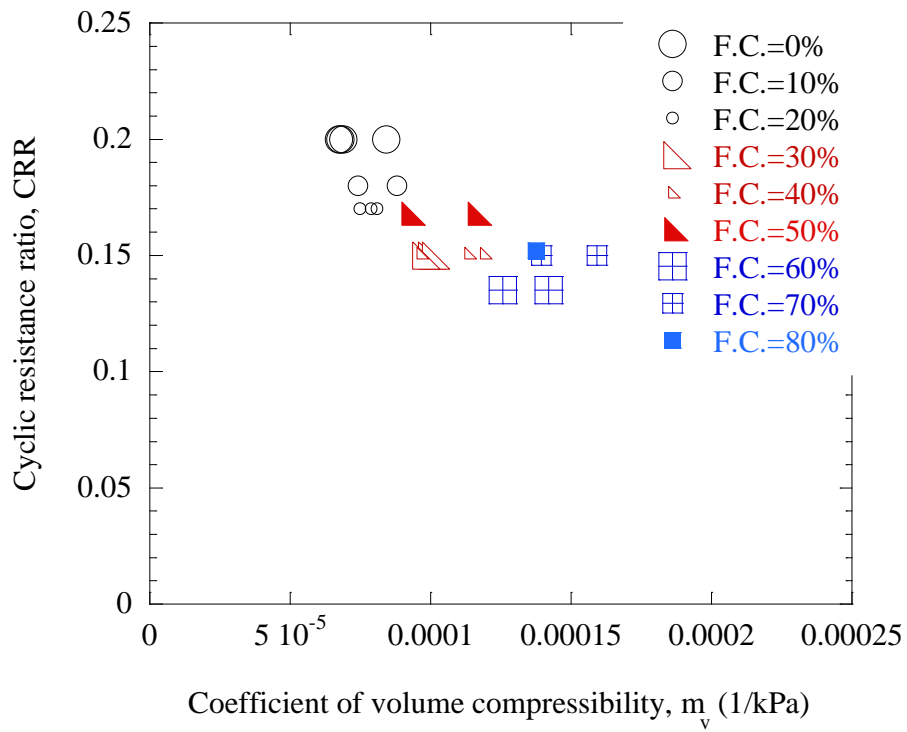


Figure 5.44. Variation of CRR₂₀ and m_v for AP-50 cm

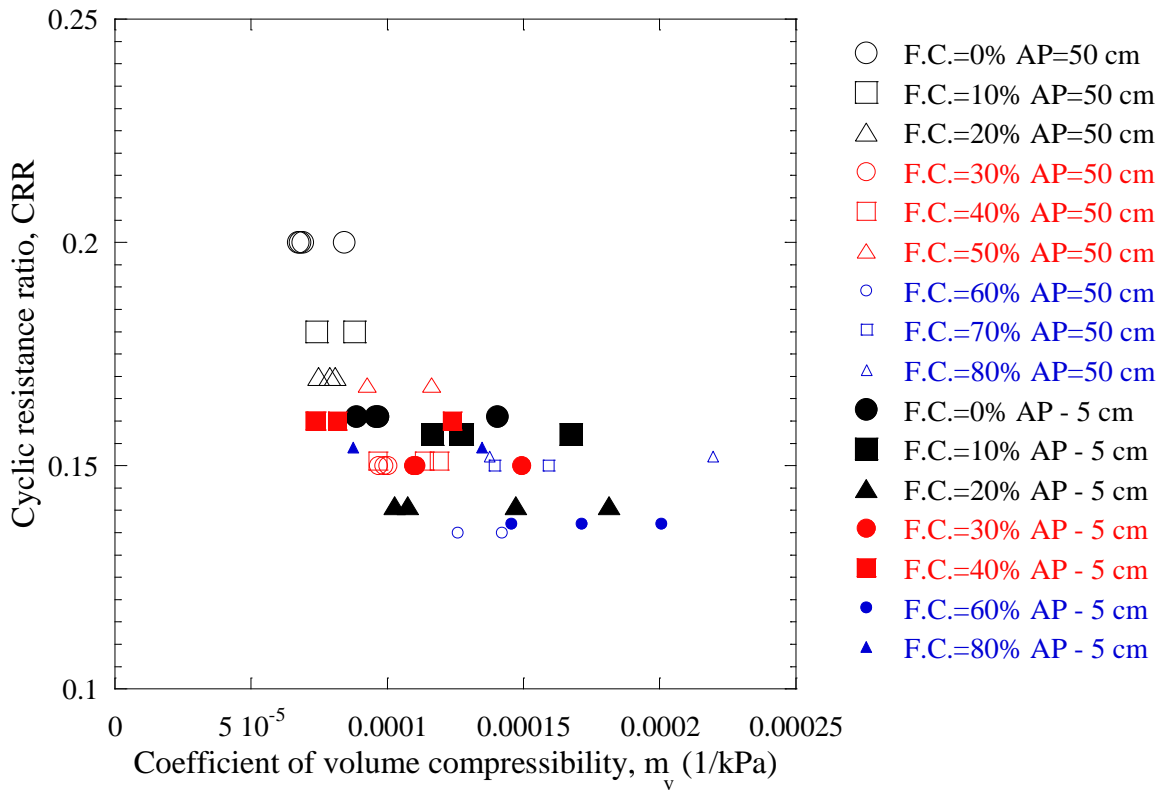


Figure 5.45. Cyclic resistance ratio and coefficient of volume compressibility for AP-5 and 50 cm

5.5. Tests at the same penetration resistance, SPT N-value (Smv)

The initial scheme to understand the influence of fines content was to keep compaction energy constant to simulate natural conditions in a very simplistic way; however, people is concerned with whether or not the SPT-based liquefaction resistance is good for sand with non-plastic fines, since most of the simplified procedures used for evaluating liquefaction potential are based on field parameters as SPT N-value. In this regard, it becomes necessary to use a laboratory parameter of comparison equivalent to SPT N.

Two different approaches were considered, first by using relative density and then by means of the coefficient of volume compressibility, the advantages and final selection of the parameter are explained in the following sections.

5.5.1. *Relative density*

Cubrinovski and Ishihara (1999) compiled data of different soils with their values of SPT N measured in situ and also information on grain size diameter and void ratio range. They found that void ratio range and grain size diameter have a strong correlation (Figure 5.46), therefore void ratio range can be used as a parameter that represents not only particle size but also a measure of packing.

Moreover, taking as a basis the relation proposed by Meyerhof where penetration resistance has a proportional relation with the effective overburden pressure and the square of relative density, they used a simplified equation for correlating with void ratio range:

$$N = \frac{C_D}{C_N} D_r^2$$

where C_D stands for a parameter representing grain size of the soil and C_N is a normalization function of effective overburden pressure. When the normalized penetration value N_1 is used, the relation is reduced to:

$$N_1 = C_D D_r^2$$

After revising an extensive amount of SPT data and D_r measured from undisturbed samples, they found the relation shown in Figure 5.47. It is observed that soil with fines is included in both figures.

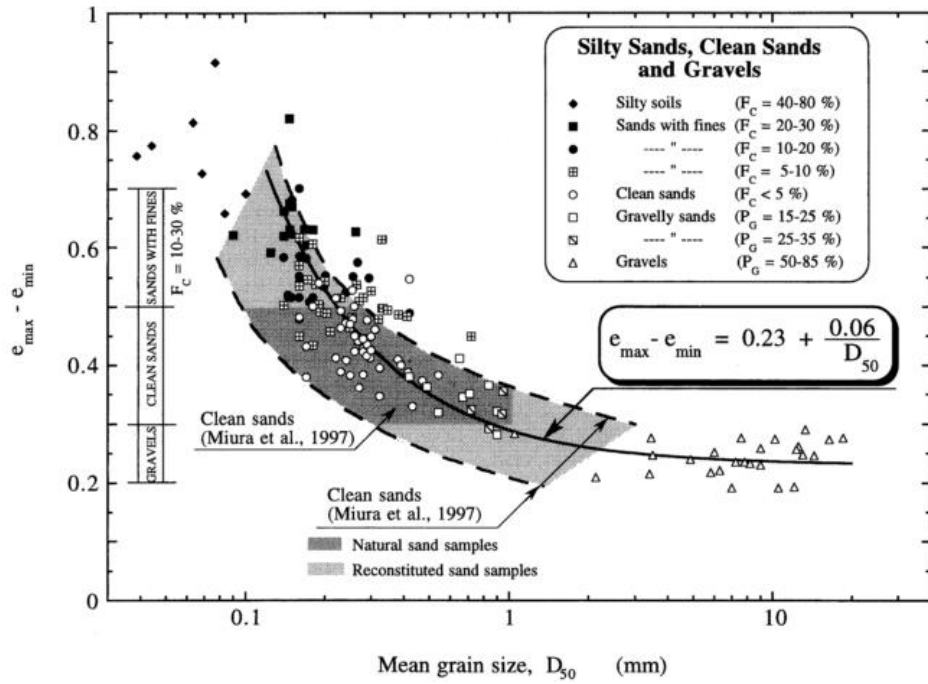


Figure 5.46. Correlation between void ratio range and mean grain size (From Cubrinovski and Ishihara, 1999)

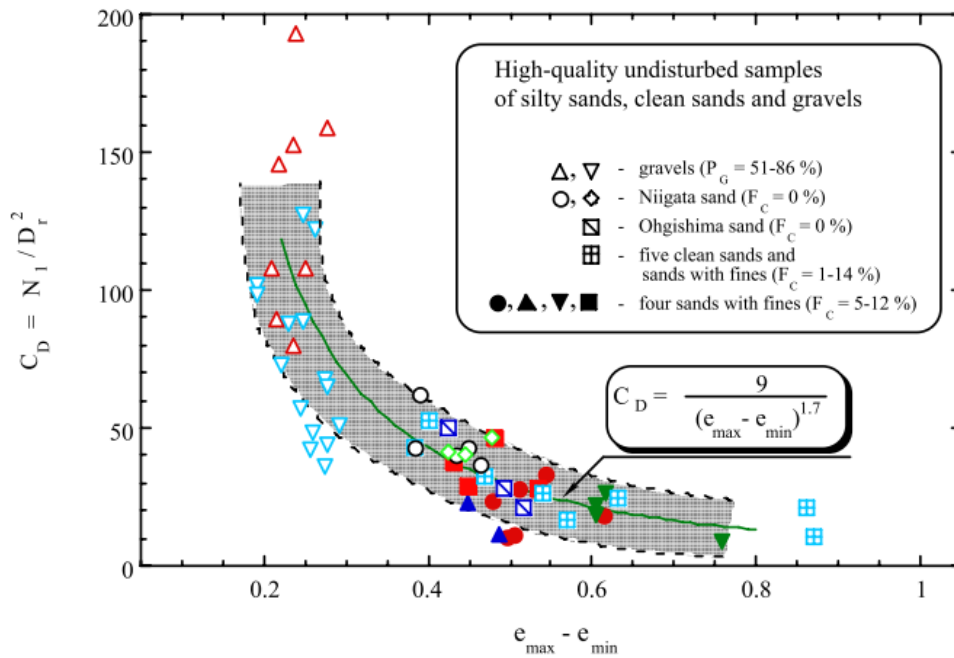


Figure 5.47. Correlation between C_D and void ratio range (From Cubrinovski and Ishihara, 1999)

By considering this approach, the range of relative density that should be tested for aiming a certain value of N_1 can be found with the equation of C_D . Figure 5.48 shows the variation of void ratio range ($e_{\max}-e_{\min}$) with fines content. It is observed that the range of values is small and a slight increase is observed as fines increase.

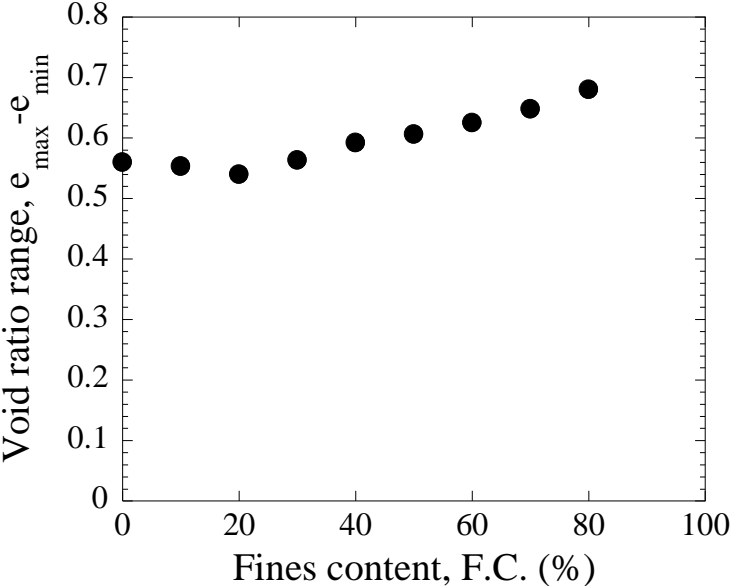


Figure 5.48. Void ratio range with fines content

Relative density was computed for two values of normalized penetration resistance, $N_1=3$ and $N_1=5$. The resulting densities are plotted in Figure 5.49 over the values of samples for AP-5 and 50 cm. It is observed that the densities measured for AP-5 cm follow the same tendency as the computed density. However the values of AP-50 cm, although similar, are out of range for $FC=10$ and 20% .

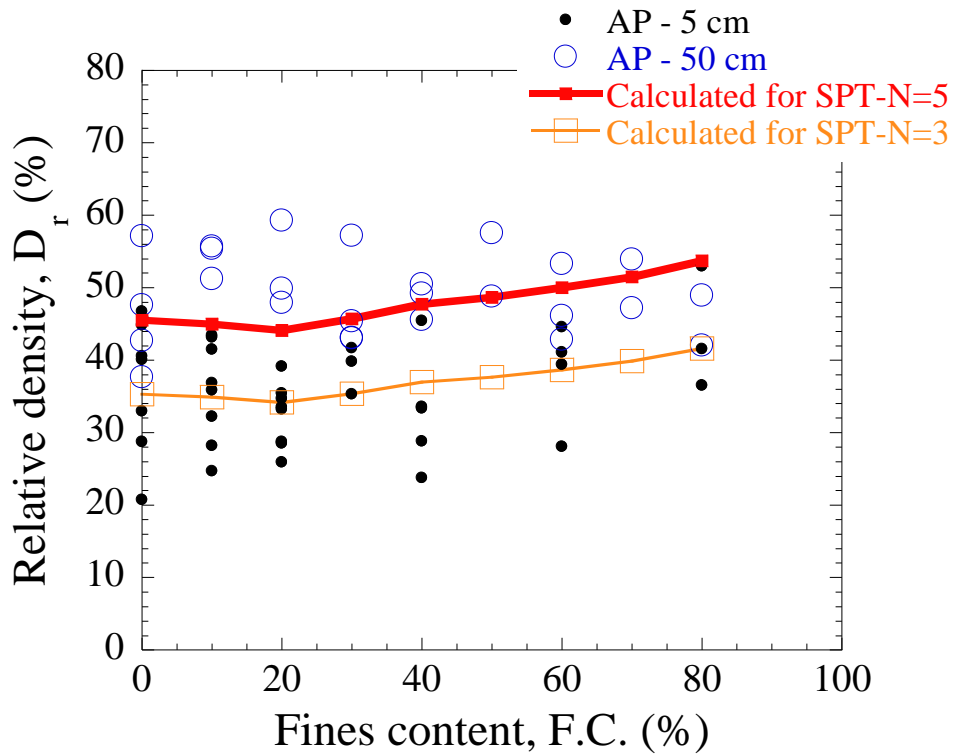


Figure 5.49. Relative density for $N_1=3$ and $N_1=5$

Viewing these results, it could be considered that tests prepared by AP-5 cm have similar values of N_1 , hence it would be expected that these results were directly applied to field conditions. However, as established before, the use of relative density as a contact index for fines content greater than 30% is not suitable. Moreover, most standards for calculation of minimum and maximum void ratios do not apply for fines content larger than 30%.

Consequently, this method was set aside and a different approach to relate a laboratory parameter to field parameters was sought.

5.5.2. Coefficient of volumen compressibility

Coefficient of volume compressibility is known to be related to the normalized penetration resistance. Stroud and Butler (1975) compiled SPT data of London soils and obtained their coefficients of volume compressibility in the laboratory to obtain a relationship between N and m_v . They found that these values are inversely related by a parameter that represents plasticity of soils:

$$N = \frac{1}{f_2 m_v}$$

Some values of f_2 for plasticity index, PI , are given in Figure 5.50

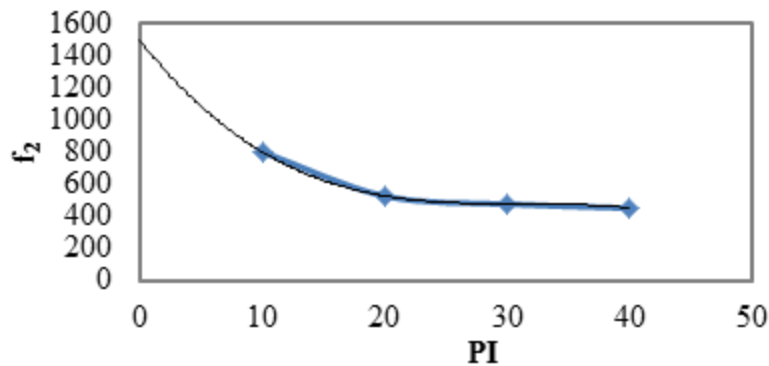


Figure 5.50. Variation of f_2 with PI . After Stroud and Butler (1975)

By assuming a certain value of m_v , it can be expected that samples are being tested at the same SPT N -value. A value of $m_v=1.20 \times 10^{-4}$ (1/kPa), equivalent to SPT $N=5$, was chosen to conduct a test program on samples at the same N .

Nevertheless, since coefficient of volume compressibility is obtained after consolidation, aiming for a particular value of m_v was a challenging task to undertake. A vast amount of tests were prepared as shown in Figure 5.51 and a range was selected with an error of 15% in order to analyze the effect of fines on the liquefaction resistance at a similar N -value (Figure 5.52).

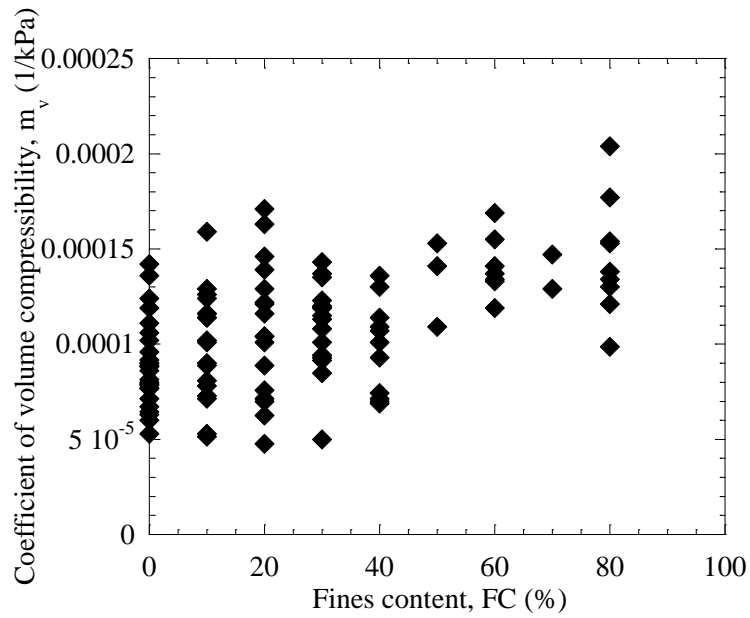


Figure 5.51. Coefficient of volume compressibility variation with fines content

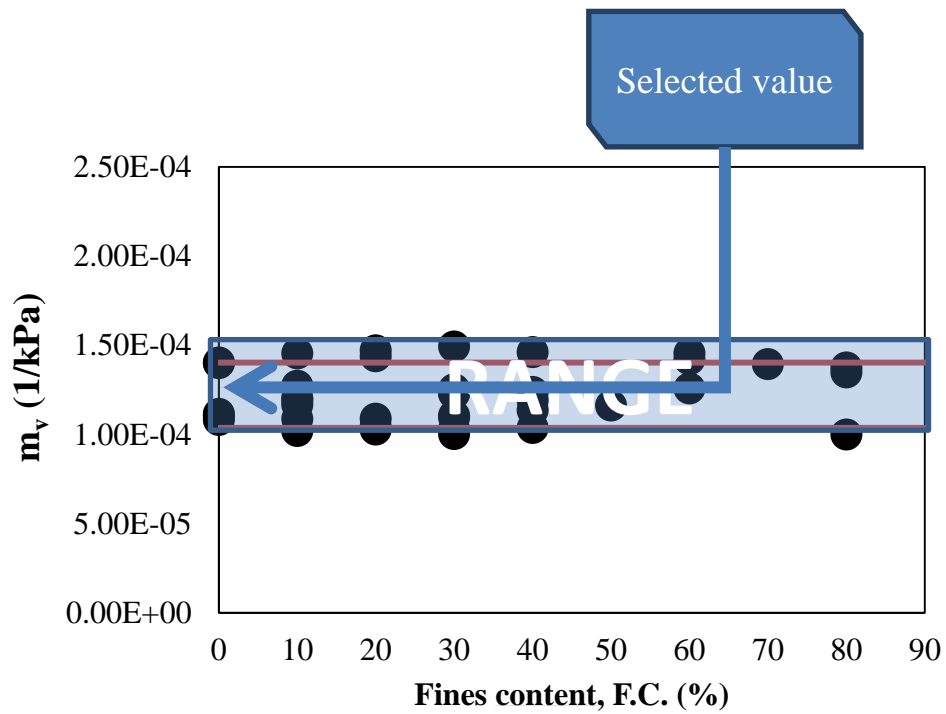


Figure 5.52. Selected range of m_v

5.5.2.1. Consolidation tests

Figure 5.53 shows the volumetric strain during consolidation for some samples prepared at the same level of mv. It is observed that creep is larger for FC=60 and 80%.

Figure 5.54 illustrates the variation of mean effective stress and volumetric strain during consolidation. It is observed that all samples depart from the effective stress at the beginning of consolidation 30 kPa, and increase up to 100 kPa. All values of volumetric strain are in the same range and during calculation of the coefficient of volume compressibility leads to the same range as well.

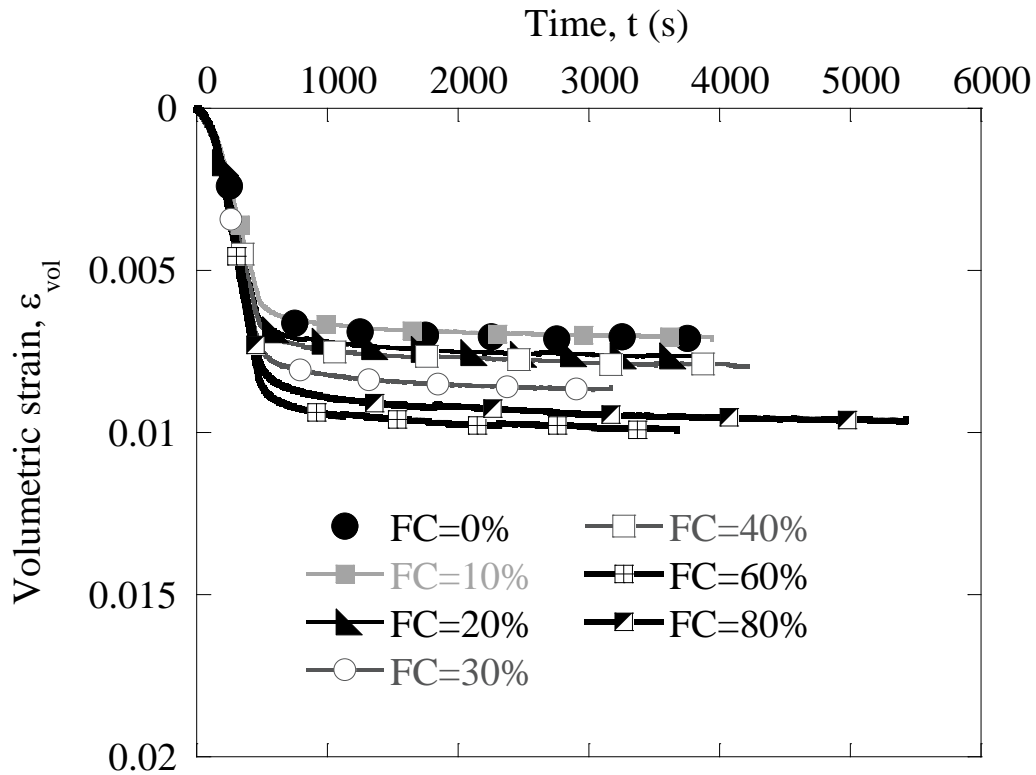


Figure 5.53. Volumetric strain during consolidation. Smv

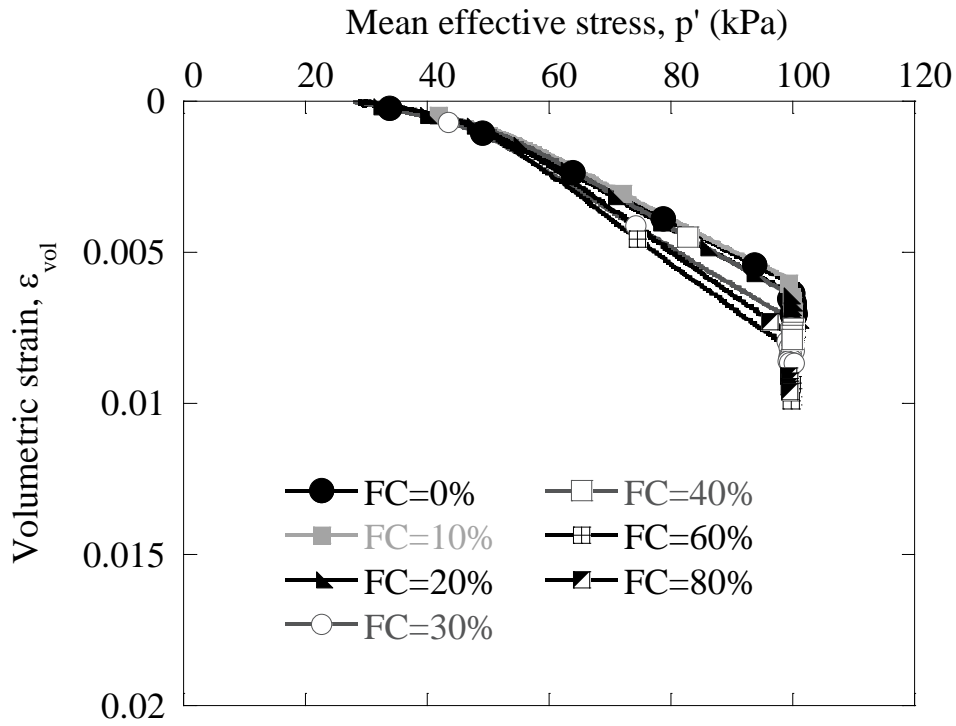


Figure 5.54. Mean effective stress and volumetric strain during consolidation. S_{mv}

5.5.2.2. Shear stress-strain curves

Kazama and Yanagisawa (2000) presented some results based on the concept of dissipated energy, W , which is the amount of energy that soil can consume as plastic strain, this was considered to be an index to evaluate ductility and is equal to the area of a shear stress-strain loop (Figure 5.55). It is defined by:

$$W = \int_0^t \tau(\gamma) \dot{\gamma}(t) dt$$

Where $\dot{\gamma}$ is the rate of strain at time t , and τ is the shear stress.

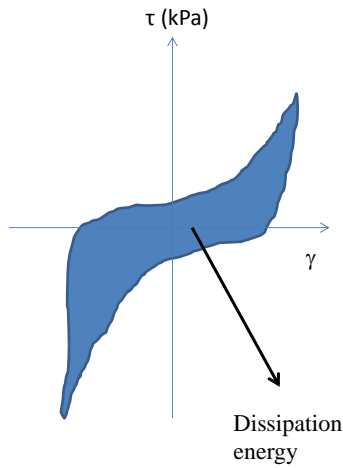


Figure 5.55. Concept of dissipation energy

Based on this concept, dissipated energy was calculated for FC=0, 30 and 80% and compared (Figure 5.56). It can be seen that FC=0% exhibits more dissipated energy and more number of cycles as compared to 30 and 80%. This is consistent with the results presented in Figure 5.17 for AP-5 cm.

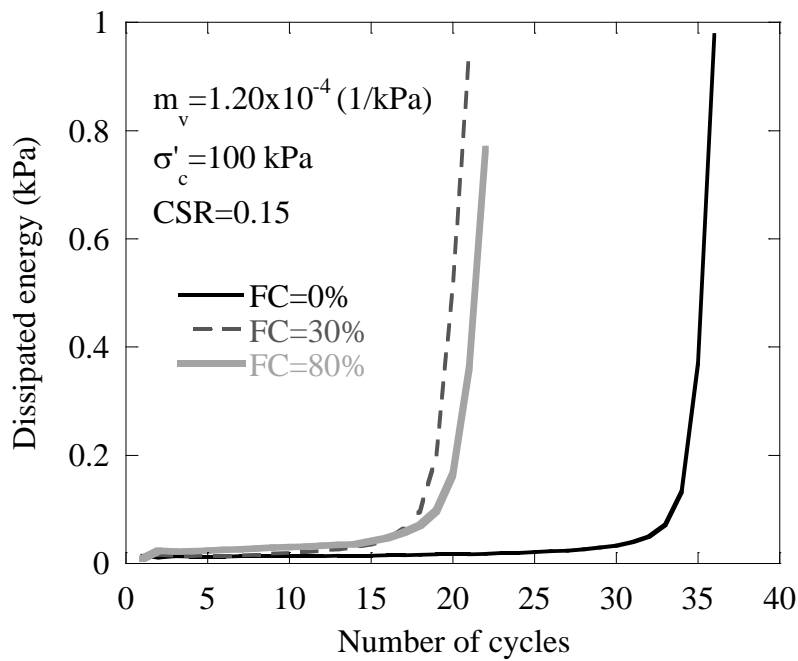


Figure 5.56. Dissipated energy for the same m_v

Following this idea, the double amplitude shear strain was measured at each cycle as a hysteresis index. Figure 5.57 shows the results for fines content equal to 0, 30 and 80%. The trend of the curves resemble the one observed in Figure 5.56.

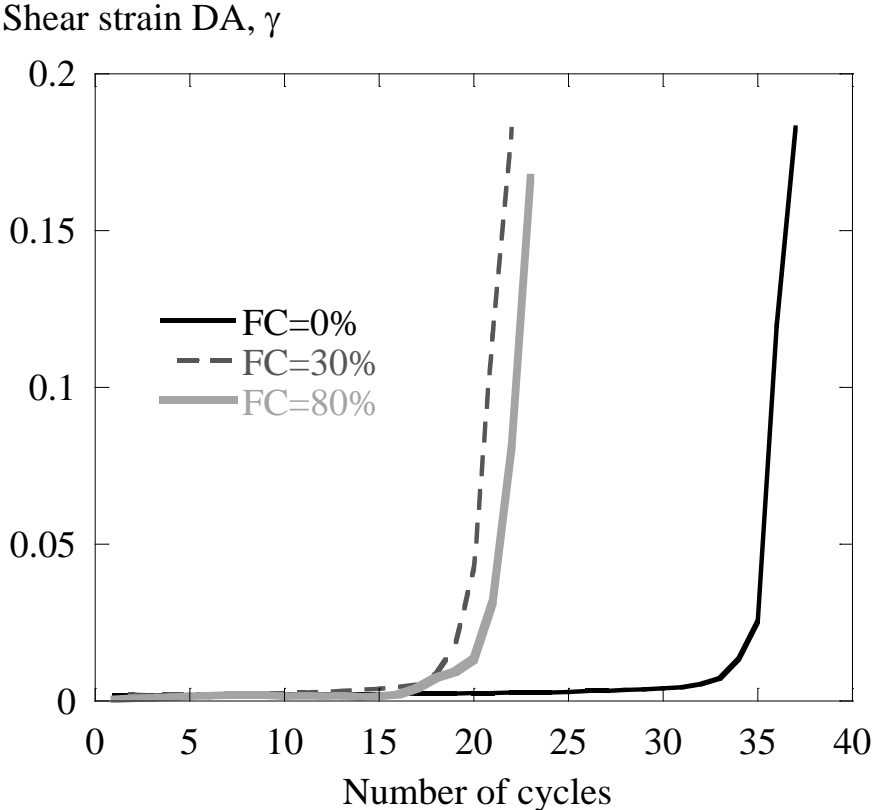


Figure 5.57. Double amplitude shear strain for $m_v=1.20 \times 10^{-4}$ (1/kPa), CSR=0.15

5.5.2.3. Excess pore-water pressure

After conducting cyclic shear tests on the samples with similar m_v , the curves of excess pore pressure ratio were plotted in order to observe the effect of fines content on the liquefaction resistance and the generation of excess pore pressure during undrained loading. Figure 5.58 exhibits the changes in excess pore pressure generation for different fines content at $m_v \approx 1.20 \times 10^{-4}$ for the same cyclic stress ratio, CSR=0.15. There it is observed

that there the 60% fines content curve has the faster development of excess pore pressure while the 0% curve has the slowest generation.

There is a decrease in the number of cycles from FC= 0 (36 cycles) to 20% (20 cycles), then an increase of one cycle from 30 (23 cycles) to 40% (24 cycles). The sample of 60% has the lower number of cycles (10 cycles) and an increment is observed for 80% (22 cycles).

Observing these results it is possible to say that clean sand has the larger resistance while sand with a large amount of fines, barely above the limiting fines content, has the lower resistance.

When a small amount of fines around the threshold fines content is added to clean sand, it decreases its resistance but they exhibit a similar response. As fines increase beyond the limiting fines content the matrix strengthens and larger resistance is observed, similar to that of sand with lower fines content.

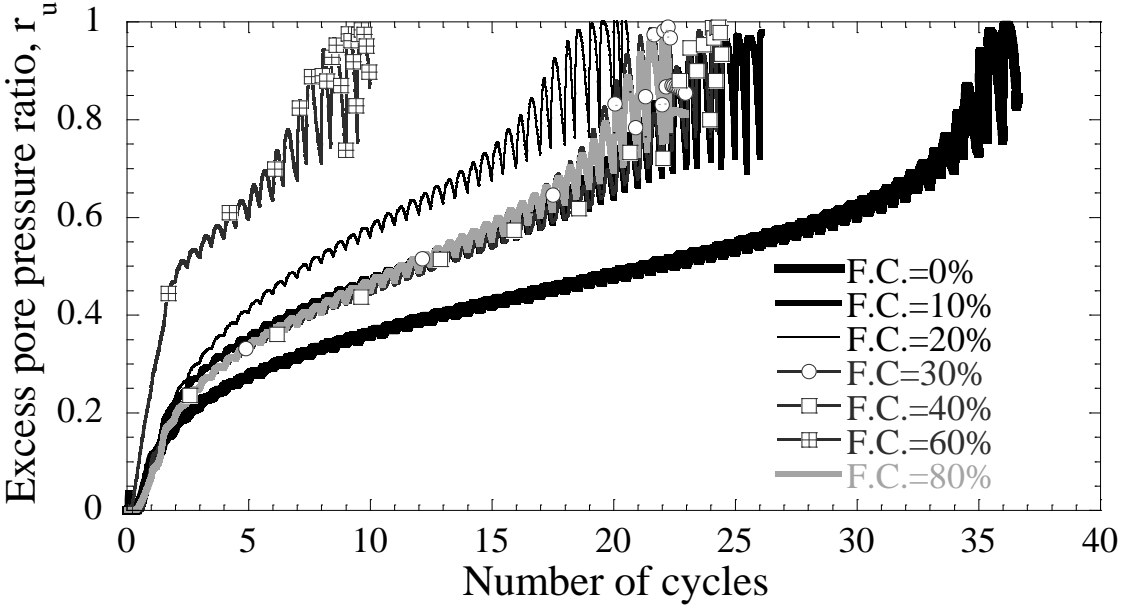


Figure 5.58. Excess pore pressure ratio for $mv \approx 1.20 \times 10^{-4}$ (1/kPa), CSR=0.15

5.4.2.3 Liquefaction curves

After the experimental program was finished, liquefaction curves were drawn to observe the effect of fines content on the cyclic resistance ratio.

In Figure 5.59 it is observed that clean sand has the stronger resistance and a decrease in cyclic resistance ratio is observed until 20% fines content. Later a slight increase is observed from 30 to 40%. Then, a decrease is observed for 60% but a larger than that observed in the previous group is observed for the sample with 80% fines content.

This behavior resembles the results found in the previous experiments of AP-5 cm and AP-50 cm.

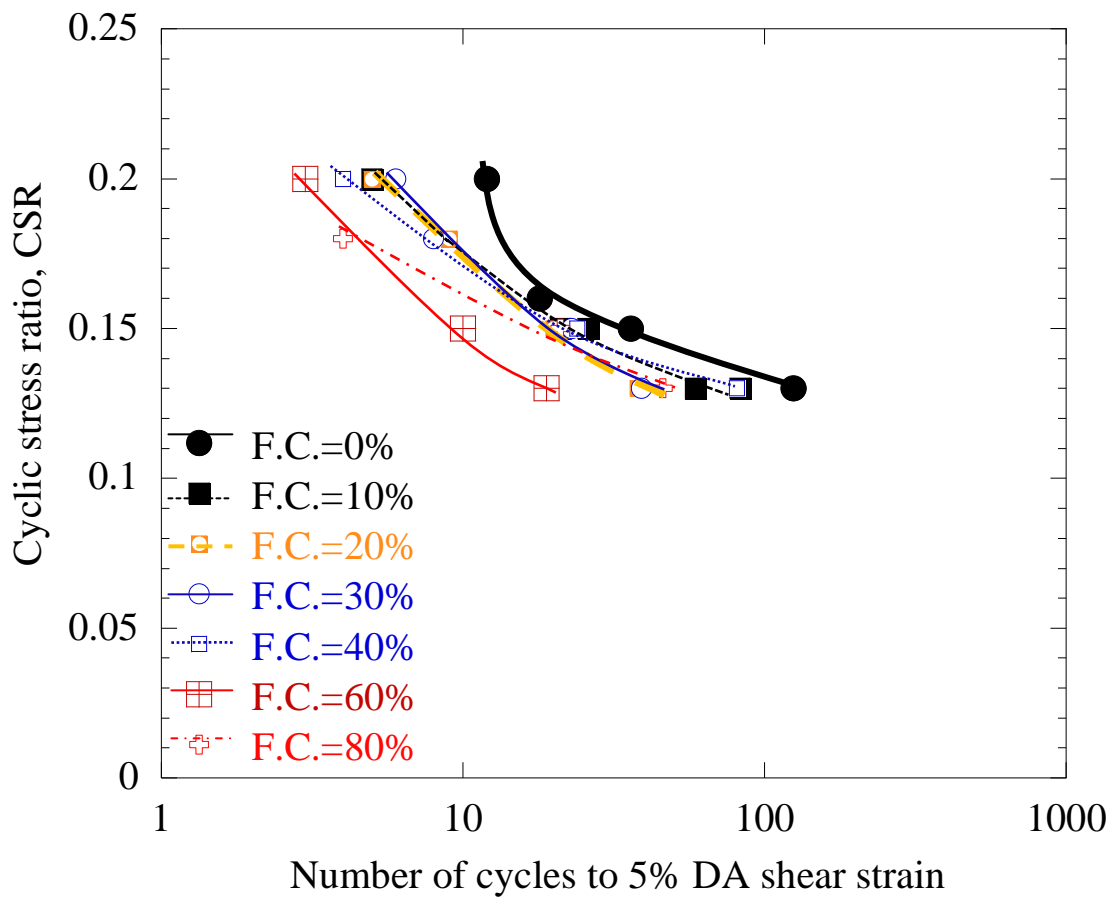


Figure 5.59. Liquefaction curves. Smv

Variation of cyclic resistance ratio for different fines contents at the same mv is depicted in Figure 5.60, compared to samples made by AP-5 cm and AP-50 cm.

It can be seen that for Smv resistance diminishes from 0 to 20% fines content then there is a slight increase in resistance from 30 to 40%, although for practical considerations it can be considered to remain constant. Finally there is an evident drop of resistance from 40 to 60% and then CRR_{20} grows again for 80%.

Results are compared to cyclic resistance ratio obtained for samples made by AP-5 and 50 cm. In all cases resistance decreases with the addition of small amount of fines and also exhibits an overall reduction for large fines contents.

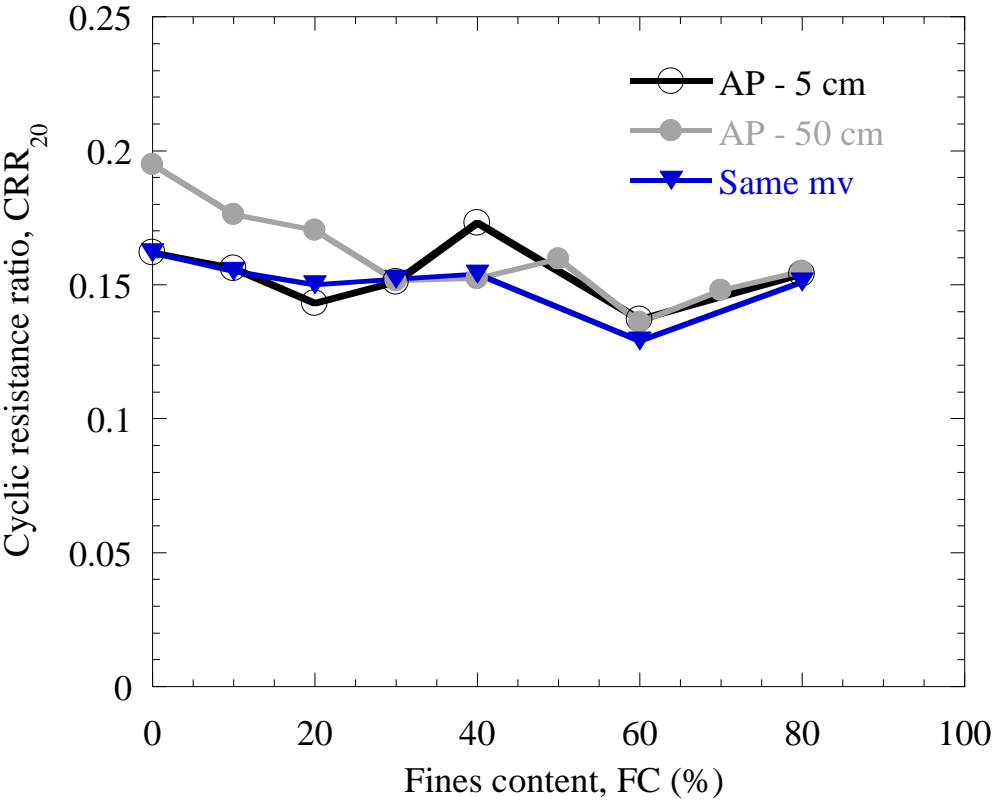


Figure 5.60. Comparison of CRR_{20} for the three different experiments

5.6. Slurry deposition procedure

A couple of tests were conducted following the procedure described by Zdravkovic (1996) for a hollow cylindrical device, and first introduced by Kuerbis (1989).

After following the initial steps describes above, some modification were made. The process then consisted on pouring the mixture in a container filled half with deaired water, removing air bubbles by agitation, add more deaired water, remove air bubbles and add more water until no air bubbles were observed.

The process of mixing was very important to avoid air in the sample. Once the mixture was perfectly blended, it was poured from the container through a hose into the molds already prepared to receive the sample. This maneuver had to be fast in order to avoid air from getting in. After pouring the whole sample, the top cap was placed and secured with three rings and backpressure was applied to achieve full saturation.

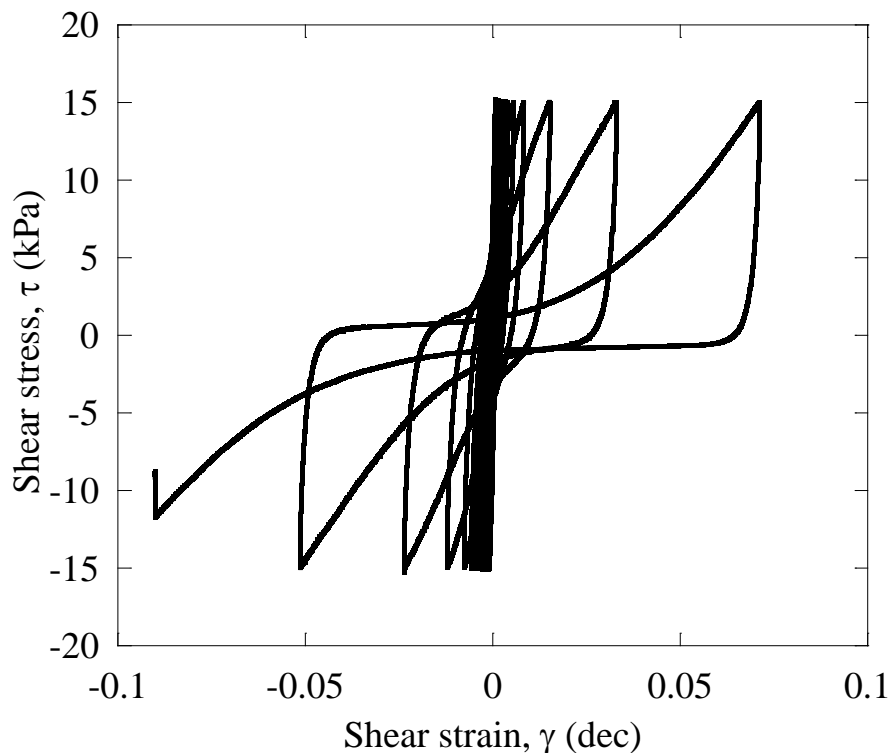


Figure 5.61. Stress-strain curve for slurry deposition sample FC=10%, e=1.10, CSR=0.15

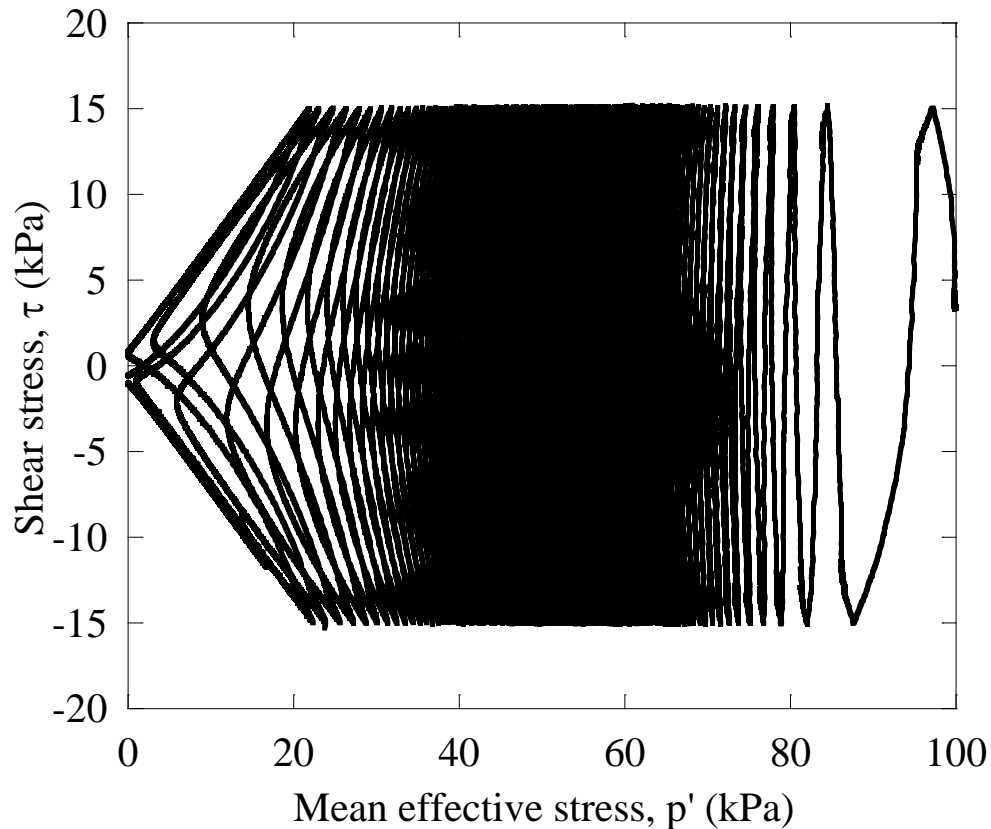


Figure 5.62. Effective stress path for slurry deposition sample FC=10%, e=1.10, CSR=0.15

In Figure 5.61 the stress strain curves obtained for a sample with FC=10% is shown and the effective stress path is depicted in Figure 5.62.

When compared to a sample of FC=10% at the same void ratio, it was observed that while the sample prepared by slurry deposition reached 5% double strain amplitude at 98 cycles, a sample made by AP-50 cm reached 5% double amplitude at 36 cycles.

This difference agrees with previous results conducted on samples made by different procedures. Nevertheless, some seams were observed in the samples retrieved as depicted in Figure 5.63. This finding remarks the possibility of obtaining non-uniform samples when using wet deposition methods. In order to avoid this issue, more practice should be gained in performing the slurry deposition method.



Figure 5.63. Layering observed in samples made by SD

Chapter 6

APPLICATION TO
DEFORMABILITY
ANALYSIS

Chapter 6. APPLICATION TO DEFORMABILITY ANALYSIS

6.1. Shear modulus degradation

The value of secant shear modulus was measured for the first cycle in the different set of tests for AP-5 cm and AP-50 cm. This secant shear modulus corresponds to 0.1% of shear strain and is compared for different fines contents. Definition of this modulus is given in Figure 6.1

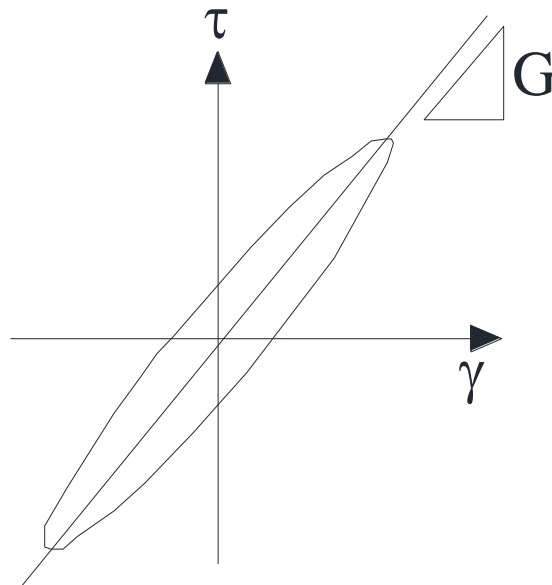


Figure 6.1. Shear modulus for the first cycle of loading $\gamma=0.1\%$

In Figure 6.2 values of the secant shear modulus for AP-5 cm can be observed, while Figure 6.3 presents the values for AP-50 cm. In each case, three or more samples are presented for each fines content, comparing the corresponding value of cyclic resistance ratio obtained in the liquefaction curves to the values of shear modulus for 0.1% shear strain.

Figure 6.4 compiles all data for AP-5 and 50 cm. It is observed that from 0 to 20% fines content, shear modulus drops while it recovers again from 30 to 40%. From 60 to 80% the

values of shear modulus increase. It is observed that for silty sand the shear modulus ranges from 1.7×10^4 to 3.7×10^4 (kPa), while it is wider for clean sand.

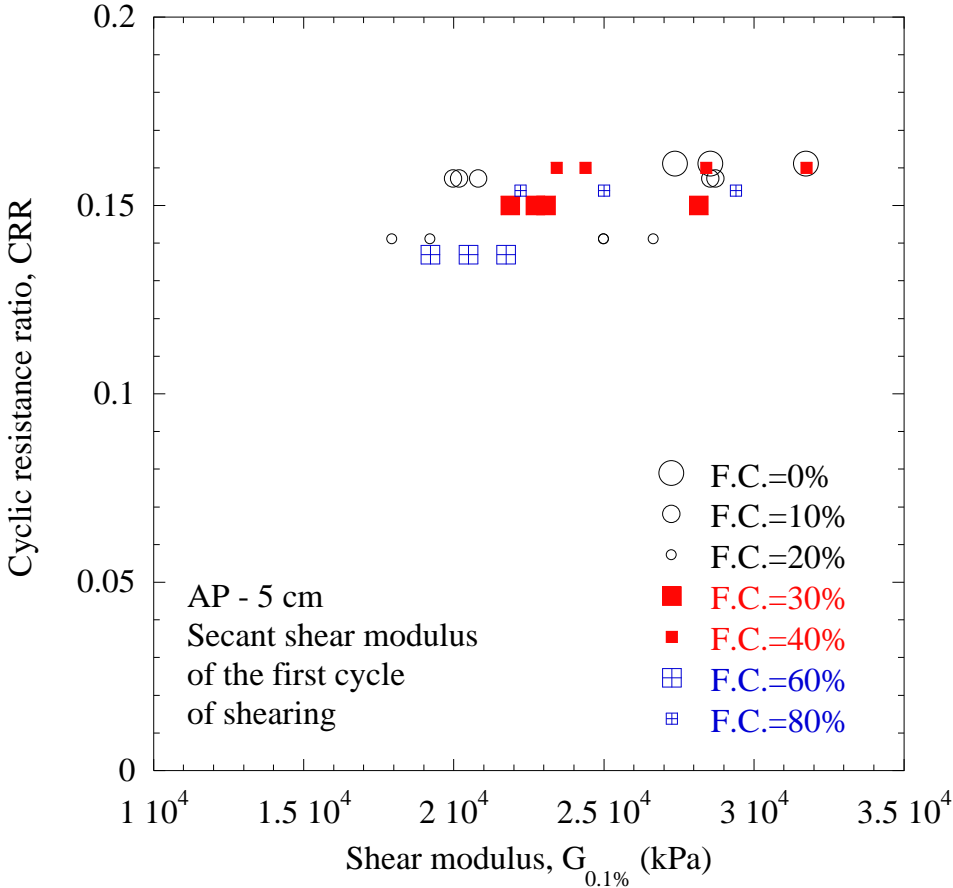


Figure 6.2. Cyclic resistance ratio and shear modulus for 0.1% of shear strain for AP-5 cm

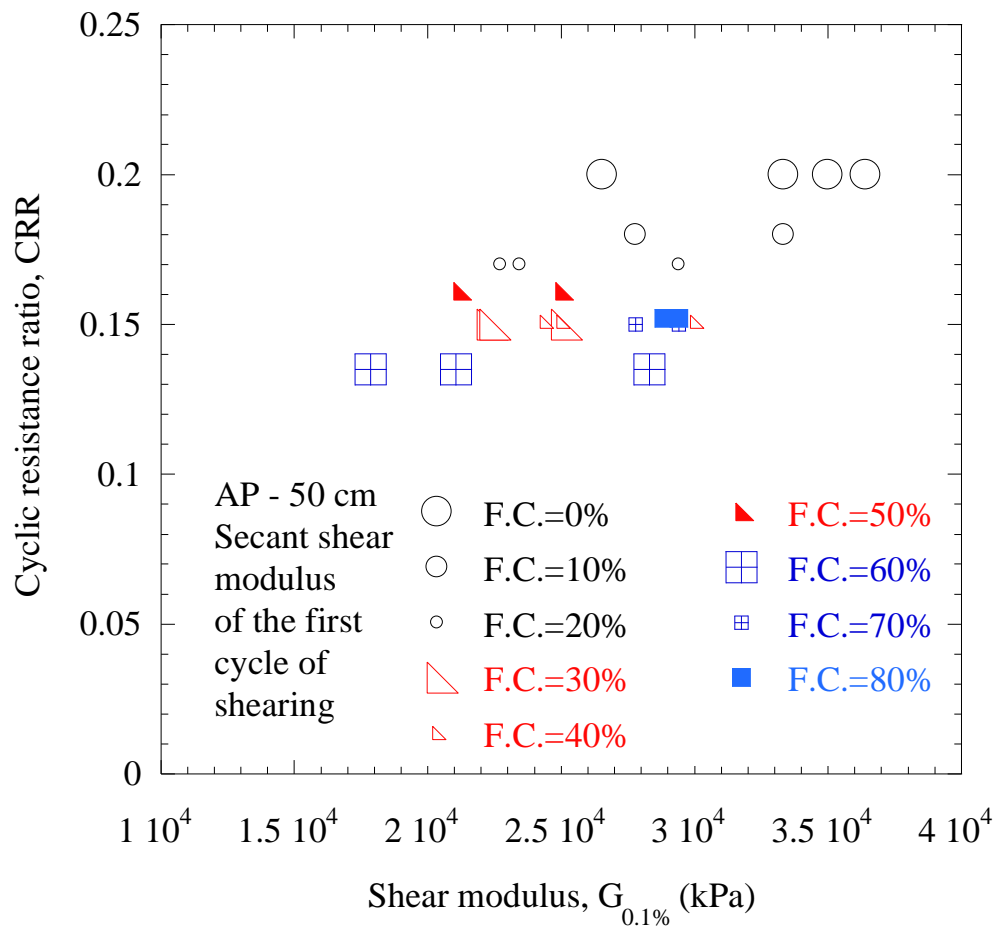


Figure 6.3. Cyclic resistance ratio and shear modulus for 0.1% of shear strain for AP-50 cm

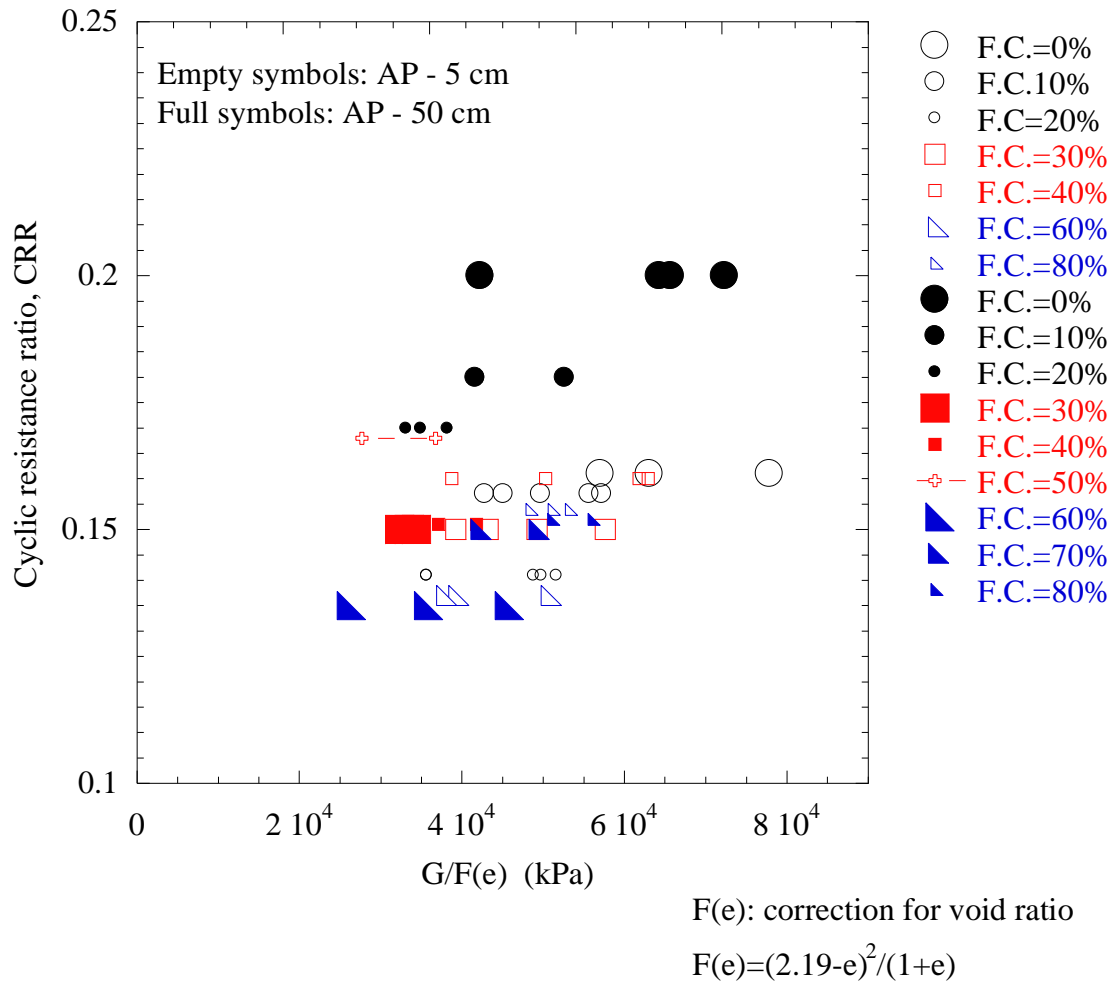


Figure 6.4. Cyclic resistance ratio and coefficient of volume compressibility for AP-5 and 50 cm

Secant shear modulus was measured during cyclic shearing to draw a shear modulus degradation curve. The value for the initial shear modulus was taken from the first cycle of shearing as explained in Figure 6.1; this modulus corresponded to 0.1% of shear strain which represents the situation of no damage from the liquefaction viewpoint, this is the pre-earthquake stage or where no damage has occurred yet. Then all cycles of the stress-strain curve were studied for determining the secant shear modulus. Definition of the secant shear modulus is shown in Figure 6.5. It is observed that the secant shear modulus is the slope of the line that connects two ends of the hysteresis loop.

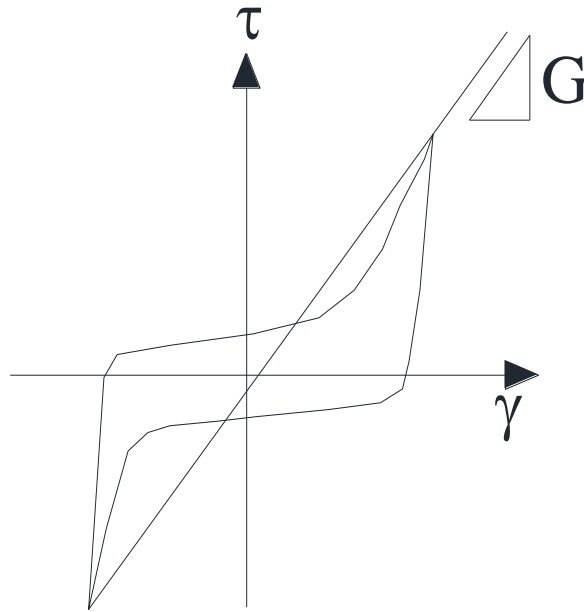


Figure 6.5. Definition of the secant shear modulus

Degradation curves for AP-5 cm are shown in Figure 6.6. Noteworthy is that this curve represents the decay of shear modulus caused by both increasing shear strain and decreasing effective stress during the progress of liquefaction. This figure illustrates that fines content does not seem to have a clear influence on the degradation of modulus during the progress of cyclic loading.

In Figure 6.7 the shear modulus degradation for AP-50 cm is depicted. Small differences can be observed in the different fines contents however there is variance, for example from the curve of 50% to the one of 60%.

Figure 6.8 shows the degradation of shear modulus for similar m_v value. Fluctuations in results are minor, however some groups can be observed, for example 0 and 80% have alike curves. Curves of 40 and 60% also exhibit comparable values. Some resonant column experiments conducted by Amini (2002) demonstrated that when comparing the shear

moduli of sand with different fines contents no correction is required for the transfer functions.

These changes in the degradation of shear modulus are relevant for calculations of lateral displacement as can be observed in the following sections.

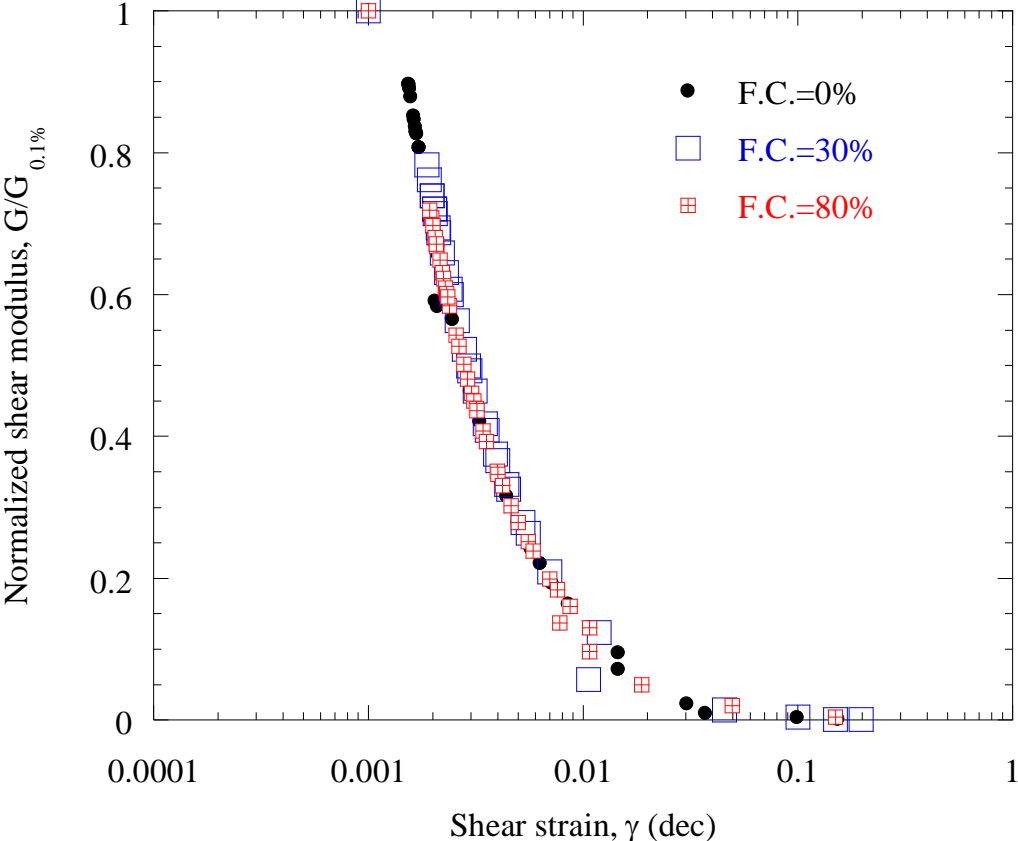


Figure 6.6. Normalized shear modulus degradation for AP-5 cm

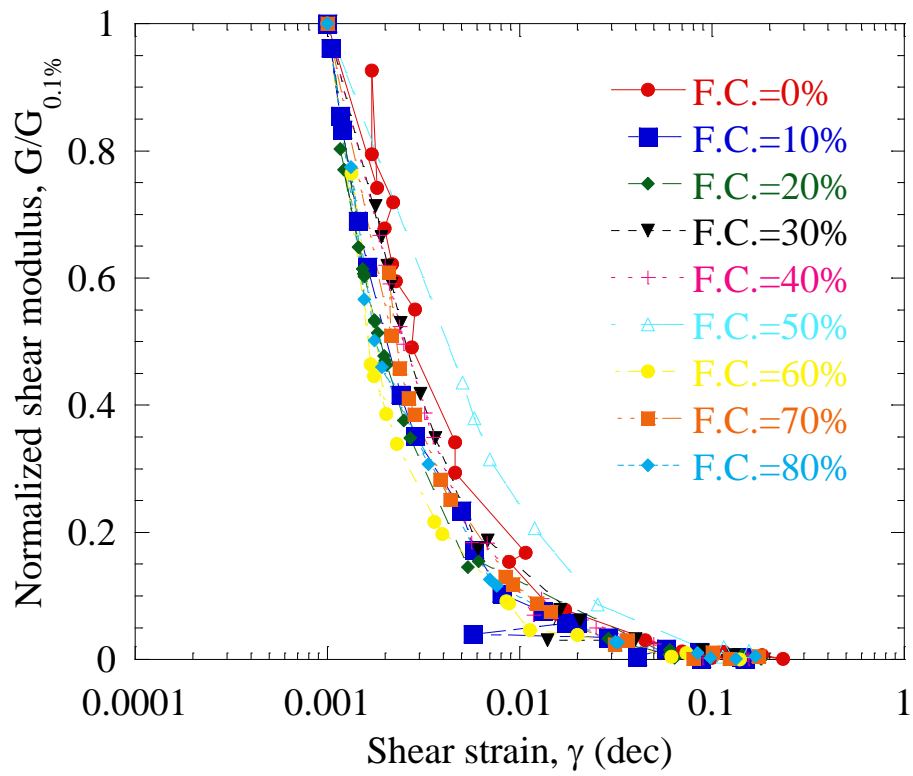


Figure 6.7. Degradation of shear modulus for AP-50 cm

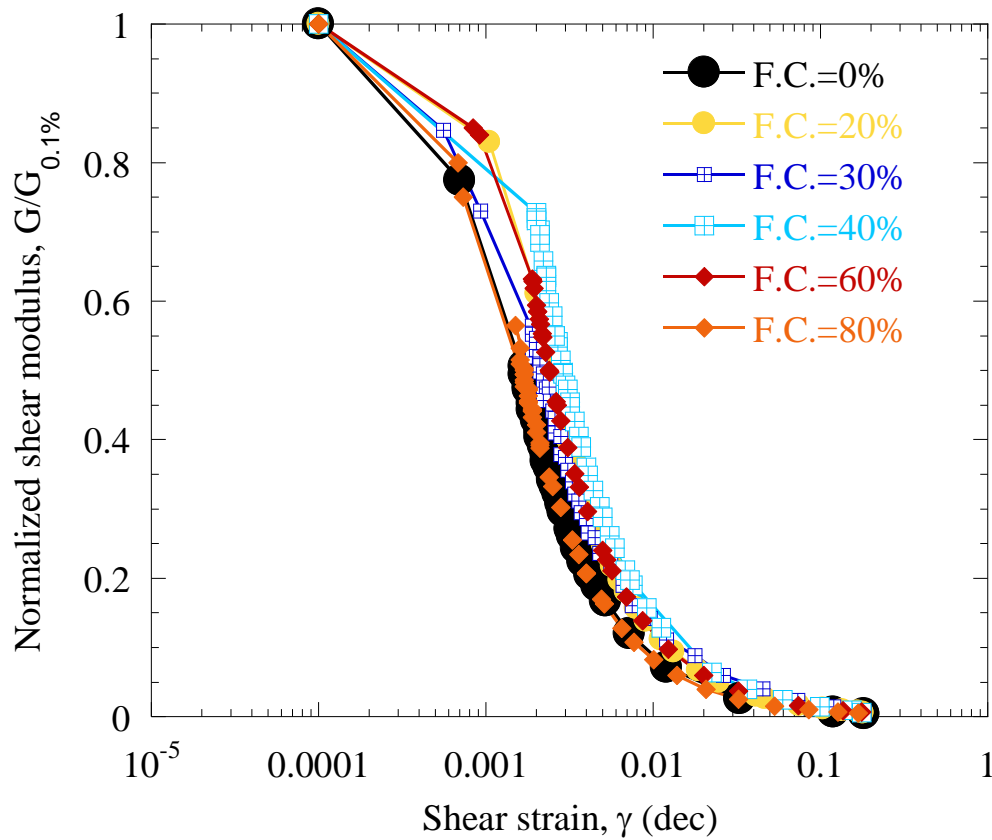


Figure 6.8. Degradation of shear modulus for similar m_v value

6.2. Calculation of lateral displacement

In order to consider the application of the curves of degradation of shear modulus for silty sand, a case analysis is shown. Gunji et al. (2013) developed a simplified formula to predict lateral displacement, which is one of the significant damages during liquefaction.

A sinusoidal curve (Figure 13) was assumed for displacement distribution, F , in the vertical direction and then in order to obtain F of the equilibrium state, after a sufficiently long time of soil flow, the variation of the potential energy due to deformation, q , was integrated over the entire length of liquefied ground and minimized:

$$q = \frac{\pi^2 G_L}{16H_2} F(x)^2 + \left(\frac{E_L H_2}{4} + \frac{E_S H_1}{2} \right) \left(\frac{dF}{dx} \right)^2 - \sin\theta \left\{ \frac{2\gamma_L H_1}{\pi} + \gamma_S H_1 \right\} F(x)$$

where E_L is the Young's modulus of the liquefied soil, E_s is the Young's modulus of the unliquefiable layer and G_L is the shear modulus of the liquefiable layer at the time of liquefaction. The relation $E_L = 2(1 + \nu)G_L$ was considered, and Poisson ratio was assumed to be $\nu = 0.5$. Degradation of shear modulus, G_L , during cyclic loading is the cause of lateral flow. Even if excess pore pressure $r_u < 1$ degradation occurs and this method can take this into account.

According to the variational principle, the Euler equation is given by:

$$\frac{\partial q}{\partial F} - \frac{d}{dx} \left\{ \frac{\partial q}{\partial \left(\frac{dF}{dx} \right)} \right\} = 0$$

It is possible to obtain an analytical solution for this differential equation, considering the boundary conditions of a fixed end at the bottom of a slope ($x=0$) and an open-crack boundary at the top ($x=L$):

$$F_0 = 0 \text{ at } x = 0, \frac{dF_L}{dx} = 0 \text{ at } x = L$$

Solution for these boundary conditions is given by:

$$F(x) = \frac{c_2}{c_1} \left[1 - \frac{\cosh\{\sqrt{c_1}(L-x)\}}{\cosh(\sqrt{c_1}L)} \right]$$

Constants c_1 and c_2 depend on soil properties and geometry:

$$c_1 = \frac{\pi^2 G_L}{(4E_L H_2 + 8E_S H_1) H_2} \quad c_2 = \frac{2 \sin \theta \left(\frac{2\gamma_L H_2}{\pi} + \gamma_s H_1 \right)}{E_L H_2 + 2E_S H_1}$$

A simple example and the definition of these variables are given in Table 6.1 and depicted in Figure 6.9, based on real gathered data. The general procedure for calculating the shear modulus of the liquefiable layer at the time of liquefaction, G_L , is described in the following chart and explained below.

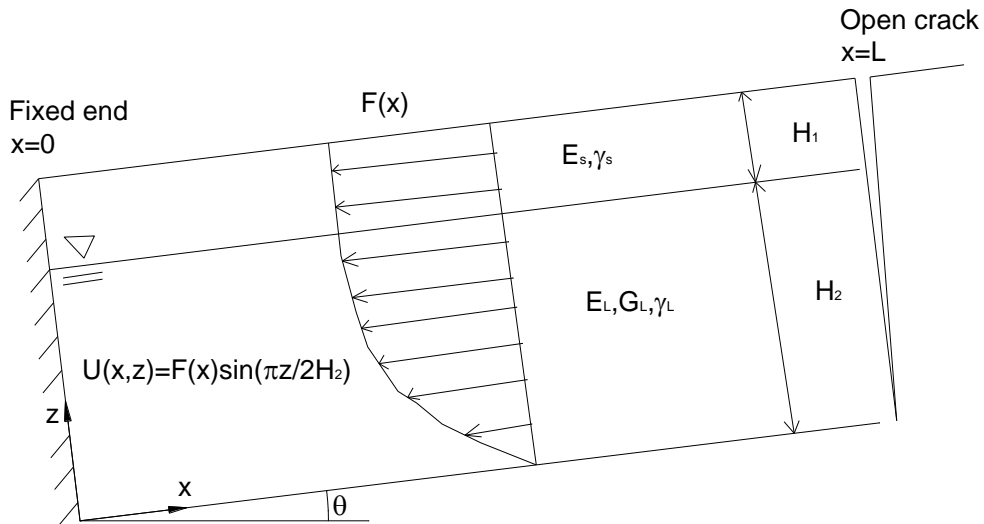
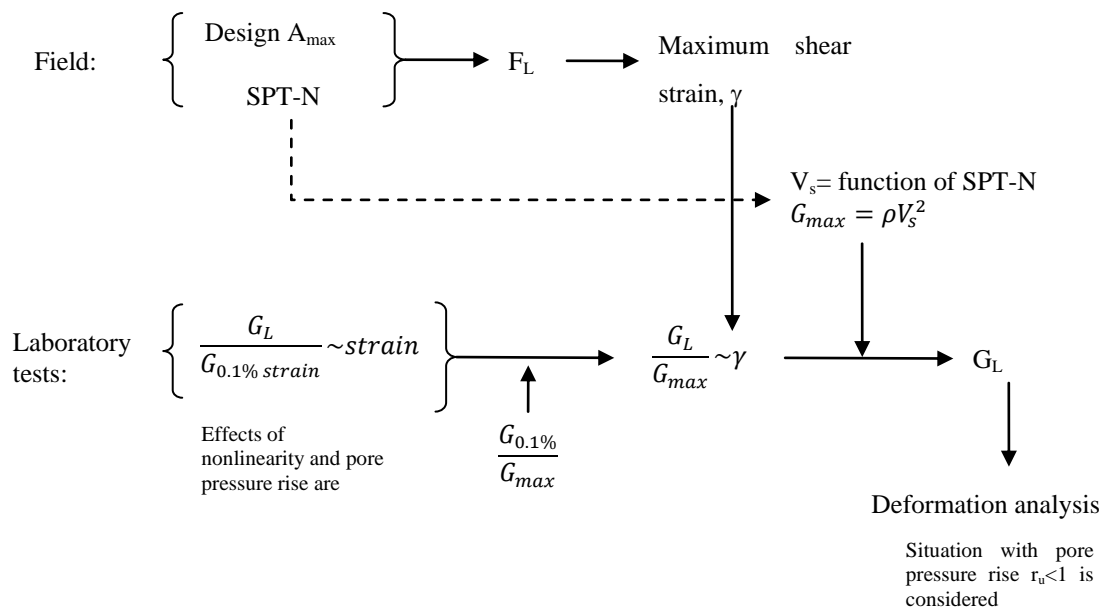


Figure 6.9. Model of lateral displacement



a) The factor of safety can be computed considering the maximum ground acceleration for design A_{max} and the in-situ measured SPT N-value for the liquefiable layer.

- b) Once having the stress ratio and the N-value, the corresponding maximum shear strain, γ , can be found in the figure for cyclic strain in the Foundation Design Code of the Architectural Institute of Japan or elsewhere.
- c) On the other hand, shear wave velocity can be computed from $V_s=80N^{1/3}$ and then, maximum shear modulus from $G_{\max}=\rho V_s^2$.
- d) The degradation curve for the normalized shear modulus $G_L/G_{0.1\%}$ was obtained from the laboratory tests. As explained earlier in this section, the shear moduli for the initial cycles of the tests are within a range of 0.1% shear strain, but the maximum modulus required traditionally for G_L/G_{\max} is given for smaller strains ($10^{-4}\%$). To account for this issue, data measured in Urayasu City by Kawasaki Geological Engineering Co. was summarized and the relation between maximum shear modulus and the shear modulus for 0.1% shear strain was $G_{0.1\%}/G_{\max}=0.44$.
- e) With the strain level, from step (b), the corresponding ratio $G_L/G_{0.1\%}$ can be taken from Figure 12 and can be multiplied by $G_{0.1\%}/G_{\max}=0.44$ to get the ratio G_L/G_{\max} . As G_{\max} was computed in step (c), G_L can be known as well as E_L .
- f) E_s , for the unliquefiable layer can be calculated from the SPT-N value for the unliquefiable layer, and the relation $E_s=2800N$ (kPa).

Table 6.1. Parameters for calculation of lateral displacement of an anonymous site

Parameter	G/G_{\max}
	0.0002
Surface maximum design acceleration, A_{\max} [Gal]	300
Standard penetration test blows for the liquefiable layer, SPT-N	6
Standard penetration test blows for the unliquefiable layer, SPT-N	1
Thickness of unliquefiable layer, H_1 [m]	1
Thickness of liquefiable layer, H_2 [m]	9
Young modulus of unliquefiable layer, E_s [kPa]	2800
Young modulus of liquefiable layer, E_L [kPa]	24.7
Shear modulus of liquefiable layer at the time of liquefaction, G_L [kPa]	8.24
Unit weight of unliquefied soil, γ_s [kN/m ³]	16.5
Unit weight of liquefied soil, γ_L [kN/m ³]	18.5
Slope length, L [m]	640
Slope angle θ (°)	0.005

Considering the set of boundary conditions, where there is no displacement at the bottom of the slope and some cracks open in the upper slope, the calculation of displacement along the slope length was carried out and results are shown in Figure 14. Strictly speaking, the earthquake-induced displacement is equal to the subtraction: Displacement (when $G=G_L$)- Displacement (when $G=G_{0.1\%}$), however if the latter one is small it can be neglected.

Calculation is comparable with the observation at an anonymous site. Thus, seismic lateral displacement of a slope composed of silty sand can be assessed.

The present method is able to assess the lateral displacement for all the extents of pore water pressure rise; not limited to the state of full liquefaction. Note that the calculated displacement is the maximum possible for the given factor of safety against liquefaction. The time development of displacement is yet to be studied.

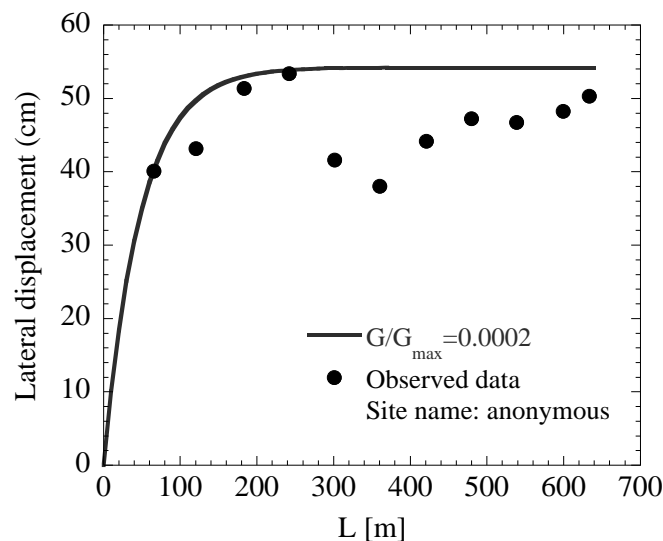


Figure 6.10. Calculation of lateral displacement

This procedure showed to be accurate if the shear modulus of the liquefiable layer is known; in this regard the curves presented herein can be used to obtain $G_L/G_{0.1\%}$ values. However, special care should be taken when considering small-strain stiffness for silty sand, as reported by Salgado et al. (2000), who performed bender element tests on Ottawa sand with silt and found that G_{max} decreased significantly with the addition of fines.

6.1. Stress-strain modified curves

Koseki et al. (2005) performed hollow cylindrical torsional shear test on Toyoura sand and presented modified curves of the ratio of corrected shear stress over corrected mean effective stress versus shear strain. These curves were intended to amend the stresses obtained during cyclic loading. Figure 6.11 shows the curves with the stress ratio t/p' without the correction and Figure 6.12 exhibits a larger scale of the same curve. Curves with the ratio t/p for the different groups of behavior are presented from Figure 6.13 to Figure 6.15. In Figure 6.16 the representative fines content of each group are shown, while the correction of the stresses is given in Figure 6.17.

These curves are also useful to easily observe the differences between the skeleton curve for different fines contents. It is observed that in all cases, the samples with FC=60 and 80% develop more deformation and shift the curves to the right side before achieving higher stress ratios and finally reaching liquefaction.

Curves were separated in three different groups from FC= 0 to 20, 30 to 40 and from 60 to 80%, to study the curves separately. It is observed that the weakest curves in every group (FC=20, 30 and 60%) exhibit larger shear strain since the first cycles but in the last cycles the deformation reduces to achieve the maximum value of $\gamma=10\%$ faster.

Without the correction, it is observed that the ratio increases to extremely large values, however for the range of $[-1,1]$ the differences are still observed, for example samples with larger fines content show immediately more shear strain than samples with FC=0, 10 or 40%.

In Figure 6.17 the correction was made for each curve and it is observed that there is a shift of the FC=80% curve to the left as shear strain is developing faster than for FC=0 and 80%. However the stress ratios remain in about the same range and for the same corrected ratio FC=80% shows the largest shear strain and FC=0% the smallest.

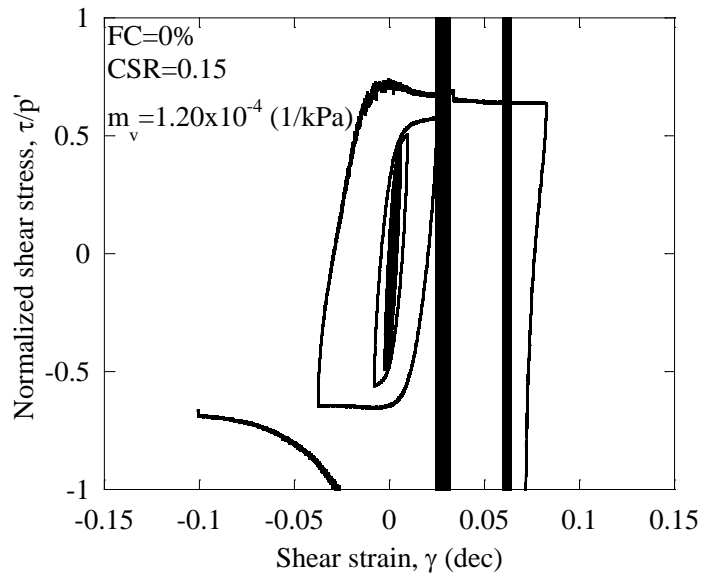


Figure 6.11. Stress-strain modified curve for FC=0% CSR=0.15 by Smv

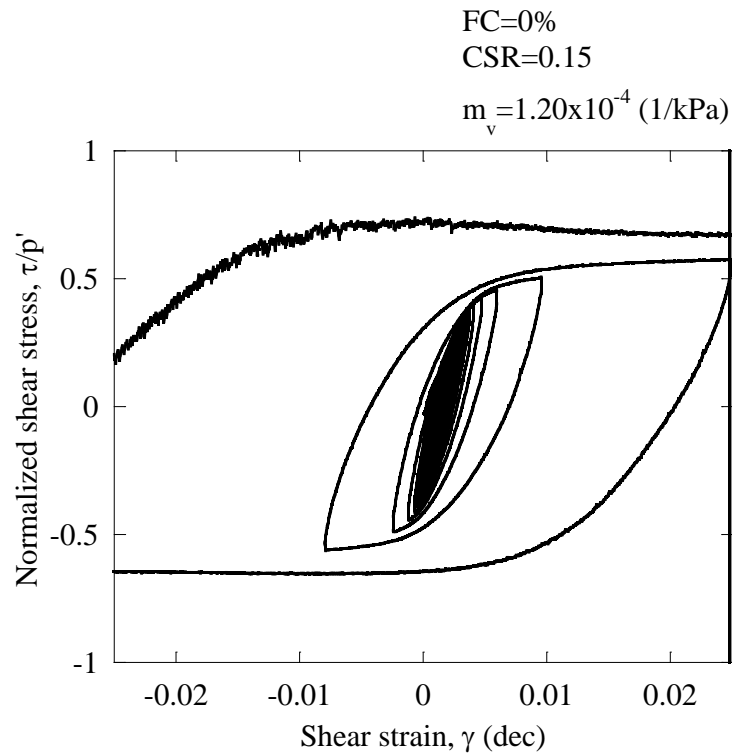


Figure 6.12. Larger scale FC=0% CSR=0.15 by Smv

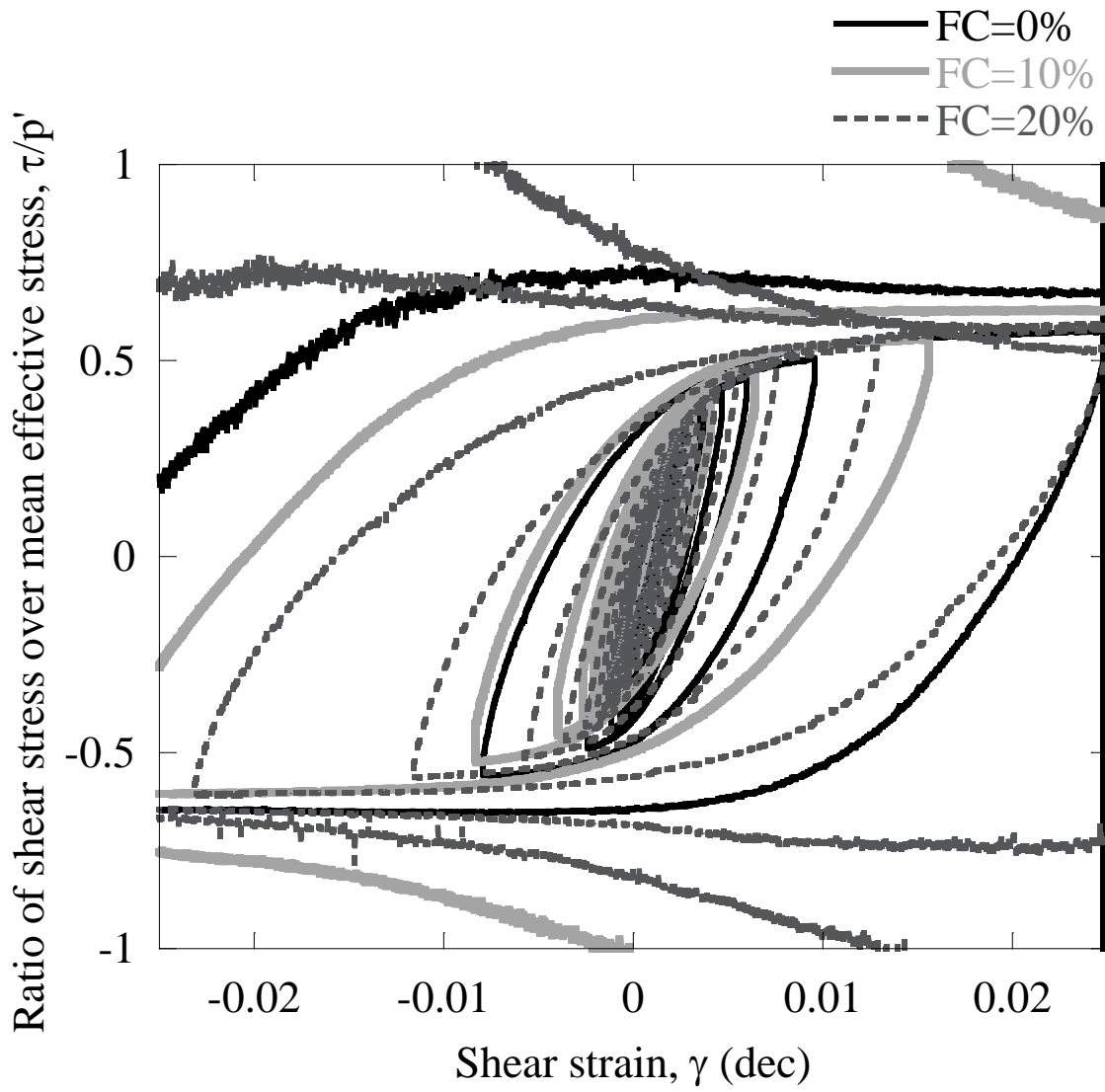


Figure 6.13. Curves of stress ratio τ/p -strain for FC=0, 10 and 20%

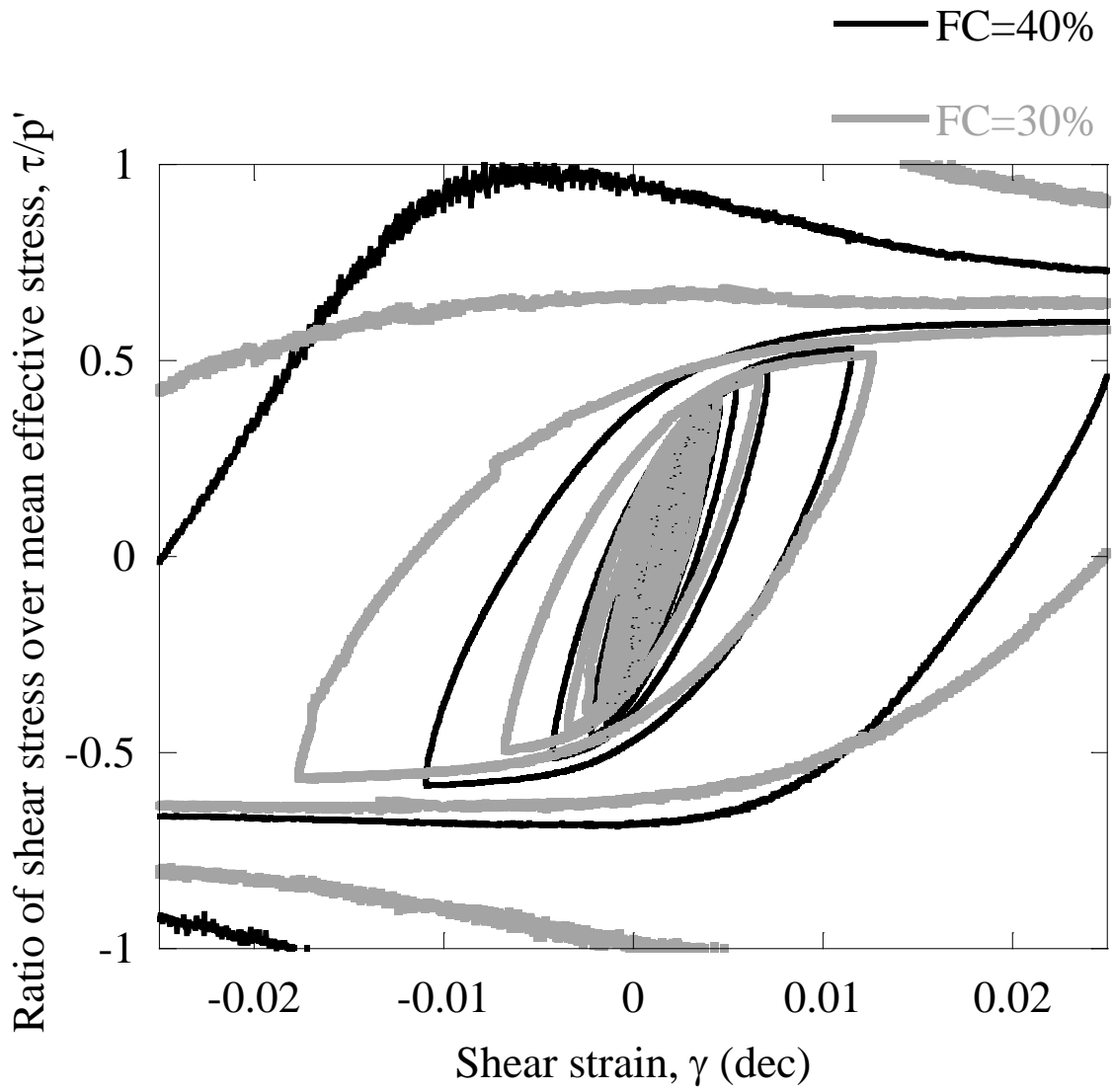


Figure 6.14. Curves of stress ratio τ/p' -strain for FC=30 and 40%

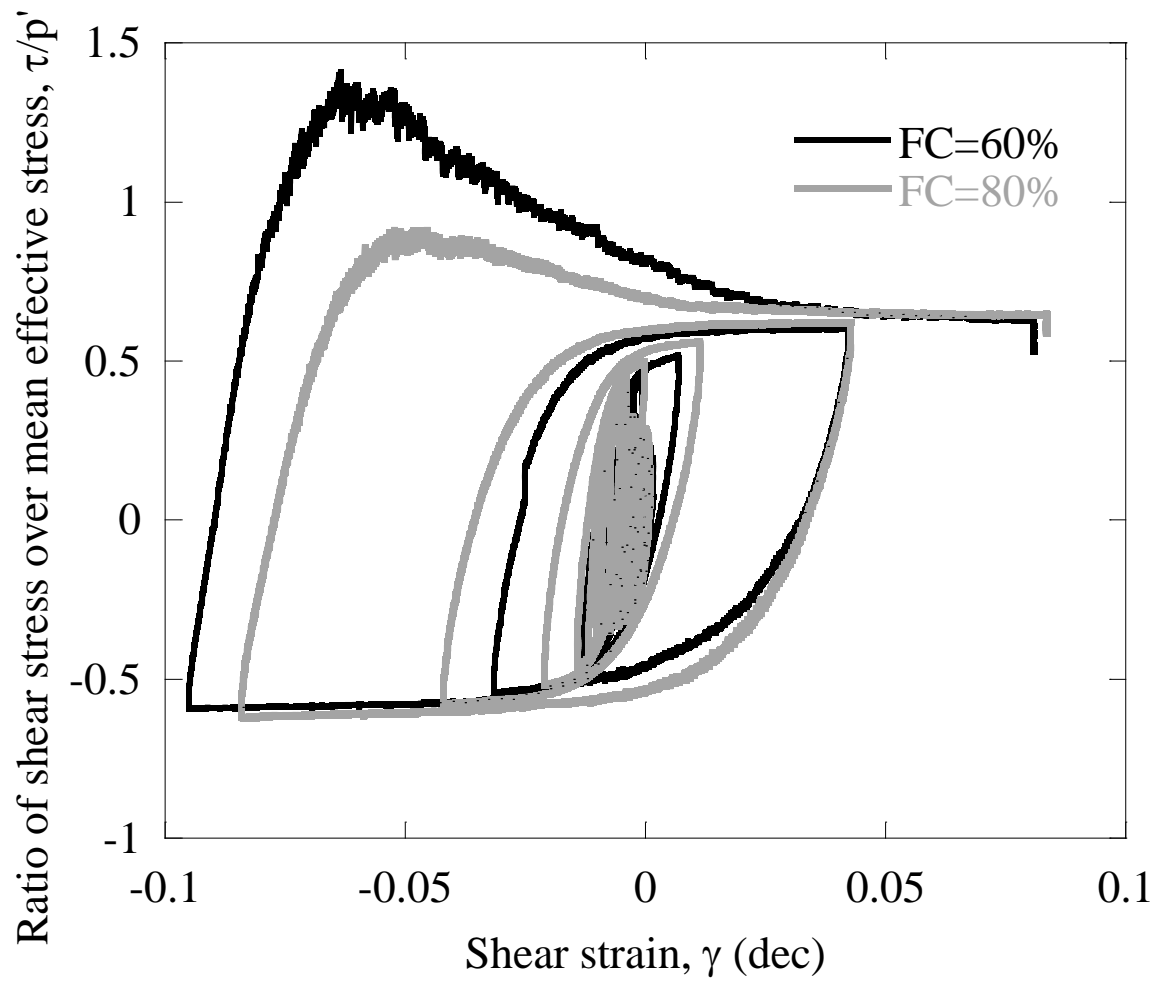


Figure 6.15. Curves of stress ratio τ/p' -strain for FC=60 and 80%

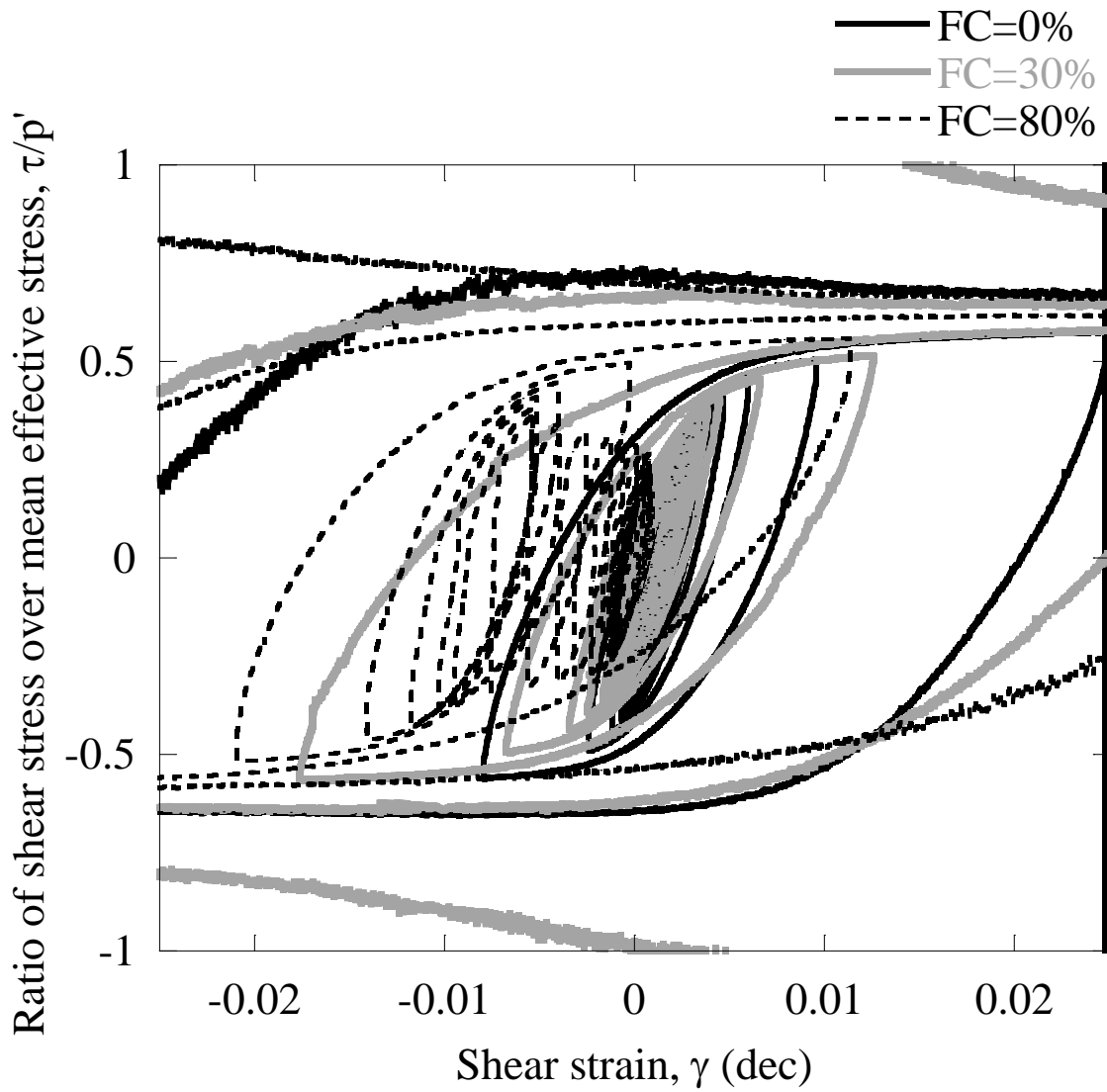


Figure 6.16. Ratio of shear stress over mean effective stress versus strain for FC=0, 30 and 80%

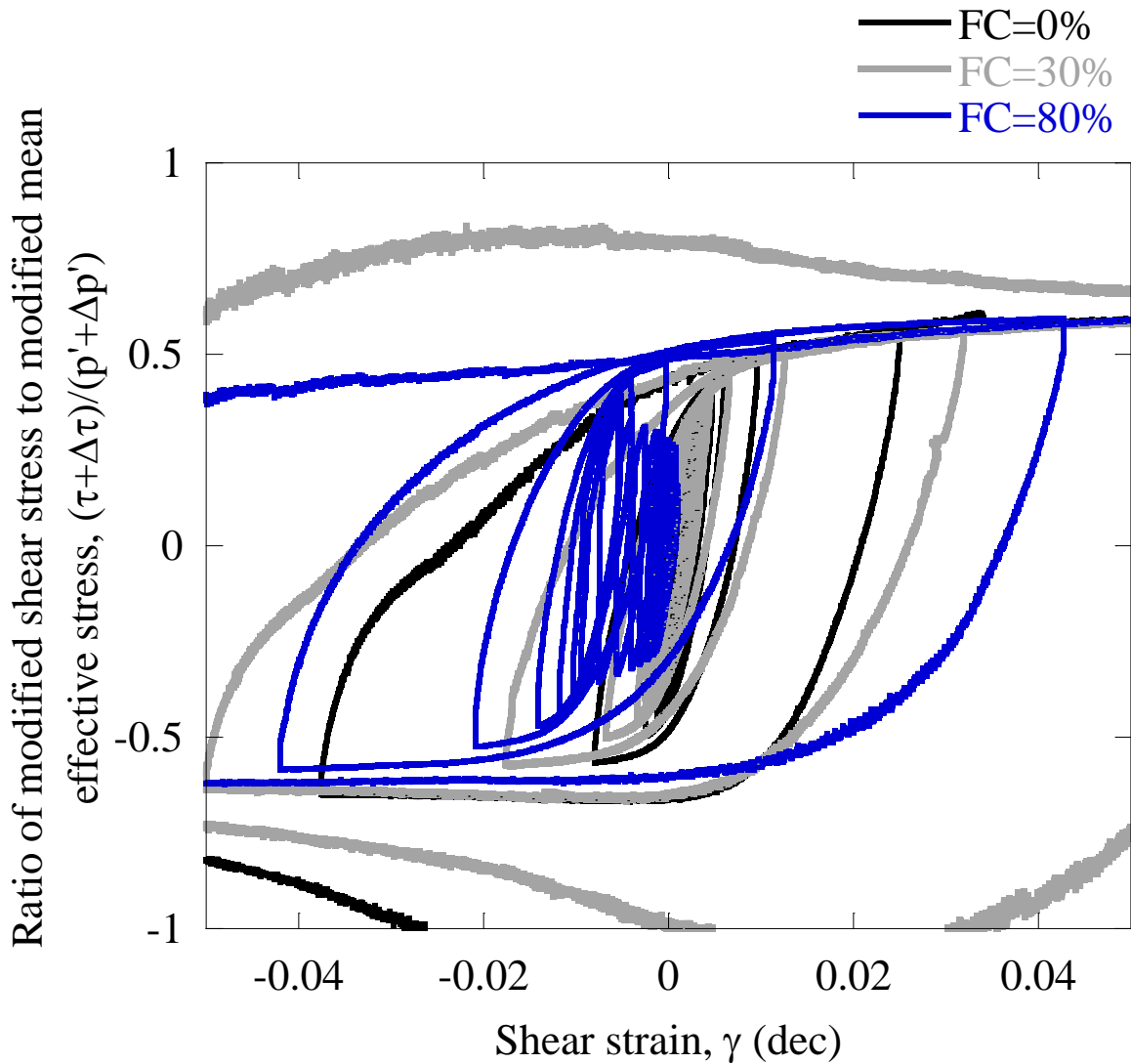


Figure 6.17. Modified stress-strain curves for FC=0, 30 and 80%

6.2. Post-liquefaction deformation

One of the main issues related to liquefaction is the deformation that occurs immediately after liquefaction and causes undesirable effects on the structures.

Several researcher have approached this issue for clean sand (e.g., Ishihara and Yoshimine 1992; Stark et al. 1997; Tokimatsu and Seed 1987; Vaid and Thomas 1995) and some

others have also studied the evaluation of settlement in silty sand deposits after liquefaction (e.g., Ishihara et al. 2004; Toriihara et al. 2000; Tsukamoto et al. 2004).

The mentioned studies did not pursue the effect of fines content on the volumetric strain after liquefaction.

In the experimental program conducted, after evaluating the undrained behavior of sand with different fines contents, the volumetric strain was measured. It is important to remark that these values were measured for uniform cyclic loading, although later results measured for random loads are also provided.

Figure 6.18 and Figure 6.19 show the values measured for different fines contents by AP-5 and 50 cm at the same shear strain, which has been found to be a parameter tightly related to volumetric strain.

In Figure 6.18 it is observed that clean sand has the lower value of volumetric strain, while the largest value is for FC=60%. This coincides to the maximum and minimum cyclic resistance ratio obtained during liquefaction tests. The other fines content remain in the middle, although it can be noted that as fines content increases, volumetric strain also increases.

In Figure 6.19 the volumetric strain measured for samples made by AP-50 cm is depicted. Similarly to the previous plot, the minimum value of volumetric strain is exhibited by the FC=0% sample, while the largest value was measured for the FC=60% sample. This is consistent with the previous results obtained, although in this case, most of the other fines contents lie on the same range of volumetric strain.

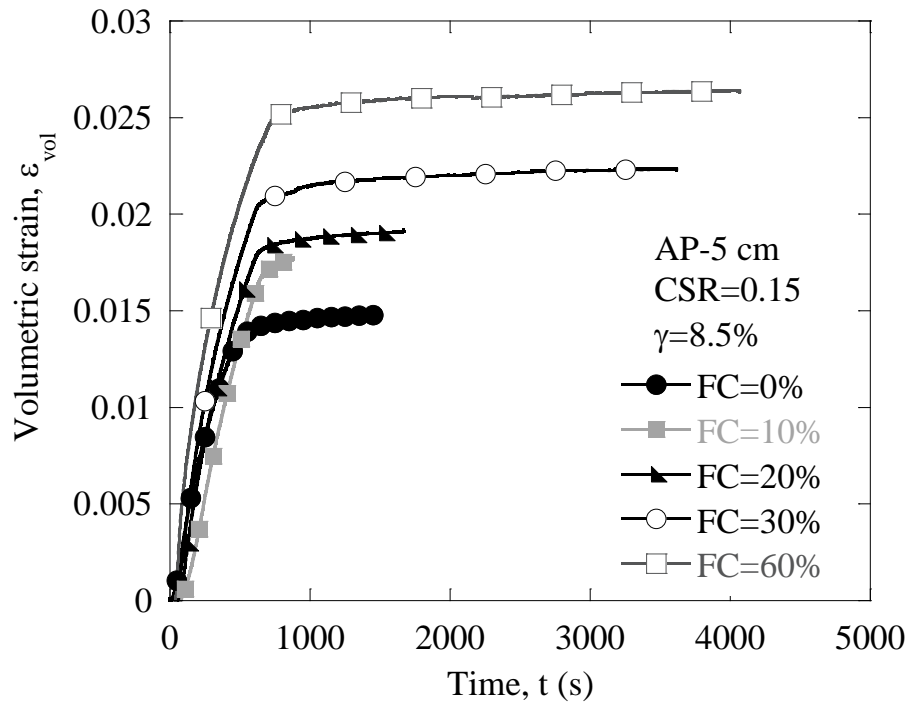


Figure 6.18. Volumetric strain after uniform loading CSR=0.15 AP-5 cm

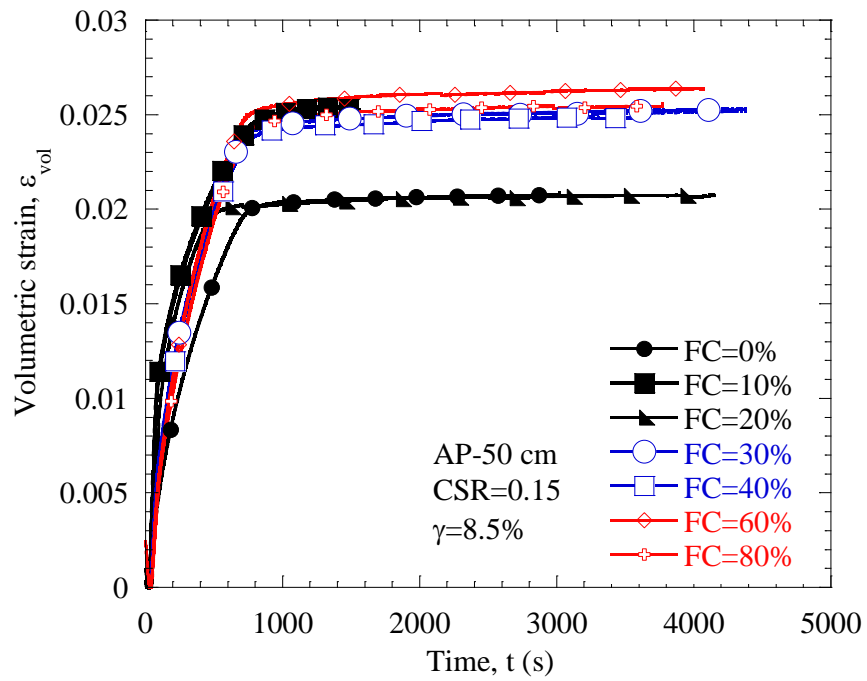


Figure 6.19. Volumetric strain after uniform loading CSR=0.15 AP-5 cm

6.2.1. Random loading

Considering the tests conducted by several researchers, undrained random loading was applied using an acceleration time history recorded in Urayasu. One example of the load applied is depicted in Figure 6.20.

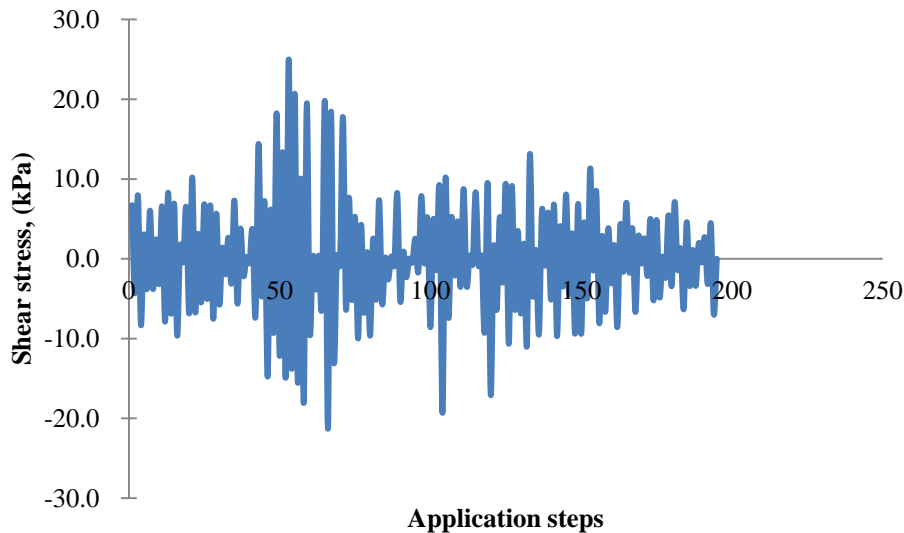


Figure 6.20. Random loading

Even though it is usually recommended to test different kinds of acceleration records in compression and extension tests, Ishihara et al. (2004) found that their results were independent of the type of acceleration and volumetric strains compared whether they were measured after compression or extension tests.

Similar tests were run by Toriihara et al. (2000) and Tsukamoto et al. (2004). Some of the results for different void ratios can be observed in Figure 6.21, where it can be appreciated that as the void ratio decreases, volumetric strain measured after liquefaction also decreases. It is also noted that after 10% of shear strain, values of volumetric strain seem to stabilize and maintain the same value of volumetric strain regardless of the value of shear strain measured during liquefaction.

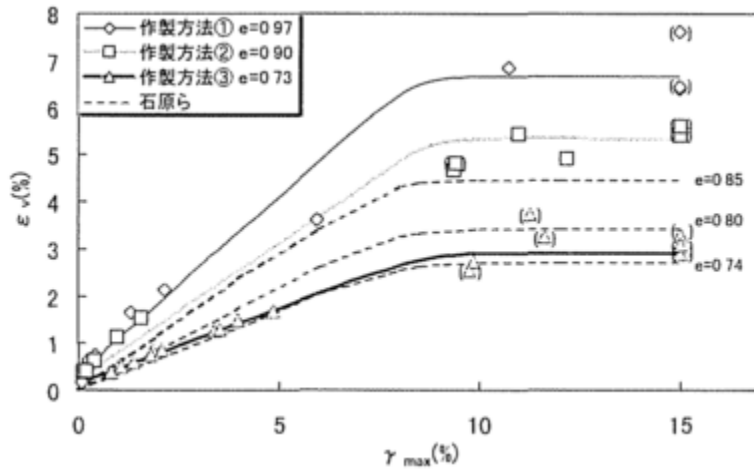


Figure 6.21. Variation of volumetric strain with shear for different shear strains (From Toriihara et al., 2000)

After applying random loads, drainage was opened at specific shear strains to measure volumetric strain. In Figure 6.22 there is an example of the load applied on a sample of clean sand (FC=0%). In this case, load was applied up to 9% shear strain before opening drainage for measuring volumetric strain. The effective stress path is depicted in Figure 6.23 for the same sample, where the different values of shear stress can be observed. Similar curves for fines content FC=20, 30 and 80% are presented from Figure 6.24 to Figure 6.29.

Samples with FC=20 and 80% seem to have the weakest resistance to the same load wave. Yet, it can be observed that the sample with 80% reaches a minimum value of 40 kPa of mean effective stress and shear strain $\gamma=0.2\%$ before actually failing. The failure resembles monotonic loading and after that shear strain increases rapidly until achieving $\gamma=10\%$. When the value of the volumetric strain of this test was compared to other with smaller shear stress amplitude that liquefied, it was observed that both coincided.

These results are very interesting since in this case it can be observed that the 80% sample has a behavior similar to that expected for clayey material.

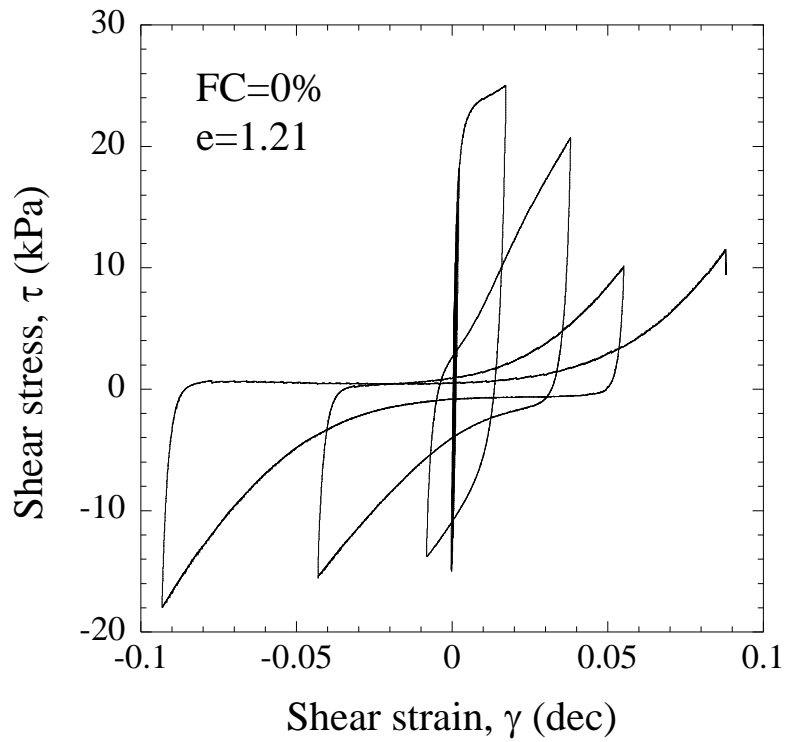


Figure 6.22. Stress-strain curves of random undrained loading on FC=0% sample

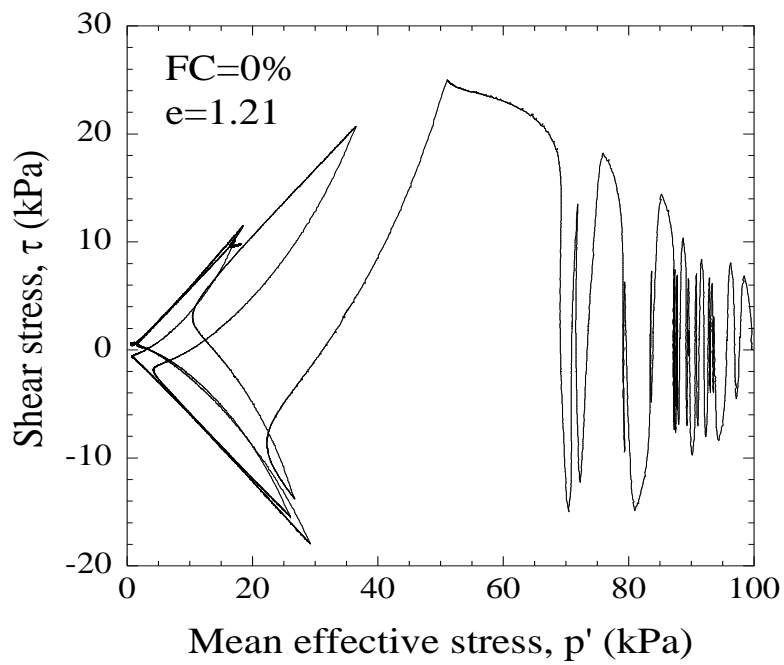


Figure 6.23. Effective stress path for random undrained loading on FC=0% sample

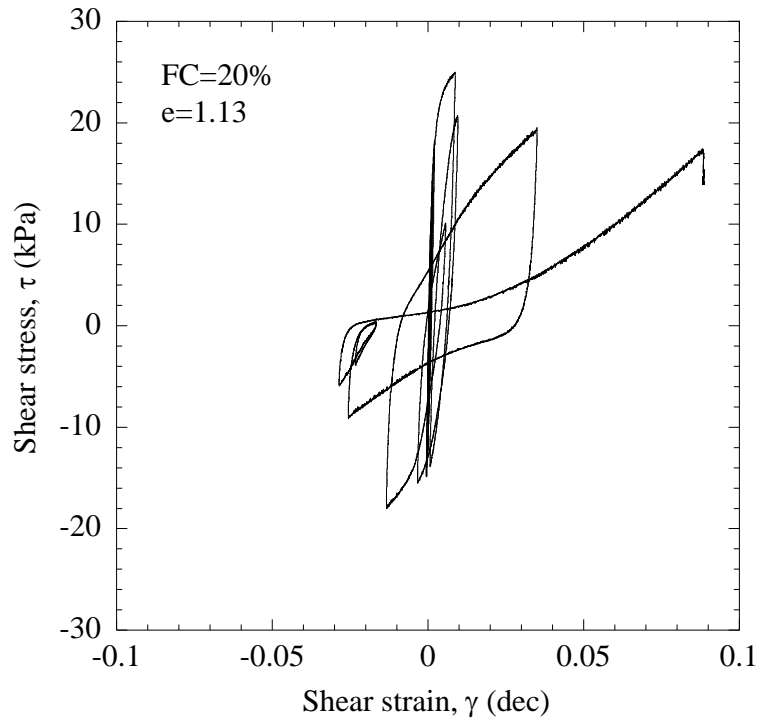


Figure 6.24. Stress-strain curves of random undrained loading on FC=20% sample

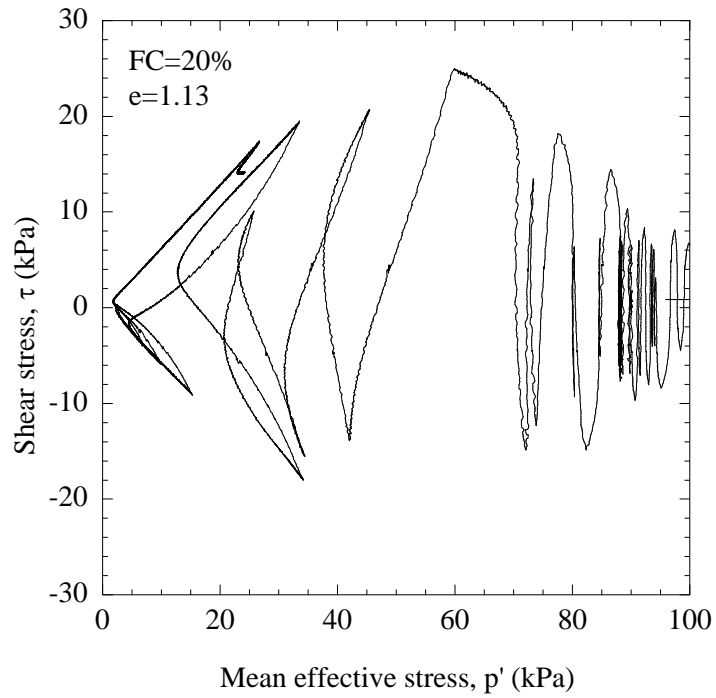


Figure 6.25. Effective stress path for random undrained loading on FC=20% sample

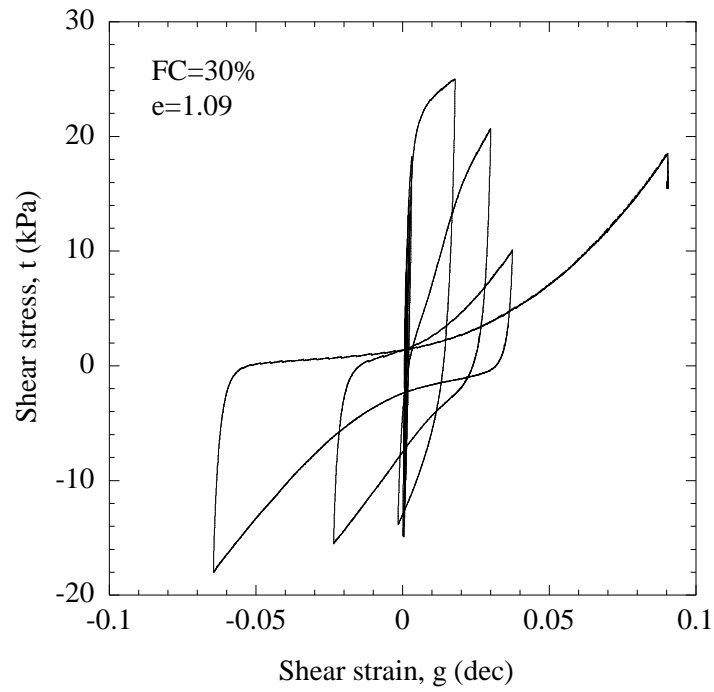


Figure 6.26. Stress-strain curves of random undrained loading on FC=30% sample

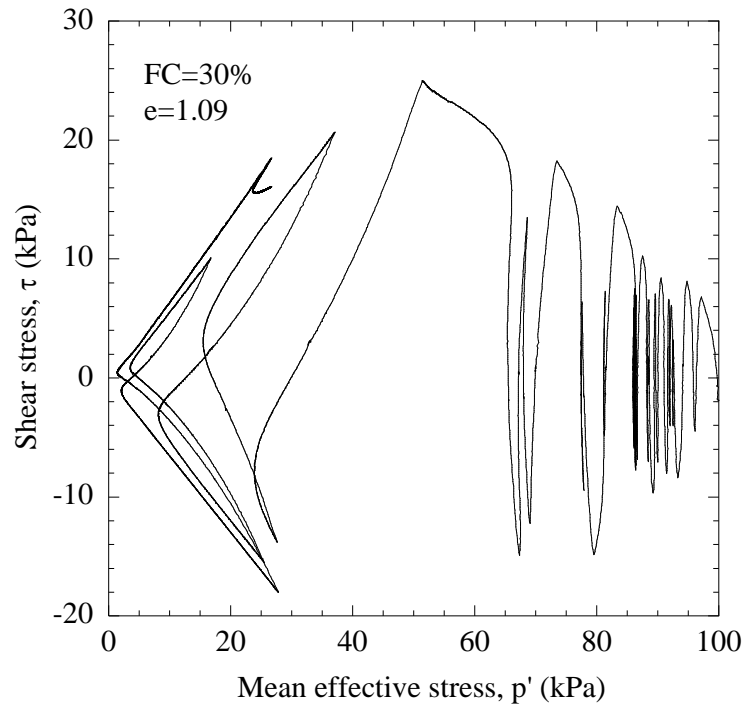


Figure 6.27. Effective stress path for random undrained loading on FC=30% sample

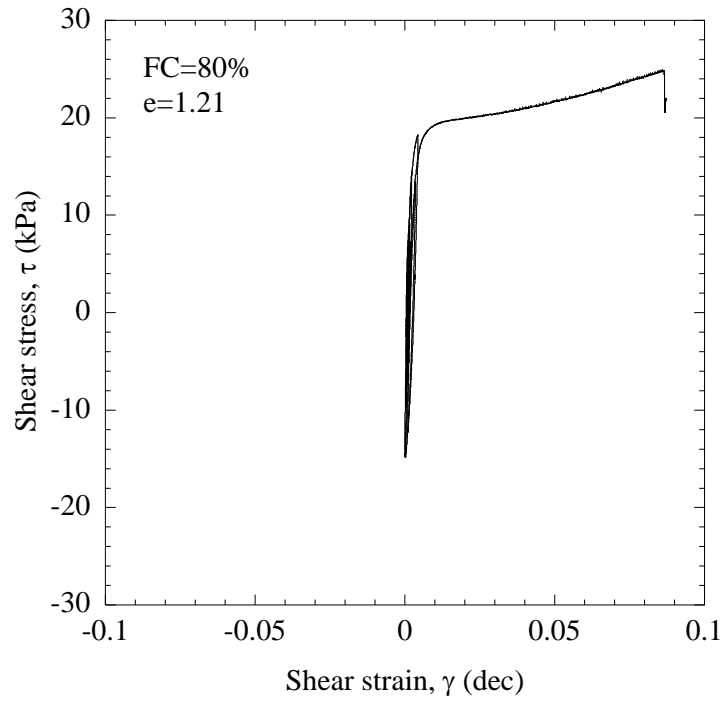


Figure 6.28. Stress-strain curves of random undrained loading on FC=80% sample

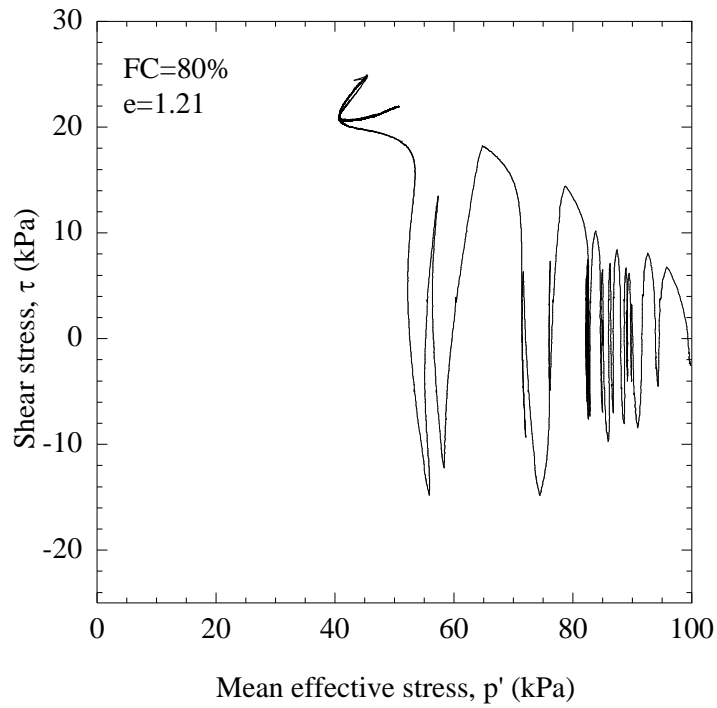


Figure 6.29. Effective stress path for random undrained loading on FC=80% sample

Modified stress-strain curves were also drawn for CSR=0.25 without (Figure 6.30) and with correction (Figure 6.31) for FC=0, 20, 30 and 80%. The clean sand sample depicts larger deformation while 20 and 80% exhibit large shear strain in fewer cycles. It is also observed in both figures that the ratio of τ/p' for FC=0% increases in the last cycle before reaching liquefaction. These curves are helpful to observe the skeleton curve and compare the behavior of different fines contents. It can be seen that the higher values of stress ratio are obtained by the FC=0% sample, then the 30% and finally 20 and 80%.

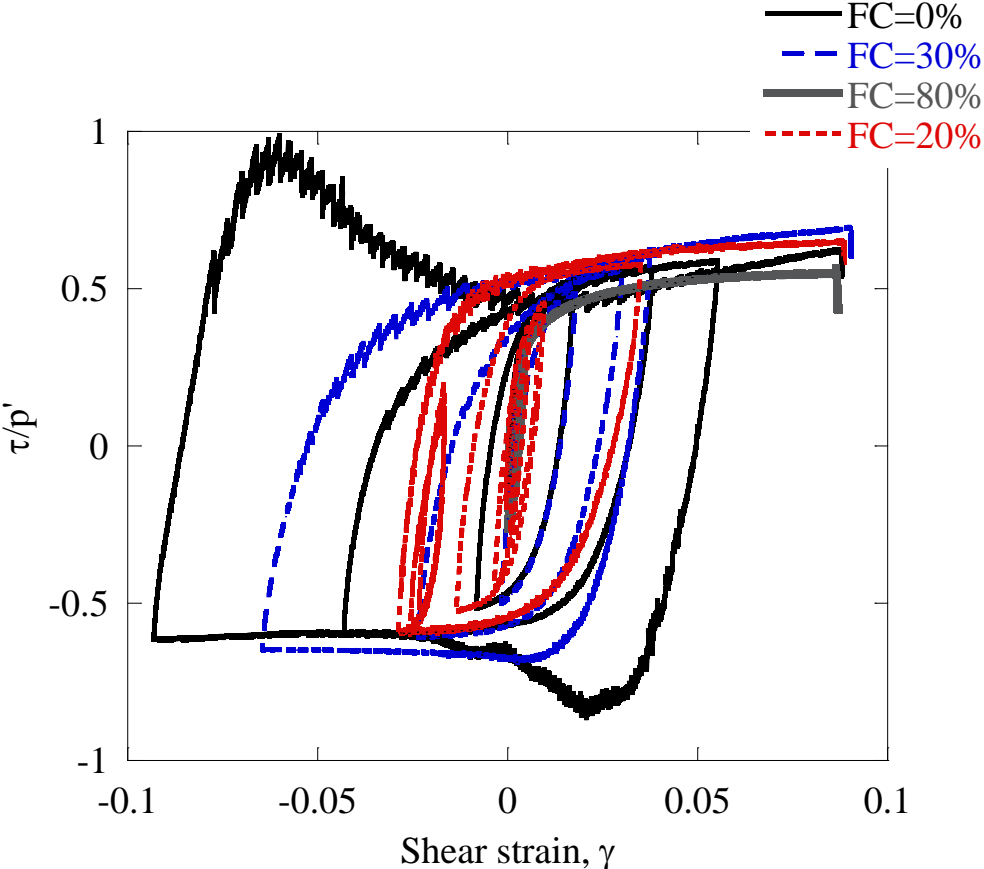


Figure 6.30. Ratio of shear stress over current mean effective stress versus shear strain for random loading. AP=5 cm, CSR=0.25

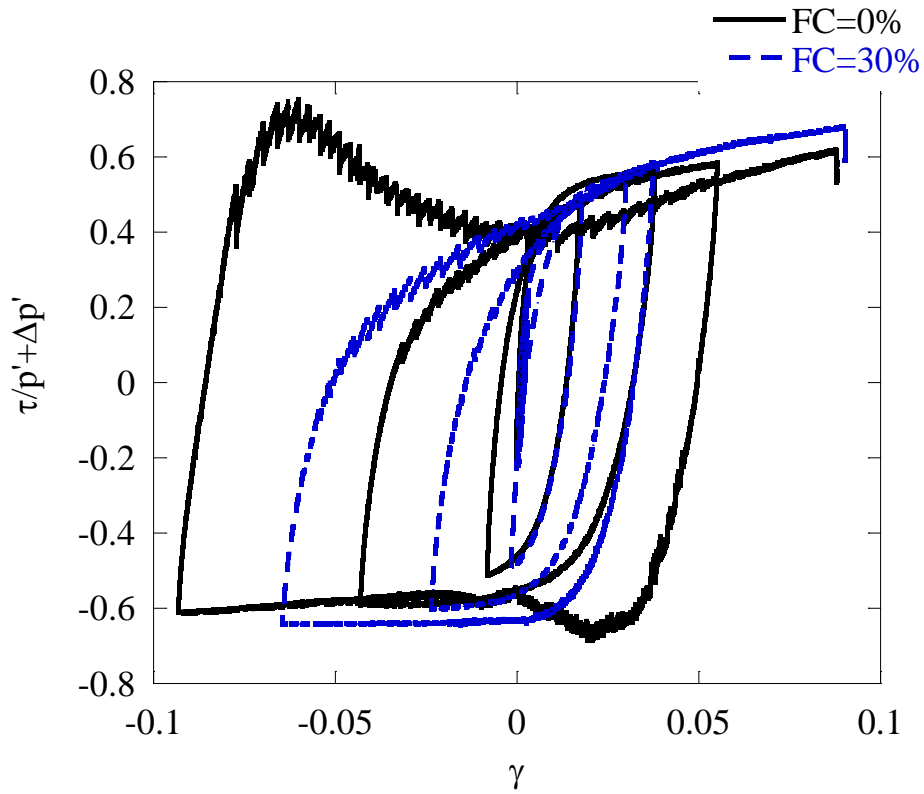


Figure 6.31. Ratio of shear stress over corrected current mean effective stress versus shear strain for random loading. AP=5 cm, CSR=0.25

As explained earlier a good index of hysteresis can be given through the curves of double amplitude of shear strain versus the number of cycles. Figure 6.32 shows the values for FC=0, 30, 80 and 20% for CSR=0.25. It is observed that FC=0% exhibits the largest value of shear strain DA, while the sample with FC=80% shows the lowest value. Results are consistent with those obtained previously for tests made by AP-5 cm and at the same value of m_v .

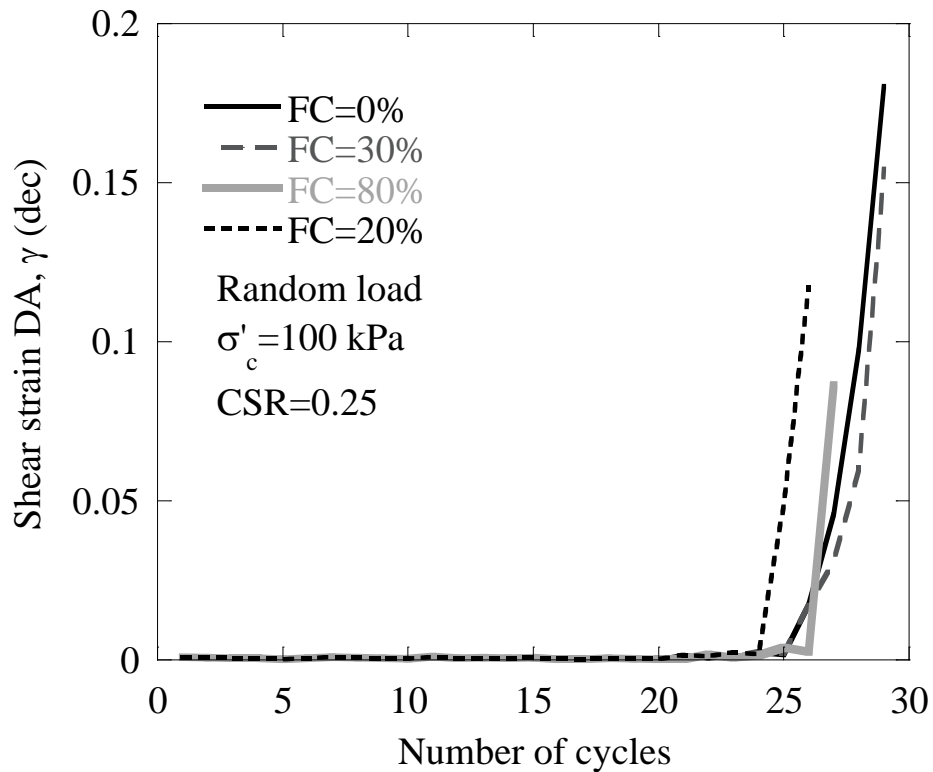


Figure 6.32. Shear strain DA with number of cycles for random loading

Figure 6.33 exhibits the volumetric strain measured after applying undrained loading and comparing the results for similar void ratios. No large difference is observed between the different values, although since all samples were prepared at AP-5 cm, there is not a large range of void ratio.

In Figure 6.34 the values are compared for different fines content: 0, 20, 30 and 80%, that were considered to be representative of the different groups.

It can be observed that the lower volumetric strains were measured for 30 and 0%, while the samples with 20 and 80% exhibit the largest volumetric strain. This result agrees with previous findings.

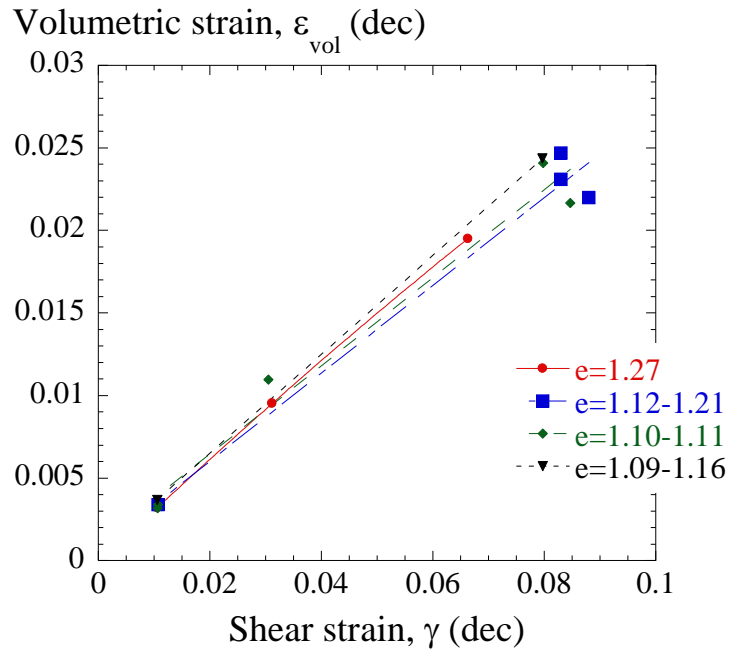


Figure 6.33. Volumetric strain after random undrained loading for different void ratios. AP-5 cm

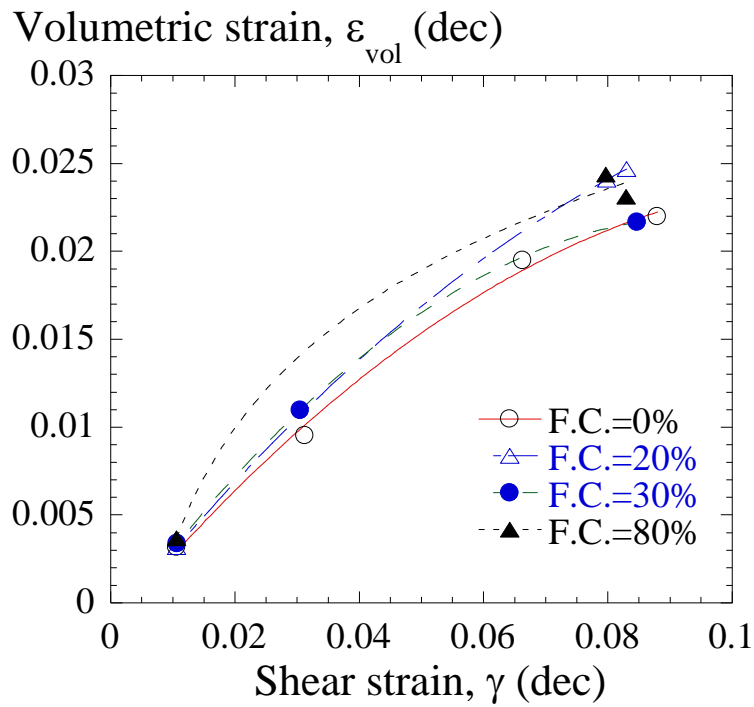


Figure 6.34. Volumetric strain after random loading for different fines contents

Chapter 7

RECONCILIATION OF PREVIOUS RESEARCH

Chapter 7. RECONCILIATION OF PREVIOUS RESEARCH

7.1. Laboratory tests on the effect of fines content

As explained in Chapter 3, the problem of liquefaction of silty sand has been approached in different studies where usually a density measurement has been used to compare different results.

In this regard, this section includes a comprehensive review of different tests on both natural sand with fines and artificial mixes of fines with fines. These results were used in this dissertation intending to analyze the behavior of void ratio range, effective confining pressure and size of particles.

7.1.1. Binary packing

The contact between sand and fine grains can be arranged in several manners. For simpler understanding some researchers assume a binary packing where sand and fine grains have only one size each (e.g., Thevanayagam 2000). In such a case, when fines are less than the threshold fines content, they only fall within the voids filling the spaces with no contribution to the force (Figure 7.1a). This can be valid when the mean size diameter of sand, D_{50} , is at least 6.5 times greater than the mean diameter, d_{50} , of fines. Otherwise ($D_{50}/d_{50} < 6.5$), the fines will fall between the sand particles creating separation between the larger contacts of sand (Figure 7.1b). This will reduce the liquefaction resistance. If fines keep increasing, they will have larger contact with sand grains and will start contributing to the force chain (Figure 7.1c) until the amount of fines is large enough to have the sand grains floating in a fine matrix, reducing now the contacts fine-to-fine (Figure 7d). Then as more fines are added, the sand grains will have zero contact and fines will increase their contact with the corresponding decrease in void ratio (Figure 7.1e).

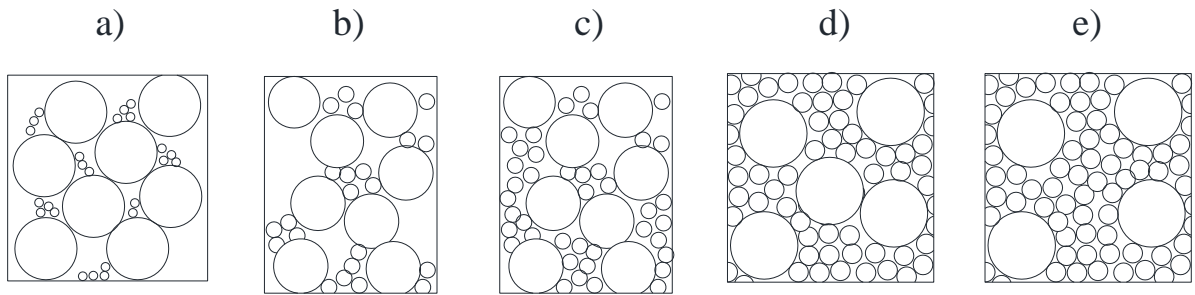


Figure 7.1. Stages of binary packing

In these stages it is possible to identify two important fines content. The first is the threshold fines content, F_{thr} , which is reached when the amount of fines completely fills the voids in the sand matrix. From this point (Figure 7.1c), fines start bearing the load and sand grains, still in contact, act as strengthening. The second is the limiting fines content (Figure 7.1e), F_{lim} , when the amount of fines impedes the contact between sand grains and isolate them one from another. From this point, fines control the overall behaviour of the soil.

The ratio of D_{50}/d_{50} affects the location of F_{thr} and F_{lim} . As shown by Lade et al. (1998), the values of e_{min} shifted according to that ratio. In Figure 7.2, they used the values reported by McGeary (1961) and shown in Figure 3.5, to convert densities into void ratios and show the influence of different ratios of D_{50}/d_{50} in the V-shape and on the minimum void ratio. It can be seen that as the ratio increases, the minimum void ratio is smaller (Figure 7.3). Also, as the value grows the location of the minimum void ratio shifts to the right for greater fines contents.

Another factor that can affect the location of the threshold and limiting fines contents is the sample preparation. In similar manner, when calculating the maximum and minimum void ratios, the use of a certain procedure can shift the minimum values for different fines contents. For instance, Cubrinovski and Ishihara (2002) collected data of the variation of e_{max} and e_{min} calculated for different sands by ASTM standards or JGS standards and found that the use of ASTM standards led to minimum values for greater values of fines contents. However, it has been shown by different researchers (e.g., Cubrinovski and Ishihara 2002; Lade et al. 1998; Rahman et al. 2008) that for most sands, the threshold fines

content is located between 20 and 40%. For the sand tested in this experimental program, the threshold fines content was found to be around 30% and the limiting fines content was around 60%.

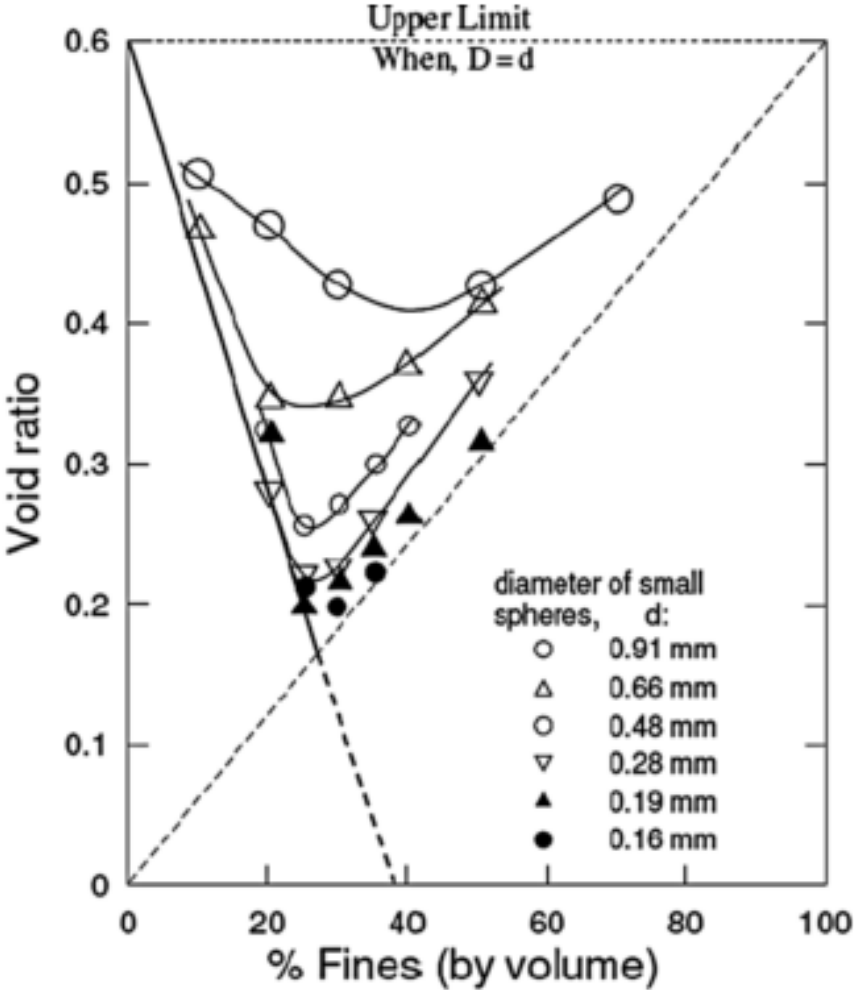


Figure 7.2. Influence of D50/d50. From Lade et al. (1998)

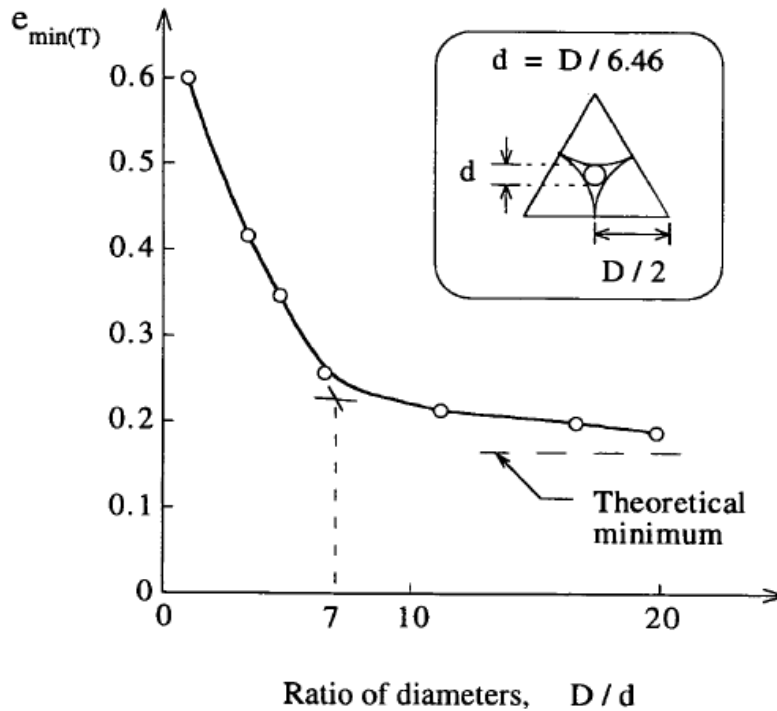


Figure 7.3. Variation of e_{min} with D_{50}/d_{50}

7.2. Reconciliation of previous results

Different results have been found depending on the selection of a density index, as void ratio, relative density or sand skeleton void ratio.

However, the variation of void ratio range for different fines contents and the characteristics of packing depending on particle shape or the ratio between mean size diameter of sand and fines particles, D_{50}/d_{50} , affect the packing and therefore liquefaction resistance.

In Figure 7.4 void ratio is kept constant and the variation in relative density can be observed. As fines content approaches F_{thr} , relative density decreases, therefore tests conducted in this range will find a reduction in cyclic resistance ratio. Figure 7.5 shows the value of relative density kept constant and the variation of void ratio with fines content. In this case, the concept of void ratio range ($e_{max}-e_{min}$) needs to be introduced. As studied by Panayiotopoulos (1989), the most important factors in the packing of sands are the concepts

of minimum and maximum void ratios; the difference between these parameters is defined as void ratio range by Cubrinovski and Ishihara (1999) and it was found to be inversely proportional to the normalized penetration resistance, N_1 , if relative density is kept constant. It can be understood then that when void ratio range reduces, liquefaction resistance increases.

Polito and Martin (2001) conducted tests on Monterey and Yatesville sand with Yatesville fines and when they compared the results of cyclic resistance ratio at the same sand skeleton void ratio, found that for the first, cyclic resistance ratio keeps constant while for Yatesville, it increases with fines content.

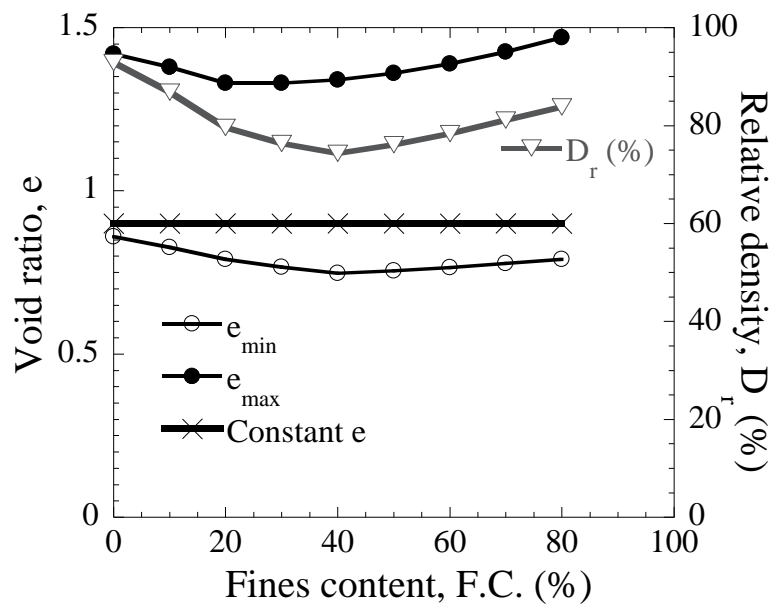


Figure 7.4. Void ratio kept constant

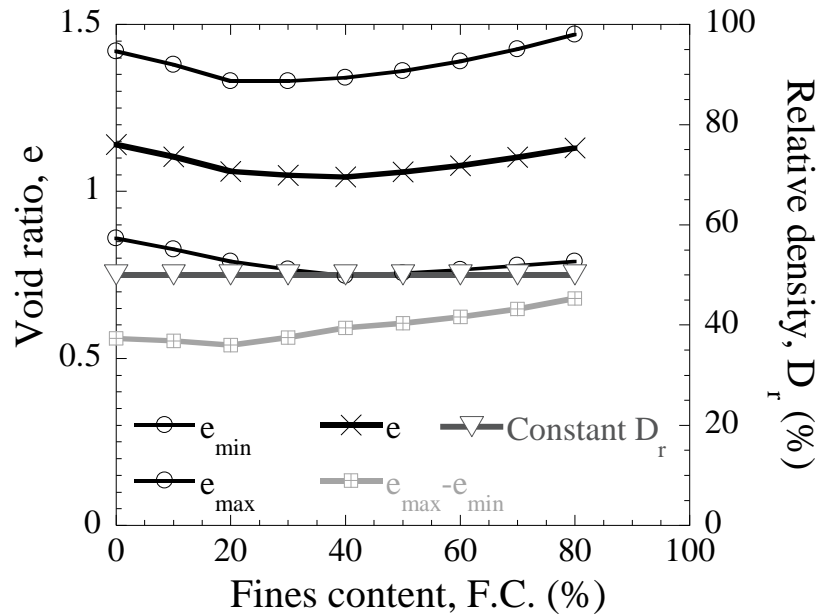


Figure 7.5. Relative density kept constant

The explanation to this behavior is also given in terms of relative density, for example for Monterey sand, when the sand skeleton void ratio is kept constant, void ratio decreases parallel to minimum and maximum void ratios, causing that relative density remains constant for all fines contents tested keeping cyclic resistance ratio constant as well (Figure 7.6).

On the other hand, for Yatesville sand, when sand skeleton void ratio is kept constant, void ratio decreases faster than the values of maximum and minimum void ratios, causing an increase in relative density that leads to the increase in cyclic resistance ratio (Figure 7.7).

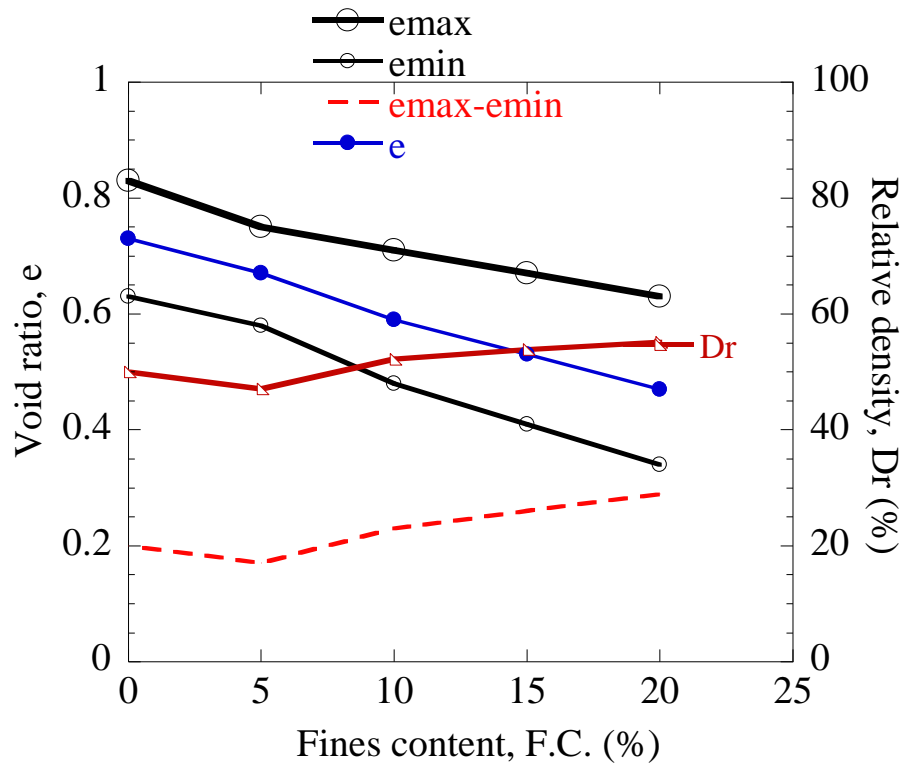


Figure 7.6. Relative density for Monterey sand at the same sand skeleton void ratio

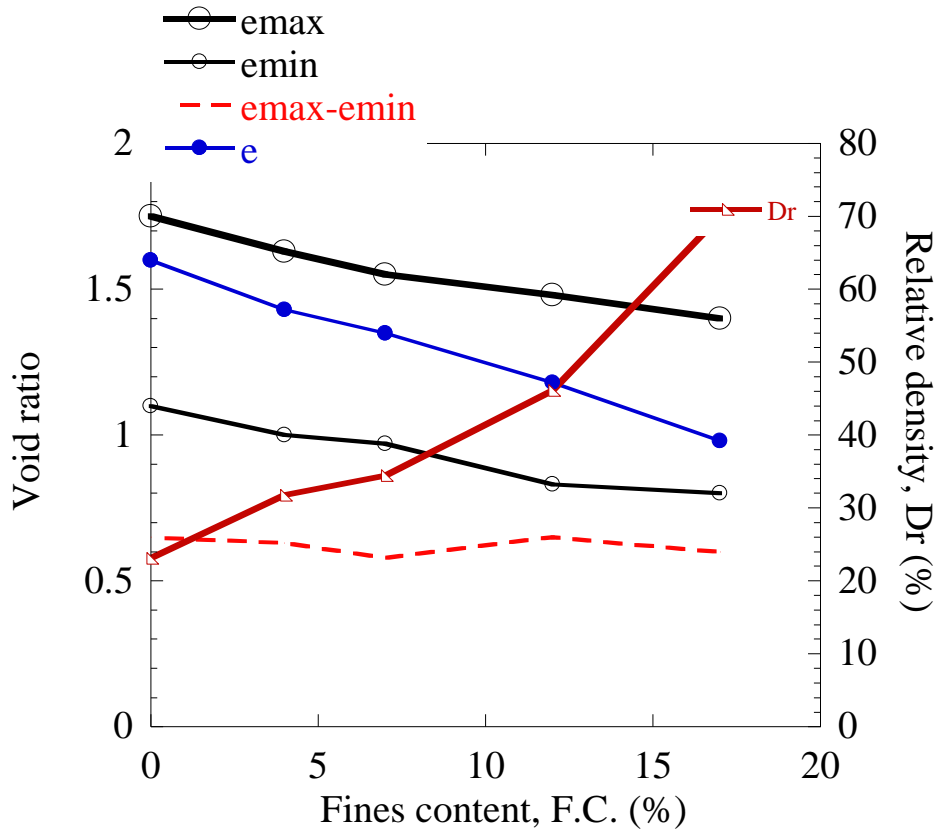


Figure 7.7. Relative density for Yatesville sand at the same sand skeleton void ratio

In the view of these results it can be explained that these parameters led to different results, which can be misleading as there is no relation to the actual parameters of assessment of liquefaction potential.

7.3. Monotonic tests for effective confining pressure, $\sigma'_c=50$ kPa

Other important aspect that must be considered while examining fines content effect on liquefaction resistance is the influence of the effective confining pressure.

To observe this effect a series of monotonic tests were carried out on samples prepared by AP-5 cm at an effective confining pressure of 50 kPa.

Stress-strain curves can be observed in Figure 7.8 and effective stress paths can be seen in Figure 7.9, where the 10% fines content curve exhibits the larger shear strength that

decreases to 30% and then shows a slight increase for 40%. The curve of 0% shows a response similar to the curve of 30%. This results agree partially with those presented by Bouckovalas et al. (2003) who explained a rotation in the critical state lines for confining stress smaller than 60 kPa.

Their idealized change of the critical state line is depicted in Figure 7.10 in an $e-\ln p'$ space.

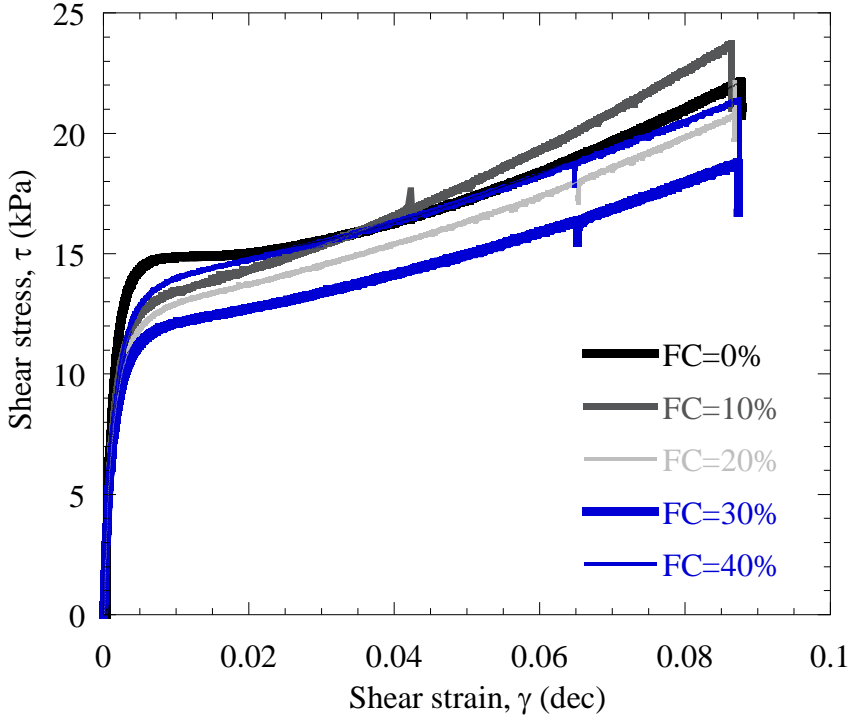


Figure 7.8. Stress-strain curves for monotonic loading at $\sigma'_c=50$ kPa. AP=5 cm

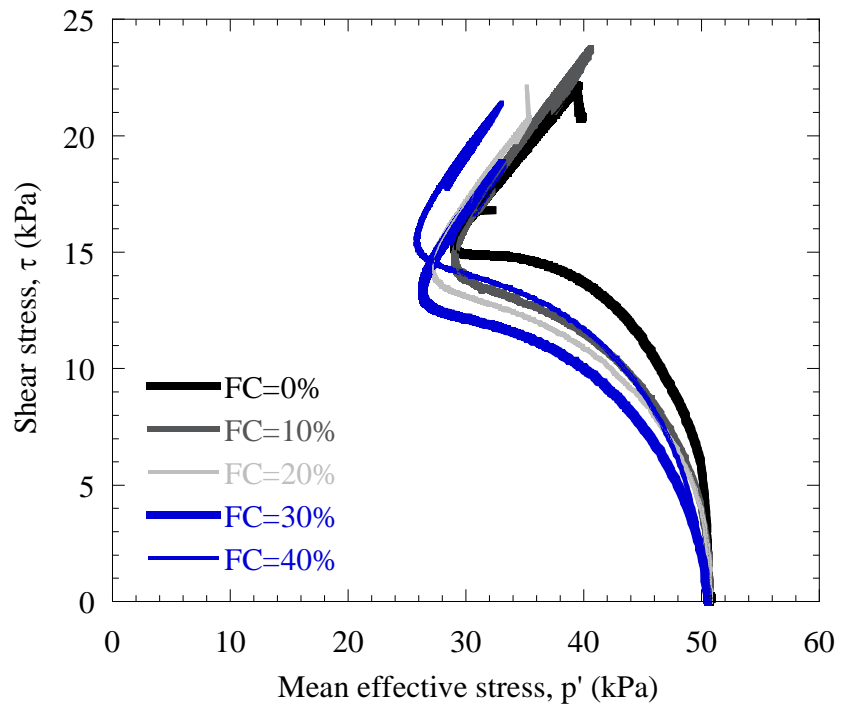


Figure 7.9. Effective stress paths for monotonic loading at $\sigma'_c=50$ kPa. AP-5 cm

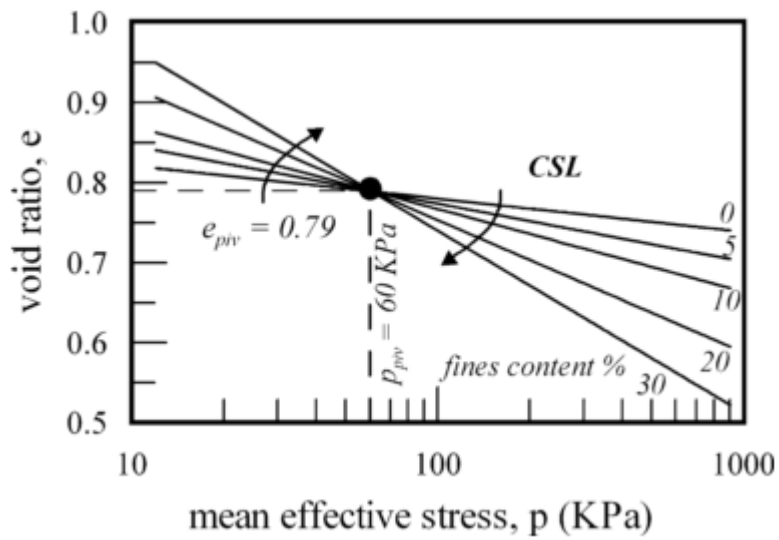


Figure 7.10. Effect of fines on the critical state line. (In Bouckovalas et al. 2003)

However results obtained by Lade and Yamamuro (1997) for Ottawa sand with fines, at a confining stress of 25 kPa in samples prepared at the maximum void ratio showed a decrease in strength with fines (Figure 7.11).

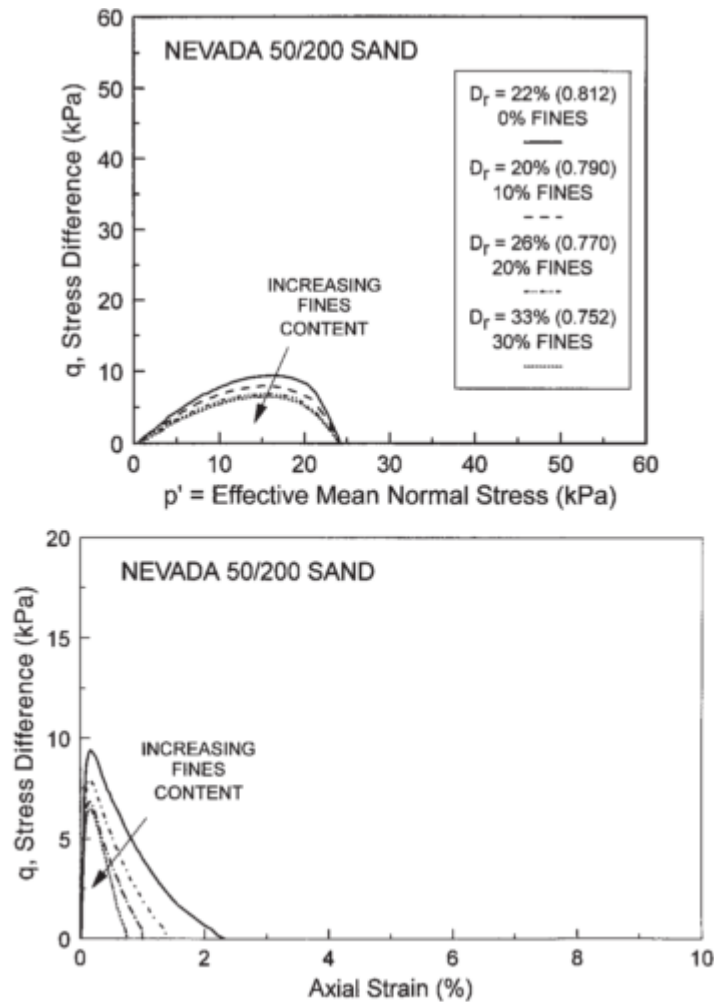


Figure 7.11. Decrease in resistance with fines content for the same compaction energy. From Lade and Yamamuro (1997)

7.4. Low-plasticity fines

As was summarized by Ishihara (1993), the plasticity index is the most important factor affecting materials containing fines. Results in Figure 7.12 show that for low values of plasticity index ($PI < 10$) there is not significant increase of cyclic resistance ratio.

Nevertheless some recent studies as Bray and Sancio (2006) presented lower values of PI for liquefied soils.

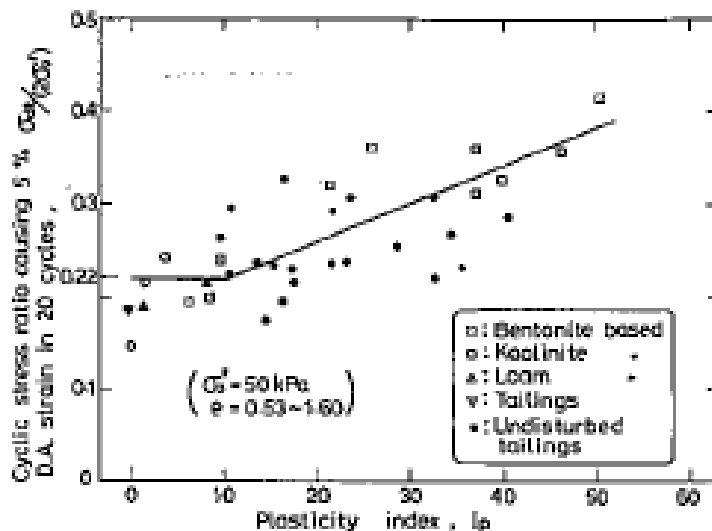


Figure 7.12. Plasticity index and cyclic resistance ratio for soil with fines (From Ishihara 1993)

Andrews and Martin (2000) compiled data of different criteria for liquefaction distinguishing clay from silt and they concluded that the most important parameters are clay content and liquid limit, which they interpreted as a measure of the net attractive force of clays.

A mixture of Tokyo Bay sand with low-plasticity fines, called LPTBS, was prepared. LPTBS contained fines with a plasticity index of 9 (liquid limit, LL=40.6% and plastic limit, PL=31.4%), below PI=12 the limit established by Bray & Sancio (2006) to define a soil as potentially liquefiable. The LPTBS samples were formed keeping a height of fall of 5 cm with 10% (LL= 27.9, PL=26.8), 20% (LL=27.1, PL=26.4) and 30% (LL=26.9, PL=26.6).

Typical curves of stress-strain behavior and effective stress paths are shown from Figure 7.13 to Figure 7.15, for both regular Tokyo Bay sand with non-plastic fines (TBS) and with low-plastic fines (LPTBS), at the same cyclic stress ratio, CSR=0.20 and fines content, FC=10%. Liquefaction was defined as 5% double amplitude shear strain. TBS sample

prepared at 50 cm of height of fall (AP-50 cm) shows higher resistance and more significant degradation of shear modulus than the one prepared at 5 cm (AP-5 cm). The LPTBS sample of AP-5 cm has even less resistance than the TBS at the same height of fall; it reaches initial liquefaction (excess pore pressure equal to 0) after 3 cycles and also shows larger shear strain.

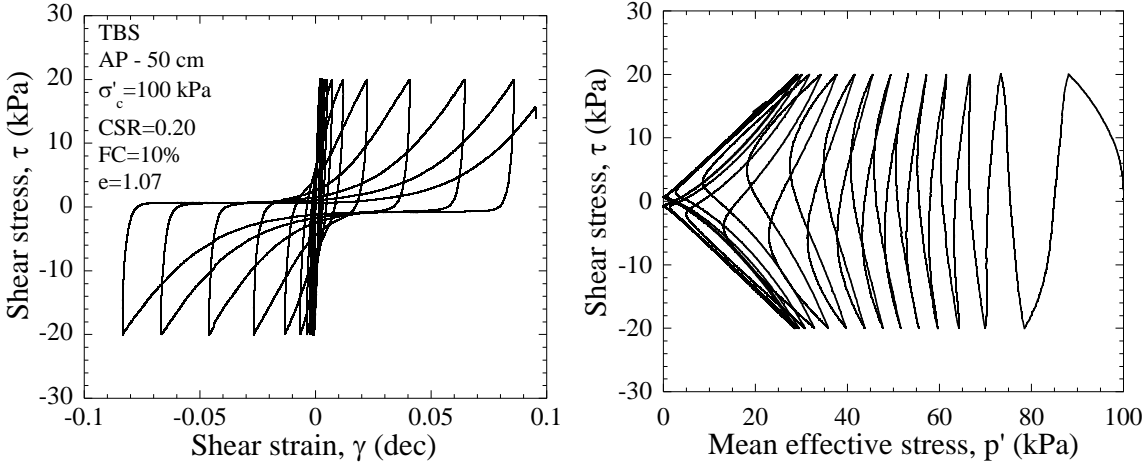


Figure 7.13. Cyclic loading on TBS, FC=10% prepared by AP-50 cm

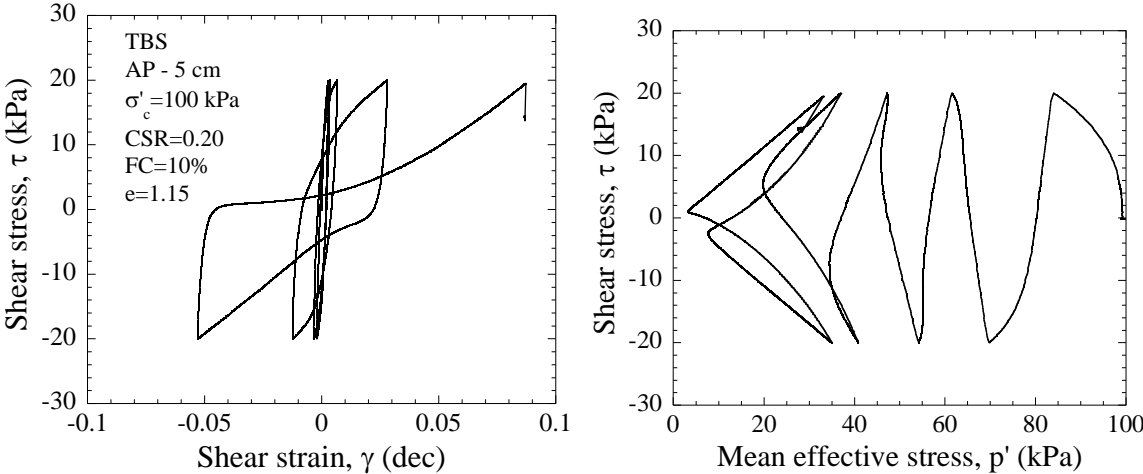


Figure 7.14. Cyclic loading on TBS, FC=10% prepared by AP-5 cm

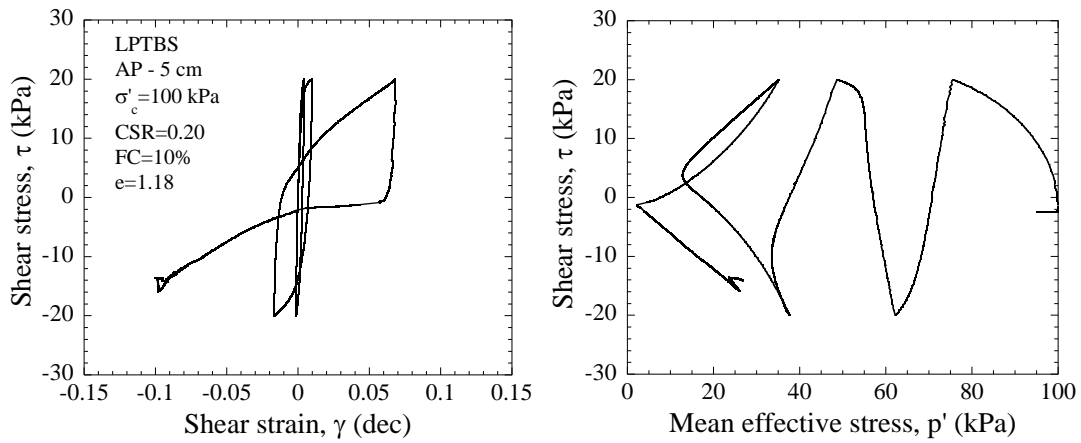


Figure 7.15. Cyclic loading on LPTBS, FC=10% prepared by AP-5 cm

This behavior shows that adding a small amount of plasticity does not necessarily reduce the liquefaction potential or increase the strength.

Excess pore pressure curves for FC=10, 20 and 30% are depicted in Figure 7.16 and compared to clean Tokyo Bay sand. It can be seen that clean sand is stronger and that the number of cycles to reach a $r_u=0.9$ is similar for all samples. Although there is a decrease from 10 to 20% and 30 and 10% exhibit similar curves.

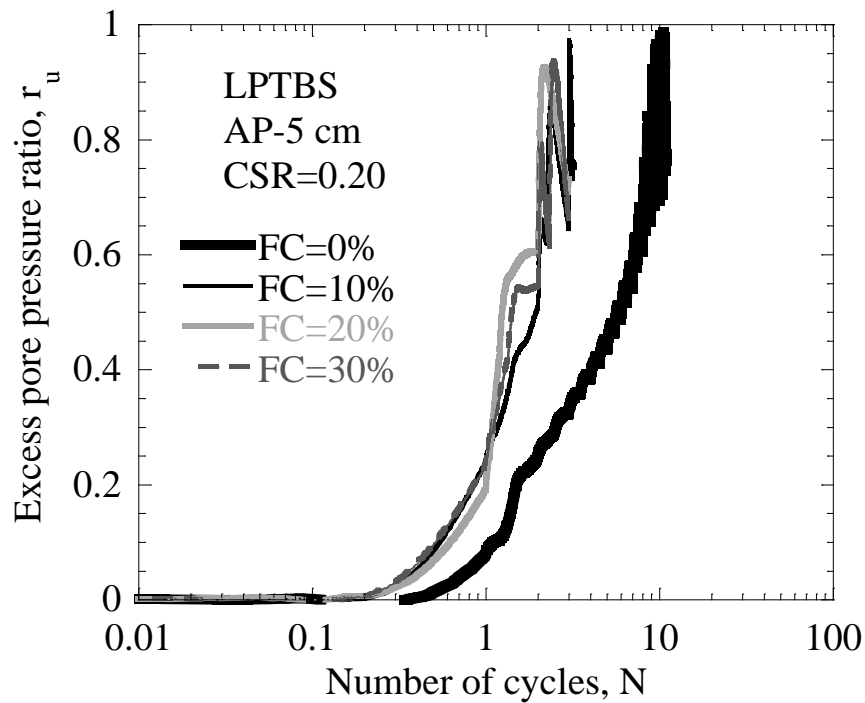


Figure 7.16. Excess pore pressure ratio for LPTBS

Liquefaction curves are shown in Figure 7.17. As observed for the previous results, there is a decrement in liquefaction resistance as FC increases.

When compared to the previous liquefaction curves obtained by AP-5 cm (Figure 7.18), it is observed that curves of the samples with bentonite actually have less resistance than the respective samples of non-plastic fines with FC=10, 20 and 30%. It can be noted that samples formed with low plasticity do not exhibit greater strength than clean sand and actually show similar results to those of large non-plastic fines content (FC>60%). This decrease in resistance can be explained if the effect of plasticity is neglected (due to the small amount of bentonite) and only the microstructure is considered. If the fines are replaced with smaller particles, void ratio increases and there is a reduction in liquefaction resistance. Guo and Prakash (1999) made similar observations of decrease in liquefaction resistance for plasticity index up to 5% and for greater PI, an increment. Moreover, Gratchev et al. (2007) conducted undrained cyclic tests in a ring-shear box on silica sand mixed with bentonite, varying the content from 0 to 15%. They found that the increase of

bentonite up to 7% actually decreased the number of cycles to liquefaction, although after 11% the increase in resistance was significantly larger and for 15% it kept increasing. After conducting tests on pore water chemistry, they stated that the presence of ions in pore water made the microstructure of the soil more prone to liquefaction.

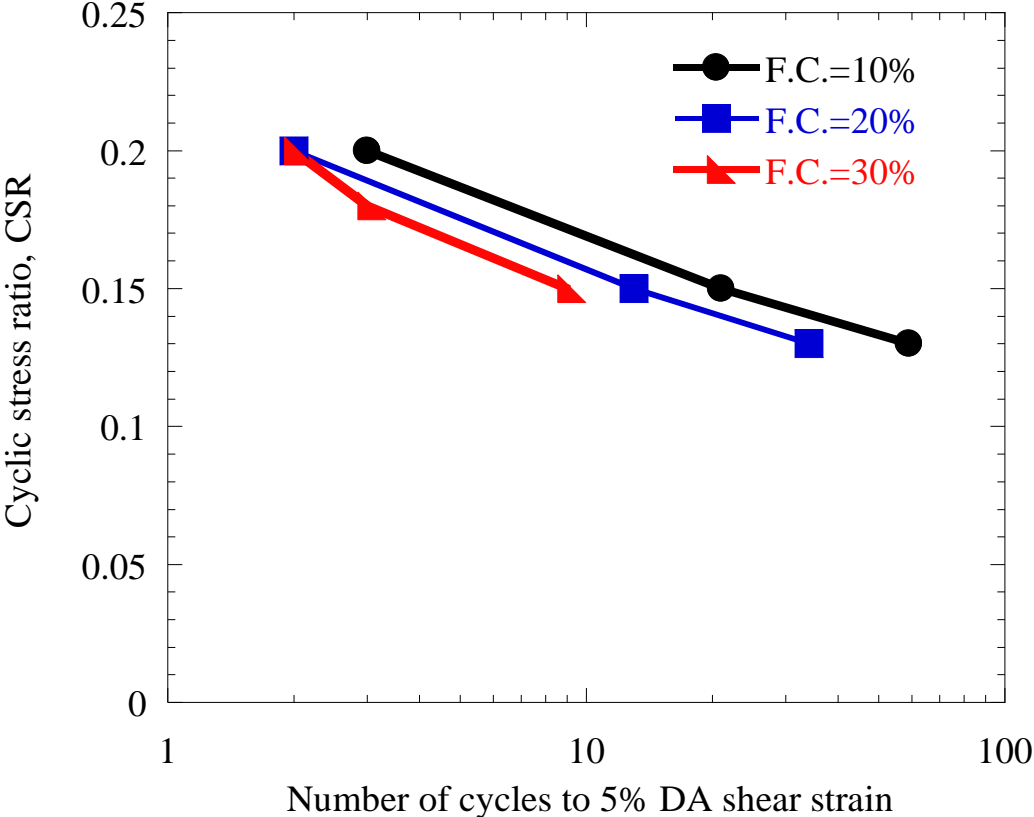


Figure 7.17. LPTBS – Liquefaction curves

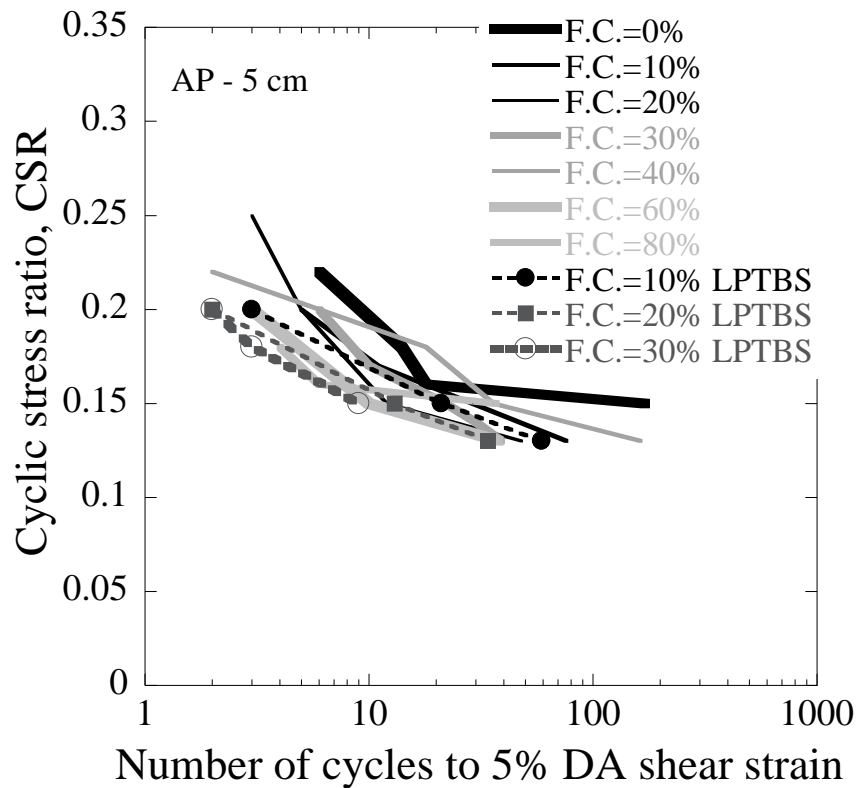


Figure 7.18. Liquefaction curves of LPTBS compared to non-plastic fines liquefaction curves

7.5. Simplified procedures for evaluation of liquefaction potential

Nowadays there are several simplified procedures used for evaluating the liquefaction potential of soil deposits. Some of the more widely used procedures are described below focusing on the effect of fines in this assessment.

7.5.1. Youd and Idriss (2001)

This procedure is based on previous studies on liquefaction by Seed and Idriss (1970). It consists of estimating two key values, the seismic demand of a soil layer (CSR) and the resistance of that layer (CRR). CSR depends on the peak horizontal acceleration at the ground surface, a_{\max} , gravity, g , total and effective vertical stresses in the soil layer, σ_{v0} and σ'_{v0} , and a stress reduction coefficient, r_d , which is a function of depth below ground surface.

$$CSR = (\tau_d / \sigma'_{vo}) = 0.65(a_{max}/g)(\sigma_{vo} / \sigma'_{vo})r_d$$

where τ_d is the amplitude of uniform shear stress cycles equivalent to actual seismic shear stress time history.

CRR is estimated from the curve presented by Seed et al. (1985) and illustrated in Figure 7.19. These curves were developed for clean sand although researchers observed that there was an increase in CRR with fines content. However, there was no distinction between plastic and non-plastic fines and it was not evident whether the increase was due to an increment in liquefaction resistance or a decrease in penetration resistance.

Therefore, in order to consider the presence of fines content, the blowcount measured in a layer with fines is corrected by parameters α and β to an equivalent value for clean sand.

$$(N_1)_{60cs} = \alpha + \beta(N_1)_{60}$$

Where $(N_1)_{60cs}$ is the equivalent corrected blowcount for clean sand and parameters α and β are defined by:

$$\alpha = 0 \text{ for } FC \leq 5\%$$

$$\alpha = \exp[1.76 - (190/FC^2)] \text{ for } 5\% < FC < 35\%$$

$$\alpha = 5.0 \text{ for } FC \geq 35\%$$

$$\beta = 1.0 \text{ for } FC \leq 5\%$$

$$\beta = [0.99 + (FC^{1.5}/1000)] \text{ for } 5\% < FC < 35\%$$

$$\beta = 1.2 \text{ for } FC \geq 35\%$$

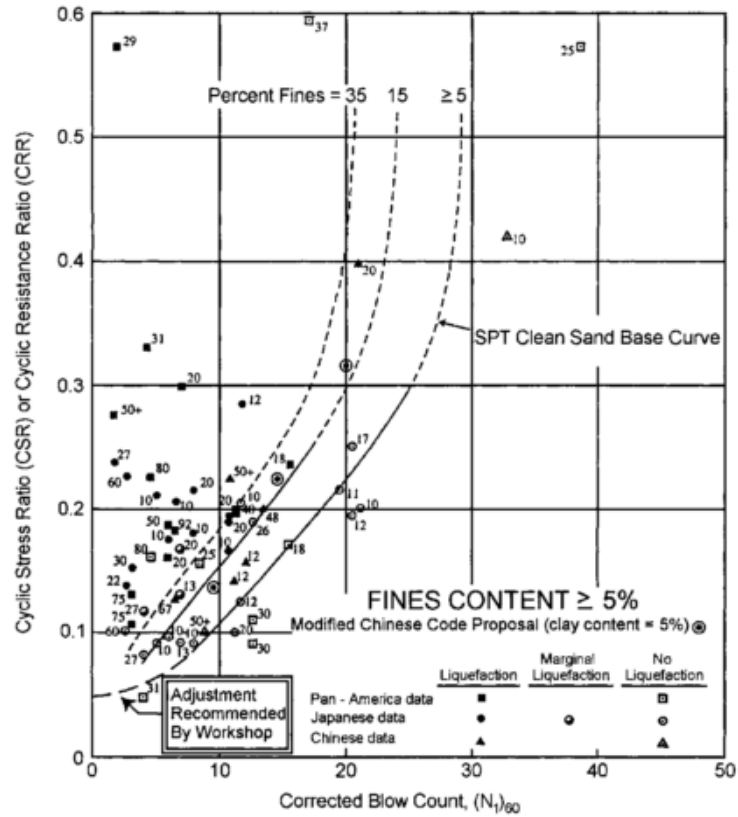


Figure 7.19. SPT clean-sand base curve (From Seed et al., 1985)

7.5.2. Japanese Highway Bridge Design Code

Factor of safety against liquefaction is evaluated as $F_L = R/L$, where the seismic stress ratio, L , is calculated as:

$$L = r_d \frac{\sigma_{vo}}{\sigma'_{vo}} c_z k_{hc0}$$

In this code r_d is calculated as $r_d = 1 - 0.015 \times \text{depth (in meters)}$. k_{hc0} is the seismic coefficient for design and is determined as a function of subsoil classification. Parameter c_z considers the regional seismic activity and ranges from 0.7 to 1.0.

Resistance, R , is evaluated as:

$$R = C_w R_L$$

Where C_w represents the effect of loading type and R_L , the resistance.

$$R_L = \begin{cases} 0.0882\sqrt{N_a/1.7} & (N_a < 14) \\ 0.0882\sqrt{N_a/1.7} + 1.6 \times 10^{-6}(N_a - 14)^{4.5} & (14 \leq N_a) \end{cases}$$

For sand, the adjusted value of blowcount, N_a , is calculated as:

$$N_a = c_1 \times \left(\frac{1.7N}{\sigma'_{vo} + 0.7} \right) + c_2$$

$$c_1 = \begin{cases} 1 & (0\% \leq FC < 10\%) \\ (FC + 40)/50 & (10\% \leq FC \leq 60\%) \\ (FC/20) - 1 & (60\% \leq FC) \end{cases}$$

$$c_2 = \begin{cases} 0 & (0\% \leq FC \leq 10\%) \\ (FC - 10)/18 & (10\% \leq FC) \end{cases}$$

C_w is computed as:

$$C_w = \begin{cases} \text{Earthquake type I} & \{1.0 \\ \text{Earthquake type II} & \begin{cases} 1.0 & (R_L \leq 0.1) \\ 3.3R_L + 0.67 & (0.1 < R_L \leq 0.4) \\ 2.0 & (0.4 < R_L) \end{cases} \end{cases}$$

Regarding fines content, this code points out soils susceptible to liquefaction as those with fines content less than 35% or plasticity index less than 15%.

As is observed in this code, coefficients c_1 and c_2 depend on fines content, although plasticity of these fines is not considered beyond the criterion mentioned above. It can be deduced that increasing fines content will increase the corrected SPT N-value.

For instance, considering SPT $N=5$ and the effective vertical stress level $\sigma'_{vo}=1 \text{ kgf/cm}^2$, the effect of fines on coefficients c_1 , c_2 and N_a can be calculated. Figure 7.20 and Figure 7.21 illustrate the variation of c_1 and c_2 with fines content, respectively. Figure 7.22 depicts the influence of fines content on the corrected value of SPT N. It is observed that a blowcount of $N=5$ measured in a layer with $FC=80\%$ can go up to 19 with the corrections for fines, which could increase resistance in 50% as shown in .

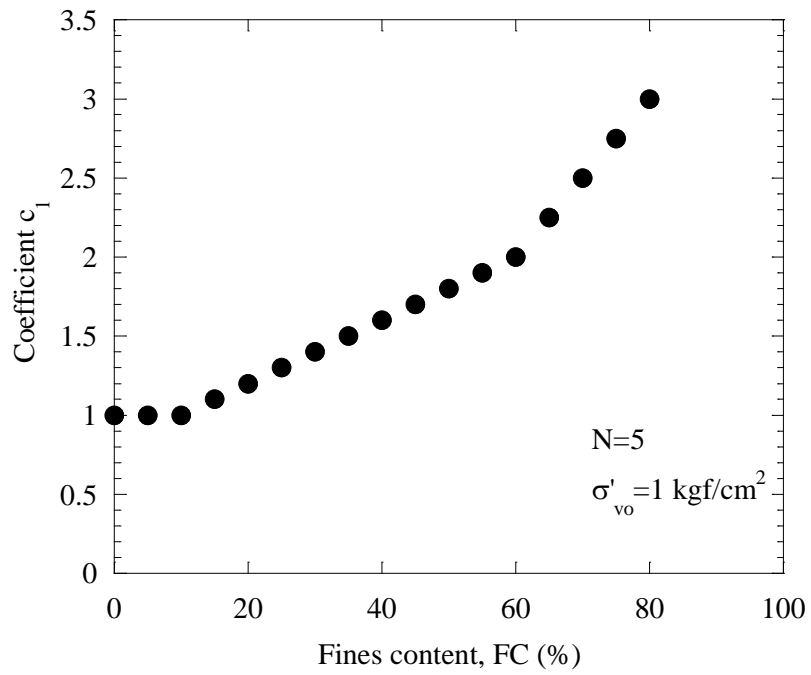


Figure 7.20. Variation of the coefficient c_1 with fines content

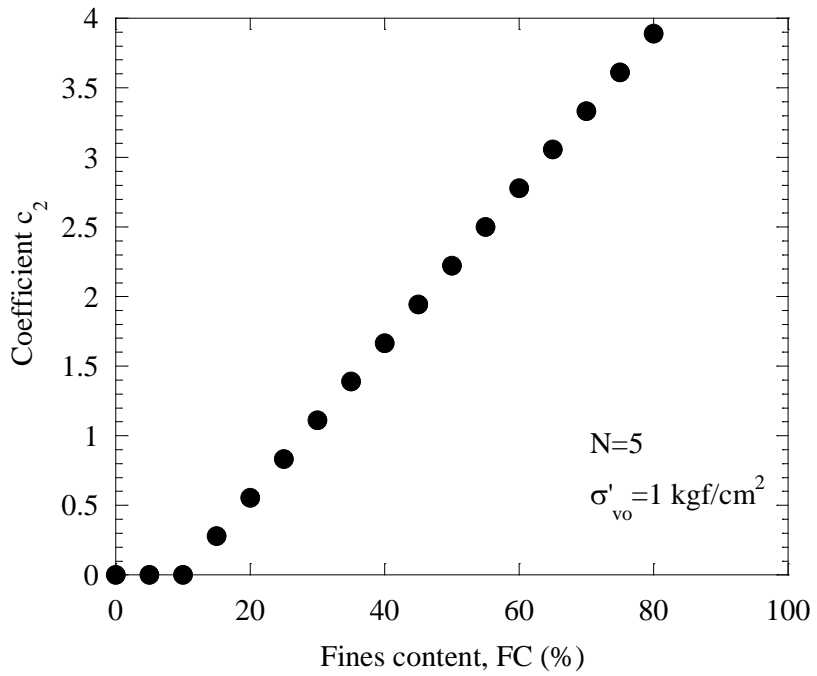


Figure 7.21. Variation of the coefficient c_2 with fines content

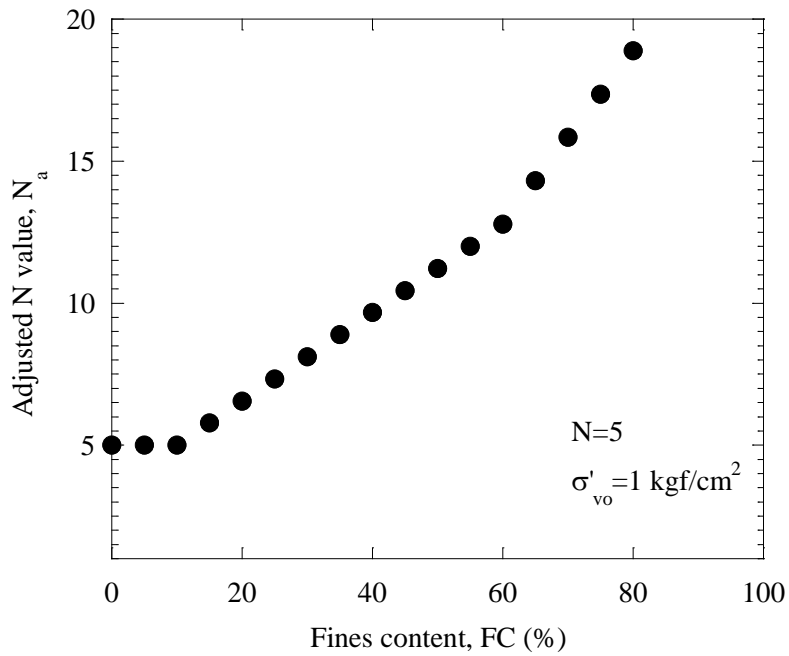


Figure 7.22. Variation of the corrected blowcount N_a with fines content

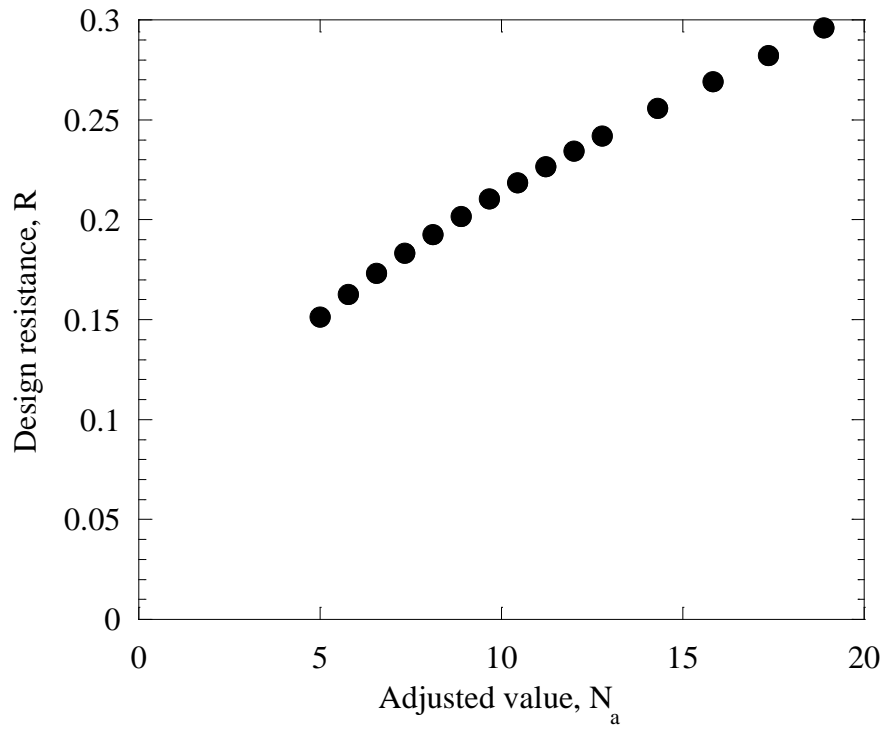


Figure 7.23. Variation of resistance with the adjusted value N_a modified for fines content

7.5.3. Tokimatsu and Yoshimi (1983)

These researchers revised a large amount of liquefaction case histories and laboratory tests on saturated sand and compared the obtained data to results of standard penetration tests in order to define a criterion to assess liquefaction potential by means of SPT.

The shear stress ratio to represent seismic ground motions was defined as:

$$\frac{\tau_d}{\sigma'_{vo}} = \frac{a_{max}}{g} \frac{\sigma_{vo}}{\sigma'_{vo}} r_d r_n$$

Where r_d and r_n stand for coefficients that account for depth and earthquake magnitude:

$$r_d = 1 - 0.015z$$

$$r_n = 0.1(M - 1)$$

Table 7.1 shows the relationship between earthquake magnitude and the coefficient r_n for the corresponding number of cycles

Table 7.1. Relationship among earthquake magnitude, number of cycles and r_n

Earthquake magnitude	Number of cycles	r_n
5.5	3	0.47
6.5	6	0.54
7.0	10	0.60
7.5	15	0.65
8.3	25	0.72

Resistance is computed as

$$\frac{\tau_l}{\sigma'_{vo}} = a C_r \left[\frac{16\sqrt{N_a}}{100} + \left(\frac{16\sqrt{N_a}}{C_s} \right)^n \right]$$

Where a and n are empirical constants, C_r is a correction factor for cyclic triaxial tests that considers the effect of system compliance, difference between triaxial and simple shear condition, effect of irregular shear stress and the effect of multidirectional shear; C_s is an empirical parameter function of strain amplitude, $C_s=94-19\log(\gamma)$; N_a is the SPT N-value adjusted for fines:

$$N_a = N_1 + \Delta N_f$$

Where ΔN_f is a correction terms that accounts for fines content and is defined in Table 7.2. The effect of fines content on the normalized SPT N-value, N_1 , can be observed in Figure 3.1 and in Figure 7.24, where for a shear stress ratio, N_1 reduces with fines content.

Table 7.2. Correlation between fines content and ΔN_f

Fines content, FC (%)	ΔN_f
0-5	0
5-10	Interpolate
10-	0.1FC+4

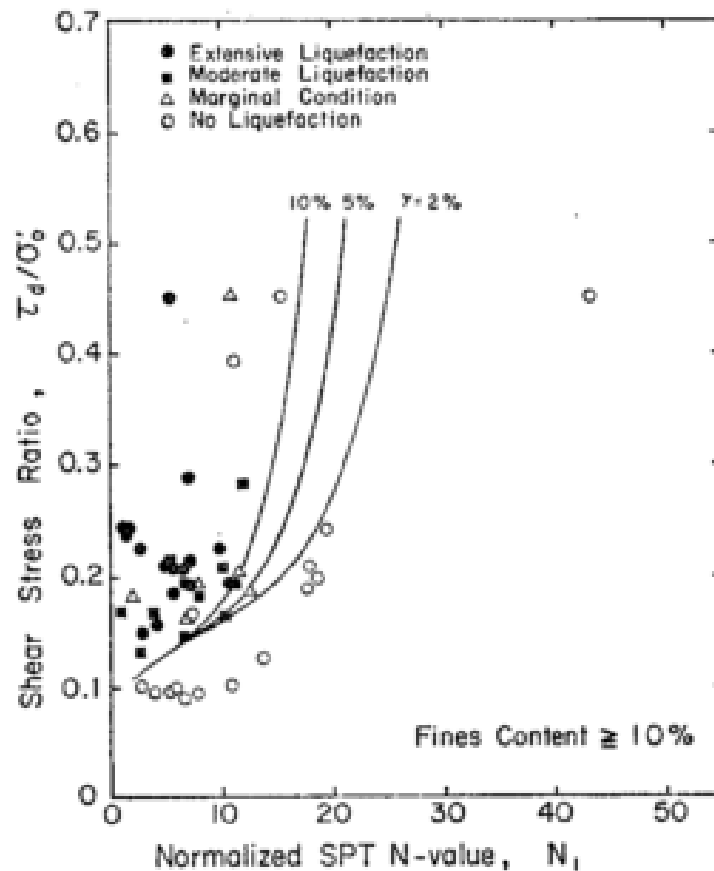


Figure 7.24. Field correlation and laboratory results for silty sands. From Tokimatsu and Yoshimi (1983).

7.5.4. Assessment through cone penetration test (CPT)

Up to now, methods based on correlations with standard penetration tests have been presented; nevertheless, other popular procedure conducted in-situ is the cone penetration test that measures penetration resistance, q_c , and sleeve friction, f_s . Robertson and Campanella (1985) proposed a correlation from CPT to SPT based on data from Seed et al. (1983).

Figure 7.25 shows the correlation between the modified cone penetration resistance, $Q_c = C_Q q_c$, and the cyclic stress ratio to cause liquefaction based on relative density and SPT N-value correlations.

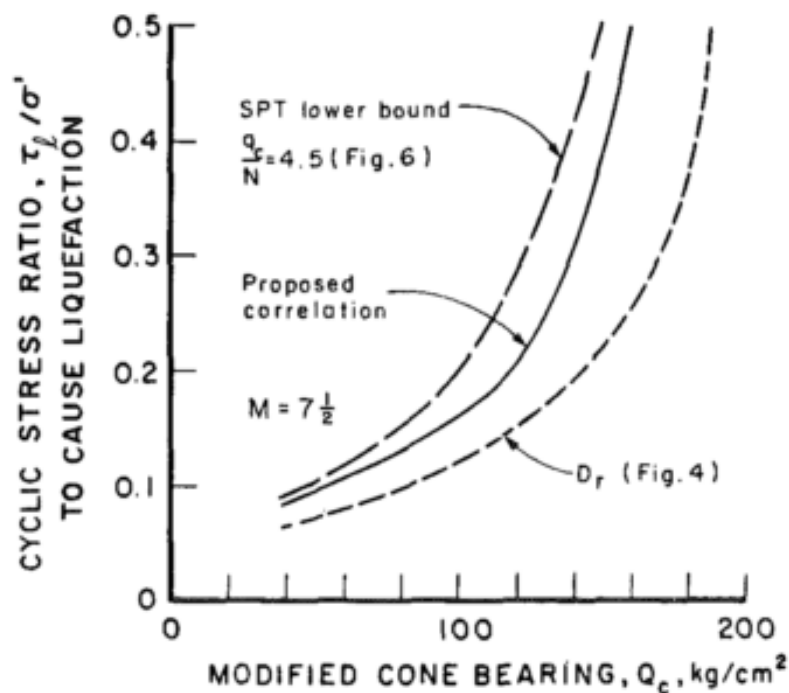


Figure 7.25. Correlation between modified cone penetration resistance and cyclic stress ratio (From Robertson and Campanella 1985).

This correlation is only valid for soils with $D_{50} \geq 0.25$ mm, in this regard researchers observed that there is a decrease in cone resistance of around 40 kg/cm^2 when there is a

reduction in mean size diameter from $D_{50}=0.25$ mm to $D_{50}=0.15$ mm for silty sand. Considering this, another correlation was proposed and is shown in Figure 7.26.

Carraro et al. (2003) proposed some curves considering non-plastic fines content. They carried out undrained cyclic tests on Ottawa sand varying the content of non-plastic silt from 0 to 15% and used a computer program called CONPOINT that allows estimation of cone penetration resistance based on cavity expansion theory. They developed the curves depicted in Figure 7.27 computing cone penetration resistance for $\sigma'_v=100$ kPa and $K_0=0.4$. It is observed that as fine content increases, the curves shift to the right. This behavior was explained considering that sands with fines are more dilative than clean sand and that cone resistance increases by dilatancy and critical-state friction angle, which grows with fines content.

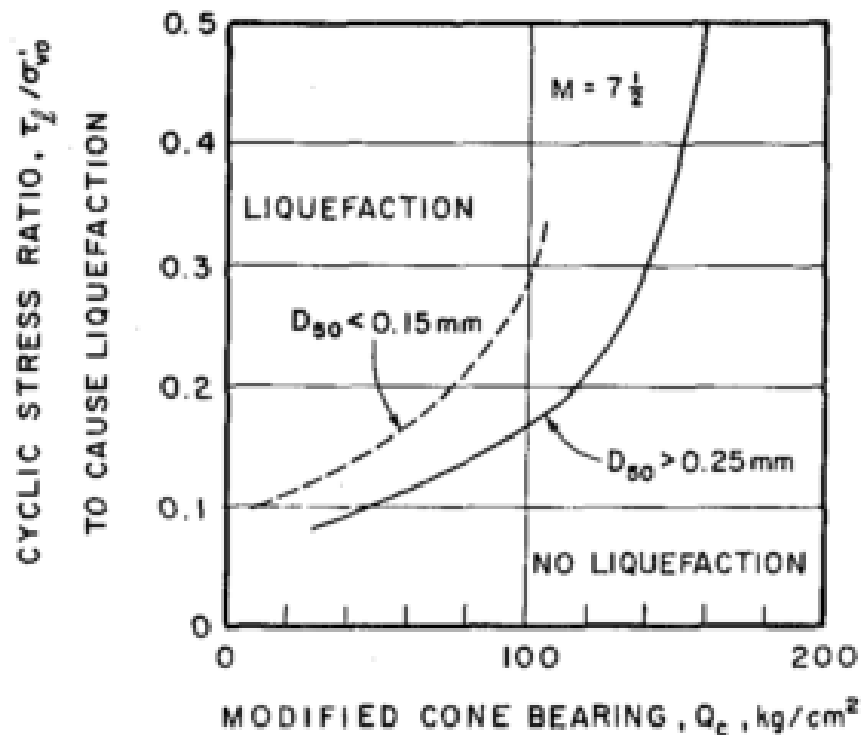


Figure 7.26. Correlation between cone penetration resistance and cyclic stress ratio for sands and silty sands. From Robertson and Campanella (1985).

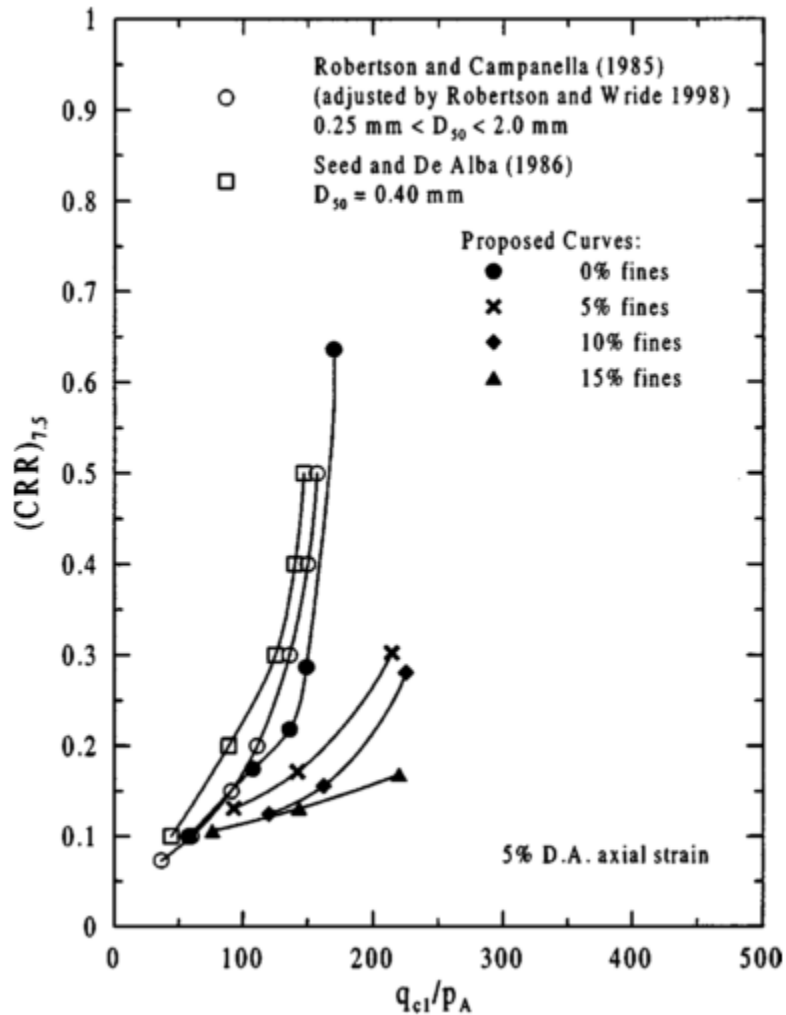


Figure 7.27. Effect of non-plastic fines content on the correlation between normalized cone resistance and cyclic resistance ratio. (From Carraro et al., 2003)

7.5.5. Results obtained in this research program

As observed, simplified procedures using standard penetration tests often use corrections of the penetration resistance observed in the field when there is presence of fines in the soil layer.

These increases respond to the fact that compressibility of fines decreases the value of SPT-N, nevertheless this not necessarily means that fines have larger resistance. Besides, Kokusho et al. (2012) carried out tests on undisturbed specimens from Pleistocene and

Holocene deposits retrieved from Chiba Prefecture, Japan and concluded that the reason why soils with high fines contents seem to have greater resistance does not depend on the fines themselves but on the cementation effect.

As stated in Chapter 5, at the same compaction energy silty sand exhibits less resistance than clean sand. Similar results were found by Lee et al. (2013) who performed cyclic triaxial tests on undisturbed samples retrieved from Urayasu City using the technique of the Gel-Push sampler. They compared liquefaction curves of samples with different fines contents at the same void ratio and found that silty sand has smaller liquefaction resistance compared to that of clean sand, therefore, when using the typical simplified procedures for assessing liquefaction potential, the resistance of non-plastic silty sand might be overestimated.

In the study presented in this dissertation all samples are at the same level of m_v which is equivalent to say that all of them correspond to a value of SPT N.

In this case, clean sand exhibits larger resistance than silty sand. As mentioned in Chapter 5, the sample with 60% of fines content consistently showed less resistance than the other samples, while from 20 to 40%, samples had similar resistance.

An idealized sketch of these results is plotted in Figure 7.28, along with the curves by Seed et al., (1985). It is important to remark that these fines are non-plastic therefore there is no contribution of cohesion, as it might be the case for the fines considered in the database for developing these curves.

This is an important fact because when considering fines content in the evaluation of liquefaction potential of a soil deposit, it is important to verify the plasticity in order to make the corrections for fines.

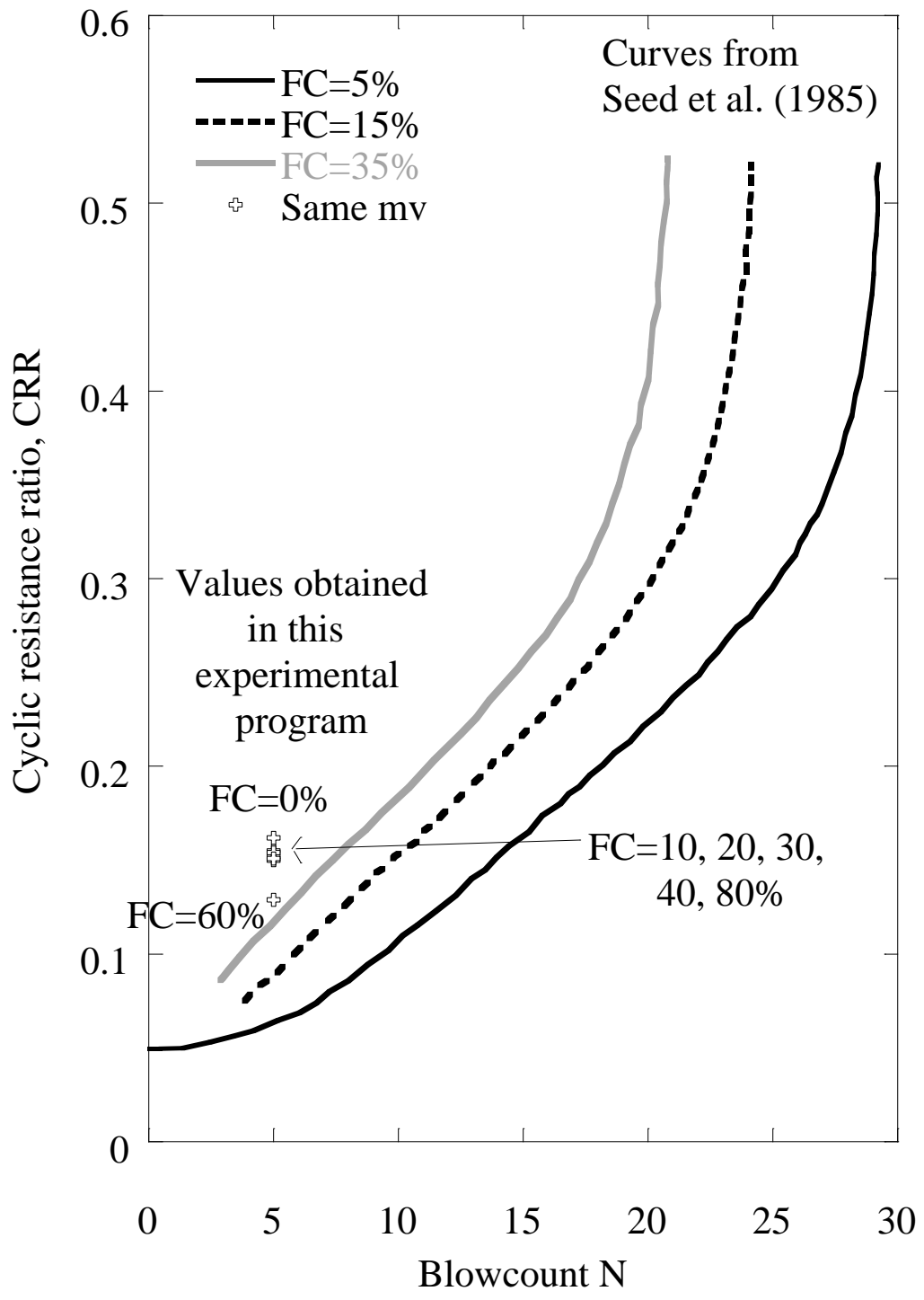


Figure 7.28. Comparison of results with current curves for SPT N-value and cyclic resistance ratio

Chapter 8

CONCLUSIONS AND RECOMMENDATIONS

Chapter 8. CONCLUSIONS AND RECOMMENDATIONS

The study on the effect of non-plastic fines content on the liquefaction resistance of sand has taken several approaches through the past decades.

Large amount of data has been collected for evaluation of liquefaction potential; however there is no clear distinction between plastic and non-plastic fines. Laboratory testing has used density parameters of comparison as void ratio, relative density or sand skeleton void ratio. Even the use of equivalent void ratio or inter-fine void ratio is not suitable for the whole range of fines contents.

Torsional shear tests were conducted on silty sand from Urayasu City, varying the fines content from 0 to 80% to consider all ranges of behavior, in four different sets: AP-5 cm, AP-30 cm, AP-50 cm, Smv. Three different responses were found and their characteristics were evaluated in terms of excess pore pressure build-up, shear strain and cyclic resistance ratio. Keeping the same energy for sample preparation gives some useful insight into the behavior of silty sand. It was found, by using this criterion, that the resistance of clean sand is always greater than that of sand mixed with fines. However, the behavior of the silty sand depends more on their relation to the threshold (F_{thr}) and limiting (F_{lim}) fines contents. When $FC < FC_{thr}$, liquefaction resistance decreases with increasing fines content, around this value ($FC \approx FC_{thr}$) liquefaction resistance increases, and for values higher than the limiting fines content ($FC > FC_{lim}$), soil behavior is dominated by the fines and liquefaction resistance increases as less sand grains are immersed into the sample. In this regard two aspects become very interesting, the microstructure of soil and the effective confining stress.

It was stated that regarding microstructure, an idealized binary packing can be used to understand the interaction between sand and fines. In this framework, two main problems arise, the effect of fines content on the variation of void ratio of the mixture, and the ratio of the mean diameter of clean sand over the mean diameter of silt (D_{50}/d_{50}). Once these problems are undertaken, interpretation of the microstructure is straightforward, as well as the effect of the density parameters on the cyclic resistance ratio and the results obtained by previous researchers.

There are three different stages of the microstructure:

1. Below the threshold fines content ($FC < F_{thr}$) in which fines are within the voids of the sand matrix. In this stage, the presence of fines decreases the void ratio, however there is no increase in the force because fines actually reduce the contacts between sand grains, which causes a decrement in liquefaction resistance.
2. Around the threshold fines content ($FC \approx F_{thr}$) fill all the voids within the sand matrix and start making contact with each other and with the sand grains, in this stage the minimum void ratio is reached and both fines and sand are contributing to the force chain of the solid skeleton.
3. After the limiting fines content ($FC > F_{lim}$), all sand grains are surrounded by fines, therefore they do not make sand-to-sand contacts and the overall resistance is reduced having an increment in overall void ratio. However, the sand grains also reduce the contact between fines, so as less sand is present, more resistance is gained.

By varying the height of fall it was seen that the effect of density through the raise in height of fall is clearly observed for samples below the threshold fines content, after F_{thr} the response of samples for both heights of fall is very similar.

When using the coefficient of volume compressibility as parameter of comparison, a similar response was observed to that seen for AP-5 cm and AP-50 cm. However it was noted that there is a small change in resistance for low fines content. This comparison is one of the biggest discoveries in this work due to the introduction of a parameter equivalent to SPT N-value. Given that the coefficient of volume compressibility relates to penetration resistance, N-value, it is expected that the same results are observed in the field. Results showed that when comparing different samples with varying non-plastic fines content, even at the same mv value, clean sand exhibits larger resistance. This is opposite to current design procedures and further studies should be carried out to offer different provisions for assessing liquefaction resistance of silty sands.

The deformability analysis showed the influence of shear modulus on permanent displacement and it was observed that the difference in fines content does not clearly affect the stiffness degradation of silty sand. This must be taken into account for design.

It was found that soil liquefaction can occur even with high non-plastic fines content, which indicated that the criteria of liquefaction susceptibility must focus more on the characteristics of the fines rather than the amount of material that passes the sieve #200 (Lee et al. 2012).

Additional results also indicated that post-liquefaction behavior is clearly affected by fines and it can be expected that soils comprised of non-plastic fines exhibit larger deformations after liquefaction.

8.1. Recommendations

The scope of this experimental program was focused on the undrained behavior of loose sands with non-plastic fines with confining stress equal to 100 kPa.

It is recommended to conduct a new program of monotonic and cyclic testing in a larger range of densities and for different effective confining pressures at the same m_v value. This would provide more data for improving the curves for design.

In that experimental program, it would be desirable to use the slurry deposition method for reconstituting the samples, to observe if the same trend is observed during testing, also in order to recreate the same magnitudes that would be observed in the field, and to incorporate the new data into design charts.

An important factor that was overlooked in this dissertation is the ageing effect. This important parameter should be included through longer consolidation times or by adding cement content as some papers have described. This is one of the main parameters affecting the results obtained in the field, when dealing with fines content.

The scope of this research can be expanded to soils containing fines and having an overall plasticity index $3 < PI < 12$. Some researchers have found that the increase in liquefaction resistance after $PI=11$ is relevant, while some others say that below 12, there is no actual influence of the plasticity. This can be a very important when considering reclaimed soils that contain some plasticity.

Finally, these tests were run on isotropic consolidated samples; however the conditions found in the field are usually for anisotropic conditions. It is recommended that samples with values of $K_0=0.75$, 0.5 and 0.3 are tested in order to obtain more insight into the problem of liquefaction-induced ground deformation.

Chapter 9. REFERENCES

- Amini, F. (2002). "Silt content effect on shear moduli using improved transfer function methods." *2002 IMAC-XX: Conference & Exposition on Structural Dynamics*, 1224–1226.
- Amini, F., and Qi, G. Z. (2000). "Liquefaction Testing of Stratified Silty Sands." *Journal of Geotechnical and Geoenvironmental Engineering*, American Society of Civil Engineers, 126(3), 208–217.
- Ampadu, S., and Tatsuoka, F. (1993). "Effect of setting method on the behaviour of clays in triaxial compression from saturation to undrained shear." *Soils and Foundations*, 33(2), 14–34.
- Andrews, D., and Martin, G. (2000). "Criteria for liquefaction of silty soils." *Proc., 12th World Conf. on Earthquake ...*, 1–8.
- Arefi, M. (2013). "Ground response evaluation for seismic hazard assessment." Doctoral thesis. University of Canterbury.
- Baki, M., Rahman, M., Lo, S. R., and Gnanendran, C. T. (2012). "Linkage between static and cyclic liquefaction of loose sand with a range of fines contents." *Canadian Geotechnical Journal*, 49(1), 891–906.
- Bayat, M., Bayat, E., Aminpour, H., and Salarpour, A. (2012). "Shear strength and pore-water pressure characteristics of sandy soil mixed with plastic fine." *Arabian Journal of Geosciences*.
- Been, K., and Jefferies, M. G. (1985). "State parameter for sands." *International Journal of Rock Mechanics and Mining Sciences & Geomechanics Abstracts*, 22(6), 198.
- Belkhatir, M., Arab, A., Della, N., Missoum, H., and Schanz, T. (2010). "Influence of inter-granular void ratio on monotonic and cyclic undrained shear response of sandy soils." *Comptes Rendus Mecanique*, Elsevier Masson SAS, 338(5), 290–303.
- Belkhatir, M., Missoum, H., Arab, A., Della, N., and Schanz, T. (2011). "Undrained shear strength of sand-silt mixture: Effect of intergranular void ratio and other parameters." *KSCE Journal of Civil Engineering*, 15(8), 1335–1342.
- Bouckovalas, G. D., Andrianopoulos, K. I., and Papadimitriou, A. G. (2003). "A critical state interpretation for the cyclic liquefaction resistance of silty sands." *Soil Dynamics and Earthquake Engineering*, 23(2), 115–125.
- Boulanger, R., and Idriss, I. (2006). "Liquefaction susceptibility criteria for silts and clays." *Journal of Geotechnical and Geoenvironmental Engineering*, 132(11), 1413–1426.
- Bray, J., and Sancio, R. (2006). "Assessment of the liquefaction susceptibility of fine-grained soils." *Journal of Geotechnical and Geoenvironmental Engineering*, 132(9), 1165–1177.

- Carraro, J., Bandini, P., and Salgado, R. (2003). "Liquefaction resistance of clean and nonplastic silty sands based on cone penetration resistance." *Journal of Geotechnical and Geoenvironmental Engineering*, 129(11), 965–976.
- Carraro, J., Prezzi, M., and Salgado, R. (2009). "Shear strength and stiffness of sands containing plastic or nonplastic fines." *Journal of Geotechnical and Geoenvironmental Engineering*, 135(9), 1167–1178.
- Chang, W., and Hong, M. (2008). "Effects of Clay Content on Liquefaction Characteristics of Gap-graded Clayey Sands." *Soils and Foundations*, 48(1), 101–114.
- Clough, G. W., Martin, J. R., and Chameau, J. L. (1994). "The geotechnical aspects." *Practical Lessons from the Loma Prieta Earthquake*, Report from a Symposium Sponsored by the Geotechnical Board and the Board on Natural Disasters of the National Research Council, 29–63.
- Cubrinovski, M., Bradley, B., Wotherspoon, L., Green, R., Bray, J. D., Wood, C., Pender, M., Allen, J., Bradshaw, A., Rix, G., Taylor, M., Robinson, K., Henderson, D., Giorgini, S., Ma, K., Winkley, A., Zupan, J., O'Rourke, T., DePascale, G., and Wells, D. (2011). "Geotechnical aspects of the 22 February 2011 Christchurch earthquake." *Bulletin of the New Zealand Society for Earthquake Engineering*, 44(4), 205–226.
- Cubrinovski, M., and Ishihara, K. (1999). "Empirical correlation between SPT N-value and relative density for sandy soils." *Soils and Foundations*, 39(5), 61–71.
- Cubrinovski, M., and Ishihara, K. (2002). "Maximum and minimum void ratio characteristics of sands." *Soils and Foundations*, 42(6), 65–78.
- Dash, H. K., and Sitharam, T. G. (2011). "Undrained Cyclic and Monotonic Strength of Sand-Silt Mixtures." *Geotechnical and Geological Engineering*, 29(4), 555–570.
- Donahue, J., Bray, J., and Riemer, M. F. (2007). *The liquefaction susceptibility, resistance and response of silty and clayey soils*. 272.
- Donahue, J. L., Bray, J. D., and Riemer, M. F. (2008). *Geoengineering liquefaction susceptibility, resistance and response of silty and clayey soils*. 271.
- Gratchev, I., Sassa, K., and Fukuoka, H. (2007). "Undrained Cyclic Behavior of Mixtures of High-Plasticity Clay and Sand." *Annals of Disaster Prevention Research Institute, Kyoto University*, 50(1), 113–118.
- Gunji, K., Alberto, Y., and Towhata, I. (2013). "Simple prediction method of liquefaction-induced displacement." *48th Annual Conference, Japanese Geotechnical Society, Toyama, June 2013*, 1847–1848.

- Guo, T., and Prakash, S. (1999). "Liquefaction of silts and silt-clay mixtures." *Journal of Geotechnical and Geoenvironmental Engineering*.
- Hara, T., Kokusho, T., and Tanaka, M. (2008). "Liquefaction strength of sand materials containing fines compared with cone resistance in triaxial specimens." *The 14th World Conference on Earthquake Engineering, October 12-17, Beijing, China*, 1–8.
- Holzer, T. (1998). *The Loma Prieta California Earthquake of October 17 1989 - Liquefaction*. 311.
- Huang, A., and Chuang, S. (2011). "Correlating cyclic strength with fines contents through state parameters." *Soils and Foundations*, 51(6), 991–1001.
- Huang, Y.-T., Huang, A.-B., Kuo, Y.-C., and Tsai, M.-D. (2004). "A laboratory study on the undrained strength of a silty sand from Central Western Taiwan." *Soil Dynamics and Earthquake Engineering*, 24(9-10), 733–743.
- Hung, V. (2012). *A Study of the Effects of Liquefaction as a Result of the 1999 Chi-Chi Earthquake*. Massachusetts Institute of Technology, 19.
- Ishihara, K. (1993). "Liquefaction and flow failure during earthquakes." *Geotechnique*, 43(3), 351–415.
- Ishihara, K. (2011). "Liquefaction in Tokyo Bay and Kanto Region in the 2011 Great East Japan Earthquake." *Proceedings of the International Symposium on Engineering Lessons Learned from the 2011 Great East Japan Earthquake, Tokyo, Japan, March 1-4*, 63–81.
- Ishihara, K., Tsukamoto, Y., and Sawada, S. (2004). "Evaluation of Settlement of Silty Sand Deposits." *The 11th International Conference on Soil Dynamics & Earthquake Engineering (11th ICSDEE). The 3rd International Conference on Earthquake Geotechnical Engineering (3rd ICEGE)*., 681–688.
- Ishihara, K., and Yoshimine, M. (1992). "Evaluation of settlements in sand deposits following liquefaction during earthquakes." *Soils and Foundations*, 32(1), 173–188.
- Iwasaki, T., and Tatsuoka, F. (1977). "Effects of grain size and grading on dynamic shear moduli of sands." *Soils and Foundations*, 17(3), 19–35.
- Jefferies, M. G., and Been, K. (2006). *Soil liquefaction. A critical state approach*. Taylor & Francis, 625.
- Juang, C., Yang, S., Yuan, H., and Fang, S. (2005). "Liquefaction in the Chi-Chi earthquake-effect of fines and capping non-liquefiable layers." *Soils and Foundations*, 45(6), 89–101.
- Kayen, R., and Mitchell, J. (1997). "Assessment of liquefaction potential during earthquakes by Arias intensity." *Journal of Geotechnical and Geoenvironmental Engineering*, 123(12), 1162–1174.

- Kazama, M., and Yanagisawa, E. (2000). "Earthquake motion intensity from liquefaction viewpoint." *12th World Conference on Earthquake Engineering*, 1–8.
- Kokusho, T., Ito, F., Nagao, Y., and Green, A. (2012). "Influence of Non/Low-Plastic Fines and Associated Aging Effects on Liquefaction Resistance." *Journal of Geotechnical and Geoenvironmental Engineering*, 138(6), 747–756.
- Kokusho, T., Nagao, Y., Ito, F., and Fukuyama, T. (2012). "Aging effect on sand liquefaction observed during the 2011 Earthquake and basic laboratory studies." *Proceedings of the International Symposium on Engineering Lessons Learned from the 2011 Great East Japan Earthquake*, 759–770.
- Koseki, J., Yoshida, T., and Sato, T. (2005). "Liquefaction properties of Toyoura sand in cyclic torsional shear tests under low confining stress." *Soils and foundations*, 45(5), 103–113.
- Kuerbis, R. (1989). "The effect of gradation and fines content on the undrained loading response of sand." The University of British Columbia.
- Kuerbis, R. H., and Vaid, Y. P. (1988). "Sand sample preparation - The slurry deposition method." *Soils and foundation*, 28(4), 107–118.
- Lade, P., Liggio, C., and Yamamuro, J. (1998). "Effects of non-plastic fines on minimum and maximum void ratios of sand." *Geotechnical Testing Journal*, 21(4), 336–347.
- Lade, P. V., and Yamamuro, J. A. (1997). "Effects of nonplastic fines on static liquefaction of sands." *Canadian Geotechnical Journal*, 34(6), 918–928.
- Law, K., and Ling, Y. (1992). "Liquefaction of granular soils with non-cohesive and cohesive fines." *Proceedings of the tenth world conference on Earthquake Engineering*, 6.
- Lee, K., and Fitton, J. (1969). "Factors affecting the cyclic loading strength of soil." *Vibration effects of earthquakes on soils and foundations, ASTM, STP 450*, 71–95.
- Lee, W., Chen, C., and Ishihara, K. (2013). "Liquefaction Potential of Non-Plastic Silty Sand." *Journal of Marine Science and Technology*, 13(3), 1–8.
- Lee, W., Ishihara, K., and Chen, C. (2012). "Liquefaction of silty sand-preliminary studies from recent Taiwan, New Zealand and Japan Earthquakes." *Proceedings of the International Symposium on Engineering Lessons Learned from the 2011 Great East Japan Earthquake, March 1-4, 2012, Tokyo, Japan*, 747–758.
- McGeary, R. (1961). "Mechanical packing of spherical particles." *Journal of the American Ceramic Society*, 58(1931), 513–522.

- Missoum, H., Belkhatir, M., Bendani, K., and Maliki, M. (2012). "Laboratory Investigation into the Effects of Silty Fines on Liquefaction Susceptibility of Chlef (Algeria) Sandy Soils." *Geotechnical and Geological Engineering*.
- Mitchell, J., and Soga, K. (2005). *Fundamentals of Soil Behavior*. Wiley, 592.
- Miura, S., Toki, S., and Tanizawa, F. (1984). "Cone penetration characteristics and its correlation to static and cyclic deformation-strength behaviors of anisotropic sand." *Soils and Foundations*, 24(2), 58–74.
- Mogami, T., and Kubo, K. (1953). "The behaviour of soil during vibration." *Proceedings of the Third International Conference of Soil Mechanics and Foundation Engineering, Switzerland 16th-17th August, 1953, Volume 1*, 152–155.
- Mulilis, J. P., Arulanandan, K., Mitchell, J. K., Chan, C. K., and Seed, H. B. (1977). "Effects of Sample Preparation on Sand Liquefaction." *Journal of the Geotechnical Engineering Division, ASCE*, 103(2), 91–108.
- Nabeshima, Y., and Matsui, T. (2003). "Role of Plastic and Non-Plastic Fines on Cyclic Shear Behavior of Saturated Sands." *13th International Offshore and Polar Engineering Conference*, 440–444.
- Naeini, S. A., and Baziar, M. H. (2004). "Effect of fines content on steady-state strength of mixed and layered samples of a sand." *Soil Dynamics and Earthquake Engineering*, 24(3), 181–187.
- Ni, S., and Fan, E. (2004). "Fines content effects on liquefaction potential evaluation for sites liquefied during Chi-chi earthquake, 1999." *13th World Conference on Earthquake Engineering, Vancouver, B.C., Canada*, 1–15.
- Noda, S., and Hyodo, M. (2013). "Effects of fines content on cyclic shear characteristics of sand-clay mixtures." *18th International Conference on Soil Mechanics and Geotechnical Engineering, Paris 2013*, 1551–1554.
- Panayiotopoulos, K. (1989). "Packing of sands—a review." *Soil and Tillage Research*, 13, 101–121.
- Polito, C., and Martin, J. R. (2001). "Effects of nonplastic fines on the liquefaction resistance of sands." *Journal of Geotechnical and Geoenvironmental Engineering*, 127(5), 408–415.
- Rad, S., and Clough, G. W. (1985). "New procedure for saturating sand specimens." *Journal of Geotechnical Engineering*, 110(9), 1205–1218.
- Rahman, M. M., and Lo, S. R. (2008). "The prediction of equivalent granular steady state line of loose sand with fines." *Geomechanics and Geoengineering: An International Journal*, 3(3), 179–190.

- Rahman, M. M., and Lo, S. R. (2008). "The prediction of equivalent granular steady state line of loose sand with fines." *Geomechanics and Geoengineering*, Taylor & Francis, 3(3), 179–190.
- Rahman, M. M., Lo, S. R., and Gnanendran, C. T. (2008). "On equivalent granular void ratio and steady state behaviour of loose sand with fines." *Canadian Geotechnical Journal*, 45(10), 1439–1456.
- Rees, S. (2010). "Effects of fines on the undrained behaviour of Christchurch sandy soils." Doctoral thesis. University of Canterbury.
- Robertson, P., and Campanella, R. (1985). "Liquefaction Potential of Sands Using the CPT." *Journal of Geotechnical Engineering*, American Society of Civil Engineers, 111(3), 384–403.
- Rollings, K. M., and McHood, M. D. (1998). "Comparison of computed and measured liquefaction-induced settlements in the Marina District, San Francisco." *The Loma Prieta California Earthquake of October 17, 1989 - Liquefaction*. USGS, B223–B239.
- Saada, A. (1988). "Hollow cylinder torsional devices: their advantages and limitations." *Advanced Triaxial Testing of Soil and Rock*. ASTM, STP 977, 766–795.
- Salgado, R., Bandini, P., and Karim, A. (2000). "Shear strength and stiffness of silty sand." *Journal of Geotechnical and Geoenvironmental Engineering*, 126(5), 451–462.
- Seed, B. H. B., Tokimatsu, K., Harder, L. F., and Chung, R. M. (1985). "Influence of spt procedures in soil liquefaction resistance evaluations." *Journal of Geotechnical Engineering Engineering*, 111(12), 1425–1445.
- Seed, H. B., Idriss, I. M., and Arango, I. (1983). "Evaluation of Liquefaction Potential Using Field Performance Data." *Journal of Geotechnical Engineering*, American Society of Civil Engineers, 109(3), 458–482.
- Seed, H., and Idriss, I. (1970). "A simplified procedure for evaluating soil liquefaction potential." *University of California, Berkeley. Report No. EERC 70-9. November 1970*, 39.
- Seed, H., Tokimatsu, K., Harder, L., and Chung, R. (1984). "The influence of SPT procedures in soil liquefaction resistance evaluations." *University of California, Berkeley. Report No UCB/EERC-84/15. October 1984*, 59.
- Seed, Idriss, I., and Arango, I. (1983). "Evaluation of liquefaction potential using field performance data." *Journal of Geotechnical Engineering*, 109(3), 458–482.
- Shen, C. K., Vrymoed, J. L., and Uyeno, C. K. (1977). "The effect of fines on liquefaction of sands." *Proc. IX Int. Conf. on Soil Mechanics and Foundation Engineering, Tokyo, Vol. 2*, 381–385.
- Stark, T., Kramer, S., and Youd, T. (1997). *Post-liquefaction shear strength of granular soils. ... Postliquefaction Shear Strength of Granular Soils, ...*, 385.

- Stroud, M. A., and Butler, F. G. (1975). "The standard penetration test and the engineering properties of glacial materials." *Proceedings of the symposium on Engineering Properties of glacial materials*, 14.
- Tatsuoka, F., Ochi, K., Fujii, S., and Okamoto, M. (1986). "Cyclic undrained triaxial and torsional shear strength of sands for different sample preparation methods." *Soils and Foundations*, 26(3), 23–41.
- Terzaghi, K., and Peck, R. (1967). *Soil mechanics in engineering practice*. Wiley, 729.
- Thevanayagam, S. (1998). "Effect of fines and confining stress on undrained shear strength of silty sands." *Journal of Geotechnical and Geoenvironmental Engineering*, 124(6), 479–491.
- Thevanayagam, S. (2000). "Liquefaction potential and undrained fragility of silty soils." *Proceedings of the 12th World Conference on Earthquake Engineering*, 1–8.
- Thevanayagam, S., Shenthan, T., Mohan, S., and Liang, J. (2002). "Undrained Fragility of Clean Sands, Silty Sands, and Sandy Silts." *Journal of Geotechnical and Geoenvironmental Engineering*, American Society of Civil Engineers, 128(10), 849–859.
- Tokimatsu, K., and Seed, H. B. (1987). "Evaluation of settlements in sands due to earthquake shaking." *Journal of Geotechnical Engineering*, 113(8), 861–878.
- Tokimatsu, K., and Yoshimi, Y. (1983). "Empirical correlation of soil liquefaction based on SPT N-value and fines content." *Soils and Foundations*, 23(4), 56–74.
- Tokimatsu, K., and Yoshimi, Y. (1983). "Empirical correlation of soil liquefaction based on SPT N-value and fines content." *Soils and Foundations*, 23(4), 56–74.
- Toriihara, M., Yamada, Y., Morimoto, I., and Ishihara, K. (2000). "The characteristics of settlement after liquefaction for sand containing fines." *Proceedings of the 35th Japan Conference on Geotechnical Engineering*, 1655–1656.
- Towhata, I., Goto, S., Taguchi, Y., and Aoyama, S. (2012). "Unsolved engineering problems after 2011 gigantic earthquake in Japan." *Conference of Australian Earthquake Engineering Society*, 1–11.
- Tsukamoto, Y., Ishihara, K., and Sawada, S. (2004). "Settlement of silty sand deposits following liquefaction during earthquakes." *Soils and foundations*, 44(5), 135–148.
- Vaid, Y. P., and Thomas, J. (1995). "Liquefaction and Postliquefaction Behavior of Sand." *Journal of Geotechnical Engineering*, American Society of Civil Engineers, 121(2), 163–173.
- Vaid, Y., Sivathayalan, S., and Stedman, D. (1999). "Influence of specimen-reconstituting method on the undrained response of sand." *ASTM geotechnical testing journal*, 22(3), 187–195.

- Wang, W. (1979). "Some Findings in Soil Liquefaction." *Chinese Journal of Geotechnical Engineering*, 2(3), 55–63.
- Wijewickreme, D., Sanin, M. V, and Greenaway, G. R. (2005). "Cyclic shear response of fine-grained mine tailings." *Canadian Geotechnical Journal*, 42, 1408–1421.
- Xenaki, V. C., and Athanasopoulos, G. A. (2003). "Liquefaction resistance of sand–silt mixtures: an experimental investigation of the effect of fines." *Soil Dynamics and Earthquake Engineering*, 23(3), 1–12.
- Yamamuro, J., and Covert, K. (2001). "Monotonic and cyclic liquefaction of very loose sands with high silt content." *Journal of Geotechnical and Geoenvironmental Engineering*, 127(4), 314–324.
- Yasuda, S., Harada, K., Ishikawa, K., and Kanemaru, Y. (2012). "Characteristics of liquefaction in Tokyo Bay area by the 2011 Great East Japan Earthquake." *Soils and Foundations*, Elsevier, 52(5), 793–810.
- Youd, T. L., and Idriss, I. M. (2001). "Liquefaction Resistance of Soils: Summary Report from the 1996 NCEER and 1998 NCEER/NSF Workshops on Evaluation of Liquefaction Resistance of Soils." *Journal of Geotechnical and Geoenvironmental Engineering*, American Society of Civil Engineers, 127(4), 297–313.
- Zdravkovic, L. (1996). "The stress-strain-strength an isotropy of a granular medium under general stress conditions." Imperial College of London. Doctoral dissertation.
- Zlatovic, S., and Ishihara, K. (1995). "On the influence of non-plastic fines on residual strength." *Proceedings of IS-TOKYO 95*, 239–244.